PERFORMANCE ANALYSIS OF GRID-CONNECTED WIND ENERGY SYSTEMS

Ph.D. THESIS

by

KANASOTTU ANIL NAIK

DEPARTMENT OF ELECTRICAL ENGINEERING
INDIAN INSTITUTE OF TECHNOLOGY ROORKEE
ROORKEE – 247667 (INDIA)
JULY, 2018

PERFORMANCE ANALYSIS OF GRID-CONNECTED WIND ENERGY SYSTEMS

A THESIS

Submitted in partial fulfilment of the requirements for the award of the degree

of

DOCTOR OF PHILOSOPHY

in

ELECTRICAL ENGINEERING

by

KANASOTTU ANIL NAIK

DEPARTMENT OF ELECTRICAL ENGINEERING
INDIAN INSTITUTE OF TECHNOLOGY ROORKEE
ROORKEE – 247667 (INDIA)
JULY, 2018

INDIAN INSTITUTE OF TECHNOLOGY ROORKEE
ROORKEE

CANDIDATE'S DECLARATION

I hereby certify that the work which is being presented in this thesis entitled "**PERFORMANCE ANALYSIS OF GRID CONNECTED WIND ENERGY SYSTEMS**" in partial fulfillment of the requirements for the award of the Degree of Doctor of Philosophy and submitted in the Department of Electrical Engineering of the Indian Institute of Technology Roorkee, Roorkee is an authentic record of my own work carried out during a period from January, 2014 to July, 2018 under the supervision of Dr. Chandra Prakash Gupta, Associate Professor and Dr. E. Fernandez, Associate Professor, Department of Electrical Engineering, Indian Institute of Technology Roorkee, Roorkee.

The matter presented in this thesis has not been submitted by me for the award of any other degree of this or any other Institute.

(KANASOTTU ANIL NAIK)

This is to certify that the above statement made by the candidate is correct to the best of our knowledge.

(Chandra Prakash Gupta)
Supervisor

(E. Fernandez)
Supervisor

Dated: _____

ACKNOWLEDGEMENTS

With GOD's grace I have got this opportunity to thank all those who have supported me all through this course of work. First and foremost, I would like to express my deepest sense of gratitude towards my supervisors Dr. Chandra Prakash Gupta, Associate Professor, Department of Electrical Engineering and Dr. E. Fernandez, Associate Professor, Department of Electrical Engineering of Indian Institute of Technology Roorkee, Roorkee, for their patience, inspiring guidance, constant encouragement, moral support and keen interest in minute details of the work. I am sincerely indebted to them for their pronounced individuality, humanistic and warm personal approach, and excellent facility provided to me in the laboratory to carry out this research.

I also express my sincere gratitude towards my research committee members Dr. N. P. Padhy (Professor EED & Chairmen SRC), Dr. D.K. Khatod, (Associate Professor, EED), Dr. R.P. Saini, (Professor, Department of AHEC) for their invaluable direction, encouragement and support, and above all the noblest treatment extended by them during the course of my studies at IIT Roorkee.

I heartily extend my gratitude to Head of the Department of Electrical Engineering, and all faculty members of the department for their help, moral support and providing the excellent infrastructure, laboratory and computing facility for the research work.

I acknowledge my sincere gratitude to the Ministry of Human Resources and Development (MHRD), Government of India for providing financial support during my doctoral research work.

I express my sincere thanks to all seniors especially to Dr. N.Venkata Ramana, Dr. D. Suresh, Dr. Aurobinda Panda, Dr. T. Ramesh Naik, Mr. K. Janardana Rao, Y. Srinivasa Rao and Mr. V. Jagan for supporting me during the whole period. I extend my sincere thanks to my colleagues Mr. A. Narendra babu, Mr. Naveen Yalla, Mr. Sanjeev Kumar, Mr. Sidhard and Miss. Rinalini lahon for sharing and supporting me during my research work. I will never forget my friends Mr. Pankaj Negi, Mr. O.P.Yadav, Mr. K. Kumaraswami and Mr. K. Raju for keeping me motivated by their caring words and whole hearted supports during the research work.

I would also like to thank all the administrative & technical staff of the Department of Electrical Engineering, Indian Institute of Technology Roorkee, Roorkee for their cooperation and necessary facility provided to me to carry out this research work. My special thanks to Mr. Amir Ahmed who made necessary arrangements during my research work.

I owe a debt of gratitude to my parents, Shri. Deepla and Smt. Krishanmma, my brother Naveen, sister-in law Mangaveni, Sister Umarani and brother-in-law Ramu for their endless support, encouragement, patience and care.

I sincerely acknowledge the ethical support from my father-in-law Shri. Bhagya Naik and mother-in-law Smt. Umarani.

No words can adequately express my deepest gratitude and love to my wife Smt. Madhuri for her unconditional support, encouragement, love and inspiration and always being there during my good and bad times. I express my deepest love to my cute daughter Adhya whose smiling faces always refresh me.

May all praise be to the Almighty, the most beneficent, and the most merciful.

(Kanasottu Anil Naik)

ABSTRACT

Wind energy has recently emerged as one of the most promising and significant sources of renewable energy that is replenishable. Unlike conventional power plants, wind power plants emit no air pollutants or greenhouse gases and therefore, wind energy provides clean and non-polluting form of electricity. Today, more than 341,320 wind turbines are spinning all over the world. However, the growing penetration of wind energy system (WES) into electric network poses significant challenges on a wide range of issues, the major ones are as follows:

a) Variable Wind speed - Wind speed is intermittent and stochastic in nature and the output of wind turbine (WT) is proportional to the cube of the wind speed. This causes the wind generator output power to fluctuate largely for even small changes in wind velocity. The power in the grid determines the frequency at which the grid will operate. When the penetration of WES in the grid is large, the wide power variations may result in significant fluctuations in grid frequency.

b) Transient faults- The induction generator is extremely sensitive to the grid faults as its stator winding is directly connected to the grid. If short-circuit faults occur in the power network, induction type WES tend to drain relevant amount of reactive power potentially causes rotor instability due to voltage collapse. In recent years this has become a major concern as the wind power penetration is increasing in the grid power mix.

(c) Grid code requirement- The grid codes are originally defined keeping in mind with conventional generators. But increasing penetration level of wind generators into power system has pushed wind farm operators to set new grid code requirements for reliable grid operation. During the disturbances, wind generating stations connecting to the grid must satisfy the grid code requirements in order to ensure power system stability and reliable operation.

However, designing a robust controller for effective power smoothing, fault ride through and smooth grid interaction operation subjected to above issues is a challenging task to the control engineers as wind energy system become highly uncertain. In response to these challenges, this thesis mainly proposes a novel control strategy with interval type-2 fuzzy sets, for handling the uncertainties in the network operating conditions. The third dimension membership functions (MFs) and foot-print-of-uncertainty (FOU) offer an additional degree-of-freedom in the controller design to take uncertainties into account. The feasibility of the controller is also investigated in some test cases by developing the real time simulations using OPAL-RT digital simulator.

Therefore, the main focus of the thesis is to investigate the applicability of the interval type-2 fuzzy logic controller (FLC) for fixed speed and variable speed wind energy systems to improve the operational performance under varying wind speed and network faults. The core objectives of the thesis are as follows:

- Transient stability enhancement and power smoothing of WES using type-2 fuzzy logic based pitch-angle controller.
- Stability enhancement of fixed speed wind farm using STATCOM equipped with type-2 fuzzy logic based damping controller.
- Performance analysis of a fixed speed wind farm using unified voltage and pitch-angle control (UVPC) strategy.
- Design and analysis of adaptive type-2 FLC-PI for a variable speed (DFIG) wind energy system.

In general, pitch-angle controller regulates the generator output power when the wind speed exceeds the rated wind turbine speed. Besides, this it can also be employed to stabilize the WES rotor speed during the transient disturbances. In this part of the thesis, therefore, a logical pitch angle controller strategy (in power and speed control modes) has been developed and an interval type-2 fuzzy logic technique is proposed to design the controller. To evaluate the effectiveness of the type-2 fuzzy logic based pitch-angle controller, the simulations have been carried out for severe network faults and fluctuating wind conditions and results are compared with conventional PI and fuzzy logic controller (called as type-1 fuzzy logic controller) that has been reported in the literature. Moreover, some key factors that affect the transient stability of wind generator have also been investigated. The electrical torque as well as mechanical torque versus rotor speed results are obtained under different pitch-angle conditions, and concept of stable and unstable electrical-mechanical equilibrium points are established. This type of investigation is very important to expand the operating limitations of the wind turbine driven induction generator under the severe faults.

The WES has an undesirable characteristic in which its power output varies with wind speed, resulting in fluctuations in the grid frequency and voltage. This part of the work initially employed *exponential moving average* (EMA) concept to generate reference power. Later on, an interval type-2 fuzzy logic based pitch-angle controller is implemented and designed for good reference tracking and therefore, it can smoothen out the WES output power more effectively. Different types of wind speed patterns are employed to validate the effectiveness of the proposed controller. Real time simulations are also developed to show the applicability of the proposed controller using the OPAL-RT digital simulator. The results show that the proposed type-2 fuzzy logic based pitch-angle controller offers better

performance in tracking reference power and hence, it offers good smoothing of output power fluctuations than conventional proportional-integral (PI) and traditional fuzzy logic (type-1) controllers. The performance of the proposed controller is also estimated using power smoothing and energy loss functions in terms of performance indices.

Fixed speed wind farms employing squirrel-cage induction generator still exist in the world with a considerable number due to their advantages. In the event of grid faults, they are extremely sensitive as their stator winding is directly connected to the grid. As for cases in which if the penetration of wind farm is large in the generator mix and therefore, supplying power to the grid have adverse impact on the power system to which they are connected. Therefore, stability of wind farm becomes an important issue and has recently attracted considerable attention. As a preliminary study, this part of the work, therefore, investigates the impact of fault ride-through on the stability of fixed speed wind farm. The effect of fault locations and fault time durations on the stability of fixed speed wind farm are studied for different types of fault such as line-to-ground (LG), double-line-to-ground (LLG) and three-line-to-ground (LLLG) faults. The simulations are then repeated incorporating a static synchronous compensator (STATCOM) to study its contribution to support the wind farm during different fault conditions. The outputs include the affected voltage profile, active and reactive power magnitudes. Later on, an interval type-2 fuzzy logic based damping controller for STATCOM is proposed to contribute an adequate damping characteristic which improves the transient stability of wind integrated power system. In this regard, three different scenarios (STATCOM-without damping controller, STATCOM-with type-1 FLC based damping controller and STATCOM-with type-2 FLC based damping controller) are considered to evaluate the effectiveness of the proposed method by comparative analysis. The simulation results are obtained for different fault cases such as LLLG, LLG and LG. All the simulations are carried out on a test system using MATLAB/Simulink® software.

The increasing penetration of wind energy system into power system has pushed grid operators to set new grid code requirements in order to maintain acceptable and reliable operation of the system. One of the most relevant grid code requirements is low voltage ride-through (LVRT) capability of wind generators. In case, whenever large voltage dip occurs due to severe network disturbances, the wind generators must remain connected, instead of tripping, in order to avoid other sequence of disturbances triggering in the power system. This part of the thesis proposes *Unified Voltage and Pitch-angle Control (UVPC)* strategy for fixed speed wind farm. The focus is put on guaranteeing the grid code compliance (i.e. LVRT) when the wind farm subjected to severe network fault. The UVPC consists of STATCOM voltage control and pitch-angle control loops which are coordinated in order to enhance the

low-voltage ride-through capability of the wind generators thereby, fulfilling the prescribed LVRT grid code requirement. To evaluate the effectiveness of UVPC strategy, different test cases have been considered which are as follows:

(a) System without STATCOM and pitch-angle controller

(b) System with STATCOM only

(c) System with STATCOM as well as pitch-angle control (i.e. UVPC).

The simulation results show that the adoption of STATCOM and pitch-angle controller helps in complying with LVRT requirement so as to ensure the continuous operation of wind turbines.

Moreover, UVPC strategy is also employed and investigated for its applicability in smoothing out the output power and voltage regulation of a fixed-speed wind generator in the partial load region subjected to varying wind speed.

In both conditions (transient fault and varying wind speed) the pitch angle control loop of UVPC has been designed using type-2 fuzzy logic controller, as it offers effective performance than other control technique such as conventional PI and type-1 FLC.

Doubly fed induction generator (DFIG) is very sensitive to voltage variations in the grid, which pose limitations for wind plants during the grid interaction. Handling the disturbances, which cause voltage variations in the grid thereby, affecting DFIG is a major challenge to make it complaint with the modern grid code requirement. This work proposes an advanced interval type-2 fuzzy logic-proportional integral (PI) controller for torque and voltage control loops of rotor-side converter (RSC) of DFIG. The gains of PI controller are determined and tuned by interval type-2 fuzzy logic method according to system operating condition. Thus, the adaptive nature of type-2 fuzzy logic and the robust nature of PI controller combined together, eventually exhibits good steady-state and dynamic responses. The performance of the proposed controller has been evaluated for different operating conditions of DFIG such as severe fault and voltage sag with reference to varying wind speed. A 1.5MW DFIG connected to the grid is modeled using MATLAB/Simulink® and then it exported to OPAL-RT digital simulator for real time simulation. The performance of the proposed controller scheme is verified through a comparative analysis with its traditional fuzzy logic-PI counterpart. The transient analysis of tuned PI gains with interval type-2 fuzzy logic shows the improved performance subjected to disturbances (i.e. three phase short circuit fault and voltage sag) as desired by the grid codes.

CONTENTS

LIST OF FIGURES

LIST OF TABLES

LIST OF SYMBOLS

Symbols	Meaning
A	Type-2 fuzzy set
$\mu_A(x,u)$	Type-2 membership function
x	Primary variable
u	Secondary variable
J_x	Primary membership of x
$\tilde{A}$	Interval type-2 fuzzy set
P_w	Available wind power
ρ	Air-density [kg/m^3]
A_r	Turbine swept area [m^2]
V_w	Wind speed [m/s]
C_p	Power coefficient
λ	Tip speed ratio
β	Pitch angle
P_m	Mechanical power
ω_r	Rotor speed
T_m	Mechanical torque
T_e	Electrical torque
V_S	Stator terminal voltage
E	Air gap magnetic field induction electro-magnetic-field
X_M	Magnetizing reactance
I_M	Exciting current
I_R , I_S	Stator and rotor currents
R_R , R_S	Rotor and stator resistances
ω_{crit}	Critical rotor speed
t_{crit}	Critical time
$\omega_{crit}new$	New critical speed
V_{wR}	Rated wind speed

P_g	Generator power
P_g^{REF}	Generator reference power
$C(s)$	Controller
ε	Error
T_β	First order lag with time constant
V_{wCI}	Cut in wind speed
V_{wCO}	Cut out wind speed
P_{gCMD}^{REF}	Reference power command
P_{WT}	The wind turbine capture power
$c\varepsilon$	Change in error
P_{smooth}	Output power smoothing function
$W_{\max}$	Maximum energy function
η	Efficiency
ω_s	Machine synchronous speed
$V_{pa}, V_{pb}, V_{pc}, i_a, i_b, i_c$	AC three phase voltage and currents
m	The modulation index
ϕ or α	Phase angle of the modulating waveform
V_{dc}	DC bus voltage
L_f	The AC filtering inductor
C_{dc}	DC capacitor of STATCOM
V_{reg}	Voltage regulation function
P_S	Stator active power
P_R	Rotor active power
T_{op}	Optimal torque

LIST OF ABBREVIATIONS

Abbreviations	Meaning
AWEA	American Wind Energy Association
NREL	National Renewable Energy Laboratory
GWEC	Global Wind Energy Council
WECS	Wind energy conversion system
SCIG	Squirrel cage induction generator
IG	Induction generator
DFIG	Doubly-fed induction generator
WRIG	Wound-rotor induction generator
PMSG	Permanent magnet synchronous generator
FRT	Fault ride through
LVRT	Low-voltage ride-through
PCC	Point of common coupling
FSIG	Fixed speed induction generator
WES	Wind energy system
FLC	Fuzzy logic controller
MF	Membership function
BESS	Battery energy storage system
SMES	Superconducting magnetic energy storage
WT	Wind turbine
NN	Neural network
BR	Breaking Resistors
SVC	Static var compensator
STATCOM	Static synchronous compensator
SFCL	Superconducting Fault Current Limiter
FACTS	Flexible AC Transmission system
MATLAB	Matrix laboratory
VSIG	Variable speed induction generator
UVPC	Unified Voltage and Pitch angle Control
EMA	Exponential moving average
RSC	Rotor side converter
OPAL-RT	OPAL Real time simulation laboratory
FOU	Foot print of uncertainty
FLS	Fuzzy logic system

TR	Type reduction
UMF	Upper membership function
LMF	Lower membership function
RTDS	Real time digital simulator
LLLG	Three line to ground fault
LLG	Double line to ground fault
LG	Line to ground fault
VSC	Voltage source converter
CSC	Current source converter
PLL	Phase locked loop
DC	Direct current
AC	Alternate current
CCT	Critical clearing time
MPPT	Maximum power point tracking
GSC	Grid side converter

CHAPTER 1: INTRODUCTION

1.1 Renewable energy

Fossil fuels (e.g. coal, gas and oil) being a major energy producer are recognized nonetheless as a major cause of environmental pollution posing severe challenges to mankind. Moreover, these resources are limited in availability and their production will be at peak in the next few decades. At the same time, nuclear energy development is receiving huge political opposition from various countries. With these compulsions, to address the ever increasing energy demands and draining out of fossil fuels, the research community is striving for use of alternative energy resources. The necessity of bulk energy production combined with the interest in clean technology has resulted in an increased development of power generation using renewable energies [20]. Renewable are highly eco-friendly, resulting in deep reductions in greenhouse gas emission with low cost of required energy.

The sun is the primary source of renewable energy, with some forms also attributed to the earth and moon. The major resources which technically use conversion methods and natural ways of conversion are listed in Table 1.1. Among them, wind energy emerging as one of the

Table 1.1: Sources of renewable energy [155]

Primary source	Medium	Natural conversion	Technical conversion
Sun	Solar energy	Solar radiation	Photovoltaic conversion, Heliothermal conversion
		Heating earth surface and atmosphere	Thermal power units, heat pumps
		Ocean current	Ocean power plant
	Wind	Wave movement	Wave power plant
		Atmospheric airflow	Wind energy conversion
	Water	Precipitation, Melting, Evaporation	Hydro power plants
Earth	Isotopic decay	Geothermal heat	Co-generation plants
	Biomass	Biomass production	Co-generation plants
Moon	Gravitation	Tides	Tidal power plants

most promising and significant renewable energy resource is suitable for bulk energy production, which is replenish-able so no matter how much is used today there will still be the same supply in the future and more.

1.2 Present status of wind energy

Several organizations such as American Wind Energy Association (AWEA), National Renewable Energy Laboratory (NREL), and Global Wind Energy Council (GWEC) are working in the world in the area of wind energy research. According to GWEC, by 2020 wind energy can supply approximately about 12% of the world's total electricity demand. Today, more than 341,320 wind turbines are operating all over the world [47]. Figure 1.1 shows the global annual installed wind capacity worldwide during the period (2001-2016). Figure 1.2 depicts the top five most countries which have installed wind power during the year 2016 itself. Finally, the global cumulative wind power capacity installed from the year 2001 to 2016 is shown in Figure 1.3.

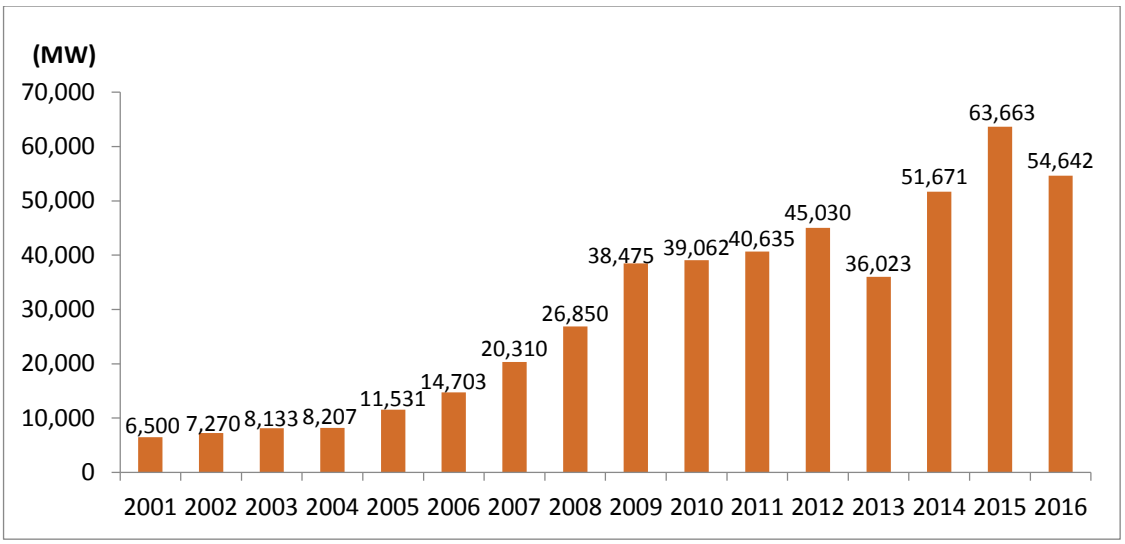

Figure 1.1: Global wind power capacity installed annually (2001-2016) [47]

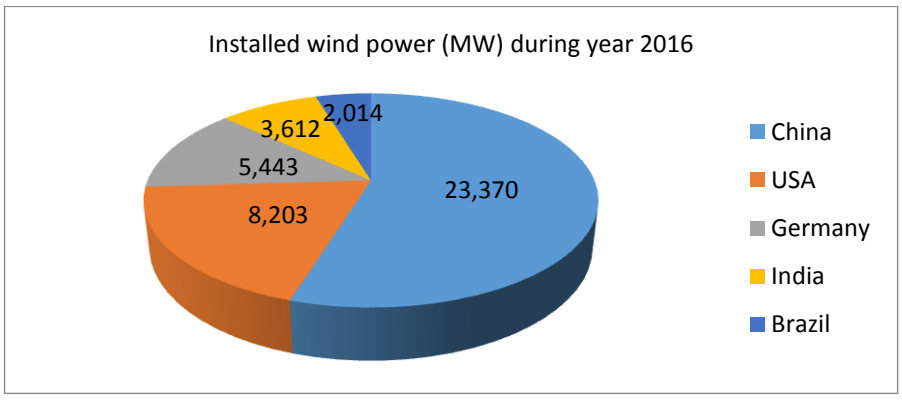

Figure 1.2: The new installed wind power capacity during the year 2016; by top five countries

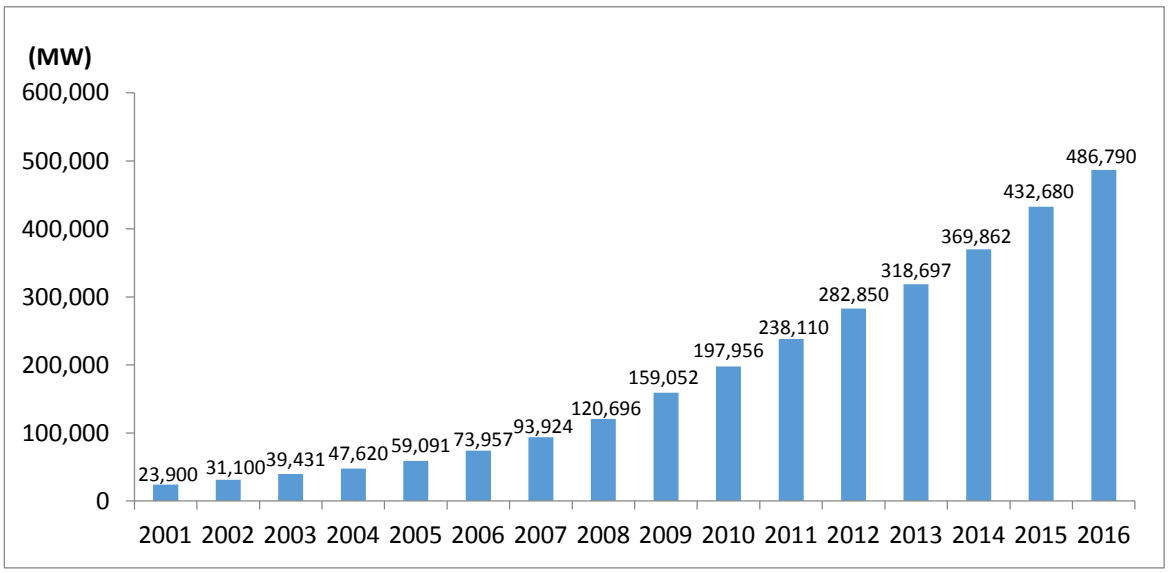

Figure 1.3: Global cumulative installed wind power capacity (2001-2016) [47]

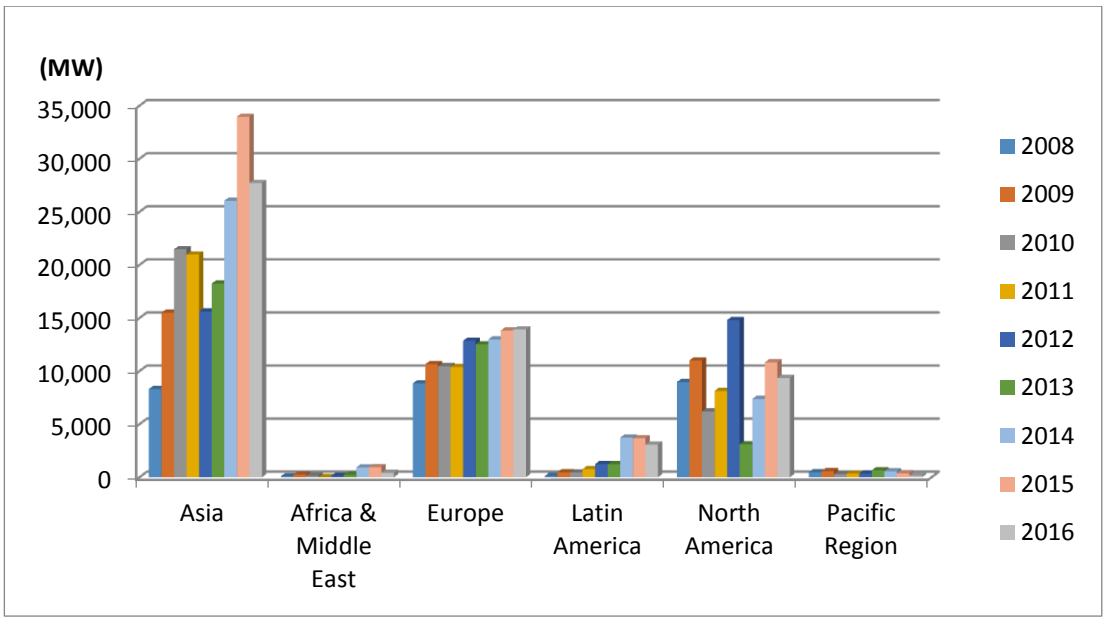

	2008	2009	2010	2011	2012	2013	2014	2015	2016
Asia	8,320	15,507	21,481	20,981	15,624	18,252	26,058	33,962	27,721
Africa & Middle East	96	251	153	8	131	240	934	953	418
Europe	8,851	10,660	10,466	10,393	12,862	12,524	12,988	13,831	13,926
Latin America	128	471	459	771	1,248	1,240	3,744	3,678	3,079
North America	8,969	11,008	6,208	8,137	14,807	3,112	7,382	10,829	9,359
Pacific Region	482	578	294	345	358	655	568	381	140
Total World wide	**28,854**	**38,475**	**39,061**	**40,635**	**45,030**	**36,023**	**51,674**	**63,634**	**54,642**

Figure 1.4: Global cumulative wind power capacity by regions (GWEC, 2008-2016) [47]

Globally, wind power installed capacity has risen exponentially from approximately 23.9GW in 2001 to 486.790GW by 2016 as shown in Figure 1.3. In every five years, the wind power installation has doubled. On 25th April, 2016 in Delhi, GWEC unveiled its flagship publication on "Global Wind Report: Annual Market Update at Wind energy". In 2016, wind power installed across the global market is around 54GW which now comprises more than ninety nations, including twenty nine nations which have now reached the 1,000MW mark, and nine nations with more than 10GW of wind power production. Cumulative capacity increased by 12.6% to reach a total of 486.790GW. Figure 1.4 shows the global cumulative wind capacity by different regions from 2008-2016. Figure 1.5 shows the top five countries contributing percentage of wind power upto the year 2016.

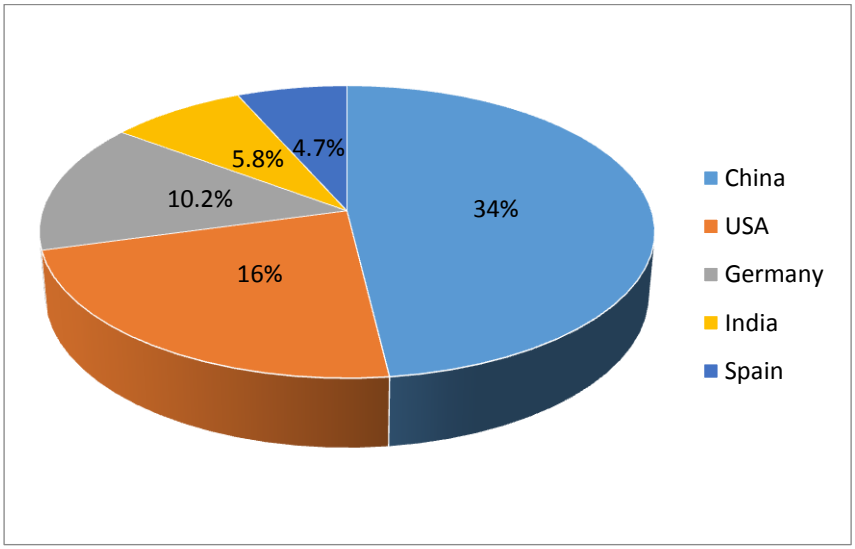

Figure 1.5: Top five countries wind power contribution by the end of 2016

Table 1.2 shows the global wind power installed capacity with different regions (with country wise contribution) by the end of year 2016. The top five most wind energy generating countries are China (168.732GW), USA (82.184GW), Germany (50.018GW), India (28.7GW), and Spain (23.074GW).Wind energy installations are increasing continuously day by day, led by Germany pushed 16%, followed by Cyprus and Spain with well over 20%, Uruguay, Portugal and Ireland around 20%, and Denmark at 40%. Moreover, the markets like Canada, US and China are getting their power from wind by 6%, 5.5% and 4%, respectively. According to five year forecasts seen by the GWEC, the new wind power installations in 2017 is around 60GW and the annual market will rise to about 75GW by 2021, which will bring the global cumulative installed capacity to more than 800GW by the end of 2021.

Table 1.2 Global wind power installed capacity region with country wise by the end of 2016 [47]

GLOBAL INSTALLED WIND POWER CAPACITY (MW)-REGIONAL DISTRIBUTION				
		End 2015	New 2016	Total 2016
AFRICA & MIDDLE EAST	Jordan	119	-	119
	Tunisia	245	-	245
	Ethiopia	324	-	324
	Morocco	787	-	787
	Egypt	810	-	810
	South Africa	1,053	418	1,471
	Other	150	-	150
	Total	**3,488**	**418**	**3,906**
ASIA	Philippines	216	-	216
	Thailand	223	-	223
	Pakistan	308	282	590
	Taiwan	647	35	682
	South Korea	835	201	1,031
	Japan	3,038	196	3,234
	India	25,088	3,612	28,700
	PR China	145,362	23,370	168,732
	Others	253	25	276
	Total	**175,970**	**27,721**	**203,685**
EUROPE	Belgium	2,218	177	2,386
	Austria	2,404	228	2,632
	Ireland	2,446	384	3,830
	Romania	2,976	52	3,028
	Netherlands	3,443	887	4,328
	Denmark	5,064	220	5,228
	Portugal	5,050	268	5,316
	Poland	5,100	682	5,782
	Turkey	4,694	1,387	6,081
	Sweden	6,029	493	6,520
	Italy	8,975	282	9,257
	France	10,505	1,561	12,066
	UK	13,809	736	14,543
	Spain	23,025	49	23,074
	Germany	44,941	5,443	50,018
	Rest of Europe	7,220	1,077	8,241
	Total Europe	**147,899**	**13,926**	**161,330**
LATIN AMERICA & CARIBBEAN	Caribbean	164	-	164
	Dominican Republic	86	50	135
	Honduras	176	-	176
	Peru	148	93	241
	Panama	270	-	270
	Costa Rica	278	20	298
	Argentina	279	-	279
	Uruguay	845	365	1,210
	Chile	911	513	1,424
	Brazil	8,726	2,014	10,740
	Others	335	24	359
	Total	**12,218**	**3,079**	**15,296**
NORTH AMERICA	Mexico	3,073	454	3,527
	Canada	11,219	702	11,900
	USA	73,991	8,203	82,184
	Total	**88,283**	**9,359**	**97,611**
PACIFIC REGION	New Zealand	623	-	623
	Australia	4,187	140	4,327
	Pacific Islands	13	-	13
	Total	**4,823**	**140**	**4,963**
	World wide	**432,680**	**54,642**	**486,790**

1.3 Wind energy systems configurations

The wind energy conversion system (WECS) consists of two main electrical components, namely, a generator and a power converter. Therefore, by combining these two components and with their different designs, WECS configuration can be classified into three different groups [16]: (1) fixed-speed WECS without power converter interface, (2) variable-speed WECS with reduced-capacity converters and (3) variable-speed WECS with full-capacity converter interface [18].

1.3.1 Fixed-speed WECS without power converter

A typical configuration of fixed-speed WECS without a power converter interface is depicted in Figure 1.6, where a generator is directly connected to the 50Hz or 60Hz utility grid. This type of WECS employs a squirrel-cage induction generator (SCIG), and its rotor speed is computed by number of pair of poles in the generator and the grid frequency. The operating range of generator speed varies within 1 to 2 percentages for different values of wind speed. As the variation of generator speed is very small and the system is often called as fixed-speed wind energy conversion system [177].

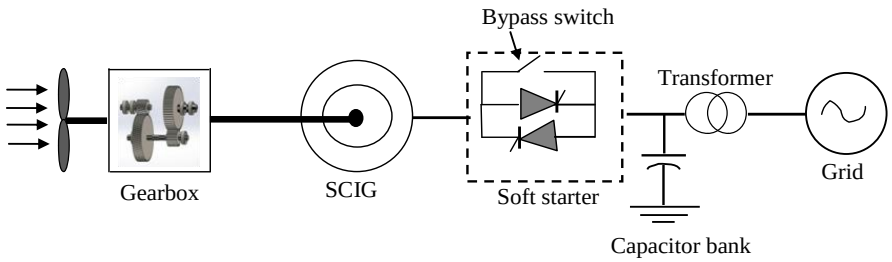

Figure 1.6**:** Fixed speed WECS configuration

Here, a gearbox is employed between the rotor of the wind turbine and the rotor of the generator in order to match the speed difference between the generator and turbine. This type of configuration incorporates soft starter in order to limit the high inrush current during system start-up, later on, it is bypassed with a switch once the system is started [136]. At the generator terminal a capacitor bank is connected to provide necessary amount of reactive power consumed by the SCIG to maintain the power factor at reasonable value.

The main features of this type of WECS are: low maintenance cost, more reliable, robust and very good for low energy yields [4, 12, 13, 30]. The disadvantages are: the generator output power fluctuates with wind speed variations cause the grid frequency disturbances, moreover, this type of WECS delivers the rated power to the grid at a given wind speed, but

for other wind speeds it produce low energy conversion efficiency. In spite of its drawbacks, this WECS is still widely accepted in industry with a power rating up to a couple of megawatts [69].

1.3.2 Variable-speed WECS with reduced-capacity converters

After the use of power electronic converters in the WECS, the whole scenario of wind power generation has significantly changed. Variable speed concept has numerous merits compared to fixed-speed WECS [32, 56, 92, 111]. In case of variable speed WECS by changing the speed of wind turbine one is able to store the variable incoming wind power as rotational energy. Therefore, it provides more energy production with less stress on the mechanical structure and leads to reduction in wear and tear on the bearings and gearbox; and also increases the life cycle of them. The rotational speed of the generator is decoupled from the grid frequency; hence, the rotor can be operating with variable speed adjusted to actual speed situation. The application of power electronic converter in the WECS decouples the generator from the grid, which enables the active and reactive power control [110].

Based on the converter capacity with respect to total system capacity the variable-speed wind energy conversion system is further classified into two types; full-capacity power converter and reduced-capacity power converter. The variable-speed WECS with reduced capacity converter employs the doubly-fed induction generator (DFIG) and wound-rotor induction generator (WRIG). Further, WRIG possess two designs configurations: one with a four-quadrant power converter system, and the other with a converter-controlled variable resistance [19].

A typical configuration of the WRIG-WECS with a variable resistance in the circuit is shown in Figure 1.7. In this configuration, the external rotor resistance is controlled by means of a power electronic converter which is mounted on therotor shaft itself. Hence, it is possible to adjust the speed range typically at about 10% above the synchronous speed of the generator [21]. This system captures more power from the wind due to variable operation, but it incurs power losses due to rotor resistance. This system also requires a capacitor bank and a soft starter for reactive power compensation and generator start-up, respectively.

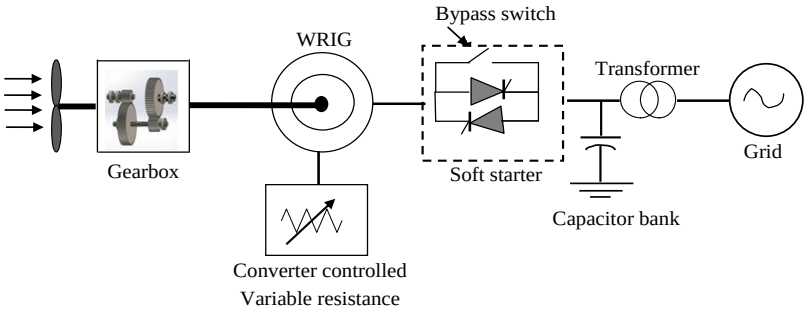

Figure 1.7: Variable-speed WECS configuration with variable rotor resistance

Therefore, the alternative configuration of DFIG based WECS system is shown as in Figure 1.8. In this type of configuration, the generator rotor is connected to the grid through a back-to-back converter and stator is directly connected to the grid. The converter employed in this system processes only the slip power which is approximately 30% of the rated power of the generator. This results in reduced converter cost over wind energy system using full converter capacity [14]. This concept is mainly motivated by two reasons:

- Less expensive configuration due to low rated power electronic converter as compared to the full rated and
- Variable speed operation over a wide speed range.

Here, the DFIG based WECS operating modes can be classified into two types with respect to rotor speed: (1) super-synchronous mode - in which the generator operates with above synchronous speed and the converter injects energy back to the grid; and (2) sub-synchronous mode - in which the generator operates with below synchronous speed and the converter draws energy from the grid.

The net power flow from the overall WECS to the grid is always positive. At the above rated wind speed, the mechanical power is reduced by changing the pitch angle of the blades.

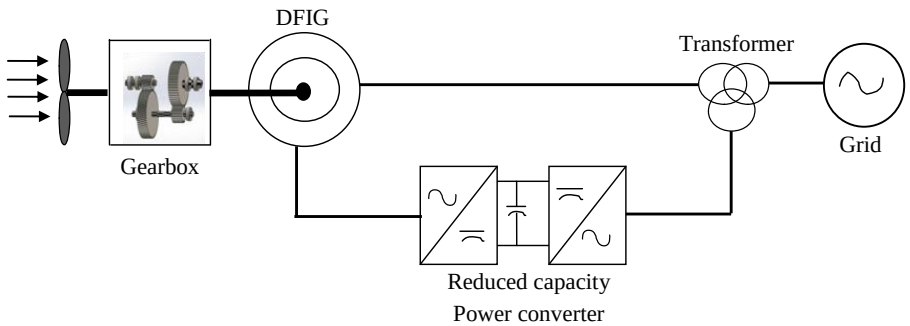

Figure 1.8: Variable-speed configuration with reduced-capacity converters

1.3.3 Variable-speed WECS with full-capacity power converters

Figure 1.9 shows another configuration for the variable speed WECS where the generator is connected to the grid through a full-capacity converter system [177]. This type of configuration utilize generators such as wound-rotor synchronous generator (WRSG), permanent magnet synchronous generator (PMSG) and squirrel-cage induction generator, upto several megawatts. The converter power rating is same as that of the generator power rating. The total turbine power goes through the converter that converts varying generator frequency (due to the variable wind speed) into a constant grid frequency. Therefore, with the help of converter, the generator is fully decoupled from the grid and can be operated in the full speed range by making use of the converter. Moreover, the converter also provides reactive power compensation and smooth grid interaction.

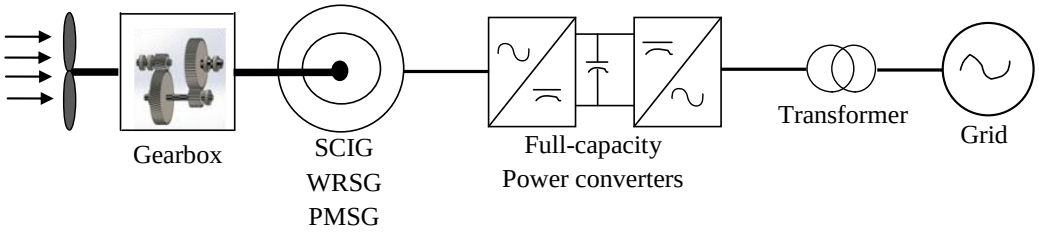

Figure 1.9: Variable-speed configurations with full-capacity converters

The main limitation of this configuration is more complexity and cost. The use of full rated power converter between the generator and grid results in extra losses in the power conversion. Besides, it will again add to the cost and technical issues such as power quality problem. It is observed that this configuration can also operate without a gearbox if the synchronous generator employed is designed for low-speeds with a large number of poles. Avoiding of gearbox can improve the efficiency and reduce maintenance and initial costs. But, a low-speed generator consists of large number of poles where it substantially requires larger diameter to accommodate these poles on the perimeter and therefore, results in increased generator fabrication and installation costs.

1.4 Grid integration issues of wind energy system (WES)

To successfully integrate a wind energy system into the grid, the major issues [8, 15] which need to be addressed are as follows:

- Transient stability
- Power, frequency and voltage fluctuations (due to wind speed variation)
- Grid code requirements

1.4.1 Transient stability

To understand the transient stability issue of a WES, let us consider a grid-integrated wind energy system. When a fault (temporary or transient fault) occurs in the connected power grid, the rotor speed of the wind generator becomes very high (as electrical torque decreases while mechanical torque remains constant due to wind flow) and as a result, active power output depressed to very low value, and terminal voltage collapses or drops to a low value. If this voltage drop condition continues, it may cause wind turbine rotor to accelerate and make rotor speed unstable and finally the WES may get disconnected from the grid. But, with increasing penetration of wind energy, the power system need that the WES must be able to stay connected (ride-through) to the transient faults and thus, contribute to the important system services such as momentary reserves and short circuit capacity during faults. In other words, the wind generator should have good fault ride-through (FRT) capability. This clearly indicates that wind generator stabilization is necessary during the network faults.

1.4.2 Power, frequency and voltage fluctuations (due to wind speed variation)

Wind speed is intermittent as well as stochastic in nature. So, as the wind speed varies, the output power of wind generator fluctuates (as wind turbine output power is proportional to the cube of the wind speed), resulting in fluctuations in frequency and terminal voltage. In other words, power quality of the wind generator deteriorates [62, 64] and it is becoming major concern as the wind power installations are increasing in number. Thus, grid voltage, frequency, and transmission line power should be maintained constant. To this end, some control means are necessary [6, 7, 63].

1.4.3 Grid code requirements

With the increasing penetration of wind generators in a power system, it is necessary to operate wind farms as much as like synchronous generator plants to support the grid frequency and voltage during the network disturbances as well as during steady-state conditions. This requirement leads many countries to develop and establish a new grid codes for wind farms' operation in the power grid. Generally, grid code incorporates all technical aspects relating to connection, operation and power transmission. It lays down the rules that define the ways that the generating stations connecting to the system must operate so as to maintain grid stability. The objective of grid codes is to ensure that the increased penetration of wind power does not compromise the security, reliability and power quality of the electric power system [159].

Although, the grid code technical requirements change from system to system, the typical requirements for the generators normally concern tolerance, power quality, protective devices, and control of active and reactive power. The manufactures of wind turbine, therefore, must include these grid code requirements and to meet these requirements, research has been conducted to develop solutions and technologies. The typical grid code requirements for grid connection and operation of wind turbines are summarized as follows:

1. *Voltage range:* The wind turbines are required to operate within the acceptable grid voltage variations.
2. *Frequency range:* The wind turbines are required to operate within typical grid frequency variations [127].
3. *Active power control:* Active power control is another requirement of grid code to ensure frequency stability of the system.
4. *Frequency control:* In this grid code requirement, the wind farm needs to provide frequency regulation capability in order to maintain the desired grid frequency.
5. *Voltage control:* Wind turbines are required to control their terminal voltage to a constant value by using a voltage regulator.
6. *Reactive power control:* In this grid code requirement, the reactive power and power factor must be maintained in the desired range for which wind farms need dynamic reactive power control.
7. *Low-voltage ride-through (LVRT):* In this grid code condition, the wind turbine must remain connected to the power grid for specific time duration before being allowed to disconnect whenever, it subjected to voltage drop or faults at its point-of-common-coupling (PCC). In addition, some utilities require that wind turbine must help support grid voltage during faults.

Grid code regulations and requirements, significantly, change from systems to system and from country to country. In certain regions, the grid codes may cover only a part of these requirements. The differences in grid code requirements are caused by different degrees of power network robustness and by different wind power penetrations. Figure 1.10 shows typical LVRT requirements for the different countries [83].

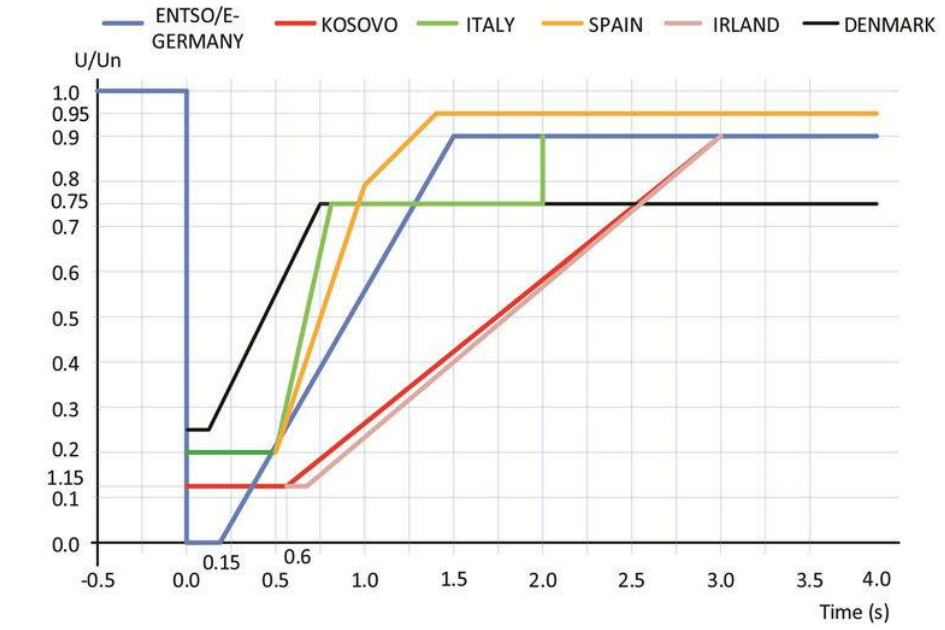

Figure 1.10: Low voltage ride through (LVRT) requirement for various grid codes

In general, LVRT can be defined as "the maximum voltage drop (either in terms of magnitude or in terms of time) for which a wind turbine is able to withstand without suffering from rotor speed instability". The fault ride-through characteristic specified by the Germany grid operator for the wind turbine is as shown in Figure 1.11. According to this grid code requirement, a FSIG is expected to ride-through zero voltage (at the PCC) for 0.15s due to solid fault, but once the fault is cleared, the connection point voltage must recover to 90% of its nominal value within 1.5s from the occurrence of fault.

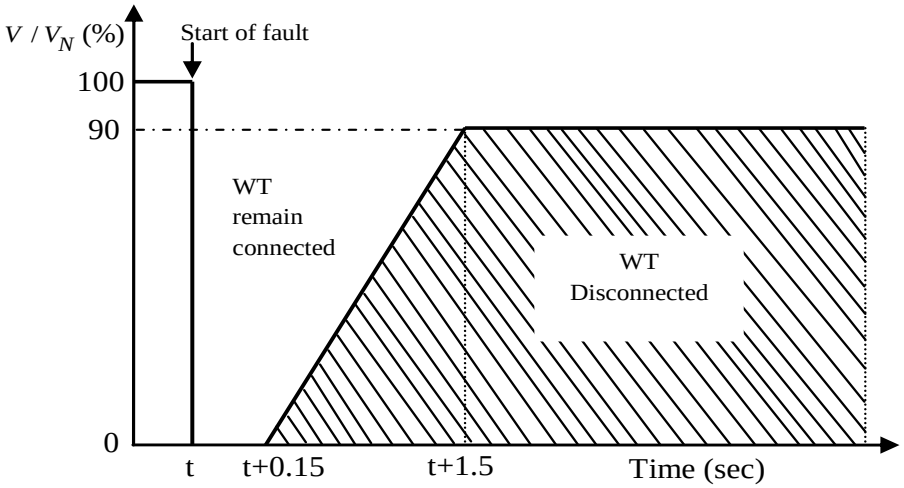

Figure 1.11: Fault ride-through characteristic specified by the Germany grid operator

1.5 Research background

There exist two types of wind turbine generator systems which are commercially available – Fixed-speed and variable-speed WESs. In the early stage of wind energy market, the most of wind power systems were employed with fixed speed induction generators (FSIGs) and, still exist due to their low cost, low maintenance and robustness. At present, 20% of the installed wind power is still being produced by Squirrel Cage Induction Generator (SCIG) based fixed speed WES. Respectively, in Australia, Germany and Denmark about 87MW, 48MW and 47.1MW of installed wind turbines (rated 1.5MW) are SCIG based wind turbines [163]. Among the many variable concepts, Doubly-Fed Induction Generator (DFIG) based variable speed WES has become most popular nowadays as the converter rating can be kept fairly low (approximately 25% of the total machine power). Currently, DFIG based WES occupies close to 50% among the total wind power generation. Due to its clean technology, the whole world shows interest towards the wind energy generation, consequently, in the very near future huge amount of wind energy systems are going to be installed. Therefore, it is necessary to investigate the performance of wind energy systems subjected to the disturbances such as wind speed variations and network faults which cause grid integration issues.

The pitch-angle controller is generally used to limit the aerodynamic power to its rated value [141] when the wind speed crosses the above rated wind speed. In some previous work [42, 70, 76, 103, 104, 131, 138, 143, 171], different methods have been proposed to design the pitch control system to regulate the generator output power at rated level and improved the output power quality with frequent wind speed changes. Beside this, pitch-angle controller is also employed to stabilize the WES during transient faults [28, 29]. Therefore, it is important to carry out the transient stability analysis so as to investigate the impact of WES into utility grid. In this regard, some of the researchers have designed rotor speed control based pitch-angle controller to enhance the transient stability [10, 112, 151, 161, 176]. In the above works - in [42, 70, 76, 103, 104, 131, 138, 171], they designed pitch angle controller for above rated wind speed where it regulate the generator output power to its rated value, and in [10, 112, 151,161, 176], they investigated the pitch angle controller for transient stability enhancement. However, none of them suggested use of the pitch-angle controller for both purposes (i.e. maintaining the power output at its rated value for above rated wind speed and transient-stability during network faults). Therefore, references [35, 36, 113, 114], have designed pitch-angle control strategy to improve the power quality and transient stability using traditional fuzzy logic controller (called as Type-1 FLC). Fuzzy logic based pitch-angle controller is best suited as it provides improved performance in tracking reference, in comparison to other

controllers. In general, based on expert knowledge and experience, membership functions (MFs) are defined and fuzzy rules are framed, accordingly. Once the MFs have been defined for designing the FLC, the uncertainties in actual degree of MFs cannot be modelled or account for. As a result, the controller (FLC) may not be robust for all types of operating conditions. Therefore, there is a need to look for the new methodology to model the uncertainties in the MFs. Moreover, the effort was made in the past [46] on stability enhancement of wind turbine driven induction generators assuming the mechanical torque constant during and after the fault which may not be accurate as the mechanical torque depends on the power coefficient and pitch angle of wind turbine system. Therefore, the accurate mechanical torque versus rotor speed characteristic required to be achieved and how these can be improved by pitch angle controller, needs to be investigated.

The next issue is power smoothing of wind energy system using a pitch angle controller. Though wind energy is considered to be very prospective source of power generation, randomly varying wind speed causes wind power to fluctuate which is still a serious issue for power grids, especially for fixed speed WESs. Depending on the wind condition, the wind power fluctuations usually occur on the timescale of a few seconds to several hours. But in case of wind farm, these power fluctuations are smaller as compared to a single WES. However, for isolated systems or future energy system with huge penetration of WESs, it is important to draw attention towards wind power smoothing. Many researchers have focused their attention and provided new methods for smoothing the power fluctuations of a wind power system. In [44], smoothing the output power of wind farm has been employed using fly-wheel energy storage system, but it involves a complicated control approach. In [60, 115], power storage system is studied for smoothing the output power of the WES. Though, this method is very effective when the power quality is targeted, but economically not feasible. In [68, 86], a battery energy storage system (BESS) is employed to mitigate the wind power fluctuations. However, BESS involve issues like chemical process, short life and slow response. The superconducting magnetic energy storage (SMES), for their fast response and efficiency, is best choice for wind energy system [149, 189]. However, with huge operating cost involved, its application is still critical from a practical point-of-view. On the other hand, the WT equipped with pitch-angle controller has become very popular method for smoothing the output power fluctuations. Various techniques like H-∞ controller [140], adaptive control [139], and predictive control [146] have been proposed for output power smoothing to ensure that the generated output power follows a command value determined by the moving average. The main limitations of these controllers are that H-∞ controllers are monolithic and their complexity/order tends to be very high as compared to other controllers, the adaptive

controller requires a model formation in order to design the controller, and in the case of predictive controller, there is no industrial development due to implementation issues. Therefore, intelligent control techniques such as fuzzy-logic controller (FLC) and fuzzy-NN are being implemented in WT pitch-angle controller [35, 114, 128, 147]. These modern techniques have numerous advantages as they do not require the mathematical model of the system and are capable of handling non-linearity. But, neural network algorithms are complicated and require more intensive computation due to online training of the system parameters. Therefore, in recent studies [26, 71], fuzzy logic controller (called as type-1 FLC) based pitch-angle controller is best suited as it provides improved performance in tracking reference in comparison to other controllers but, it has limitations such as uncertainties in the rules and MFs cannot be accounted for. Therefore, an improved and appropriate control technique needs to be adopted.

In case of fixed-speed wind farms, the reactive power compensation is a major problem [142] in both, transient and steady-state operating conditions. Usually, a capacitor is connected to the low voltage terminal of the wind turbine generator to provide the required amount of reactive power during the normal operating condition. But, it fails (under severe faults conditions) to supply adequate reactive power demanded by the WES leading to stability issue. Therefore, various studies have been reported for stability improvement of fixed speed wind farms. Usually, a pitch-angle controller is employed to limit the aerodynamic power at rated level which in addition, can also improve the transient stability of the wind generator [114, 164]. According to some reports, Breaking Resistors (BR) can be employed for stabilization of induction generator [22, 41, 43]. References [2, 162] employed SVC for voltage support and for transient stability improvement by providing sufficient reactive power to the generator during its acceleration. However, STATCOM performs better than the SVC for a given contingency if the same rating devices are assumed [108]. Recently, Superconducting Magnetic Energy System (SMES) has also been employed for grid connected wind generator stabilization [150]. Moreover, in the event of faults, the Superconducting Fault Current Limiter (SFCL) can suppress short-circuit current thereby, it can improve transient stability of induction generator [123]. Table 1.3 provides the comparative analysis of wind generator stabilization methods discussed above. However, in all aspects (principle functions), STATCOM suits well for fixed-speed wind farm, in comparison to other methods. Therefore, in recent time STATCOM has been employed to enhance the transient stability of induction generator [37, 134, 137,157, 174] by recovering the voltage effectively.

Table 1.3: Comparative analysis of all fixed speed wind farm stabilization techniques

Principle functions	Pitch angle control (PAC)	Breaking resistor (BR)	SVC	STATCOM	SMES	SFCL
Control of both active and reactive power	Able to control only active power	Consume and dissipates only active power	Can only controls reactive power	Only controls reactive power	Active and reactive power can be controlled	Control active power
Voltage and active power fluctuations minimization	Minimize only active power fluctuations	Not able to minimize the voltage and active power fluctuations	Minimize only voltage fluctuations	Minimize voltage fluctuations better than SVC	Can minimize the fluctuations in voltage and active power	Not able to minimize the voltage and active power fluctuations
Complexity of controller	Little complex than BR	Simplest	More complex than PAC	Complex than SVC	Most complex	More complex than BR
Enhancement of transient stability during successful reclosing	Stabilize the overall system, but slower than the BR, SVC and STATCOM	Stabilize overall system	Stabilize overall system	Stabilize overall system and effective	Most effectively stabilize the overall system	Effectively stabilize the overall system
Enhancement of transient stability during unsuccessful reclosing	Cannot stabilize the conventional generator, but stabilize the wind generator	Stabilize overall system	Stabilize overall system	Stabilize overall system and effective	Most effectively stabilize the overall system	Cannot stabilize the wind generator
Cost of manufacturing	Economical	Expensive than PAC	Expensive than BR	Costlier than SVC	Most Costly	Costly

"The ability of a wind farm to stay connected during disturbance is important to avoid the time of reconnection process, which need from 4 to 5 minutes and also to avoid cascading disturbance due to lack of generation" [89]. Therefore, it is needed to investigate the responses of FSIG-wind farm during the faults and possible impacts on the system stability, in order to handle the faults without disconnecting the wind farm from power network. In this

trend, literature [89] has done interesting work in which, different types of faults were considered and their impact on the stability of FSIG-wind farm has been investigated. This approach has a prominent importance so as to explore and extend the operating limitations of wind farm, in order to, stay connected to the grid during the faults. However, the analysis reported by authors [89] has not been completely explored (they have only considered limited types of faults) for the stability analysis of wind farms and hence, a partial solution is presented.

Moreover, FSIG-wind farm extremely sensitive to network faults as its stator winding is directly connected to power grid leads to wind farm power fluctuations. These inherent power fluctuations have adverse impacts on the power system to which wind-farm connected. Much of the literature addressed the stability enhancement of wind farm using STATCOM [37, 134, 137,157, 174]. However, STATCOM with damping controller exhibits better transient response [193]. Therefore, in recent study STATCOM with damping controller strategy is proposed to improve the transient stability of wind power system by damp the power oscillations [124, 169, 193], where the damping controller is designed using different control techniques such as fuzzy-logic, Neuro-fuzzy and PID-fuzzy. However, these control techniques have limitations such as uncertainties in the rules and MFs as they incorporating type-1 fuzzy logic. Therefore, need to look for the appropriate control technique for damping controller of the STATCOM in order to improve the transient stability of wind power system.

The grid codes are originally defined keeping in mind conventional generators. But increasing penetration level of wind energy into power system has forced wind farm operators to set new grid code requirements, in order to ensure the security of power system. Different countries have the different grid codes, and the performance behaviour of wind turbines are monitored. For the wind turbines, the network grid codes have incorporated the requirements such as power quality, voltage control, LVRT and protection related requirements. During contingencies, a critical issue that arises in the power system is voltage collapse, due to weak support of reactive power. Closely related to this issue is - low voltage ride through (LVRT) of wind energy systems, which is the most important requirement, incorporated in the grid codes. Therefore, for ride-through severe faults, these wind farms need dynamic reactive power support.

In order to provide adequate amount of reactive power to the induction generators, the power compensator devices such as FACTS are employed consequently, they can enhance the rotor stability margin or increases the critical clearing time of fault. Therefore, in recent time STATCOM has been employed for reactive power compensation of induction generators [34,

122, 153, 158]. In addition, it can also improve the transient stability of the wind generator by reducing the mechanical torque with suitable pitch-angle generation as discussed above [10, 112, 151, 161, 176]. In the above literature, some of them [34, 122, 153, 158] proposed STATCOM to improve wind generator stability and some [10, 112, 151, 161, 176] employed pitch-angle controller as it can control the mechanical torque and thus, enhances the transient stability of IG. But the effectiveness of the simultaneous control of STATCOM and pitch-angle controller was not explored. In [23], though the unified voltage source inverter (VSI) and pitch-angle control has been proposed to reach effective voltage control and the generator rotor speed stability, but the study did not evaluate the effect of transient fault condition which is a severe concern to the fixed-speed induction generators. A STATCOM and pitch-angle control [57, 192] is proposed to improve LVRT capability of wind farm subjected to three-phase-to-ground fault. The idea of mixing electrical (e.g. STATCOM) and mechanical (e.g. pitch control system) parts seems to be interesting. But, it does not provide the coordination control of STATCOM in combination with pitch-angle controller for successful LVRT.

Moreover, the reactive power absorption by the induction generator is coupled with its active power generation, thus any variation of wind speed also causes fluctuations in the reactive power requirement of the generator. These fluctuating active and reactive power interactions with power network leads to fluctuations in the grid voltage and frequency [75]. The main purpose of STATCOM connected at the wind farms is to improve the transient stability as well as fault ride-through capability but in addition, it is well suited for reducing voltage fluctuations at the generator terminal due to wind speed variations and thus, providing voltage flicker mitigation at the wind farm connection point. In this regard, a lot of research work on STATCOM with wind energy systems has been reported [39, 109, 116, 132, 165, 175, 180]. Since the classical STATCOM are operated in lagging and leading mode, its role in the wind power system is limited to reactive power support. As a result, since it does not have an active power control capability, the wind generator output power fluctuations due to wind speed variations cannot be smoothen out by using STATCOM only. On the other hand, STATCOM with the pitch-angle controller is the best choice for controlling the active and reactive power of the wind farm. Although studies made in the past employed the simultaneous control of STATCOM and pitch-angle control to enhance the wind farm low voltage ride-through capability when subjected to network faults [57, 192], they have not been explored in respect of wind speed variations, due to which the output power and voltage of the wind generator fluctuates.

The variable speed wind energy systems (especially using DFIG) have become more popular as DFIG has decoupled active and reactive power controls. However, the DFIG is sensitive to voltage variations which were caused by the disturbances such as load changes, network faults and wind speed variations. The voltage dip occurs at the generator connection point due to grid faults resulting in the stator current to increase. As there is a magnetic coupling between the rotor and stator circuits, the stator current reflects in the rotor circuit which may damage the rotor side converter [51]. When the penetration levels of wind farms are very high, the large voltage drops occurring during the network disturbances, such as short circuit faults, may trigger a sequence of other events in the power network. Moreover, after the fault is cleared, the oscillations (voltage and power/frequency) in the power network are also matter of concerns. The wind farms in general located far from the demand centres, where they operated with low short circuit levels known as weak grid. Therefore, the uncertain wind speed causes generator output to fluctuate which poses another challenge to maintain the steady-state voltage levels. In order to operate the grid reliably and keeping it stable, the WES must stay connected and withstand the network disturbances which are transient in nature and successfully eliminated. The recent grid code also demands LVRT capability from the wind farms for power transfer to the grid.

In the existing literature, various control schemes are proposed for variable speed induction generators (VSIGs) for grid operation [1, 166] after their integration in the grid. For their reliable grid operation, the converters are controlled by direct power and direct torque techniques with the objectives of supplying adequate active power together with the reactive power, and electromagnetic torque together with rotor flux, respectively [11, 24, 144]. Meanwhile, the vector control schemes are employed to control the electromagnetic torque and excitation current, independently [9, 59]. Compared to vector control, the direct control (torque and power) may have advantages such as robust, easy-implementation and fast response, but they cause fluctuations in the generator current, flux and electromagnetic torque, as their switching frequency is not fixed, resulting in reduction in gearbox reliability [166, 191]. Therefore, the vector control is more widely employed in industrial applications. Most of these control schemes are employing PI controllers to access the references from stator and rotor variables. The performance of the above techniques greatly depends on tuning of PI controller gains, since the plant is highly nonlinear with uncertainties in operating conditions. For determined operating point, the fixed gain of PI controller provides an acceptable steady-state performance, but poor transient performance is often obtained when the converter operating point varies continuously due to changing of plant dynamics. Moreover, grid

specifications such as grid frequency and voltage might change during the converter operation [117]. Therefore, the performance of the linear controllers (PIs) with fixed gains is limited.

Moreover for severe disturbances, such as short circuit faults and wind speed variations, with the fixed gains PI controller does not predict the system behaviour correctly. Therefore, converter control schemes with adaptive nature must be used in these applications to overcome the limitations of PI controllers. The most popular adaptive method employed in the literature is fuzzy logic controller (FLC) which exhibits superior performance subjected to the plant disturbances [129]. Recent studies show tuning of gains of PI controller using fuzzy logic method is of paramount importance as it improves dynamic and steady-state performance of the system [52, 90, 154, 170]. Fuzzy-PI controller is obtained by combining the adaptive and detached natures of the FLC and fast response characteristics of PI controller. In this method, FLC determine the gains of the PI controller according the system operating conditions.

Since the operating condition of WES is variable with grid disturbances or wind speed changes, the adaptive controller (Fuzzy-PI) is most suited for converter control to improve the performance of the wind energy system. In this regard, converter control schemes are switching towards the fuzzy-PI controller [50, 87, 145] so as to obtain better dynamic response and good stability, resulting in fulfilling the grid code requirement. However, traditional fuzzy logic technique does not fully handle the high level of uncertainties which exists in the DFIG based WES, since fuzzy logic method itself incorporates uncertainties in the rules. Therefore, there is a need to evolve new methodology which will improve performance of the fuzzy-PI controller.

1.6 Objectives of the thesis and author's contribution

In the renewable energy sector, electric power generation from the wind has emerged as one of the most successful program. It has started making meaningful contributions to the overall power requirements in India and worldwide. However, the growing penetration of WES equipped with fixed-speed and variable-speed systems in electric network pose significant challenges on a wide range of issues, namely, wind speed disturbances and network fault disturbances. From the gaps in the literature review, the following objectives have been suggested for the present work.

- *Transient stability improvement of a WES using pitch-angle controller*

  In general, pitch-angle controller regulates the generator output power when the wind speed exceeds the rated wind speed. Besides, this it can also be employed to stabilize the WES rotor speed during the transient disturbances. Therefore, in this thesis, a logical pitch-angle controller strategy (in power and speed control modes) has been developed and an interval type-2 fuzzy logic method is proposed to design the controller. In order to verify the effectiveness of the Type-2 fuzzy logic based pitch-angle controller, the simulations have been carried out for different cases such as severe network faults and fluctuating wind conditions and results are compared with proportional-integral (PI) controller and traditional fuzzy logic controller (called as type-1 fuzzy logic method).

  Moreover, in this, some key factors that affect the transient stability have been investigated by deriving steady-state equivalent model of the induction generator. The electrical torque and mechanical torque versus rotor speed results are obtained under different pitch-angle conditions and concept of stable and unstable electrical-mechanical equilibrium points is established. This type of investigation is very important to expand the operating limitations of the wind turbine driven induction generator under the severe faults to guarantee the wind farm connection to the grid.

- *Output power smoothing of WES using pitch-angle controller*

  In the previous objective, pitch-angle controller is employed to stabilize the WES, but in this case, pitch-angle controller is employed to smoothing out the wind generator output power when it subjected to wind speed variations. An exponential moving average (EMA) concept has been implemented and incorporated to the pitch-angle controller to generate reference power. Later on, type-2 fuzzy logic equipped with EMA incorporated pitch-angle controller is implemented and designed for good reference tracking and therefore, it achieves good output power smoothing. Controller performance is evaluated by developing real-time simulations using OPAL-RT digital simulator. Different types of wind speed patterns are employed to validate the effectiveness of the proposed controller. Moreover, the performance indices of the proposed controller have also been estimated by using power smoothing and energy loss functions.

- *Fixed-speed wind farm stabilization using static synchronous compensator (STATCOM)*

  In this objective, at first, a 36MW fixed-speed wind farm exporting power to 120kV grid has been designed using MATLAB/SIMULINK®. Thereafter, a static synchronous compensator (STATCOM) model has been developed, designed and employed to support the studied wind farm. As a preliminary study, this part of the work, therefore, investigates the impact of the fault ride-through on the stability of fixed speed wind farm. The effect of fault locations and fault time durations on the stability of fixed speed wind farm are studied, subjected to different types of faults such as line to ground (LG), double line to ground (LLG) and three line to ground (LLLG). The simulations are then repeated incorporating a static synchronous compensator (STATCOM). The outputs include the affected voltage profile, active and reactive power magnitudes. Later on, an interval type-2 fuzzy logic based damping controller for STATCOM is proposed to achieve damping improvement, and thus enhances the stability of wind integrated power system. To evaluate the effectiveness of the proposed method by comparative analysis, three different scenarios (STATCOM-without damping controller, STATCOM-with type-1 FLC based damping controller and STATCOM-with type-2 FLC based damping controller) are considered subjected to different types of faults (LLLG, LLG, and LG).

- *Low voltage ride-through capability of fixed-speed wind farm using STATCOM and pitch-angle control*

  In this objective, Unified Voltage and Pitch-angle Control (UVPC) strategy is developed for wind farm to guaranteeing the LVRT grid code requirement when it subjected to severe network perturbations. The UVPC consist of STATCOM voltage control loops with adequate pitch angle control loops which are coordinated to enhance the low-voltage ride-through capability of the wind generators thereby, complying the LVRT grid code requirement as desired by the Germany grid code. Specially, an interval type-2 fuzzy logic technique is incorporated in the fault ride-through (FRT) scheme of pitch-angle controller as it is very efficient in handling the uncertainties in membership functions and rules than their traditional fuzzy logic

counterpart. To evaluate the effectiveness of UVPC strategy, the following different test cases have been considered:

(a) System without STATCOM and pitch-angle controller

(b) System with STATCOM only

and (c) System with STATCOM as well as pitch-angle control (i.e. UVPC)

- *Generator output power smoothing and terminal voltage regulation of a wind generator using UVPC*

  In this objective, the UVPC (which is developed in the previous objective) is employed to smoothing out the output power and voltage regulation of a fixed-speed wind generator in the partial load (below rated wind speed) region. At first, a typical pitch angle control strategy is developed by employing an exponential moving average (EMA) concept from which the controller reference power (signal) can be set for below-rated wind speed. Later on, the developed pitch-angle controller together with STATCOM, namely, the unified voltage and pitch-angle controller (UVPC), addresses the objective of smoothing out the output power and terminal voltage regulation of a wind generator, subjected to below-rated wind speed variations. An interval type-2 fuzzy logic technique has been incorporated in the pitch angle controller design, as it offered better performance than its traditional fuzzy logic counterparts as discussed above.

- *Transient stability improvement of variable speed (DFIG) wind energy system*

  In this objective, an adaptive control technique i.e. type-2 fuzzy logic-PI controller is designed for torque and voltage control schemes of rotor-side converter (RSC). Type-2 fuzzy-PI controller can be achieved by combining type-2 fuzzy logic controller, which is adaptive and PI controller which has a robust response results in superior dynamic and steady-state responses from the system. Here, proportional and integral gains of PI controller are adjustable and they are computed by using type-2 FLC approach according to as system operating condition changes. Thus, it achieves the adaptive structure required for RSC converter for smooth interaction of DFIG to the grid. The controller performance is evaluated by developing the real time simulations using OPAL-RT digital simulator. Since many researchers have considered the OPAL-RT technology as a real time platform for controller prototyping and hardware-in loop

simulations. The studied DFIG-WES model developed in MATLAB/SIMULINK® is exported to OPAL-RT digital simulator for real time simulation. Different operating conditions such as severe fault and voltage sag with reference to the varying wind speed are considered. The results of type-2 FLC-PI compared with type-1 FLC-PI in order to investigate effectiveness of the proposed controller (i.e type-2 FLC-PI).

1.7 Organization of the thesis

The thesis has been organized in seven chapters and the work included in each chapter has been presented in the following sequence:

Chapter-1 gives a brief introduction about renewable energies and present scenario of wind energy generation worldwide. The different types of wind energy systems are discussed in short and later on, various issues which arise in the grid integrated WES are elaborated. The various aspects of the topic presented in the thesis and research background are discussed. This chapter also highlights the author's contributions towards the problem area, and finally, outlines the organization of the thesis.

Chapter-2 discusses an interval type-2 fuzzy logic system, which is employed to design the various controllers in the rest of thesis. At first, it provides a brief review on fuzzy logic controller (type-1) and mathematical analysis of type-2 fuzzy logic systems. The comparative features of type-1 and type-2 fuzzy sets are also elaborated. The structure of the type-2 fuzzy logic controller (FLC) is presented and discussed in details.

Chapter-3 reported two types of pitch-angle controllers (for transient stability and power smoothing) where they are equipped with an interval type-2 fuzzy logic technique. First, type-2 FLC based logical pitch-angle controller is presented. This controller maintains the generator output power at rated value when speed is above the rated speed. Besides, it also improves the transient stability during severe network faults. An analytical method has been employed to obtain the electrical equivalent of the induction generator. The performance of the proposed interval type-2 fuzzy logic method is compared with PI and type-1 fuzzy logic technique. Another contribution of this chapter is the generator output power smoothing using pitch-angle controller. EMA concept is incorporated to generate reference power for pitch angle controller. An interval type2- FLC is proposed for pitch angle controller for better smoothing to achieve. Different types of wind speed patterns are considered and real-time simulations are developed which make the controller more practical.

Chapter-4 provides the detailed modelling and control strategy of the static synchronous compensator (STATCOM) which supports the employed wind farm. A 36MW of fixed-speed wind farm exporting power to 120kV grid has been designed using MATLAB/SIMULINK®. Different faults locations and fault durations have been considered with and without STATCOM and fault ride-through capability of the fixed-speed wind farm has been investigated. Later on, an interval type-2 fuzzy logic based damping controller is adopted in STATCOM to achieve improved damping which enhances the stability of wind integrated power system.

Chapter-5 introduces unified voltage and pitch-angle control (UVPC) strategy which consists of STATCOM voltage control and pitch-angle control loops, coordinated in such a way to improve the LVRT capability of WES thus compliance the grid code requirement. Moreover, UVPC also investigated for voltage regulation and power smoothing under the partial load region subjected to wind speed variations. This chapter employs the wind farm which is developed in the chapter 4.

Chapter-6 details the mathematical modelling of the DFIG and the design of the RSC voltage and torque controllers using type-2 fuzzy logic-PI controller. The DFIG based WES which is integrated to the grid has been developed using MATLAB/SIMULINK® and it is later on exported into OPAL-RT simulator for real time environment is elaborated. The performance of the real time simulations results are discussed and comparative analysis done using type-2 fuzzy logic-PI and type-1 fuzzy logic-PI under disturbances such as three phase short-circuit fault and voltage sag with reference to varying wind speed.

Chapter-7 compiles the salient conclusions of the present study regarding the controller designs and control strategies for WESs and recommended directions for further investigations.

CHAPTER 2: AN INTERVAL TYPE-2 FUZZY LOGIC SYSTEM

2.1 Introduction

This chapter discusses an interval type-2 fuzzy logic system, which is employed to design the different controllers in the rest of thesis. The concept of type-2 fuzzy set was introduced by Zadeh [184] as an extension to the traditional type-1 fuzzy set. In type-1 fuzzy set, the membership grade is a crisp number in [0, 1], whereas in type-2 fuzzy set the membership grades themselves are type-1 fuzzy sets. This feature of type-2 fuzzy set is very useful in conditions where, it is difficult to determine exact membership grade for fuzzy set and also for incorporating uncertainties. This chapter provides an overview of type-2 fuzzy logic sets and its characteristics. The objective of this chapter is to introduce type-1 fuzzy logic controller and its uncertainties in the membership functions and rules. Later on, it provides a background on several aspects related to type-2 fuzzy sets and mathematical analysis.

2.2 Type-1fuzzy logic system

In 1965, Professor Lofti Zadeh proposed the concept of fuzzy logic (FL) [182]. The aim of the FL is to develop the output by allowing the set of membership rather than crisp value. It has been found to be an excellent choice for many control applications [72, 77, 78, 93, 94,126, 183, 185, 186], as it mimics the human control logic. The fuzzy rules are framed on the basis of the expert knowledge gained upon the performance of the system over a time. The well-known block diagram of a conventional FLC (named as type-1 FLC) is as shown in Figure 2.1.

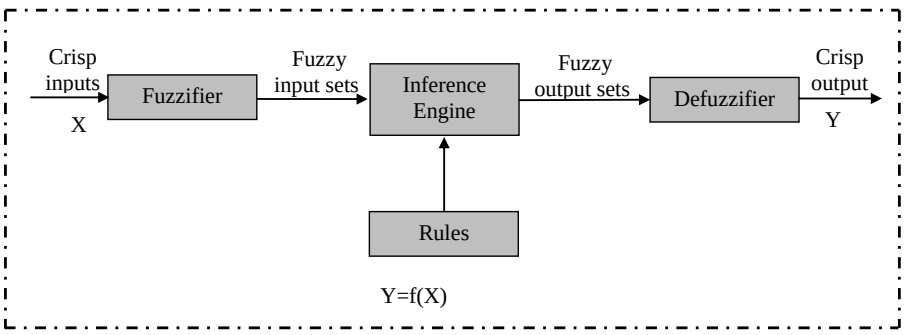

Figure 2.1: Schematic diagram of classical (type-1) Fuzzy Logic Controller

It consists of a fuzzifier, inference engine and a de-fuzzifier [183]. Here, the fuzzifier converts the crisp value of the input parameter into fuzzy set and depending upon the fuzzy rules

framed based on the membership functions for a given parameter of the system and then, fuzzy outputs are obtained with the help of the Inference Engine. In the end, de-fuzzifier converts these fuzzy outputs to a crisp output of the FLC to be used for the control purpose. It is being assumed that the concept of the type 1 FLC is clear and therefore, this will not be discussed further.

2.3 Uncertainties in type-1 fuzzy logic

Quite often, the expert knowledge that is used to construct the rules in a type-1 FLC is uncertain as the knowledge possessed by different experts may not be the same. There are three ways in which uncertainty involved with the fuzzy rules can occur:

1) the rules utilize the words in antecedent and consequent, which can mean different things to different people [96],
2) the consequents obtained from the group of experts can be different for the same rule,
3) due to noisy training data, uncertainty in antecedent and consequent can transfer into membership functions (MF).

In order to understand the uncertainties present in the type-1 fuzzy systems, Jerry M. Mendel [96] has performed an experiment as follows: First he established sixteen words that would designate the numerical interval from 0-10, and selected engineering undergraduate students for this test. The following instructions were given to them:

1. Below are a number of labels (sixteen) that describe an interval or a range that cover some-where between 0 to 10.
2. For each label, provide where this range would start and where it would stop. For example, label "quite a bit" might start at 6 and end at 8.
3. It is not necessary that all the ranges or intervals are of the same size.

After providing these instructions, a table was provided to the students where they only had to fill-in two numbers (where to start and where to end) for each label. A survey results from the 70 respondents are summarized in Figure 2.2. Each label identified with solid line and mean start and end points marked with circles. The dashed lines to the right of the right hand circle and left of the left hand circle are each terminates in a vertical bar, which represents the standard deviation for the mean start and end points. It is observed that the standard deviations are not the same for the start and end values for each labels.

It is also noticed from the Figure 2.2 that: (1) there is gap between the labels 'None' and 'Very little', it implies that they should be combined or other word should be inserted between them. (2) it is commonly agreed that 'None' should starts at zero, but there is little uncertainty about this, (3) similarly, for the word 'A maximum amount', it is seen that the

right hand value is 9.7572 instead of 10, (4) there is a small degree of overlap between the labels ‘Some’ and ‘A moderate amount’ which seems to be a linguistic gap between them. So, the sixteen words do not quite cover the 0-10 interval and the dashed portions of each label represent the word’s uncertainty. The uncertainty associated with words in case of type-1 fuzzy sets can be translated into a foot print of uncertainty (FOU) by employing type-2 fuzzy sets [96]. By doing this, uncertainty in the words potentially reduced.

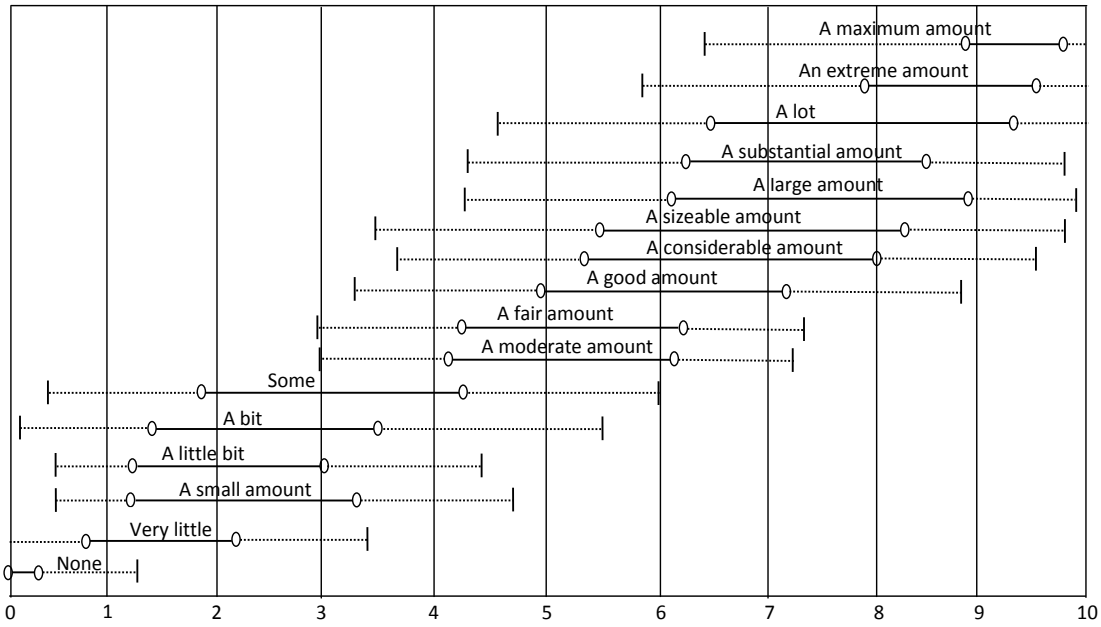

Figure 2.2: All sixteen labels and their uncertainty bands and intervals

2.4 Type-2 fuzzy logic system

Generally, type-1 fuzzy rules and membership functions (MFs) are defined based on experts’ knowledge and experience. However, once the membership functions have been defined for designing the controller, the uncertainties in actual degree of MFs cannot be modelled [49]. Quite often the knowledge used to design the type-1 FLC ignore the uncertainties in spread of MFs, rules and membership grade etc. and such system cannot guarantee the optimal performance of the system when it subjected to the disturbances.

For example: 1) The fuzzy rules are defined by experts, which varies form case to case, this causes statistical uncertainties about locations and spread of antecedents and consequent fuzzy sets. Such uncertainties can be easily modelled and accounted for using type-2 membership functions [5]. 2) The noise in training data is ignored in most of the cases, which leads to uncertainties in antecedents and consequents. If the level of uncertainty information is known, it is easily accounted by designing the type-2 fuzzy sets [85].

In addition, for the same rule-question, the expert often gives different answers. This leads to different consequences but have the same antecedents for the given rules. In such a case, it

is also possible to represents the output of the fuzzy logic system built from these rules as a fuzzy set rather than a crisp number. This can also be achieved within the type-2 framework [48]. In order to increase the fuzziness of a relation, higher type (i.e type-2) fuzzy relation is one way. According to [55], increased fuzziness means increased ability to handle inexact information in logically correct manner. Detailed description of algebraic structure of type-2 sets are given in [100].

From the literature survey, it is found that type-2 fuzzy systems have been successfully applied in many science and engineering applications [80, 81, 101, 133]. In data process applications, the system with type-2 fuzzy system seems to be more promising method than the type-1 counterpart in processing of noisy data with uncertainties [61]. Type-2 fuzzy system has been applied in decision making [33], survey processing [79], solving fuzzy relation equations [99] and function approximation [178] by comparing the performance with its type-1 counterparts. In real world applications which exhibits measurement noise and parameters uncertainties, type-2 fuzzy controllers are better option than type-1 FLC [58]. The controllers with type-2 FLC have shown to have better tracking capability in real-time mobile robots [95]. Recently, many power system applications have adopted type-2 FLC as an alternative for handling uncertainties in operating conditions [40, 74, 167, 173]. The type-2 FLC also offers better performance in automation controller than type-1 FLC [17, 25, 102, 187]. The type-2 FLC is also applied in network domain, in order to control of video transmission across the IP networks, where it provided superior video quality compared to existing traditional type-1 FLC counterparts [66, 67, 84, 152]. Type-2 FLC applications are also found in health-care and medicine domain due its robust performance than type-1 FLC [53, 125]. It is believed that a type-2 fuzzy system performs better than type-1 fuzzy system in various areas including communication networks, pattern recognition, mobile communications and renewable energy operated systems, in which the frequently supplied information to be processed is uncertain. Hence, wind energy systems, being highly uncertain in output, can utilize the special features of type-2 FLSs to improve its operational efficiency during the grid interaction.

2.5 Mathematical concept on type-2 fuzzy sets

In this section, the detailed information about the concept of type-2 fuzzy set is explained. The MF of a standard type-1 fuzzy system is shown in Figure 2.3(a), with a crisp membership grade varying in [0 1]. The type-2 MF can be imagined as blurred type-1 MF by shifting the points on triangle MF not necessarily by the same amounts either to the right or to the left, as shown in Figure 2.3(b). At a specific point of, x say x', the type-1 MF having a value of

membership grade u' whereas in type-2 case, it has the values where the blur intersected by the vertical line. These intersect points do not necessarily have the same weights, and hence, we can assign an amplitude distribution to all of those points. Doing this for all $x \in X$, a three dimensional membership function or a type-2 MF can be formed.

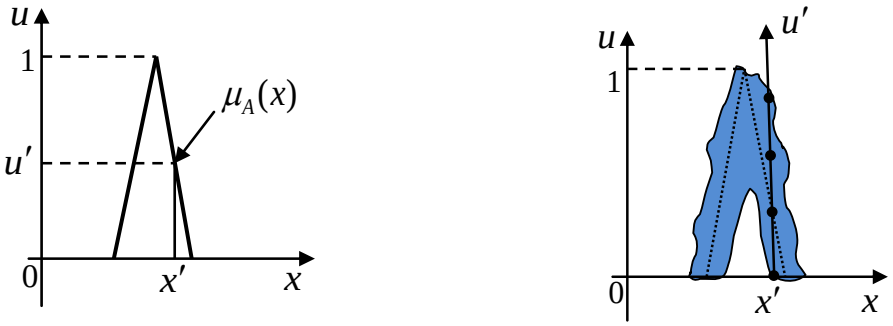

(a) (b)

Figure 2.3: (a) Type-1 membership function (b) Blurred type-1 membership function

A type-2 fuzzy set, denoted as 'A' with a type-2 MF $\mu_A(x,u)$ can be described as

$$A = \left\{ \left((x,u), \mu_A(x,u) \right) \quad \forall x \in X, \forall u \in J_x \subseteq [0,1] \right\} \tag{2.1}$$

Where $x \in X, u \in J_x \subseteq [0,1]$ and $0 \le \mu_A(x,u) \le 1$. A can also be characterized as

$$A = \int_{x \in X} \int_{u \in J_x \subseteq [0,1]} \mu_A(x,u) / (x,u) \tag{2.2}$$

$$= \int_{x \in X} \left[\int_{u \in J_x \subseteq [0,1]} \mu_A(x,u) / u \right] \Big/ x \tag{2.3}$$

Where $x \in X$ and $u \in U$ are the primary and secondary variables, respectively. The secondary variable has domain J_x at each $x \in X$; J_x is called the primary membership of x.

The graphical representation of type-2 fuzzy set with discrete universe is as shown in Figure 2.4. The axis u represents the domain of primary membership function and μ_A denotes the secondary MF. The secondary MF is also represented as vertical slice of the axis μ_A. J_x is the domain of the secondary MF also called as primary membership of x which varies in the range [0 1]. The uncertainty in the primary memberships of a type-2 fizzy set 'A' consists of a shaded region that is called as footprint-of-uncertainty (FOU) as shown in Figure 2.4.

$$FOU(A) = \cup_{\forall x \in X} J_x \tag{2.4}$$

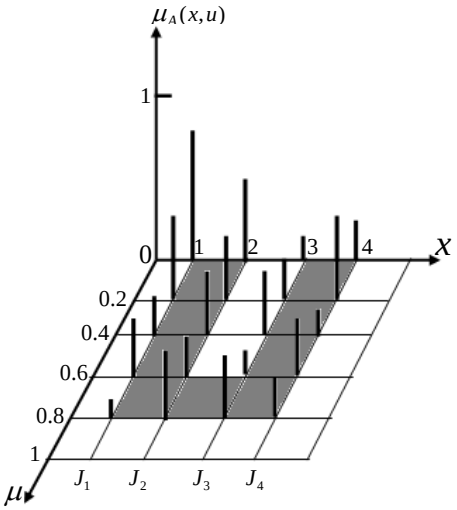

Figure 2.4: Three dimensional representation of type-2 fuzzy set

The footprint of uncertainty draws a special attention towards type-2 FSs, because it is framed to represent the uncertainties inherent in a specific type-2 membership function, whose shape is a direct consequence of the nature of these uncertainties. The type-2 FSs, represented in three-dimensional, cause difficulties in depicting them graphically. To this effect, the FOU provides two dimensional representation of type-2 FSs, which provides a convenient verbal description of the domain of secondary membership grades. The shaded FOUs imply that there is a distribution that sits on top of it (known as the third dimension of type-2 fuzzy sets) and its depends on the specific choice of the secondary grade.

2.5.1 Structure of type-2 FLS

The structural diagram of type-2 FLC is as shown in Figure 2.5. It is very similar to the structure of a type-1 fuzzy logic system (FLS) [97]. In case of type-1 FLS, the output fuzzy sets are processed through the de-fuzzifier and obtain the crisp output. Here we discuss the type 2 FLS in detail as follows:

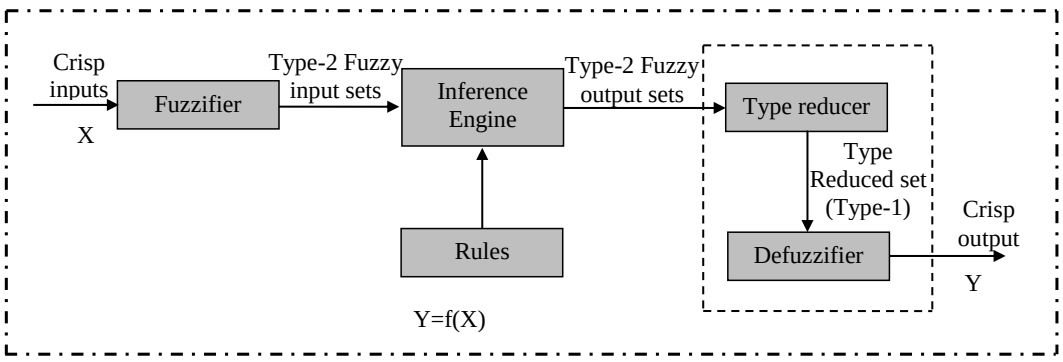

Figure 2.5: The structure of type-2 FLS

A. Fuzzifier

The fuzzifier maps the crisp input into a type-2 fuzzy set. This operation can be done by choosing the appropriate type-2 FSs in the range of the input variable. The challenge lies here in the definition of membership grade fuzziness. Therefore, the secondary and primary membership functions should be developed in such way that it reduces the problem of complexity as much as possible.

B. Rules

The rules are generally framed based on "IF-THEN" logic, where the n^{th} rule has the form

$$R^n: \text{IF } x_1 \text{ is } F_1^n \text{ and } x_2 \text{ is } F_2^n \text{ ....and } x_p \text{ is } F_p^n \text{ THEN } y \text{ is } G^n$$

where, x_i are inputs: F_i^n are antecedent sets ($i = 1, 2.....n$); y is the output; G^n are consequent sets.

The difference between type-2 and type-1 fuzzy methods is the nature of MFs associated with them and it is not important while forming the rules. Hence, the type-2 rules structure remains exactly same as that of the type-1 and the only difference is that - all of the sets involved are of type-2 [88].

C. Inference Engine

In the type-2 FLCs, the union and intersection functions are defined by join and meet operations to map the input and output sets with fired rules. Therefore, the inference engine utilizes min-method and max-method for meet and join operations, respectively. Using the extension principle, a detailed mathematical relation between the meet and join operations is presented in [107]. To do this, one needs to find unions and intersections of type-2 sets, as well as compositions of type-2 relations.

D. Type reduction

In a type-1 FLS, the output corresponding to each fired rule is a type-1 set in the output space. The crisp output is obtained by combining all the fired rules through a de-fuzzifier using some fuzzy relations. Most of the de-fuzzifiers use centroid method for obtaining the crisp output. In contrast, in type-2 FLS, the output set corresponding to the each fired rules is a type-2 set. On which the centroid method cannot be applied directly. In order to calculate the crisp output, the type-2 sets are combined in some way to get the type-1 form known as type reduction (TR) operation. The type reduction method, in the type-2 FLC system, convert

type-2 output fuzzy sets to type-1 fuzzy sets. A detailed description on type reduction can be found in [121].

For example, an embedded type-2 fuzzy set A_e has 'N' elements, where A_e contains exactly one element from $J_{x1}, J_{x2}, ..., J_{xN}$ namely $u_1, u_2, ..., u_N$, each with its associated secondary grade, namely $f_{x1}(u_1), f_{x2}(u_2), ... f_{xN}(u_N)$, i.e

$$A_e = \sum_{i=1}^{N} [f_{xi}(u_i) / u_i] / x_i \qquad u_i \in J_{xi} \subseteq U = [0,1] \tag{2.5}$$

Height, center-of-sets, center-of-sums and modified-height are the most accepted TR methods.

E. Defuzzification

The output of inference engine is converted to type-1 under type reduction operation and then, the type reduced sets are converted back to crisp value using various de-fuzzification techniques as done in the type-1 FLC. The simple way to get a crisp value is through finding the centroid of all the type-1 sets embedded in type-2 FLS. The other way of doing this operation is by choosing the highest membership point in the type-reduced set. For example, if the type reduced set y for an input x is discredited into 'N' points, then the centroid is expressed as

$$C_y(x) = \frac{\sum_{k=1}^{N} y_k \mu_Y(y_k)}{\sum_{k=1}^{N} \mu_Y(y_k)} \tag{2.6}$$

where $\mu_Y(y_k)$ represents the membership grade.

2.5.2 Centroid type reduction methods

Type reduction (TR) method is suggested in the type-2 FLC system to convert type-2 output fuzzy sets to type-1 fuzzy sets first and thereafter, the normal de-fuzzification techniques are applied. Height, center-of-sets, center-of-sums and modified-height are the most accepted TR methods [73], in which centroids of the embedded type-2 sets are calculated. If larger is the FOU width, the number of embedded fuzzy sets increases and this leads to increase in the computational time of TR method. In the present work, 'height' TR method has been used for the calculation of the centroid of Type-2 FLCs as it involves simpler computations as compared to other methods [73].

2.6 Interval type-2 fuzzy sets

As explained in [98], if all the distribution points which sit on the FOU is uniform, then the resulting type-2 fuzzy sets are called *interval type-2 fuzzy sets* [97]. These fuzzy sets have less computational complexity with secondary memberships, made either zero or one. Such Such sets are the most widely used type-2 fuzzy sets to date [101].

An interval type-2 fuzzy set (denoted $\tilde{A}$) can be characterized as:

$$\tilde{A} = \int_{x \in X} \int_{u \in J_x \subseteq [0,1]} 1/(x,u) \tag{2.7}$$

$$= \int_{x \in X} \left[\int_{u \in J_x \subseteq [0,1]} 1/u \right] \Big/ x \tag{2.8}$$

$\tilde{A}: X \to \{[a,b]: 0 \le a \le b \le 1\}$. Structurally, the membership functions of both type-2 FSs and interval type-2 FSs (IT-2FSs) are three dimensional, with only difference of secondary membership grades of IT-2FSs are either zero or one. Figure 2.6 shows the IT-2 Gaussian membership function in which the secondary membership grade is highlighted. The union of all the primary memberships is called the footprint-of-uncertainty (FOU) of $\tilde{A}$ and is shown as the shaded region of Figure 2.7. Uncertainty about $\tilde{A}$ is conveyed by union of all primary memberships, called FOU, can be expressed as:

$$FOU(\tilde{A}) = \cup_{\forall x \in X} J_x = \{(x,u): u \in J_x \subseteq [0,1]\} \tag{2.9}$$

As shown in Figure 2.7, the FOU of type-2 fuzzy set ($\tilde{A}$) has bounded by two type-1MFs called as lower membership function (LMF) and the upper membership function (UMF). The UMF and LMF are denoted as $\bar{\mu}_{\tilde{A}}(x)$ and $\underline{\mu}_{\tilde{A}}(x)$, respectively, and are defined as follow:

$$\bar{\mu}_{\tilde{A}}(x) = \overline{FOU(\tilde{A})} \qquad \forall_{x \in X} \tag{2.10}$$

$$\underline{\mu}_{\tilde{A}}(x) = \underline{FOU(\tilde{A})} \qquad \forall_{x \in X} \tag{2.11}$$

Note that J_x is an interval set; i.e.

$$J_x = \{(x,u): u \in [\underline{\mu}_{\tilde{A}}(x), \bar{\mu}_{\tilde{A}}(x)]\} \tag{2.12}$$

An embedded fuzzy set (FS) $\tilde{A}_e$ for a continuous universe of discourse X and μ is expressed as

$$\tilde{A}_e = \int_{x \in X} [1/u]/x, \quad u \in J_x \tag{2.13}$$

The set $\tilde{A}_e$ is embedded in $\tilde{A}$ in such a way that the secondary MF is always one at each value of X. A large number of such embedded type-1 fuzzy set (FS) are combined to form the type-2 FS. According to [133], the type-2 FS can be considered as a combination of many different type-1 FSs where each type-1 FS is embedded to form the FOU. The detailed analysis of embedded interval type-2 FSs are given in [82].

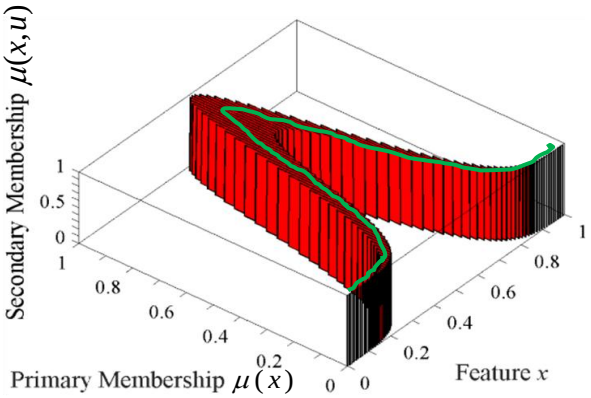

Figure 2.6: Type-2 FS with FOU and Embedded FS

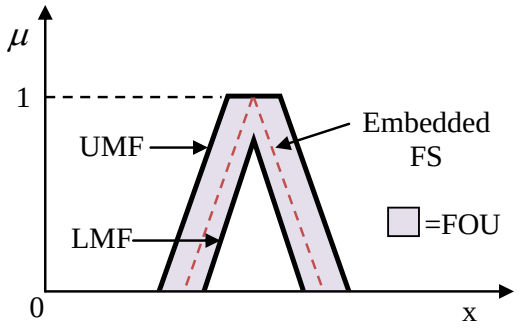

Figure 2.7: Type-2 Fuzzy Sets with FOU and Embedded Fuzzy Set (FS)

2.7 Conclusion

This chapter gives an overview of the interval type-2 fuzzy logic system. Firstly, traditional fuzzy concept has been discussed, later on type-2 fuzzy sets are introduced by brief explanation on interval type-2 fuzzy logic system. The structure of the interval type-2 fuzzy logic controller is presented and the roles of individual blocks used in the structure are discussed in detail.

CHAPTER 3: TRANSIENT STABILITY ENHANCEMENT AND POWER SMOOTHING OF WES USING PITCH-ANGLE CONTROLLER

3.1 Introduction

The increasing penetration of wind energy system into the utility grid has forced wind farm operators to perform the transient stability analysis of the wind turbine generator (WTG). Moreover, the wind energy system (WES) has an undesirable characteristic that its output fluctuates with wind speed variation, resulting in fluctuations in the grid frequency and voltage. Therefore, the objective of this chapter is to design the pitch-angle controller with an appropriate control technique for achieving improved transient stability and effective generator output power smoothing.

In this chapter, an interval Type-2 fuzzy logic controller (Type-2 FLC) based pitch-angle control system (in power and speed control modes) has been proposed, which can enhance the transient stability performance of the WTG (in speed control mode) subjected to severe network disturbances and maintain the IG output power when the wind speed is higher than rated speed (in power control mode). Moreover, some key factors that affect the transient stability have been investigated by deriving steady-state equivalent model of the induction generator.

This chapter also proposes an interval Type-2 fuzzy logic based pitch-angle controller that can smoothen the WES output power more effectively. Different types of wind speed patterns are employed to validate the effectiveness of the proposed controller. Real time simulations are developed to show the applicability of the proposed controller using the OPAL-RT digital simulator. The performance of the proposed controller has been estimated using power smoothing and energy loss functions to validate its application for WES.

The major contributions of this chapter are as follows:

- A steady-state equivalent model of the induction generator has been developed using analytical approach. The electrical torque and mechanical torque versus rotor speed performance were obtained under different pitch-angle conditions and concept of stable and unstable electrical-mechanical equilibrium points were presented.
- An interval Type-2 FLC based pitch-angle controller was designed and developed to enhance the transient stability of the WES subjected to transient fault.

- An interval Type-2 FLC based fuzzy logic controller is also incorporated in order to smoothing out the wind generator output power more effectively when it subjected to varying wind speed.
- In order to validate the proposed control strategy for power smoothing, real-time simulation is developed using OPAL-RT technology digital simulator.

3.2 Aerodynamic conversion

The mechanical power developed by a typical wind turbine is directly proportional to the cube of wind speed as

$$P_m = \frac{1}{2}\rho A_r C_p(\lambda,\beta)V_w^{\,3} = C_p(\lambda,\beta)P_w \tag{3.1}$$

where, P_w is available wind power, ρ is the air-density [kg/m^3], A_r is the turbine swept area [m^2] and can be written as $A_r = \pi R^2$, V_w is the wind speed [m/s] and C_p is the power coefficient.

The typical wind turbine is characterized by the power coefficient (C_p) which depends upon the ratio of rotor-tip speed (λ) and blade pitch-angle (β). The power coefficient (C_p) employed in this study is as follows [3]:

$$C_p(\lambda,\beta) = c_6\lambda + e^{-c_5/\lambda_i}\left(-c_4 - c_3\beta + c_2/\lambda_i\right)c_1 \tag{3.2}$$

where

$$\frac{1}{\lambda_i} = \frac{1}{0.008\beta + \lambda} - \frac{0.035}{1+\beta^3} \tag{3.3}$$

The coefficients $c_6 - c_1$ are: $c_6 = 0.0068$, $c_5 = 21$, $c_4 = 5$, $c_3 = 0.4$, $c_2 = 116$ and $c_1 = 0.5176$ and the tip-speed ratio (λ) can be defined as:

$$\lambda = \frac{\text{tip speed of the blade}}{\text{wind speed}} = \frac{\omega_r R}{V_w} \tag{3.4}$$

where, R is the radius of turbine rotor [m] and ω_r is rotor speed [rad/s]

According to equations (3.1) - (3.4), for different values of pitch-angle (β), the power coefficient versus tip-speed ratio ($C_p - \lambda$) curve for the studied system has been obtained as shown in Figure 3.1. For different values of wind speed (V_w), the turbine output power versus turbine speed characteristics is as shown in Figure 3.2.

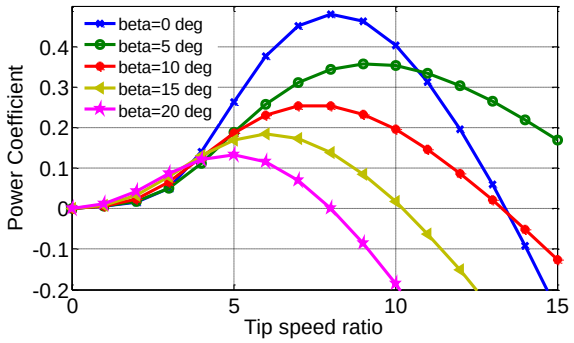

Figure 3.1: Wind turbine $C_p - \lambda$ curve

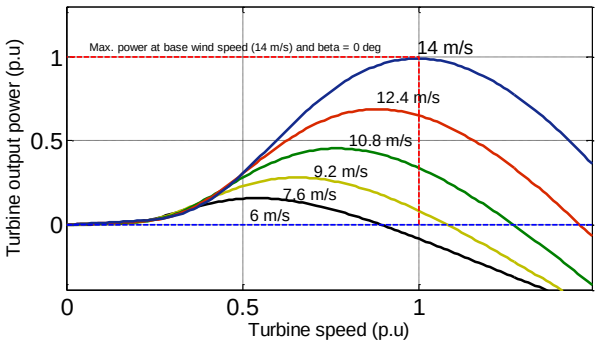

Figure 3.2: Turbine Power characteristics

The mechanical power (P_m) shown in equation (1) can be expressed as:

$$P_m = \frac{1}{2}\rho\pi R^2 C_p(\lambda,\beta)V_w{}^3 = \frac{1}{2}\rho\pi R^2 C_p(\lambda,\beta)\omega_r^3\left(\frac{R}{\lambda}\right)^3 = C_p(\lambda,\beta)K\omega_r^3 \tag{3.5}$$

where, $K = \frac{1}{2}\rho\pi R^2\left(\frac{R}{\lambda}\right)^3$

Hence, the mechanical torque output of induction generator (IG) can be derived as [156]:

$$T_m = \frac{P_m}{\omega_r} = \frac{C_p(\lambda,\beta)P_w}{\omega_r} \tag{3.6}$$

The relation between mechanical torque (T_m) and pitch angle (β) with respect to rotor speed (ω_r) as shown in Figure 3.3, which is obtained using information from Figure 3.1 and equation (3.6). As observed from equation (3.6), the mechanical power output (P_m) of wind turbine depends upon power coefficient (C_p) and the rotor speed (ω_r) of wind turbine. However, the turbine speed varies very little as the fixed speed squirrel-cage generators have a speed variation range as less than 1% [177]. Therefore, variation of mechanical power solely depends on power coefficient $C_p(\lambda,\beta)$ which is not constant and varies with tip speed ratio (λ) and pitch angle β. However, in transient stability studies, tip-speed ratio variation is

very small [168]. As a result, the mechanical torque mostly depends on the pitch angle (β). Figure 3.3 shows the relation between T_m and β as a function of ω_r. It can be noticed from Figure 3.3, in particular point onwards of rotor speed, the mechanical torque decreases, when the pitch angle is increased.

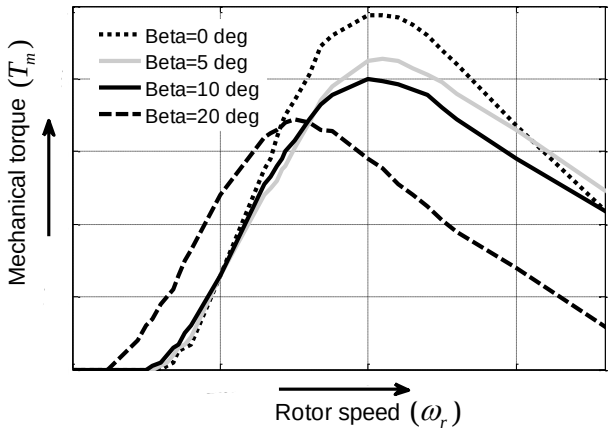

Figure 3.3: Mechanical torque versus rotor speed

3.3 Induction generator modelling

In order to obtain the induction generator (IG) model, the network from IG to PCC of the test system (see Figure 3.14) is considered and the corresponding equivalent circuit from IG to PCC is as shown in Figure 3.4. In this figure, IG is being represented by its steady-state equivalent circuit as shown in Figure 3.4 inside dotted box, and all the variables and parameters are referred to stator side.

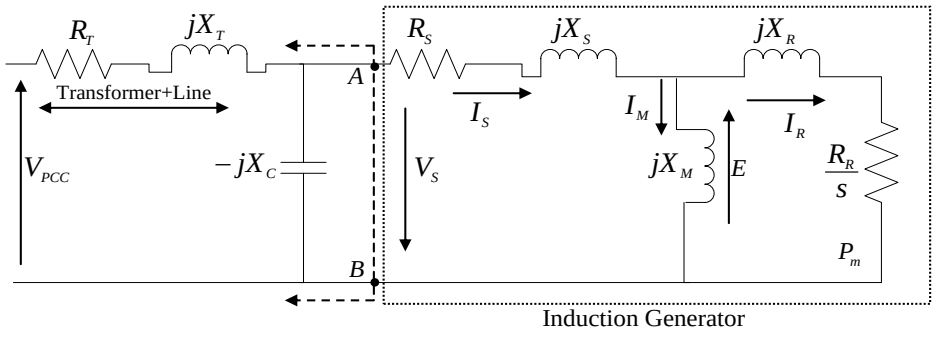

Figure 3.4: Electrical equivalent of the test system

According to the IG equivalent circuit, the mathematical expression for stator terminal voltage (V_S) of fixed speed induction generator (FSIG) is:

$$V_S = I_S(R_S + jX_S) + E \tag{3.7}$$

where, E is air-gap magnetic field induction electro-magnetic-field (EMF) given by

$$E = jI_M X_M \tag{3.8}$$

where X_M magnetizing reactance and I_M is the exciting current of the FSIG. Now the rotor current I_R can be determined from stator current I_S after deducting I_M as follows:

$$I_R = I_S - I_M \tag{3.9}$$

And, then the corresponding mechanical power input to the IG will be given by

$$P_m = 3I_R^2\left(\frac{R_R}{s}\right) \tag{3.10}$$

Where, R_R and R_S are the rotor and stator resistance, respectively and 's' is the slip which is less than zero for the IG.

3.4 Concept of critical rotor speed

There would be a critical value for the rotor speed of FSIG, after the occurrence of a fault, above which the rotor may become unstable and cause the disconnection of the IG from the grid. To understand the rotor stability concept of the studied wind energy system, it is required to calculate the electrical torque of the generator from the equivalent circuit of the system shown in Figure 3.4. From Figure 3.4, Thevenin equivalent circuit representing the left hand side portion of the equivalent circuit across point A and B, the modified circuit can be shown as given in Figure 3.5. Where, Thevenin equivalent voltage is:

$$V_{1TH} = \frac{V_{PCC}(-jX_C)}{R_T + jX_T - jX_C} \tag{3.11}$$

and the series parameters are:

$$R_{1TH} = R_T \text{ and } X_{1TH} = X_T - X_C$$

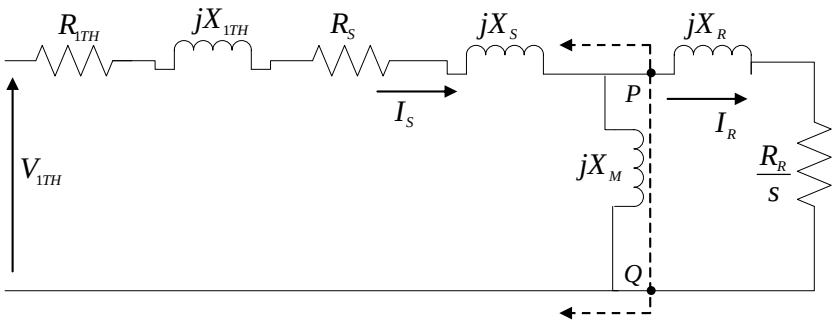

Figure 3.5: Reduced Equivalent circuit of the system

From Figure 3.5, by applying Thevenin concept again at the point P and Q, the further reduced equivalent circuit is obtained as shown in Figure 3.6. The Thevenin equivalent voltage obtained as:

$$V_{TH} = \frac{V_{1TH}(jX_M)}{R_{1TH} + R_S + jX_{1TH} + jX_S + jX_M} \tag{3.12}$$

and the equivalent Thevenin resistance and reactance can be obtained as: $R_{TH} = R_{1TH} + R_S$ and $X_{TH} = X_{1TH} + X_S + X_M$.

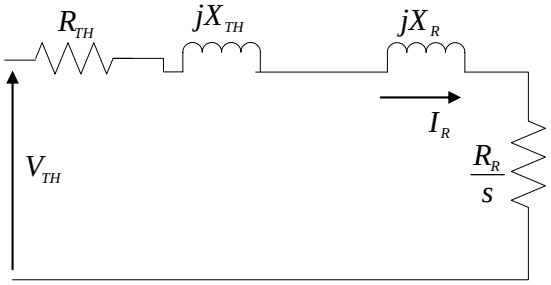

Figure 3.6: Complete Reduced Equivalent circuit of the system

Finally, from the Figure 3.6, the rotor current can be computed as [46]:

$$I_R = \frac{V_{TH}}{\sqrt{\left(R_{TH} + R_R/s\right)^2 + \left(X_{TH} + X_R\right)^2}} \tag{3.13}$$

From which, the generator electrical toque can be determined as:

$$T_e = \frac{R_R}{s} I_R^2 = \frac{R_R}{s} \frac{V_{TH}^2}{\left(R_{TH} + R_R/s\right)^2 + \left(X_{TH} + X_R\right)^2} \tag{3.14}$$

Generally, the slip is defined as:

$$s = \frac{\omega_s - \omega_r}{\omega_s} \tag{3.15}$$

When the induction machine is operated as generator, the sign convention for the electrical (T_e) and mechanical (T_m) torques are considered as negative. Therefore, the mechanical-electrical equilibrium of the IG can be expressed as

$$\frac{d\omega_r}{dt} = \frac{1}{2H}\left(T_e - T_m\right) \tag{3.16}$$

Where, H is the inertia constant of WTG. By using equations (3.6) and (3.14) the mechanical and electrical torques versus rotor speed can be plotted as shown in Figure 3.7. For better visualization, the mechanical and electrical torques were multiplied by -1.

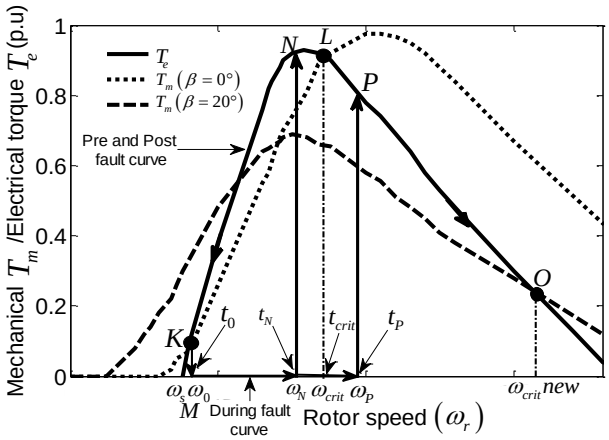

Figure 3.7: Characteristics of T_e and T_m versus rotor speed

As observed from Figure 3.7, let the IG is being at an operating point K, now the occurrence of fault at time t_0, the electrical torque (T_e) suddenly reduces to zero and operating point of the generator shifted from K to M where the rotor speed is ω_0. Due to which, the existing mechanical torque (T_m) (with no pitch-angle control (i.e. β=0) shown in Figure 3.7) causes the IG rotor to accelerate as governed by the Equation (3.16) and start increasing (during the fault). At the instant t_N, the fault is cleared and operating point of the generator shifted to point N where, the T_e is greater than T_m causing the net torque $(T_e - T_m)$ to be negative which causes the rotor speed to decrease and therefore, it eventually leads the generator to return back to its initial operating point K. This clearly shows that the IG will be stable as long as the fault is cleared before a critical speed ω_{crit} without making use of the pitch-angle control (i.e. β = 0).

3.4.1 Effect of pitch angle control

In the absence of pitch-angle control, in case the fault is not cleared before time t_{crit} (corresponding to critical rotor speed ω_{crit}), the rotor speed ω_r will increase further. If the fault

is cleared at t_P the operating point of generator T_e is shifted to point P where the T_m greater than T_e thus, the net torque $(T_e - T_m)$ is positive, which results in increase of rotor speed and thus, generator will become unstable. In this condition, it observed from the Figure 3.7 that by increasing of pitch angle by $\beta = 20°$, the mechanical torque gets reduced below the electrical torque and system retains its stability, thus, the intersection of T_e and T_m at point O provides the new critical speed ($\omega_{crit}new$). It clearly shows that by increasing the pitch angle with the help of wind turbine pitch-angle controller, the critical speed limit can be raised from ω_{crit} to $\omega_{crit}new$. Thus, the stable operation of the system can also be maintained at the higher rotor speeds (upto $\omega_{crit}new$).

The critical fault clearance time can be determined, by solving the equations (3.14) and (3.16) at the equilibrium points as follows.

$$\left(R_{TH}^2 + \left(X_{TH} + X_R\right)^2\right)s^2 + \left(2R_R R_{TH} - R_R V_{TH}^2 / T_m\right)s + R_R^2 = 0 \tag{3.17}$$

which is a second order equation. Now, solving the equation (3.17) and using equation (3.15), the steady-state ω_0 and critical rotor speed ω_{crit} can be calculated as:

$$\omega_0 = 1 - \frac{b + \sqrt{\Delta}}{2a} \tag{3.18}$$

$$\omega_{crit} = 1 - \frac{b - \sqrt{\Delta}}{2a} \tag{3.19}$$

where $\Delta = b^2 - 4ac$, $a = R_{TH}^2 + \left(X_{TH} + X_R\right)^2$, $b = 2R_R R_{TH} - R_R V_{TH}^2 / T_m$ and $c = R_R^2$

Substitute the equations (3.18) and (3.19) in equation (3.16) and integrate both side, the critical clearing time is determined as follows:

$$\begin{aligned} t_{crit} = &\left(\frac{-2H}{T_m}\frac{1}{R_{TH}^2 + \left(X_{TH} + X_R\right)^2}\right) \\ &\times\left(\sqrt{\frac{R_R^2}{T_M^2}\left(-4\left(X_{TH} + X_R\right)^2 T_m^2 - 4R_{TH}V_{TH}^2 T_m + V_{TH}^4\right)}\right) \end{aligned} \tag{3.20}$$

For improving the dynamic stability of the WES, equations (3.19) and (3.20) show that ω_{crit} and t_{crit} can be improved by temporary reduction of mechanical torque (T_m) which can

be achieved by increasing the pitch-angle (β) of the wind turbine. From the Figure 3.7, it is observed that by increasing of the pitch angle by $\beta = 20°$, the mechanical torque reduced and ω_{crit} changes from its initial value to $\omega_{crit}new$. Thus, one can understand that stable operating point of the system can be improved from ω_{crit} to $\omega_{crit}new$ by make use of pitch-angle controller. In other word, the pitch-angle control of the WES can be utilized to extend the stable operation over higher wind speeds. So, a pitch-angle controller is designed for the WES as follows:

3.5 Pitch angle controller design

The block diagram of a typical pitch-angle control system is as shown in Figure 3.8. When the wind speed crosses above rated wind speed (V_{wR}), the pitch angle controller limit the aerodynamic toque to maintain the generator output power at its rated value. The difference between the measured power (P_g) and reference power (P_g^{REF}) goes through the controller $C(s)$, which regulates the output power in accordance with error (ε), by generating suitable pitch angle.

The pitch-angle control strategy mathematically can be expressed as follows

$$\beta_c = \frac{\Delta\beta}{\Delta P}\left(P_g - P_g^{REF}\right) + \beta_i \tag{3.21}$$

where, ΔP and $\Delta\beta$ are small-signal state variables of mechanical power and pitch angle, respectively, and β_i is initial pitch-angle.

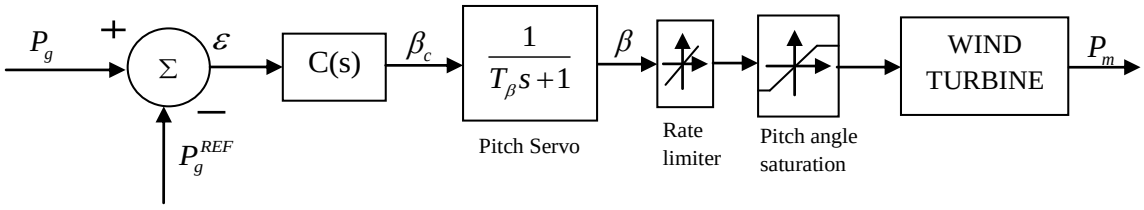

Figure 3.8: The typical pitch-angle control system

The optimum pitch angle (β_c) from the controller $C(s)$ is used as reference to the pitch actuator/servo system. The purpose of the pitch servo is for proper positioning of the blades. The first order transfer function of the electric or hydraulic pitch servo is as follows:

$$\beta = \frac{1}{T_\beta s+1}\beta_c \tag{3.22}$$

The pitch angle (β) follows the reference pitch or optimum pitch (β_c) by a first order lag with time constant T_β, which is depends on the pitch actuator. In order to get the realistic response from the pitch control system, the pitch rate and the regulations range of pitch angle are set to $\pm 2^\circ / \sec$ and $0^\circ - 45^\circ$, respectively.

As discussed in the research background of chapter 1, the pitch angle controller is mainly employed for above rated wind speed where it regulates the generator output power. Besides, it can also improve the transient stability of the WES. The following section discusses how the pitch angle controller can serve these tasks well.

3.6 Pitch angle controller in power and speed control modes

The controller shown in Figure 3.9 can be operated in two control modes (power and speed) in order to achieve above tasks effectively. The operating mode of the controller can be determined using selection switch. The controller works in power control mode with switch set to input 1, when the wind speed exceeds its rated speed to maintain the output power of the generator at rated value. However, for below rated wind speed controller not in operation where $\beta = 0^\circ$ to extract the possible maximum wind power as governed by the Figure 3.1. On the other hand, if the rotor speeds of induction generator increases to a threshold rotor speed (ω_r^{TH}) due network disturbances the controller input set to 2, as a result, it works in speed control mode where the transient stability enhancement is achieved with suitable pitch angle generation.

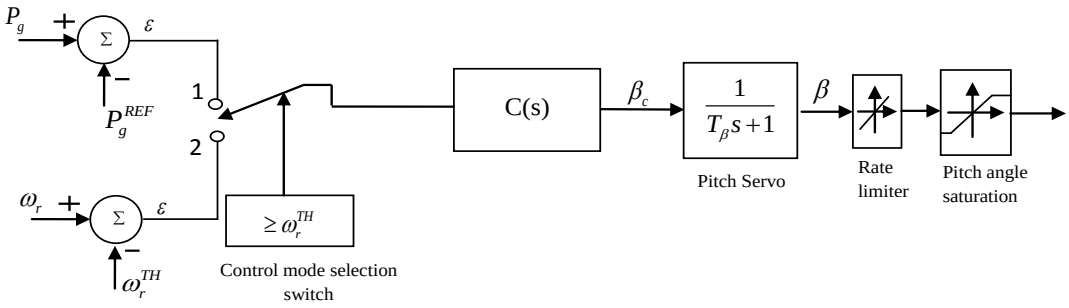

Figure 3.9: A typical pitch angle controller in power and speed control modes

In order to achieve the effective performance of the wind energy system, the controller C(s) of pitch control system need to be designed with an effective control method.

3.6.1 Proportional Integral (PI) controller

A PI controller based pitch angle control system is as shown in Figure 3.10. The PI controller has designed using linearized model of the WES where *Ziegler-Nichols* method is employed to determine the controller gains in an appropriate way. During the above rated wind speed the PI controller is used to regulate the output power at its rated value by generating suitable pitch angle. Though, this method has a simple structure, better steady-state response and easy to implement, but exhibit poor transient response due to fixed controller gains. Therefore, the alternative method for controller design is fuzzy logic. It has numerous advantages as they do not require the mathematical model of the system and are capable of handling nonlinearity. In addition, they achieve excellent dynamic responses.

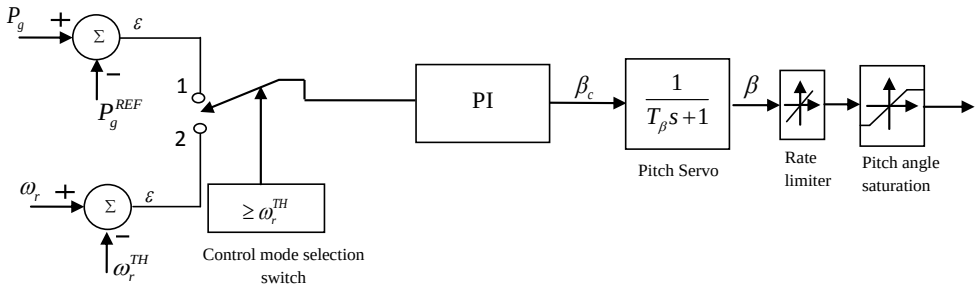

Figure 3.10: Proportional-Integral (PI) based pitch angle controller

3.6.2 Design of fuzzy logic controller (Type-1FLC)

In 1965, Professor Lofti Zadeh has proposed the concept of fuzzy logic. It consists of fuzzifier, inference engine and de-fuzzifier. Here, the fuzzifier converts the crisp value of the input parameter into fuzzy set and depending upon the fuzzy rules framed based on the membership functions for a given parameter of the system and then, fuzzy outputs are obtained with the help of the inference engine. In the end, de-fuzzifier converts these fuzzy inputs to a crisp output of the FLC to be used for the control purpose.

The employed fuzzy logic based pitch angle controller is shown in Figure 3.11.

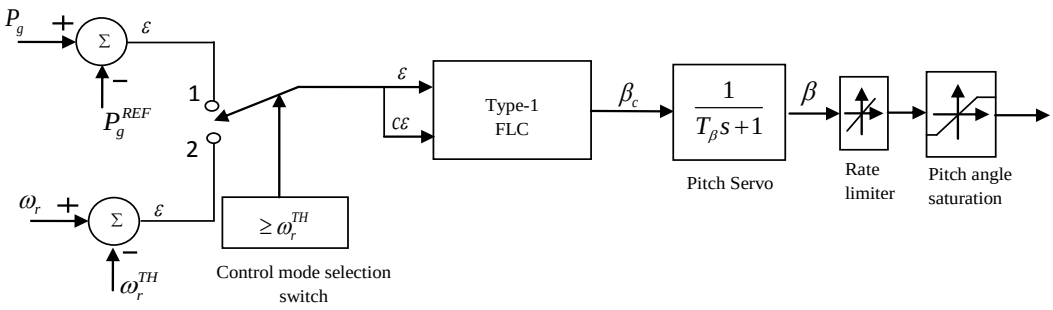

Figure 3.11: Fuzzy logic (Type-1) based pitch angle controller

3.6.3 Type-2 FLC based pitch angle controller

The Figure 3.12 shows the proposed Type 2 FLC based pitch angle controller. According to selection switch as discussed above the error ($\mathcal{E}$) signal of power or speed control modes passes through the Type-2 FLC algorithm from where it generate the suitable pitch angle.

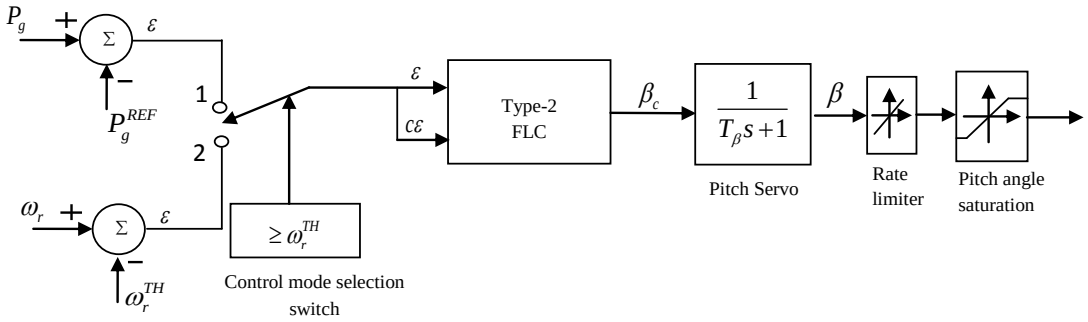

Figure 3.12: Proposed Type-2 FLC based pitch angle controller

The MFs and rules framed for the Type-1 and Type-2 FLCs as given in Figure 3.13 and Table 3.1, respectively.

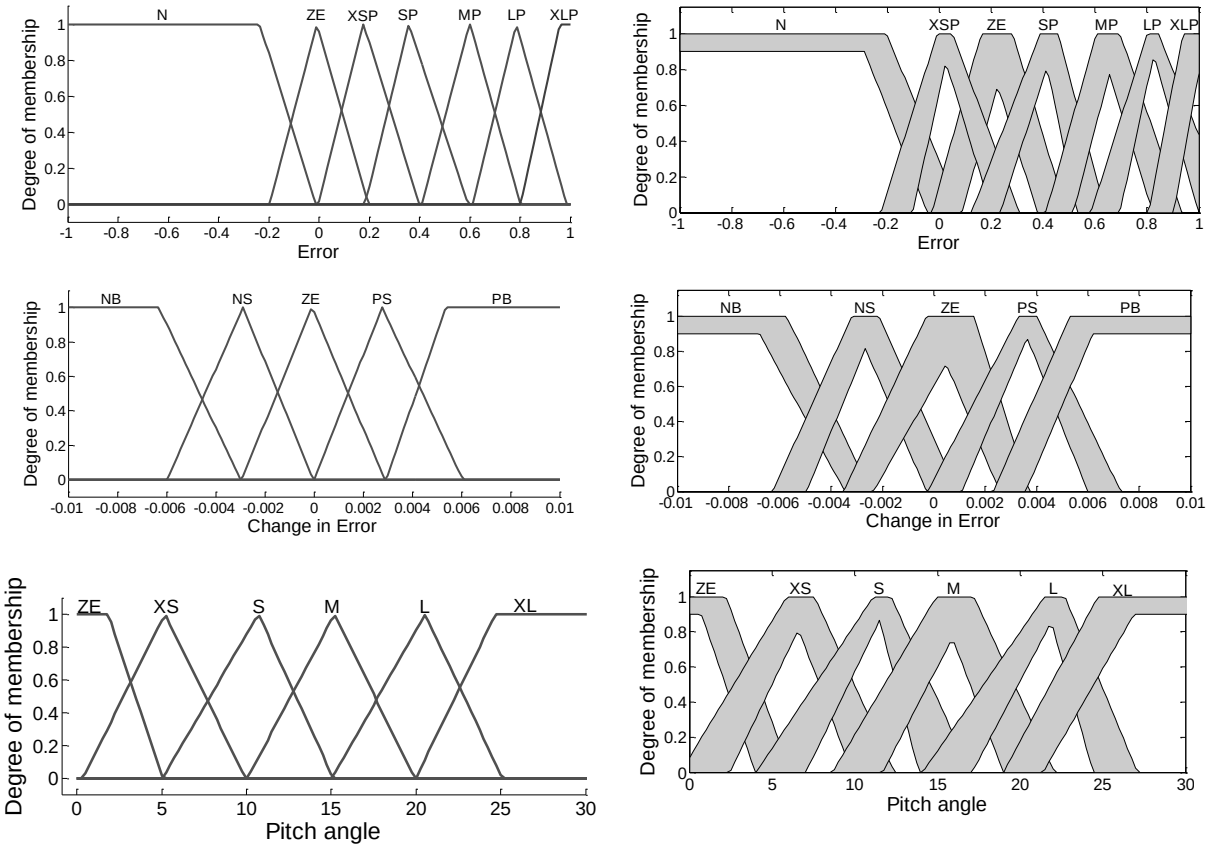

(a)Type-1FLC

(b) Type-2 FLC

Figure 3.13: The designed input and output MFs (a) Type-1 FLC (b) Type-2 FLC

Table 3.1: Fuzzy rules table for pitch angle generation

Change in Error ($\mathcal{CE}$)	Error ($\mathcal{E}$)						
	N	ZE	XSP	SP	MP	LP	XLP
NB	ZE	ZE	ZE	XS	S	M	L
NS	ZE	ZE	XS	S	M	L	XL
ZE	ZE	ZE	XS	S	M	L	XL
PS	ZE	ZE	XS	S	M	L	XL
PB	ZE	ZE	S	M	L	XL	XL

The triangular membership functions (MFs) employed for design the input and output variables of Type-1 and Type-2 FLCs are depicted in Figure 3.13. The fuzzy sets for error ($\mathcal{E}$) have been defined as: XLP(Extra Large Positive), LP(Large Positive), MP(Medium Positive), SP(Small Positive), XSP(Extra Small Positive), ZE (Zero) and N(Negative). For the change-in-error ($\mathcal{CE}$) the fuzzy sets chosen as ZE (Zero), NB (Negative Big), PB (Positive Big), NS (Negative Small), and PS (Positive Small). While for the output pitch-angle control, six membership functions have been defined and notation as XL (Extra Large), L (Large), M (Medium), S (Small), XS (Extra Small) and ZE (Zero). The MFs are selected based on prior knowledge and observations from the various simulation results.

The major function in the inference engine is the rules' implementation, aggregation and type reduction. With help of the experts' knowledge on the pitch-angle control of the wind energy system, a control strategy is framed as set of IF-THEN rules and are:

If ($\mathcal{E}$ is x_1) and ($\mathcal{CE}$ is y_1) then (β_c is w_1)

Similarly, 35 rules have been defined for all input-output MFs as shown in Table 3.1.

The common defuzzification methods used for the Type-2 FLC are the first (or last) of maxima, centroid-of-area and mean-of-max methods. In this study, centroid-of-area method has been utilized which is the most reasonable and popular method among the others. The centroid of the Type-2 fuzzy set is the collection of centroids of all of its embedded sets. The defuzzification method converts the output fuzzy to crisp value. Therefore, the output (for example power control mode) of pitch angle controller can be obtained as:

$$\beta^* = \frac{1}{T_\beta s+1}\beta_c' \tag{3.23}$$

Where $\beta_c' = \frac{\Delta\beta}{\Delta P}\left(P_g - P_g^{REF}\right) + \beta_i$

The starred value is the final output of the pitch controller, whereas the prime term is the outputs of the Type-2 fuzzy controller.

3.6.4 Configuration of the System

A typical wind energy system consisting of a wind turbine driven induction generator (IG) is as shown in Figure 3.14. The stator winding of the IG is connected to the point-of-common-coupling (PCC) through a step-up transformer (0.69/25kV) which exports power to the 120kV grid through step-up transformer (25/120kV) and a transmission line ($R_{TL} + jX_{TL}$) operating at 120kV. The rotor of the IG is driven by a variable pitch wind turbine. The power factor correction capacitor(C) is connected to the low voltage terminal of the wind turbine generator. It provides required amount of reactive power to the IG for reasonable terminal voltage. The design parameters of the generator and the wind turbine are presented in Appendix.

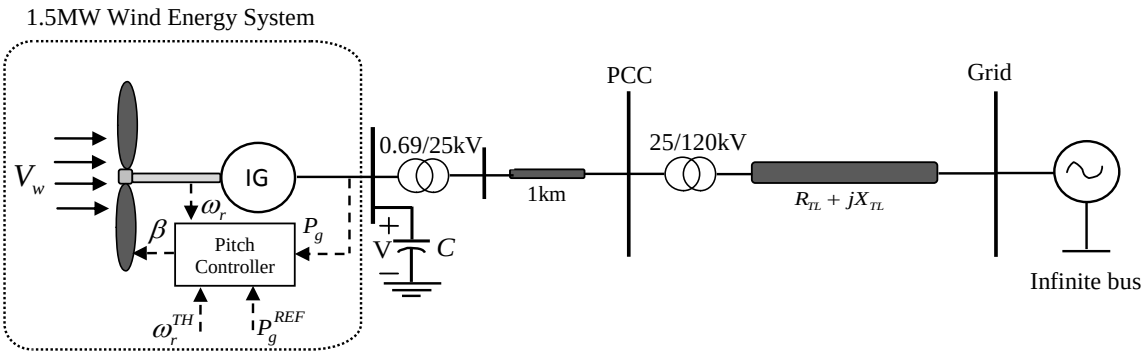

Figure 3.14: Single-line diagram of the studied grid-connected WES

3.6.5 Steady-state operating characteristics of the studied WES

In this sub-section, the WES has been analyzed under steady-state operating conditions at different wind speeds. The Figure 3.15(a)-(c) illustrate the steady-state operating conditions of the studied system where the wind speed is varied from cut-in wind speed (V_{wCI} of 4 m/s) to the cut-out wind speed (V_{wCO} of 24 m/s). Whereas the rated wind speed (V_{wR}) is 14 m/s. The various quantities of the wind energy system such as real, reactive power, voltage, current, rotor speed and the variation in pitch-angle of the wind turbine are shown in Figure 3.15(a)-(c).

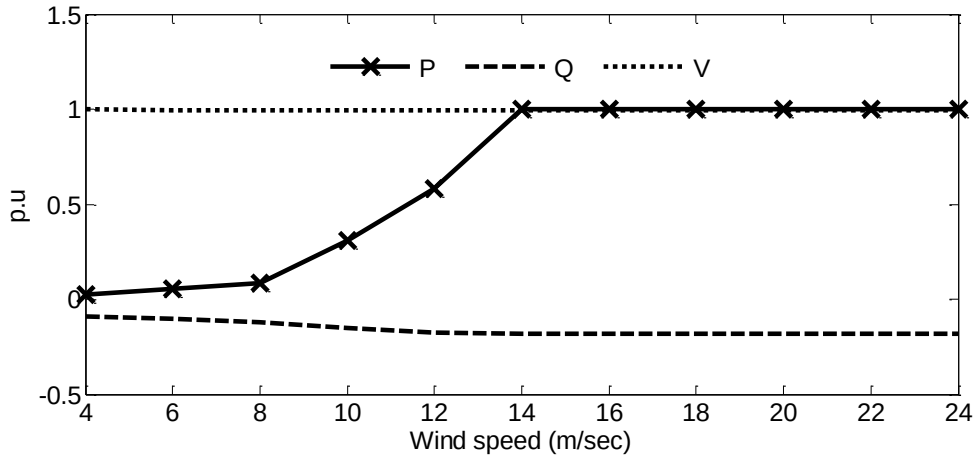

(a)

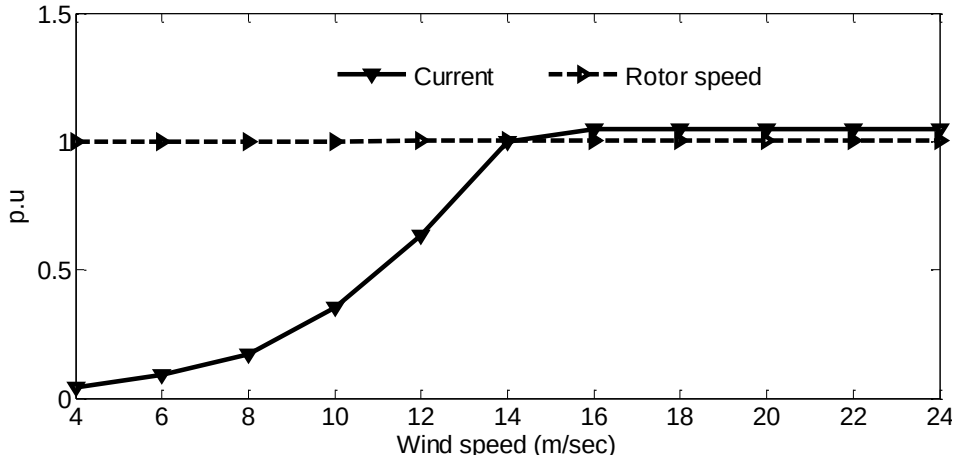

(b)

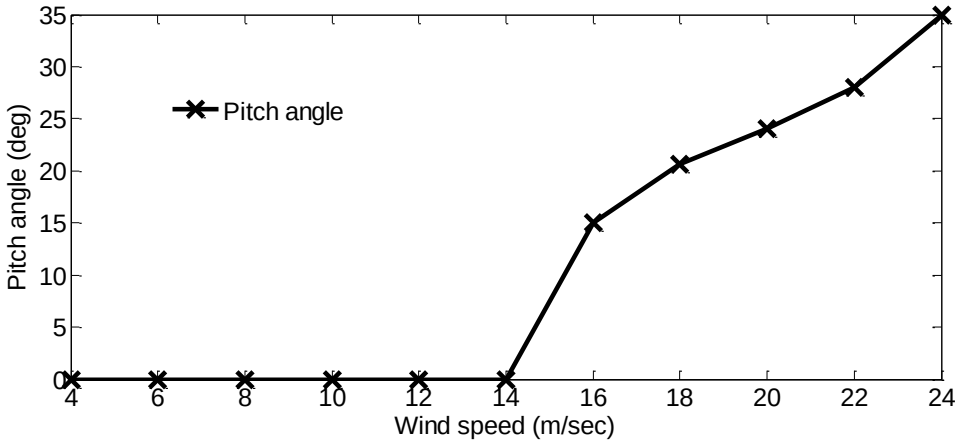

(c)

Figure 3.15: Studied system operating conditions under various values of wind speed (a) Wind Generator active (P), reactive power (Q) and voltage (V). (b) Wind Generator rotor speed and current (I) (c) Wind turbine pitch angle profile

It is seen from the Figure 3.15 that as the wind speed (V_w) is varied from V_{wR} to V_{wCO}, all quantities of wind energy system are maintained at steady values except the pitch angle.

(i) It can be observed from Figure 3.15(a) that the wind generator (WG) output voltage (V) is maintained around 1.0 p.u. for all values of wind speed (V_w).

(ii) When the wind speed varies from V_{wCI} to V_{wR}, both wind energy system real power output (P) shown in Figure 3.15(a) and the current (I) shown in Figure 3.15(b) increase almost linearly with the increase of V_w. Thereafter, both $\boldsymbol{P}$ and $\boldsymbol{I}$ are maintained at rated values when V_w exceeds V_{wR}, but the wind turbine pitch-angle (β) shown in Figure 3.15(c) increases almost linearly so as to control the active power as well as generator current within their rated values.

(iii) The WG reactive power output ($\boldsymbol{Q}$) increases slowly in negative direction, as shown in Figure 3.15(a), for the wind speed V_w below V_{wR} and then maintained at a constant value by the capacitor bank when V_w exceeds V_{wR}. With this, the power factor of the wind energy system can be maintained at a reasonable value.

(iv) It can be observed from Figure 3.15(b) that as V_w varies from V_{wCI} to V_{wR}, the rotor speed (ω_r) of the generator increases slowly from 1.0001 p.u. to 1.0045 p.u whereas, as the wind speed V_w exceeds V_{wR}, rotor speed remains almost constant at 1.0045 p.u. It has accomplished with the help of pitch-angle control of the wind turbine as shown in Figure 3.15 (c). It is observed that as the wind speed V_w exceeds the rated value V_{wR}, the pitch-angle continuously increases from 0^0 (at rated wind speed V_{wR},) to around 35^0 (at cut-out wind speed V_{wCO}).

3.6.6 Results and Discussions

In order to observe the applicability of the proposed Type-2 FLC based pitch-angle controller, a test system as shown in Figure 3.14 has been employed. Two cases (case 1: windy condition and case 2: a transient fault in the grid) have been considered to analyse the performance of the proposed controller. To show the efficacy of the proposed controller, the simulation results obtained are compared with conventional PI, and Type-1 FLC.

3.6.6.1 Case 1: Windy condition

In this case, the effectiveness of the proposed controller has been investigated for a given wind speed pattern as shown in Figure 3.16 which consists of variation of wind speed in the ranges - above, below and rated wind speeds. It can be observed from wind speed pattern that the wind speed varies at randomly – some time goes below rated value, sometime attains rated value of 14 m/s and sometime even blows with speeds above rated value. With this wind speed variation, a solid three-phase-to-ground fault is initiated to occur on the PCC at 30s for the duration 150s where the wind speed is below. The results of the WES with all the controllers have been presented in Figure 3.17 to Figure 3.20.

When the fault occurred at 30s, at which the wind speed is below rated. It is seen that the generator rotor speed did not cross the threshold rotor speed and therefore, the pitch angle controller did not operate in speed control mode. Moreover, in below rated wind speed region, all the controllers are able to extract maximum energy and hence, no generations of pitch-angle till 50s (see Figure 3.20). Therefore, it can be observed from Figure 3.16 and 3.17, response of WES in terms of its real power output follows the same trend as the wind speed pattern in the absence of pitch-angle control (no role of pitch control system) whenever the wind speed is below rated value.

On the other hand, whenever the wind speed exceeds its rated level, the pitch-angle controller operates in power control mode to maintain the power output to its rated value. It is observed from the generator output power as shown in Figure 3.17 that during the above rated wind speed, though PI controller maintains the power at rated value but it has significant oscillations which vary from around 1.38MW to 1.68MW. If this fluctuating power is exported to grid, it results in frequency variation. Therefore, the fuzzy logic controller (Type-1FLC) employed here suppressed power oscillations up to some extent but, when we introduced Type-2 FLC the power fluctuations drastically damped out as compared to Type-1 FLC. Therefore, the pitch-angle controller equipped with Type-2 FLC in power control mode offered lower overshoot compared to PI and Type-1 FLC and hence produced quality of power output. Almost similar trends are observed in the reactive power and rotor speed as depicted in Figure 3.18 and Figure 3.19, respectively. The pitch-angle profile of the wind energy system is as shown in Figure 3.20. However as observed from Figure 3.20 that the pitch-angle variations with Type-2 FLC are of smaller amplitudes than PI and Type-1 FLC and therefore, pitch-actuator system using Type-2 controller utilizes less energy to change the blades orientation.

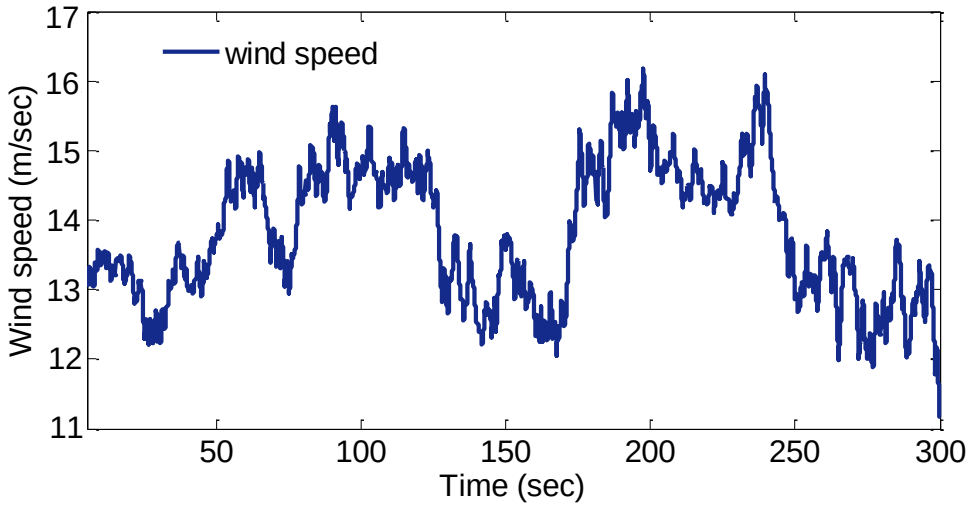

Figure 3.16: Wind speed profile

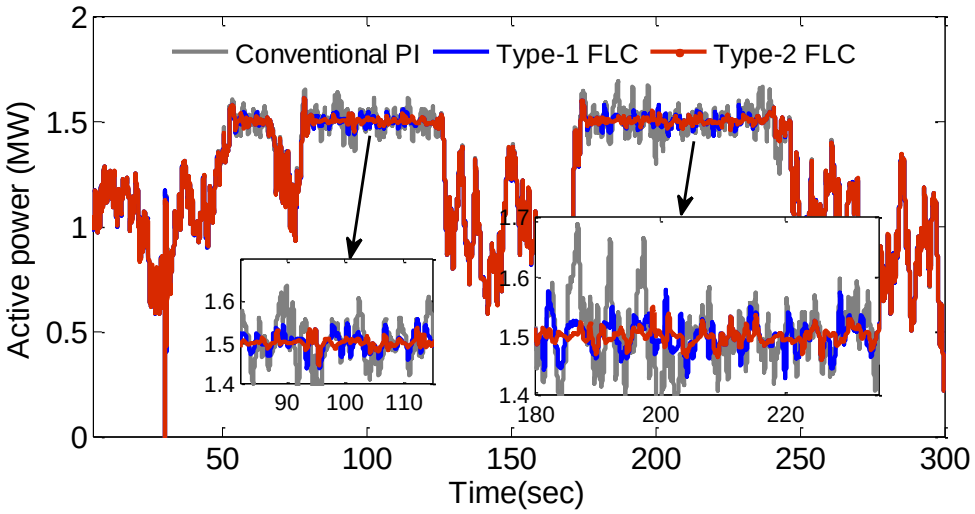

Figure 3.17: Generator active power

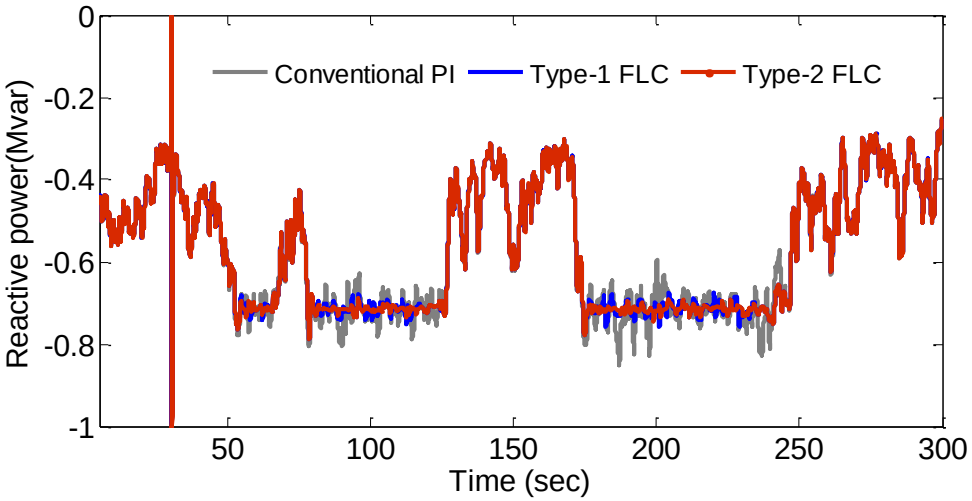

Figure 3.18: Generator reactive power

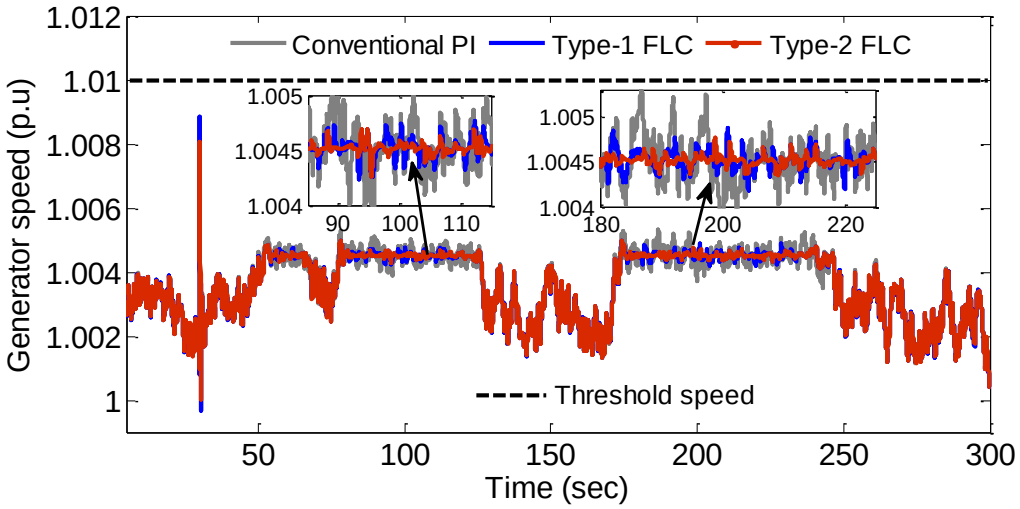

Figure 3.19: Generator rotor speed

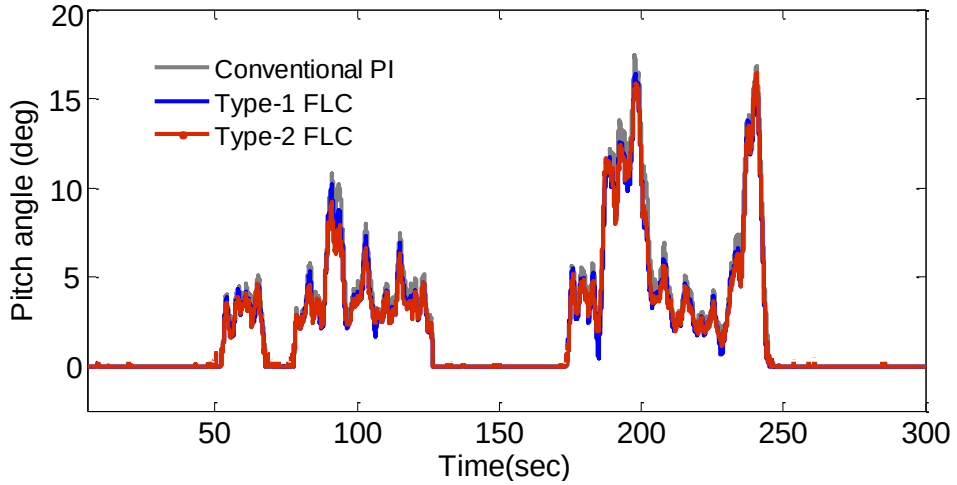

Figure 3.20: Pitch angle generation by different controllers

3.6.6.2 Case 2: Transient fault

In this case, the transient performances of the WES with all the controllers are investigated. Here wind speed is assumed as constant and maintained at rated level, the fault has been initiated from 10s to 10.15s. After the fault occurs, the generator rotor speed start increasing rapidly and when the rotor speed surpasses the threshold rotor speed (1.01p.u), the pitch-angle controller enters into the speed control mode to bring WES into stable state as shown in Figure 3.21 to Figure 3.23. It is noted from Figure 3.24 that the increase of the pitch angle causes the mechanical torque to decrease (as shown in Figure 3.23) resulting in decrease in rotor speed (as shown in Figure 3.21). All the controllers (PI, Type-1 and Type-2 FLCs) are working well in speed control mode of pitch-angle controller during transient fault condition. However, due to effective pitch-angle generation by the type-2 FLC, the mechanical torque reduces to around 0.87p.u (see Figure 3.23, whereas with PI and Type-1 FLC it is around 0.96p.u and 0.945p.u, respectively. As a result, the maximum rotor speed variation with Type-

2 FLC limited to about 1.0175p.u only, whereas with PI and Type-1 FLC it is approximately 1.019p.u and 1.024p.u, respectively. Therefore, the proposed Type-2 FLC offered better transient performance than conventional PI and Type-1 FLC. As the pitch-angle controllers limit/control the mechanical torque, it control rotor speed and consequently the generator power. Therefore, the active power of generator obtained with all types of controller is as shown Figure 3.22. It noticed that active power also damped more effectively with proposed Type-2 FLC controller.

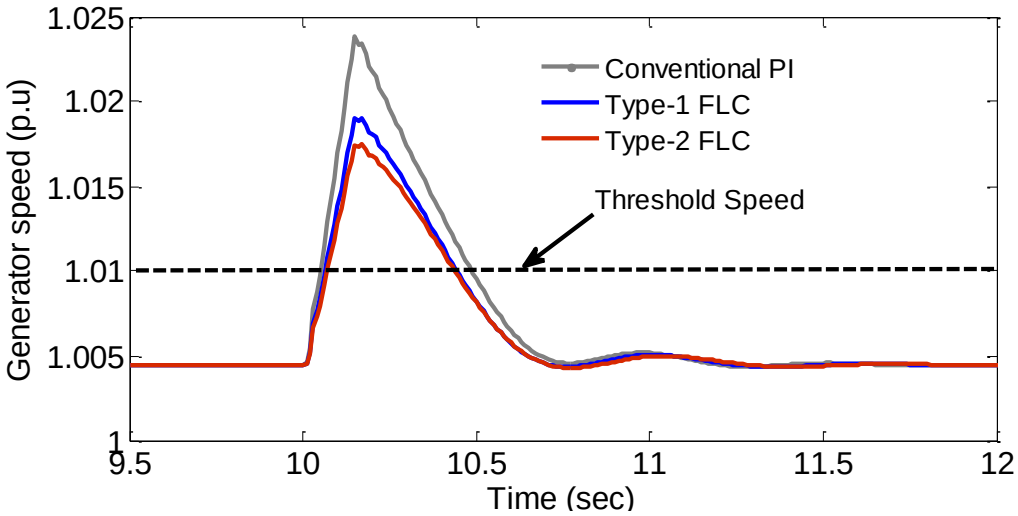

Figure 3.21: Generator rotor speed

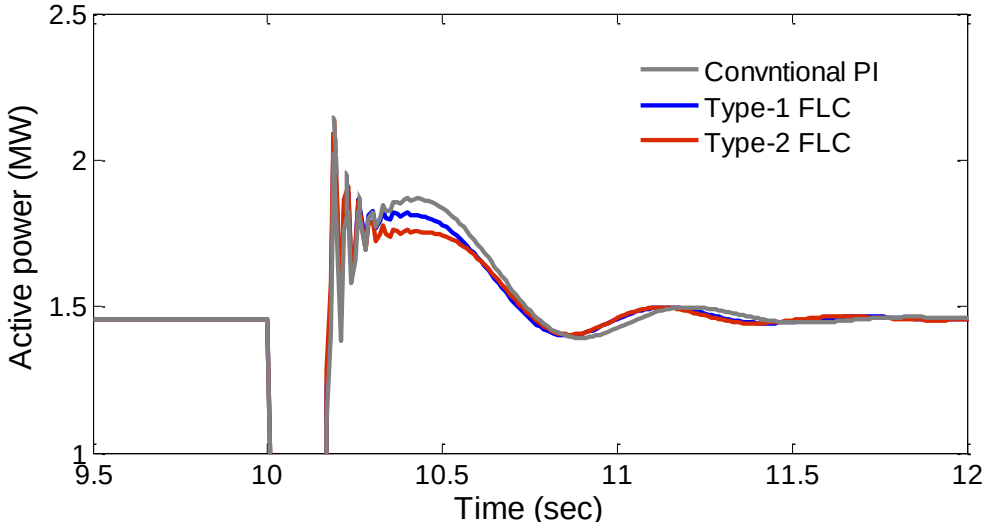

Figure 3.22: Generator active power

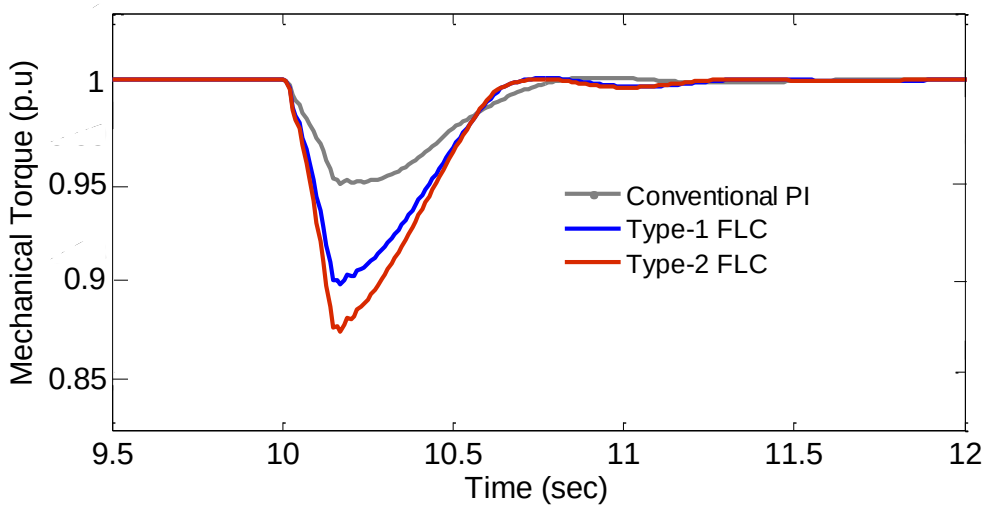

Figure 3.23: Generator mechanical torque

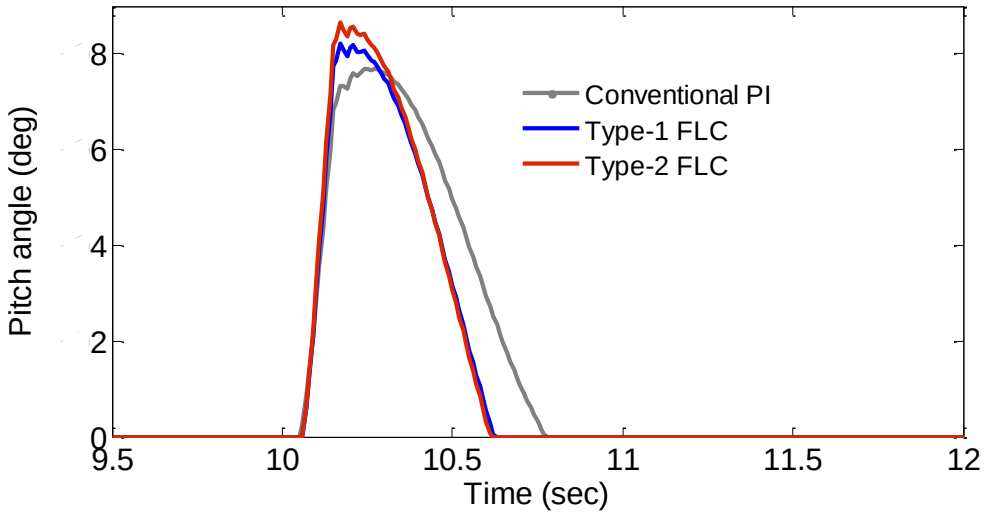

Figure 3.24: Pitch angle generation by different controllers

The control surface of the type-2 FLC uses the Karnik Mendel type reduction algorithm which results in very smooth surface by aggregating the outputs of large number of embedded type-1 fuzzy sets [194]. This smooth surface will consequently make it less sensitive to uncertainties in parameters and disturbances, offering a very good control performance. As illustrated in Figure 3.25, the designed control surface of the type-2 fuzzy controller is much smoother than that of type-1 fuzzy logic controller counterpart, which further supports the claim that the performance of the proposed controller is superior than the PI and type-1 FLC.

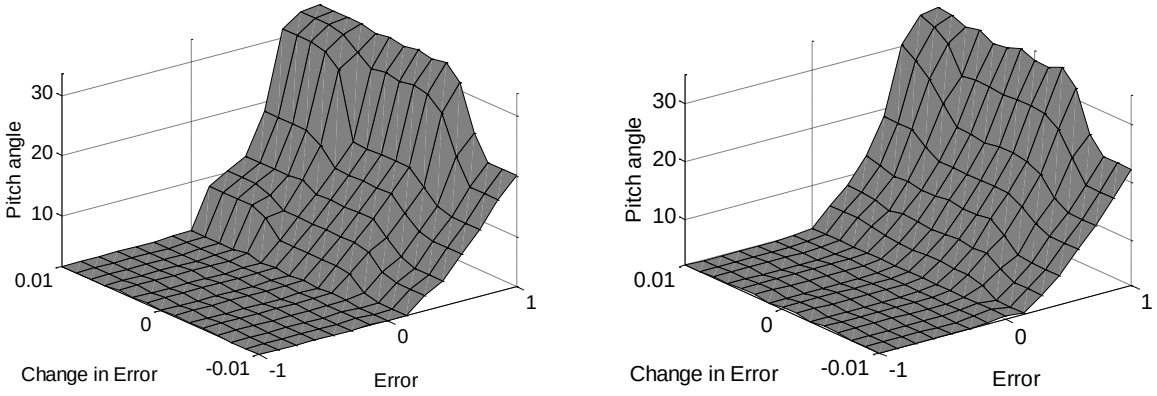

(a)Type-1 FLC (b) Type-2 FLC

Figure 3.25: Fuzzy control surfaces for (a) Type-1 FLC (b) Type-2 FLC

3.7 Output power smoothing using pitch angle control

As discussed, wind generator output power varies with wind speed, resulting in fluctuations in the grid frequency and voltage. It is, therefore, becoming a major concern as the wind power installations are increasing in number. Hence, in this work, a pitch-angle controller has employed to smoothing the generator output power. *However, one major challenge in wind power smoothing is setting of reference power, specially, when the wind speed is below its rated value*. Constant reference power is not always a good choice as there may be some cases where the wind speed is below the rated wind speed and appropriate output power cannot be obtained. As a result, exponential moving average (EMA) is the best suited to generate a reference power. Thus, in this thesis, EMA concept has been implemented and incorporated to the pitch-angle controller to generate reference power. Later on, Type-2 FLC technique is proposed for pitch angle controller in order to smoothing out the wind generator output power more effectively when it subjected to varying wind speed.

3.7.1 Computing of reference power command (P_{gCMD}^{REF})

In order to obtain the output power smoothing, an essential task is to calculate the reference power (P_{gCMD}^{REF}) for the pitch-angle controller. Different approaches [114] have been presented to determine the reference power command. However, exponential moving average (EMA) method offers better performance. The superiority of the EMA method over other approaches is that it follows wind speed quickly [114].

The numerical expression for EMA is given as

$$\mathrm{EMA}=\left[\left(\mathrm{C\text{-}P}\right)\times\mathrm{K}\right]+\mathrm{P} \tag{3.24}$$

Where C is the current value, the previous period's of EMA is P, and K is weighting factor. For period based EMA, weighting factor (K) is equal to 2/ (1+N), where N is the number of periods. A detailed explanation has presented in [114]. For example, for 50 periods EMA weighting factor K is calculated as: 2/(1+50)=0.0196. Figure 3.26(a) demonstrates the average EMA values calculated for a given wind speed. It can be observed that the EMA starts from 50secs (each of 1 period) onwards. However, in this work, the average EMA values are calculated for generated wind power (not for wind speed).

The reference power command (P_{gCMD}^{REF}) for the pitch-angle controller is calculated as follows:

Step 1: The wind turbine capture power (P_{WT}) can be obtained from equation (3.1).

Step 2: The average EMA value of captured wind turbine power ($\overline{P}_{WT}$) is calculated from equation (3.24). In this work, 50 periods of average value is used in simulation. Therefore, for every 50sec the EMA of the wind power computation has done. The EMA calculation are as follows: if the generated wind power is equal to 0.82MW at 50^{th} period and 0.81MW at 51^{st} period, respectively, the value of EMA at the time 51sec becomes [(0.81-0.82)*0.0196]+0.82=0.819MW. If wind power generated becomes 0.8MW at 52 sec, then the value of EMA at this instant calculated as [(0.8-0.819)*0.0196] + 0.8=0.799MW and so on.

Step 3: The standard deviation can be calculated as:

$$P_{WTstd}=\sqrt{\frac{\int_0^t\left(P_{WT}-\overline{P}_{WT}\right)^2 dt}{t}} \tag{3.25}$$

Step 4: Finally, the reference command power of the controller can be obtained as

$$P_{gCMD}^{REF}=\left(\overline{P}_{WT}-P_{WTstd}\right) \tag{3.26}$$

Figure 3.26(b) explains the whole calculation process of reference power command of this work.

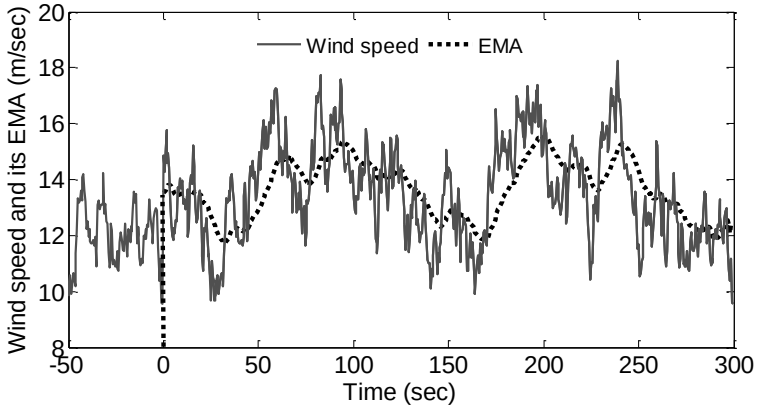

(a)

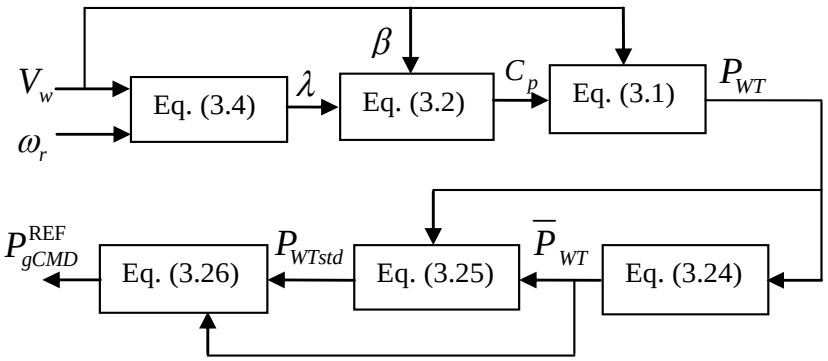

(b)

Figure 3.26: Diagram of EMA calculation (a) Comparison of wind speed and EMA (b) Computation of controller reference power command

3.7.2 Pitch-angle control design phase

In general, the wind turbine pitch-angle is not controlled until the rated power is generated. When the wind speed is above the rated speed, the pitch controller is activated to keep the output power at the rated level. In this section, a new pitch controller is presented where the turbine blade pitch angle is controlled even when the wind speed is below the rated speed. A typical pitch controller employed in this section is as shown in Figure 3.27. The controller gains K_e and K_d are used as a scaling gains for input and K_u for the output signals. These scaling gains can be variables or constants. During the FLC design these can play an important role to achieve suitable steady-state and transient responses. In this work, these gains considered to be constant and chosen as $K_e = 1$ $K_d = 100$ and $K_u = 10$.

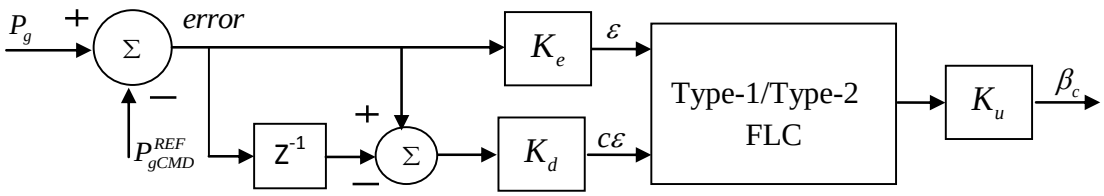

Figure 3.27: Pitch angle controller with Type-1/Type-2 FLC

3.7.3 Type-2 FLC design for the studied wind energy system

The MFs and rules are framed for the Type-1 and Type-2 FLCs as given in Figure 3.28 and Figure 3.29 and Table 3.2, respectively. The triangular MFs with overlap are used for the input and output fuzzy sets. For all the inputs and outputs, the universe of discourse is chosen as [-1, +1].

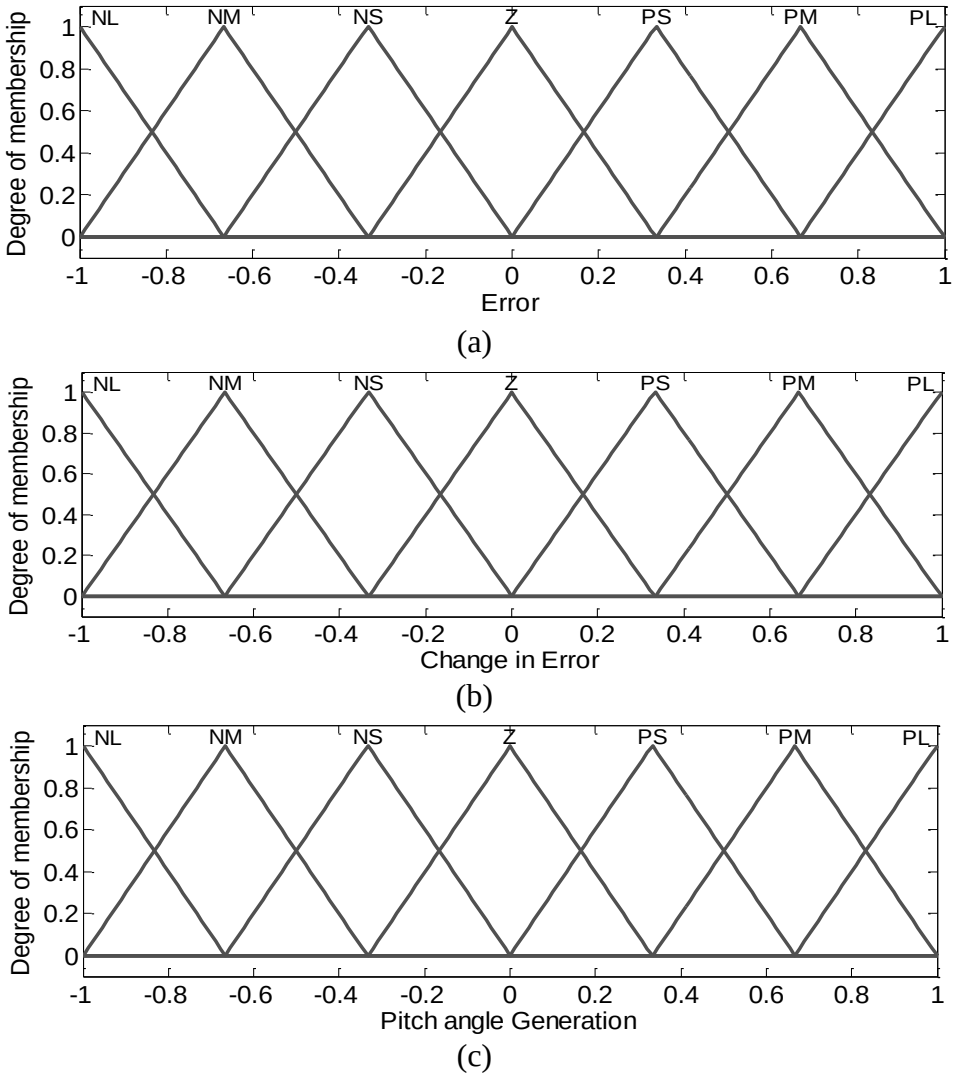

Figure 3.28: Designed MFs ofType-1 FLC (a) Error (b) Change in error (c) Pitch angle generation

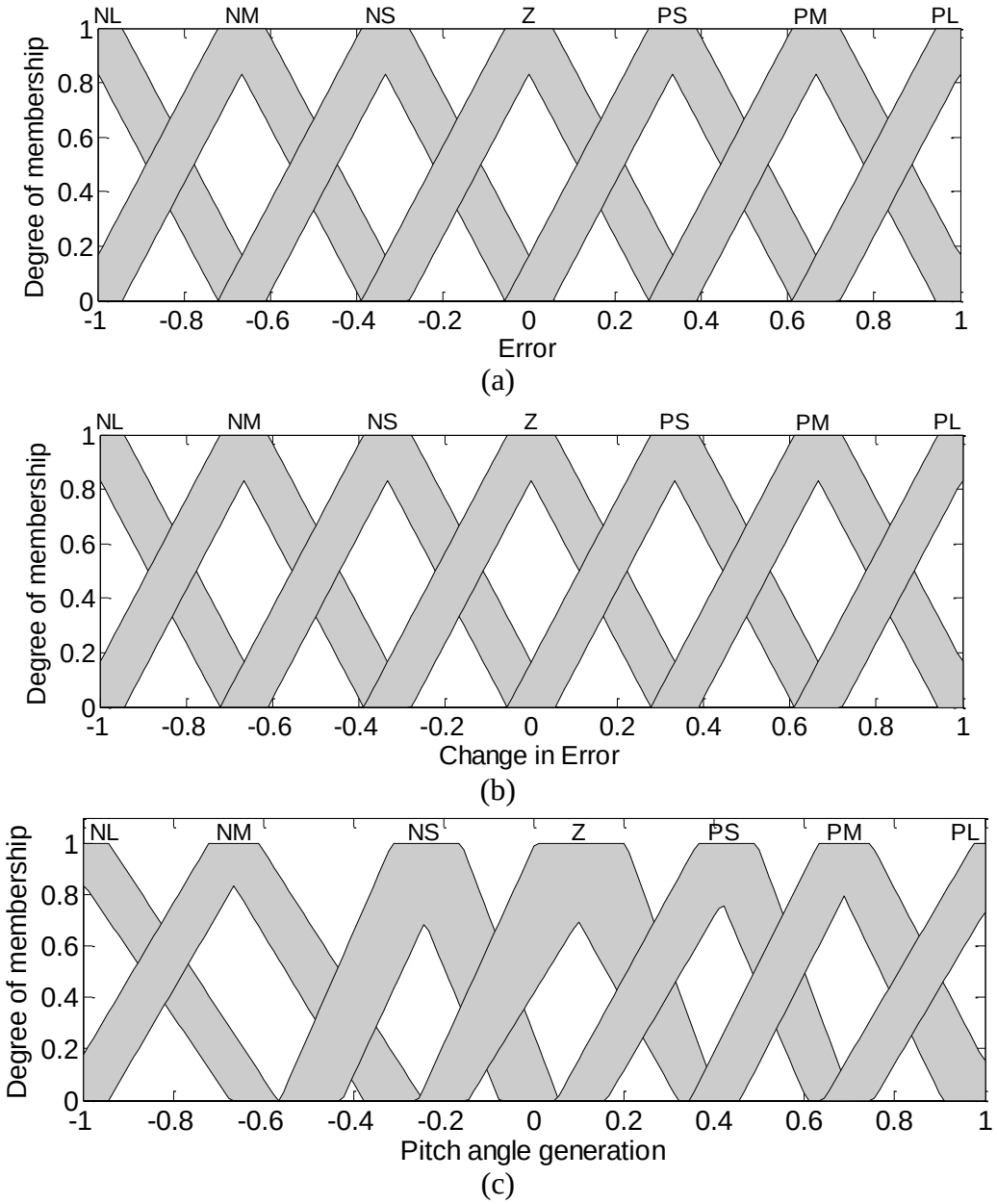

Figure 3.29: Designed MFs ofType-2 FLC (a) Error (b) Change in error (c) Pitch angle generation

The input and output variables used for the controller design are expressed with the help of fuzzy sets using seven triangular linguistic variables MFs. Notation for the fuzzy sets as: LP (Large Positive), MP (Medium Positive), SP (Small Positive), Z (Zero), SN (Small Negative), MN (Medium Negative), LN (Large Negative). The MFs are selected based on prior knowledge and observations from the various simulation results. The width of the FOU is decided by observing its effect on the WES output power oscillations. The similar MFs and rules have been designed for Type-1 and Type-2 FLCs to distinguish their performance subjected to wind speed variations.

With the help of the experts' knowledge on the pitch-angle control of the wind energy system, control strategies are framed as a set of IF-THEN rules, e.g.

If ($\mathcal{E}$ is x_1) and ($\mathcal{CE}$ is y_1) then (β_c is w_1)

Similarly, 49 rules have been defined for all input-output MFs as shown in Table 3.2.

Table 3.2: Fuzzy rules for pitch angle generation

Change in Error ($\mathcal{CE}$)	Error ($\mathcal{E}$)						
	LN	MN	SN	Z	SP	MP	LP
LN	LN	LN	LN	LN	MN	SN	Z
MN	LN	LN	LN	LN	SN	Z	SP
SN	LN	LN	MN	MN	Z	SP	MP
Z	LN	MN	SN	Z	SP	MP	LP
SP	MN	SN	Z	MP	MP	LP	LP
MP	SN	Z	SP	MP	LP	LP	LP
LP	Z	SP	MP	LP	LP	LP	LP

3.7.4 Real time simulation

The real time simulation of the studied system is carried-out on OPAL-RT digital simulator. The RT-lab, which is fully integrated with MATLAB/Simulink®, provides the flexibility and scalability to achieve the most complex real-time simulation applications in the power systems, power electronics, automotive, aerospace and industries [105, 135, 172]. The simulator uses advanced fixed-time step solvers (ARTEMIS) for strict constraints of real-time simulation of stiff systems. The sampling time used to realize the system is $50\mu s$. To run the models in real-time simulation, the RT-lab allows user to readily converted Simulink models through real-time workshop (RTW). The steps involved in implementation of MATLAB/Simulink model to real-time have been provided in detail in [106]. The RT-lab can

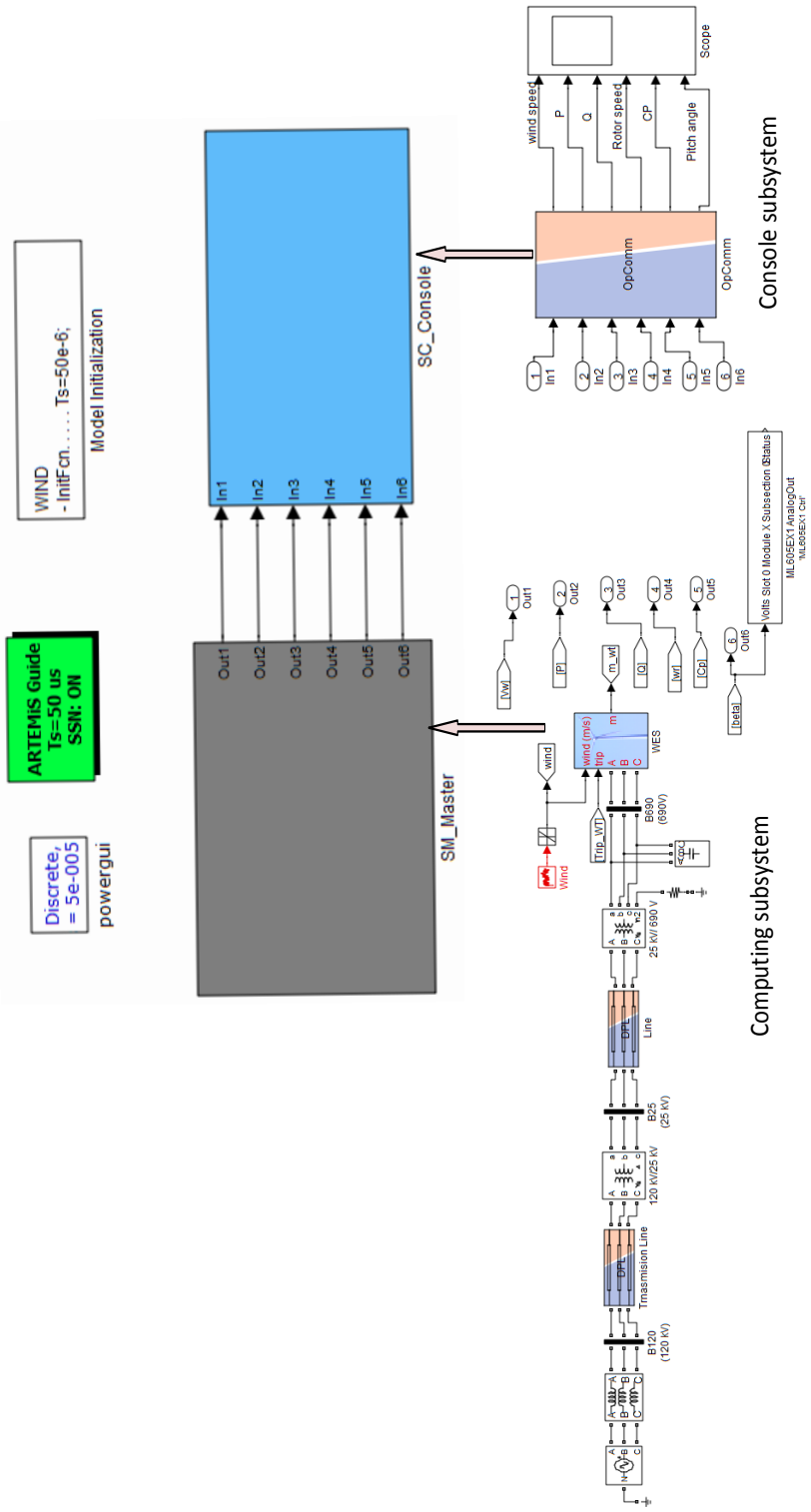

Figure 3.30: Distributed model of the WES for real time simulation

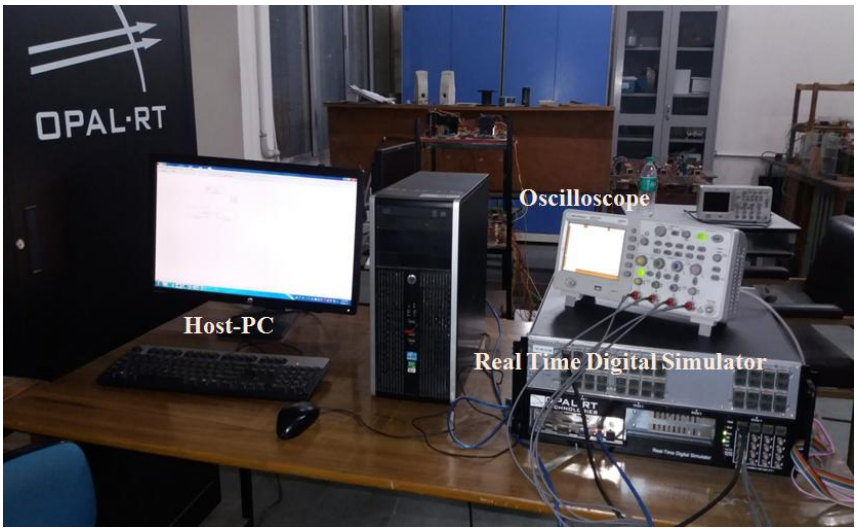

Figure 3.31: Real time digital simulator laboratory setup

separate a complex system into simple sub-systems and performs parallel operation in multiple cores. Hence, one needs to separate the model into suitable sub-systems for real time simulation [65, 190]. The studied WES as shown in Figure 3.14 can be divided into two sub-systems as shown in Figure 3.30. The console subsystem denoted as SC_Console which contains parameters accessing and displaying blocks. This sub-system runs on the host PC, which can receive simulation results and display through the scope. Another sub-system is a computing sub-system named as SM_Master which contains all the calculation blocks (of studied WES). This sub-system runs on the target machine with real-time condition.

The real-time digital simulation laboratory setup is as shown in Figure 3.31; it consists of host personal computer (Host-PC), target (real-time digital simulator) and oscilloscope. The simulator employed here is OP5600 with one processor and four 3.33-GHz dedicated cores to perform parallel computations. The work station computer (Host-PC) executes the WES model and interacts with the real-time digital simulator (RTDS) to produce the results of real-time simulation. The digital oscilloscope is also employed to observe the real-time results of pitch angle generation.

The results of Type-2 FLC are compared with Type-1 FLC and PI controller used, one at a time, for the pitch controller designed for the test WES. To present the effectiveness of the proposed controller, the following cases have been considered.

3.7.4.1 Case-1: Below rated wind speed

The wind speed pattern considered for below rated wind speed is as shown in Figure 3.32. Under this wind speed characteristics, the performance of the PI, Type-1 FLC and the proposed Type-2 FLC was investigated and the real-time simulation results were obtained through opcomm block for generator active power, generator rotor speed, power coefficient and pitch angle as shown in Figure 3.33 to Figure 3.36, respectively. When the wind speed is below rated value, there is no pitch angle generated with PI controller which ensures no point of limiting the rotor speed and the wind turbine operates with its maximum possible power extraction. As a result, the generator active and rotor speed followed the wind speed disturbances and exhibits huge fluctuations (see Figure 3.33 and Figure 3.34). If these fluctuating power exported to grid causes grid frequency to fluctuate.

Thus, it is needed to smoothen out these power fluctuations. For smoothing the output power fluctuations, at first it is required to determine the reference power command (P_{gCMD}^{REF}) as discussed in the previous sub-section 3.7.1 and thereafter, fuzzy logic approaches (Type-1 and Type-2 FLC) are implemented. These FLCs are good at tracking reference power (command power) irrespective of system operating conditions by generating a suitable pitch-angle. On comparing, it is observed from Figure 3.33 that the active power output of the wind energy system follows the command output power with small variations with Type-1 and Type-2 controllers but real power fluctuations are being smoothened more effectively by the Type-2 FLC pitch-angle controller. The similar results are also seen with generator rotor speed too, it has been more efficiently smoothen out by the proposed controller as shown in Figure 3.34. The power-coefficient of wind turbine with conventional PI, Type-1 and Type-2 FLCs controllers are as shown in Figure 3.35. The power-coefficient with PI controller is always maintained at its maximum value of 0.48, since there is no pitch angle generation. However, with Type-1 and Type-2 FLCs, the power-coefficient varies according to the pitch-angle variations in order to smoothing the output power. The pitch-angle profiles of the WES with all employed controllers are as shown in Figure 3.36. The pitch controller action with conventional PI, Type-1 and Type-2 FLCs are also observed in the digital oscilloscope and depicted in Figure 3.37(a)-(c). As there is no pitch angle generation with PI controller thus straight line (zero) has been observed in oscilloscope (see Figure 3.37(a)). But with Type-1 and Type-2 FLCs pitch-angle activity has been achieved and recorded in the digital oscilloscope as shown in Figure 3.37(b) and (c), respectively.

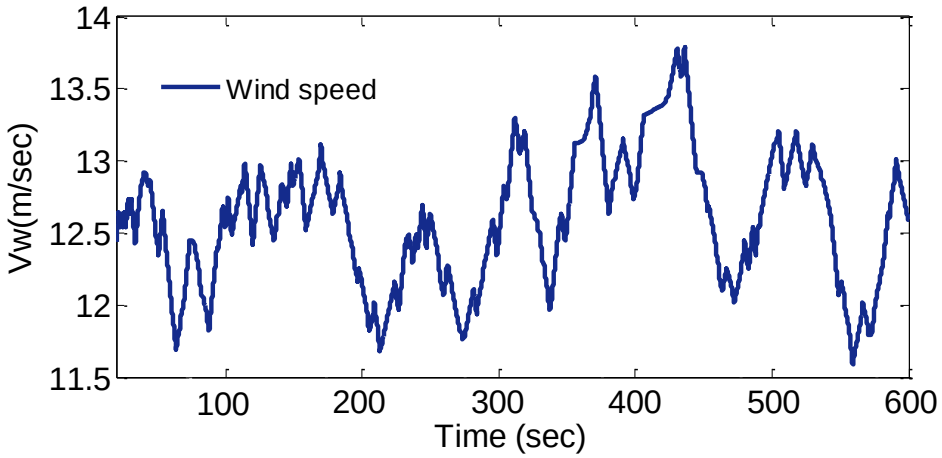

Figure 3.32: Below rated wind speed profile

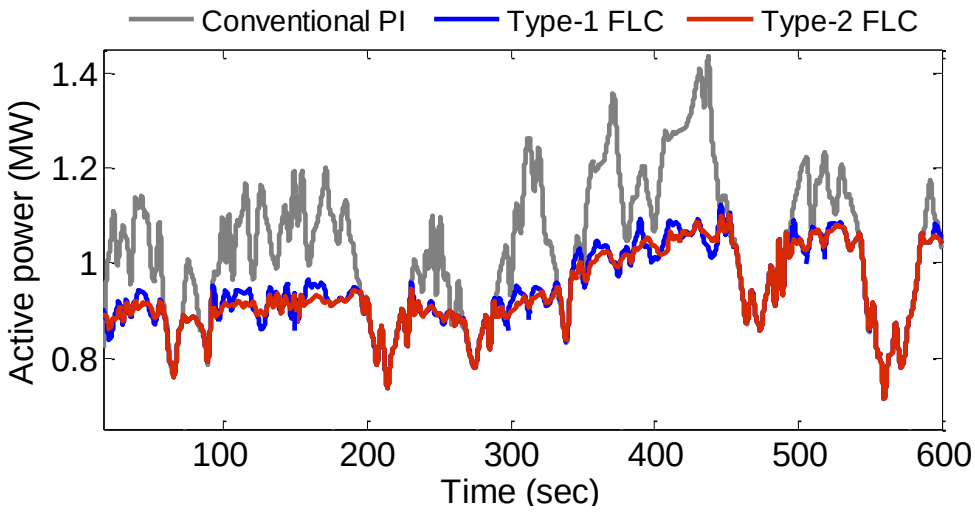

Figure 3.33: Generator active power

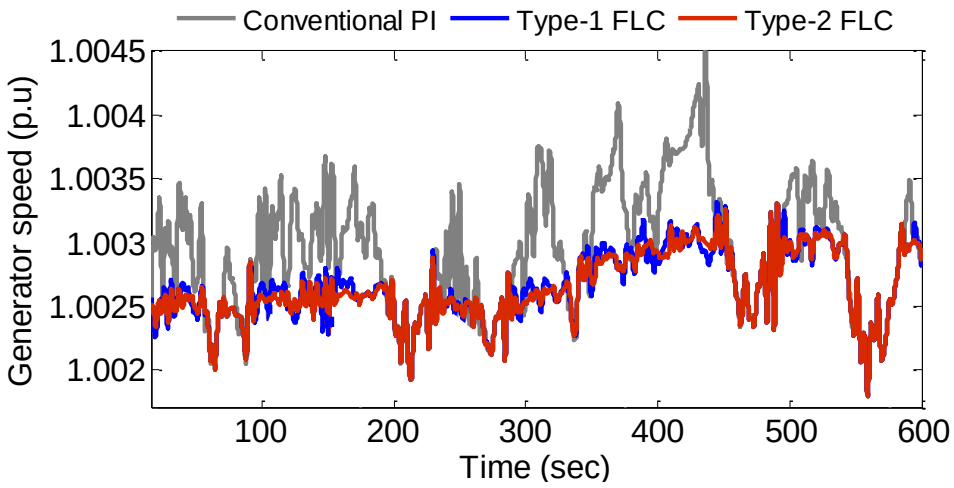

Figure 3.34: Generator rotor speed

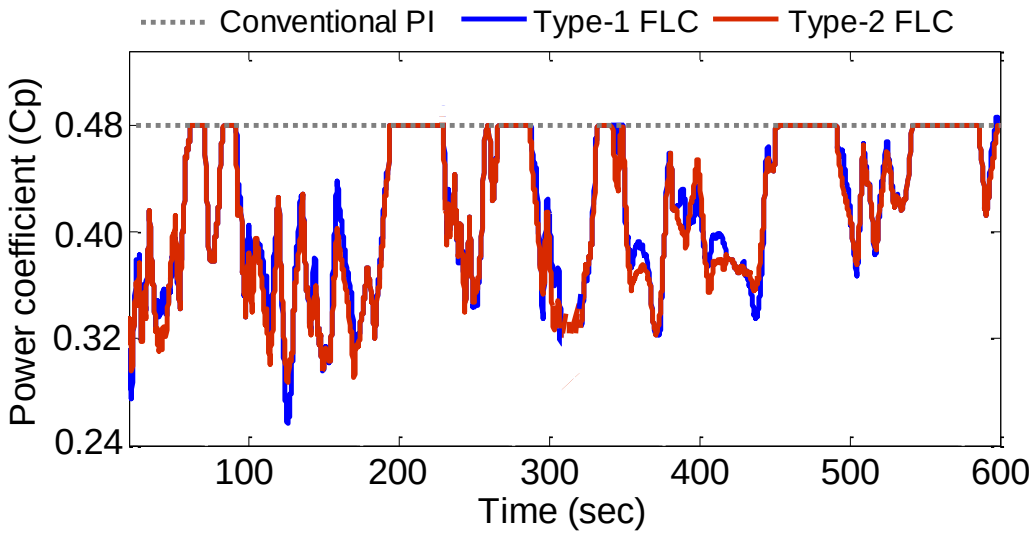

Figure 3.35: Power coefficient

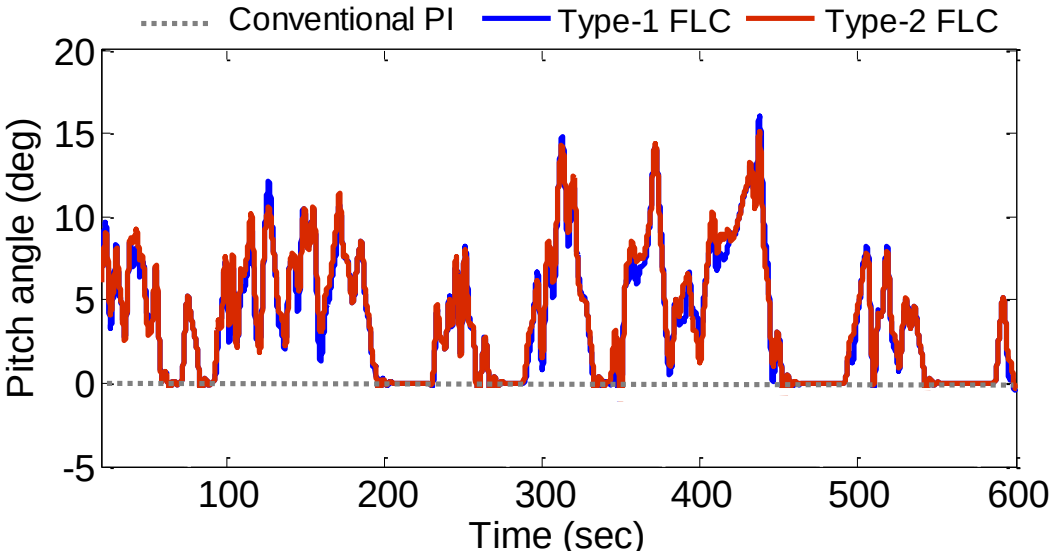

Figure 3.36: Pitch angle generation by different controllers

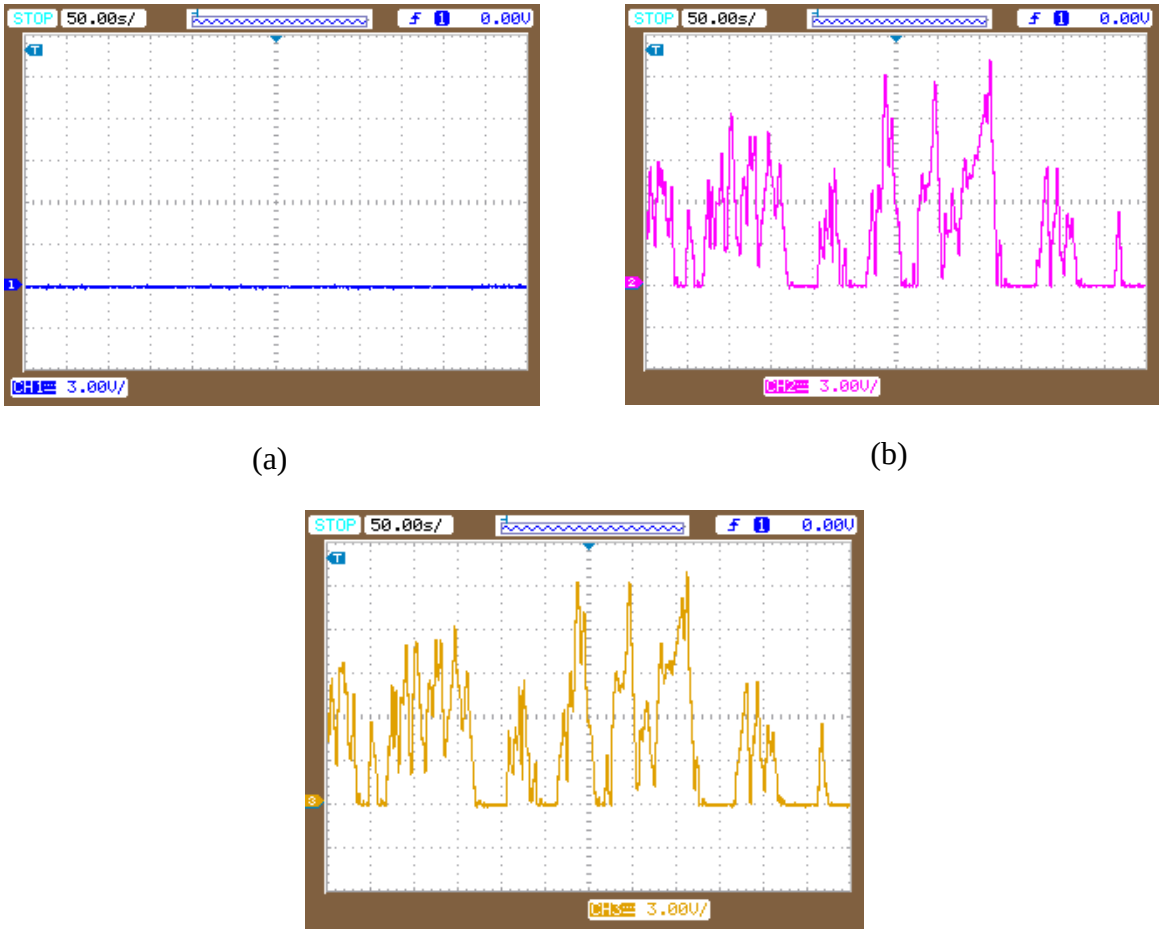

(a) (b)

(c)

Figure 3.37: Pitch angle profile obtained in oscilloscope (a) PI controller (b) Type-1 FLC (c) Type-2 FLC

3.7.4.2 Performance indices

To estimate the performance of the proposed technique (Type-2 FLC) with PI and Type-1 FLC, the output power smoothing P_{smooth} and maximum energy ($W_{\max}$) functions are calculated as [26]:

$$P_{smooth} = \int_0^T \left| \frac{dP_g(t)}{dt} \right| dt \tag{3.27}$$

$$W_{\max} = \int_0^T P_g(t) dt \tag{3.28}$$

Where, P_g is the generated output power and T is the total simulation time. In equation (3.27), P_{smooth} is the integral of the absolute value for the differentiation of the generated output

power P_g. Thus, if P_{smooth} is small in magnitude, it indicates that the generated power fluctuations of the wind energy system are smoothen-out more effectively. The Figure 3.38 shows that the power smoothing function with Type-2 FLC method has smaller magnitude as compared to PI and Type-1 FLC throughout the wind speed pattern considered.

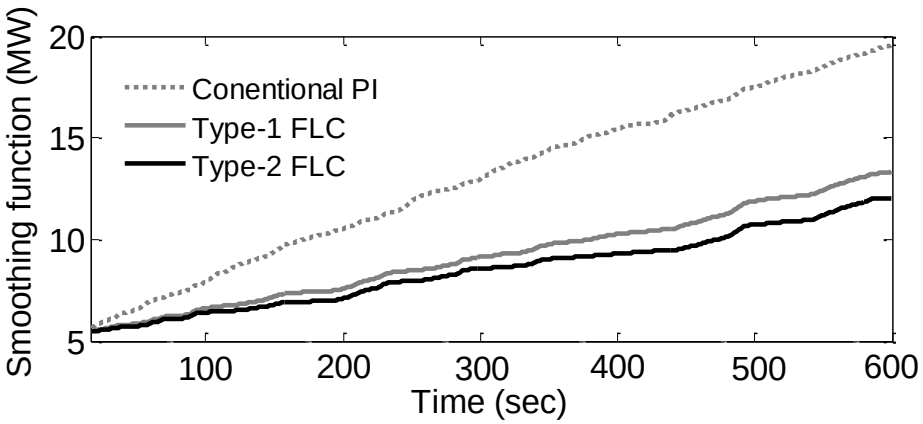

Figure 3.38: Generator output power smoothing index

Using equation (3.28), the maximum energy output of WES over the disturbance period was also determined considering all the three controllers but one at a time. The trend is as shown in Figure 3.39. The maximum energy has been obtained with conventional PI controller, as there is no pitch angle generation it remains fixed at zero degree. But with Type-1 and Type-2 FLCs there is a drop in the output power due to pitch angle generation. The purpose of this work is to smoothing the output power and thus drop cannot be avoided. From the Figure 3.39, the percentage of drop during the 600sec for Type-1 and Type-2 FLCs are calculated with respect to PI controller. The energy losses of Type-1 and Type-2 FLC (with respect to the conventional PI controller) are respectively, 30.02% and 30.31% approximately.

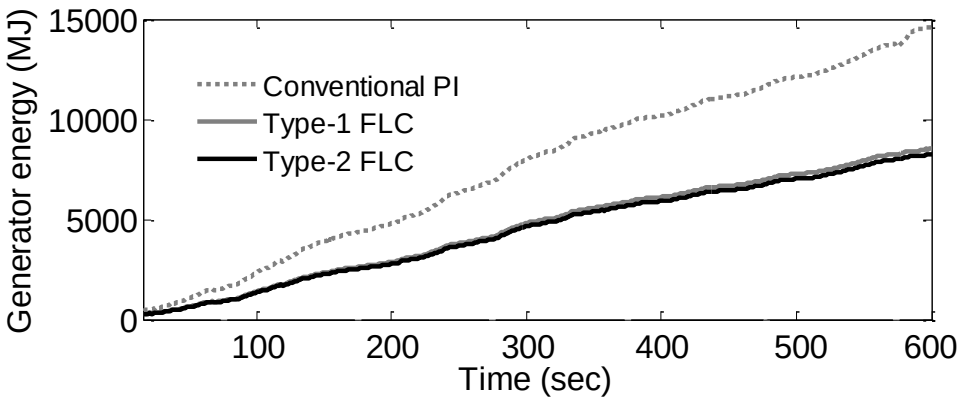

Figure 3.39: Generator total energy generation index

3.7.4.3 Case-2: Moderate wind speed

In this case, the moderate wind speed pattern has been considered i.e wind speed consists both below and above rated trends as shown in Figure 3.40. Similar trends have been observed from the active power and rotor speed of the WES system as shown in Figure 3.41 and Figure 3.42. From the simulation results, it is clear that compared to PI, Type-1 FLC and the proposed Type-2 FLC give much better smoothing for the generator output power. The power-coefficient and pitch-angle responses of the WES are also presented in Figure 3.43 and Figure 3.44, respectively. The pitch-angle generations with all the controllers are also recorded in the digital oscilloscope as shown in Figure 3.45(a)-(c).

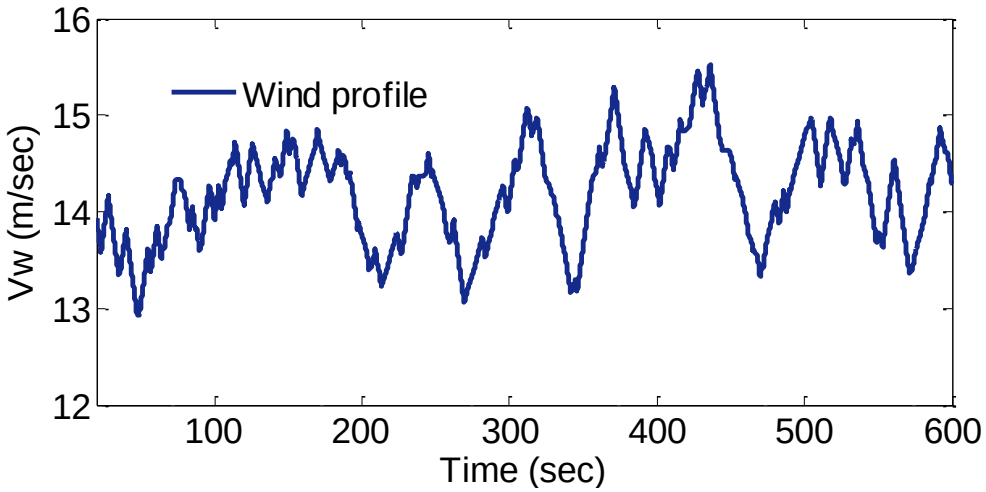

Figure 3.40: Moderate wind speed profile

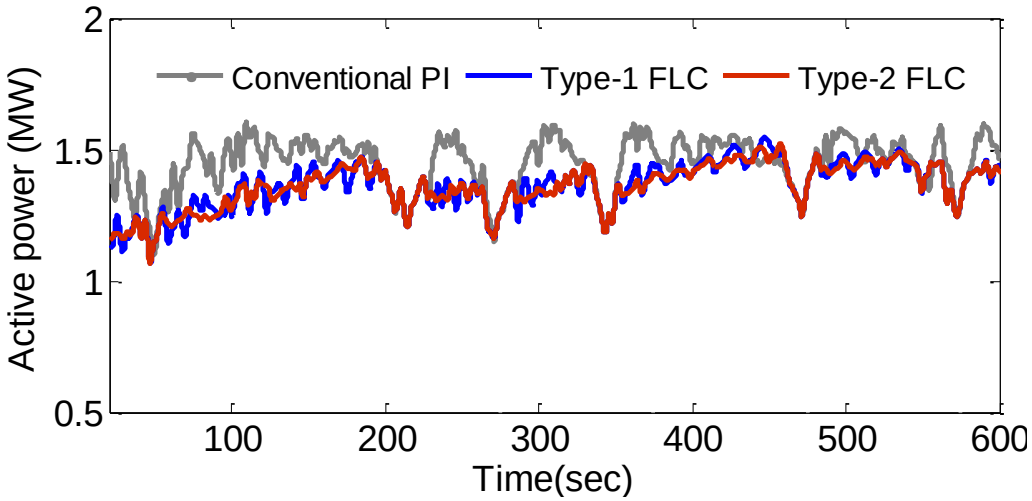

Figure 3.41: Generator active power

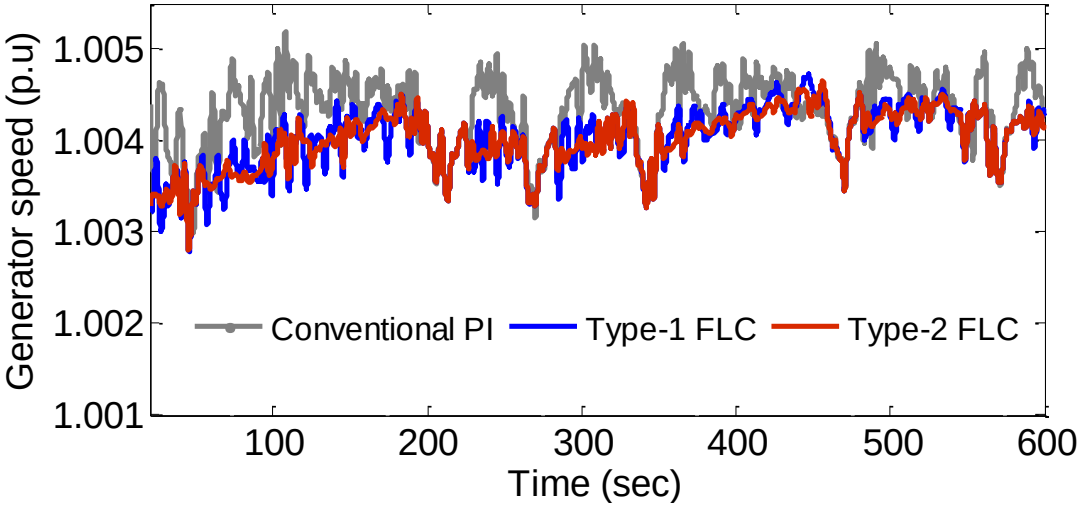

Figure 3.42: Generator rotor speed

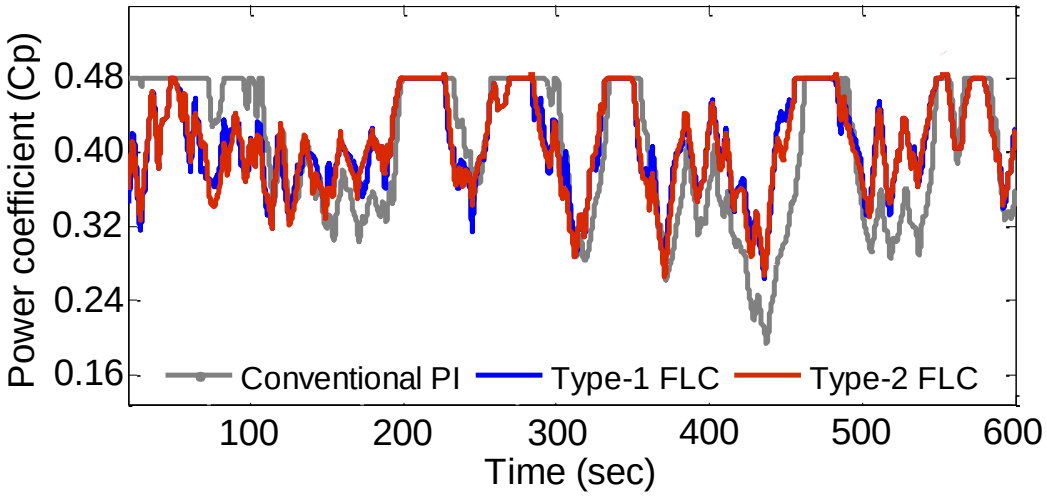

Figure 3.43: Power coefficient

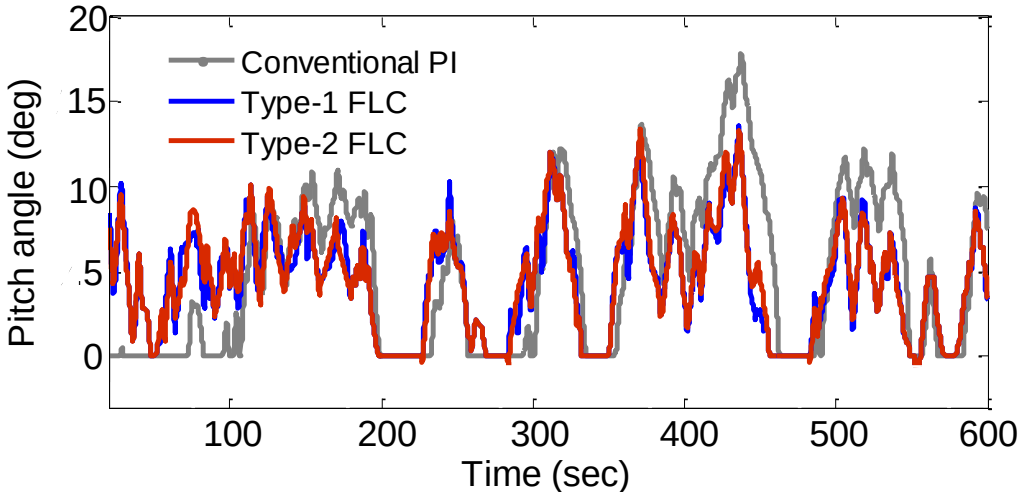

Figure 3.44: Pitch angle generation by different controllers

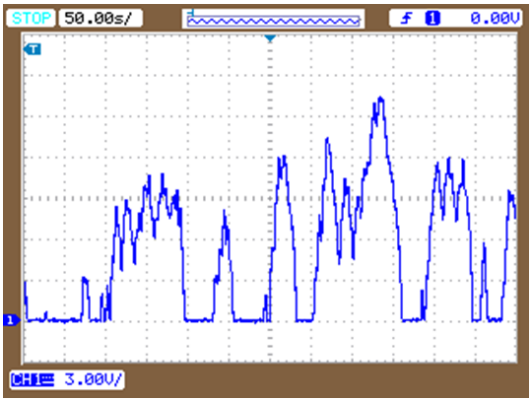

(a)

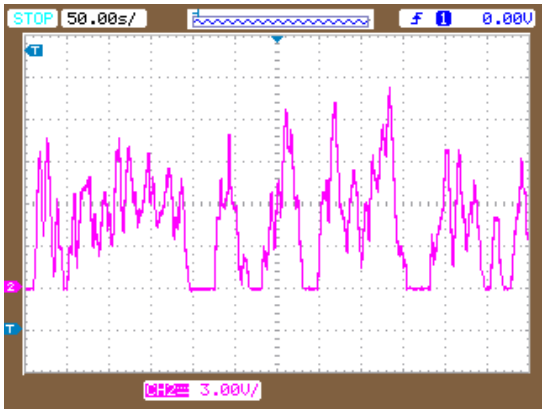

(b)

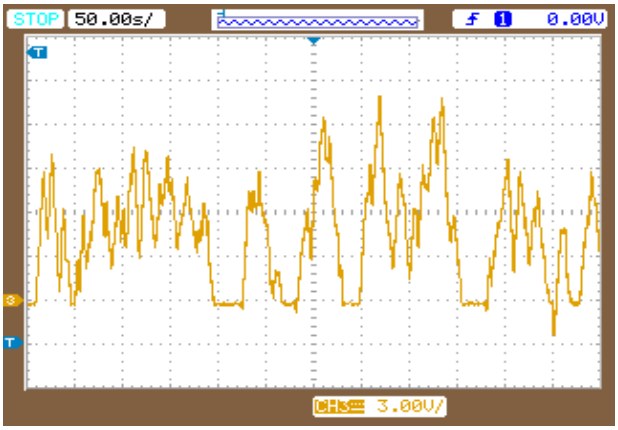

(c)

Figure 3.45: Pitch angle profile obtained in oscilloscope (a) PI controller (b) Type-1 FLC (c) Type-2 FLC

The smoothness function (performance indices) for this case with all the controllers is presented in Figure 3.46. It is seen that lower value denotes better smoothness and hence, the proposed Type-2 FLC based pitch angle controller offered smoother results than PI and Type-1 FLC. The total energy generation of IG with PI, Type-1 and Type-2 FLCs are obtained from equation (3.28) are as shown in Figure 3.47. The percentage of energy loss for Type-1 and Type-2 FLCs are calculated as approximately 4.32% and 4.51%, respectively with respect to PI controller response.

The obtained control surfaces of the type-1 and type-2 controllers are shown in Figure 3.48(a) and (b), respectively. It is observed from Figure 3.48 that as its control surface is formed with large number of embedded Type-1 FSs, the proposed Type-2 controller surface is very smooth as compared to Type-1 FLC. This smooth surface is less sensitive to disturbances and therefore, its effect is clearly visible on the responses of the wind generator output power as shown in Figure 3.33 and Figure 3.41.

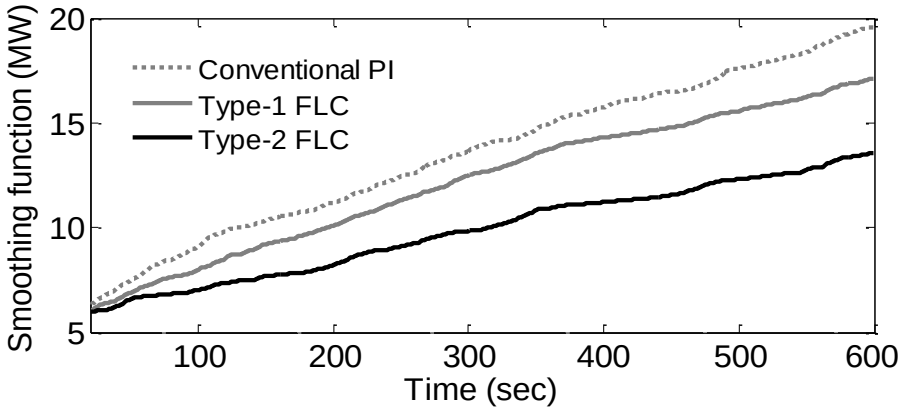

Figure 3.46: Generator output power smoothing index

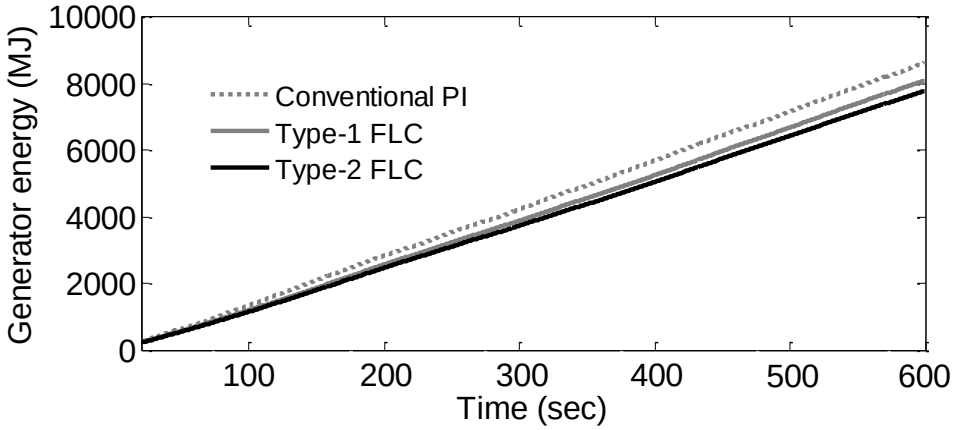

Figure 3.47: Generator total energy generation index

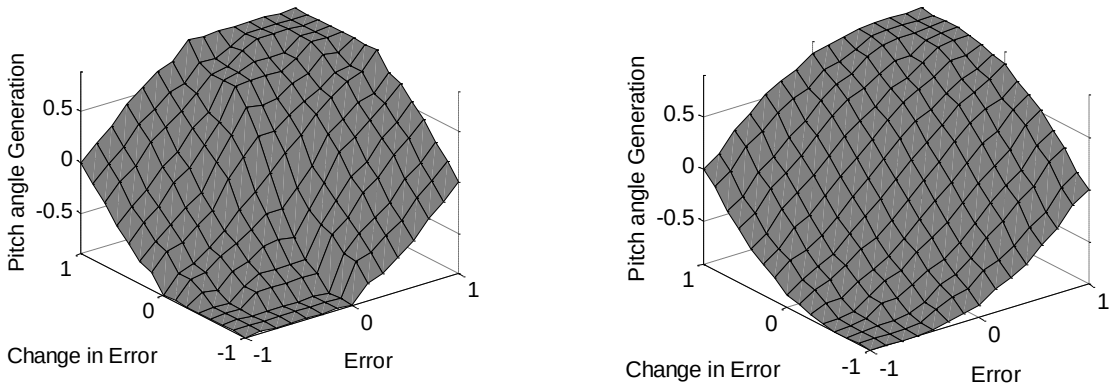

Figure 3.48 Fuzzy control surfaces for (a) Type-1 FLC (b) Type-2 FLC

3.8 Conclusions

In this chapter, a Type-2 fuzzy logic based pitch-angle controller is proposed for wind energy system to achieve major objectives such as enhancement of transient stability and generator output power smoothing.

In the first objective, pitch-angle controller implemented in power and speed control modes equipped with Type-2 FLC is investigated. Two cases (windy and transient fault) have been considered to operate pitch-angle controller in both, power and speed control modes. Simulation results of the pitch-angle controller equipped with Type-2 FLC compared with Type-1 FLC and PI controller. The proposed Type-2 FLC based pitch-angle controller out-perform in power quality and transient stability improvement, which are the main drawbacks of this type of IGs. Moreover, an analytical approach has been introduced from which some key factors that may affect the transient stability of the IG were investigated. This type of investigation is very important to expand the operating limitations of the wind turbine driven IG under the severe faults to guarantee the wind farm connection to the grid.

Concerning the generator output power smoothing, a Type-2 FLC based pitch-angle controller is proposed for WES when it subjected to varying wind speed. At first, reference power command based on EMA concept is obtained and then, fuzzy controllers (Type-1 and Type-2) are implemented to follow the reference power command. To validate the present work, the studied system has designed in MATLAB/Simulink and then exported to RT-lab via RTW for real time simulation. Two different types of wind speed patterns are employed to study the effectiveness of the proposed controller. The simulation results show the pitch-angle controller with Type-2 FLC offers better performance in smoothing the output power of WES than PI and Type-1 FLC. To estimate the smoothing level of proposed controller, power smoothing function (index) has been incorporated. Due to good output power smoothing achieved with proposed controller, the system frequency which is affected with power fluctuations can be controlled within the acceptable limit.

CHAPTER 4: STABILITY ENHANCEMENT OF FIXED SPEED WIND FARM USING STATCOM

4.1 Introduction

Modern wind energy systems (WES) nowadays utilize variable-speed Doubly-Fed Induction Generators (DFIGs) but fixed-speed wind farms still exist in the world in a considerable number due to their advantages. These wind farms generally employ Squirrel-cage Induction Generators (SCIGs) which are directly linked to the grid to export power. However, the main drawback of these wind farms is that they need large amount of reactive power during the disturbances such as network faults. Under such conditions, the terminal voltage and active power drastically decreases resulting in the increase of rotor speed, assuming the mechanical torque of SCIG to be constant. Though, the fault is cleared, but a large amount of reactive power is drawn by the induction generator during its speedup. If the needed amount of reactive power is not available, the machine will cause rotor to accelerate and make rotor speed unstable and gets disconnected from the grid. For cases in which fixed-speed wind farms supplying a large amount of active power to the network, they must stay connected to the grid. Therefore, the stability of wind farm becomes an important issue and therefore, has attracted considerable attention recently and hence, it is necessary to examine the responses of them during the faults and their possible impact on the system stability.

Moreover, these wind farms themselves are very sensitive to the grid faults and wind energy is a kind of stochastic energy implying that the output of wind farm can vary in a certain range. The inherent power fluctuations of these wind farms have adverse impacts on the power system to which they are connected. Therefore, we need to look for a novel controller design for wind integrated power system to improve its stability.

The contribution of this chapter: As a preliminary study, this chapter investigates the impact of fault ride-through on the stability of the fixed speed wind farm connected to power grid. The effect of fault locations and fault time durations on stability of fixed-speed wind farm, subjected to different types of faults were studied. Thereafter, a static synchronous compensator (STATCOM) has been employed to support the studied wind farm and its contribution to the different fault locations and durations are investigated.

Later on, an interval type-2 fuzzy logic based damping controller for STATCOM is proposed to achieve damping improvement which enhances the stability of wind integrated power system. To evaluate the effectiveness of the proposed method by comparative analysis,

three different scenarios (STATCOM-without damping controller, STATCOM-with type-1 FLC based damping controller and STATCOM-with type-2 FLC based damping controller) are considered. The performance of the proposed control scheme is analyzed by considering different network faults such as LLLG, LLG and LG. All the simulations are carried out on a test system using MATLAB/SIMULINK® software. The behaviour of the SCIG and the designing aspects of the STATCOM are discussed in the following sections:

4.2 SCIG terminal voltage and rotor speed relationship

From previous chapter 3, during the stable operation of wind power system, variation in slip of SCIG is very small and hence voltage equation can be expressed as [188]:

$$V_S \approx \frac{I_R}{|s| X_M} K_P \tag{4.1}$$

where $K_P = \sqrt{X^2 + Y^2}$ with

$$\begin{aligned} X &= -(sX_R R_S + sX_M R_S + X_M R_R + X_S R_R) \\ Y &= R_R R_S - sX_M X_S - sX_M X_R - sX_R X_S \end{aligned} \tag{4.2}$$

The relation between mechanical to electrical power with efficiency η is:

$$P_m = \eta . P_w \tag{4.3}$$

From the equations (3.5) and (3.10) the corresponding rotor current is:

$$I_R = \sqrt{\frac{\eta C_P(\lambda, \beta) K \omega_r^3 s}{3R_R}} \tag{4.4}$$

where, the slip (*s*) is defined as:

$$s = \frac{\omega_s - \omega_r}{\omega_s} \tag{4.5}$$

where, ω_s is the synchronous speed of SCIG.

From the equations (4.1), (4.4) and (4.5), the stator terminal voltage V_S of the SCIG can be written as:

$$V_S = K_R \sqrt{\frac{\omega_r^3}{|\omega_s - \omega_r|}} \tag{4.6}$$

where, $K_R = \frac{K_S \sqrt{\omega_s C_P(\lambda,\beta)\eta K}}{\sqrt{3R_R}\, X_M}$

From equation (4.6), the behaviour of generator terminal voltage (V_S) of SCIG is as shown in Figure 4.1, by taking the rotor speed as variable.

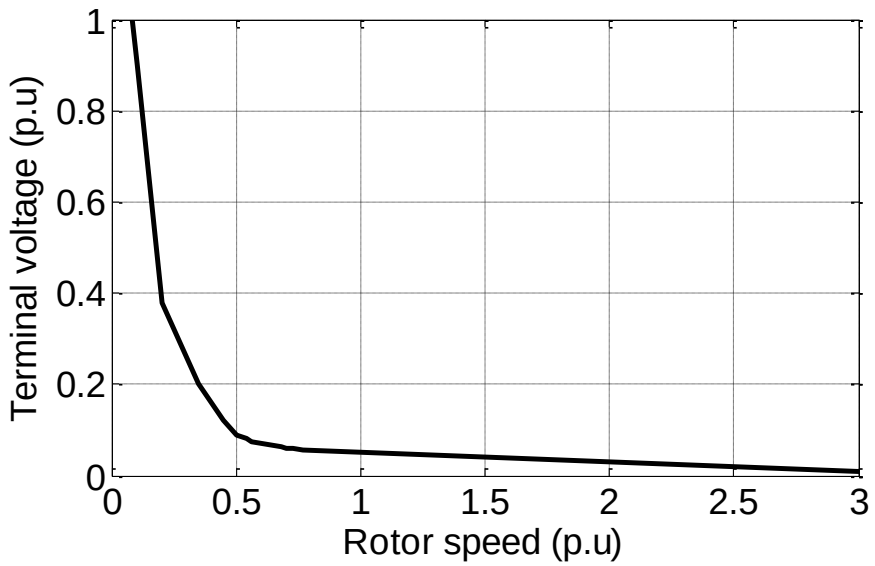

Figure 4.1: IG terminal voltage versus rotor speed characteristics

From Figure 4.1, it is observed that as the SCIG speeds up, its terminal voltage decreases very fast and reduces to a extremely low value.

4.3 STATCOM working principle

As described above, as the terminal voltage of the SCIG reduces because of its speeding up after the clearing of the network faults which may result in the possible dis-connection of SCIG. Therefore, to arrest this fall in the terminal voltage of SCIG and to provide necessary fault ride-through capability, an STATCOM is proposed to be installed at the PCC of the SCIG.

The topology of STATCOM can be classified in to two groups: voltage source converter (VSC) and current source converter (CSC). The VSC based STATCOM has efficiency relatively higher than CSC based STATCOM; therefore, in large scale wind farm it preferable [179]. In this work, we adopt VSC based STATCOM as a dynamic reactive power compensator.

The simplified basic equivalent circuit of STATACOM is as shown in Figure 4.2, where, V_s denotes the AC source, V_c is controllable STATCOM output voltage, R and X are the interfacing resistance and reactance, respectively. V_X represents the voltage drop across the

resistance and reactance and I^* is current flowing through R and X. This current can be leading or lagging to the source voltage (V_s), and the vector diagrams are as shown in Figure 4.3 and Figure 4.4.

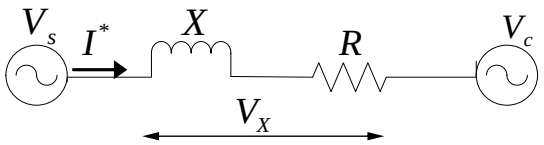

Figure 4.2: Basic equivalent circuit of STATCOM

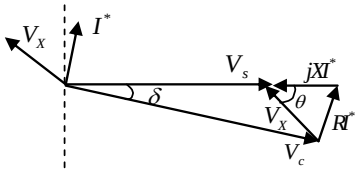

Figure 4.3: Capacitive reactive power vector diagram of STATCOM

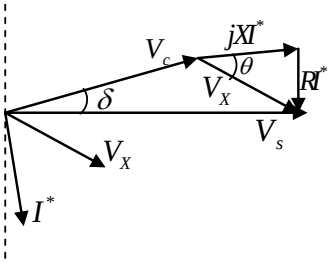

Figure 4.4: Inductive reactive power vector diagram of STATCOM

Assuming the positive direction of power transfer from power network to the STATCOM and $X >> R$, the active and reactive power expressions can be deduced from Figure 4.3 and Figure 4.4 as follows:

$$P = \frac{V_c V_s}{X} \sin \delta \tag{4.7}$$

$$P = \frac{V_c \left(V_s \cos \delta - V_c \right)}{X} \tag{4.8}$$

Here, the assumptions has been made that voltage generated by VSC (V_c) is in phase with power network voltage (V_s). Therefore, $\delta = 0$ causes active power $P = 0$ and only reactive power (Q) is flowing. If the V_s i.e bus voltage is higher than V_c, then STATCOM absorb the reactive power. On the other hand, if V_s is lower than the V_c, STATCOM injects reactive

into the grid to maintain the voltage profile of V_s. The amount of reactive power exchanged by the STATCOM with the grid can be expressed as:

$$Q = \frac{V_c\left(V_s - V_c\right)}{X} \tag{4.9}$$

The voltage regulation mode *V-I* characteristics of STATCOM is as shown in Figure 4.5 [54]. This shows that the STATCOM can be operated over its full output current rating even at very low (zero) system voltage level. As long as the reactive current stays within the maximum capacitive and inductive output current ($I_{C\max}, I_{L\max}$) imposed by the converter rating, the voltage will be regulated at the reference voltage (V_{ref}). The slope (X_s) or droop is normally employed between 1% and 4%.

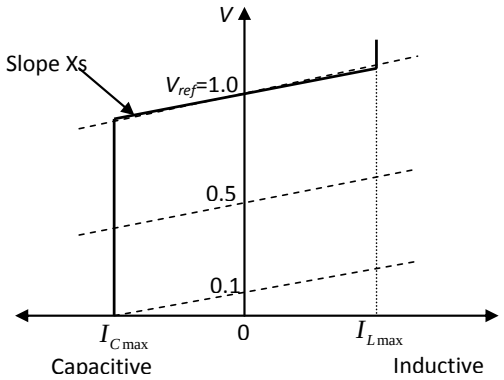

Figure 4.5: V-I characteristics of STATCOM in voltage regulation mode

4.4 Employed STATCOM

The detailed block diagram representation of STATCOM is shown in Figure 4.6. The output of inverter is connected to the point of common coupling through an AC filtering inductor. It employs PWM technique to synthesize a sinusoidal waveform from a DC voltage source with a typical switching frequency of few kilohertz. The angular position (θ) of the supply voltage vector is established by a phase-locked-loop (PLL). Thereafter, its output ($\theta = \omega t$) is used to compute the *d*-axis and *q*-axis components (V_{pd}, V_{pq} and $I_{d,} I_q$) of the AC three-phase voltage and currents (V_{pa}, V_{pb}, V_{pc} and $i_a, i_{b,} i_c$).

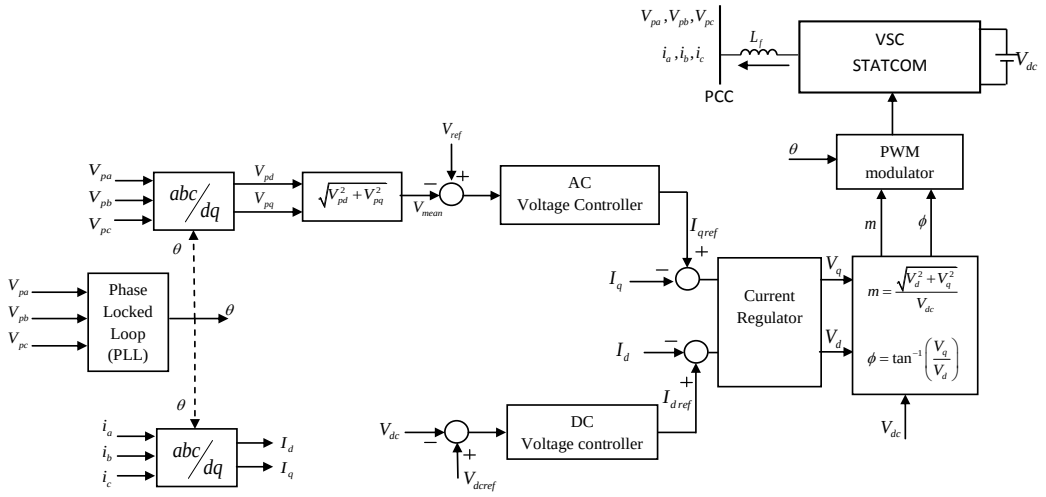

Figure 4.6: Block diagram representation of STATCOM

The current regulator is assisted by feed-forward type regulator which determines the V_d and V_q from the I_{qref} and I_{dref} currents (produced by AC voltage controller and DC voltage controller, respectively). Therefore, it controls the magnitude and phase of the generated voltage (V_d and V_q). The modulation index (m) and phase angle of the modulating waveform (ϕ or α) can be expressed as shown in Figure 4.6 [181]:

4.5 The STATCOM Control Scheme

A schematic diagram of a typical STATCOM is as shown Figure 4.7 which includes a voltage source converter (VSC), AC filtering inductor and the associated control system. The well-known control scheme [153] is used as a control strategy for the VSC based STATCOM.

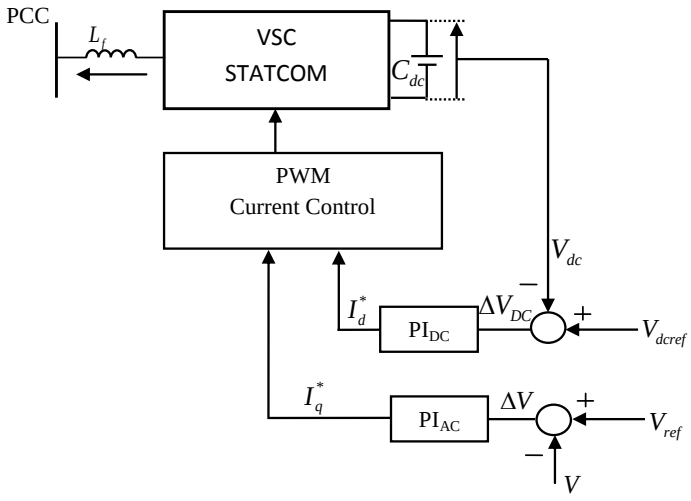

Figure 4.7: Control Scheme of STATCOM

For maintaining the voltage at PCC constant, the AC line voltage (V) is compared with the reference voltage (V_{ref}) and the error/deviation (ΔV) is processed through the controller $\mathrm{PI_{AC}}$. The AC voltage error (ΔV) at the n^{th} instant is

$$\Delta V_{(n)} = V_{ref} - V_{(n)} \tag{4.10}$$

where, $V_{(n)}$ is the magnitude of the three phase voltages sensed at the PCC at n^{th} instant, V_{ref} is the amplitude of the reference voltage.

The voltage regulation controller ($\mathrm{PI_{AC}}$), reacts to a sudden voltage variation and inject the appropriate amount of reactive power and therefore, it is well adapted for system disturbances. For an AC voltage control loop, the controller $\mathrm{PI_{AC}}$ output (I_q^*) determines the amount of reactive power to be generated by STATCOM. The AC voltage controller ($\mathrm{PI_{AC}}$) output ($I_{q(n)}^*$) at n^{th} sampling to regulate the PCC voltage can be expressed as

$$I_{q(n)}^* = I_{q(n-1)}^* + K_{Pac}\{\Delta V_{(n)} - \Delta V_{(n-1)}\} + K_{Iac}\Delta V_{(n)} \tag{4.11}$$

where, K_{Pac} and K_{Iac} are the proportional and integral gain constants of the AC voltage controller, $\Delta V_{(n)}$ and $\Delta V_{(n-1)}$ are the error voltages at the n^{th} and $(n-1)^{th}$ instants and $I_{q(n-1)}^*$ is the quadrature component of the reference current at the $(n-1)^{th}$ instant.

At the same time, in order to support the DC bus of STATCOM, DC bus voltage (V_{dc}) is also compared with the reference DC voltage (V_{dcref}) and the error voltage (ΔV_{DC}) is passed through another controller $\mathrm{PI_{DC}}$. The output (I_d^*) of this controller determine the source current active power component so that no real power injection is made by STATCOM at the PCC. Similarly, the DC bus voltage error (ΔV_{DC}) at n^{th} sampling is

$$\Delta V_{DC(n)} = V_{dcref} - V_{dc(n)} \tag{4.12}$$

where, $V_{dc(n)}$ is the DC link voltage of the STATCOM sensed at the n^{th} instant and V_{dcref} is the reference DC voltage. The output of the $\mathrm{PI_{DC}}$ controller is to support the STATCOM DC voltage at the n^{th} sampling and expressed as

$$I_{d(n)}^* = I_{d(n-1)}^* + K_{Pdc}\{\Delta V_{DC(n)} - \Delta V_{DC(n-1)}\} + K_{Idc}\Delta V_{DC(n)} \tag{4.13}$$

Where $I^*_{d(n)}$ and $I^*_{d(n-1)}$ are the active power components of the source current at the n^{th} and $(n-1)^{th}$ instants. K_{Pdc} and K_{Idc} are the proportional and integral gain constants of the DC voltage controller. The gains ($K_{Pac}, K_{Iac}, K_{Pdc}$ and K_{Idc}) of two PI controllers of the STATCOM are obtained at a specific operating point.

4.6 Design of STATCOM

4.6.1 Selection of DC link voltage of STATCOM

For satisfactory control of pulse-width modulation (PWM), the DC bus voltage (V_{dc}) is expressed by following relationship [118].

$$V_{dc} > \left(2\sqrt{2/3}V_{ac}\right)m \tag{4.14}$$

Where, V_{ac} is root-mean-square (RMS) value of the line-voltage on the AC side of the converter, m is modulation index which in the range of $0 > m > 1$. The maximum converter terminal voltage rating is 2.5kV, so that the DC bus voltage can be computed as:

$$\begin{aligned} V_{dc} &> \left(2\sqrt{2/3}\times 2500\right)\times 0.96 \\ &> 3919.18\text{V} \end{aligned} \tag{4.15}$$

The final value of DC voltage chosen as 4000V.

4.6.2 Selection of rating of STATCOM converter

Neglecting the switching and transformer losses, the DC voltage source should be constant and STATCOM does not provide active power to the system i.e $P_{SC} = 0$ and the maximum amount of reactive power delivered by the STATCOM $Q_{SC} = 15\text{Mvar}$, the converter rating (VA_{SC}) is calculated as [31]:

$$VA_{SC} = \sqrt{P_{SC}^2 + Q_{SC}^2} = \sqrt{0^2 + 15^2} = 15\text{MVA} \tag{4.16}$$

and thus, the maximum converter current is given by

$$I_{SC} = VA_{SC}/\sqrt{3}V_{ac} = 15\text{MVA}/\left(\sqrt{3}\times 2500\text{V}\right) = 3464.10\text{A} \tag{4.17}$$

4.6.3 Selection of filtering inductor

The AC filtering inductor is placed in series on PCC side of the STATCOM for ripple free current. The inductance (L_f) is given as [118].

$$L_f = \left(\sqrt{3}/2\right) m V_{dc} / \left(6 f_s a I_{r(p-p)SC}\right) \tag{4.18}$$

where, f_s is the switching frequency which is equal to 4 KHz, a is the steady state current margin, and $I_{r(p-p)SC}$ is the peak-to-peak ripple current which can be taken as 5% of peak current of I_{SC} :

$$I_{r(p-p)SC} = 0.05 \times \sqrt{2} I_{SC} \tag{4.19}$$

Therefore, the inductance (L_f) can be calculated as:

$$L_f = \left(\sqrt{3}/2\right) \times 0.96 \times 4000 / \left(6 \times 4000 \times 1.2 \times (0.05 \times \sqrt{2} \times 3464.10\right) = 0.47\text{mH} \tag{4.20}$$

For designing purpose, the inductance selected as 0.5mH. Whereas, the resistance (R_f) of the series filtering inductor is chosen as 0.25Ω so as to account for its losses.

4.6.4 Selection of DC link STATCOM capacitance

The design of DC capacitor of STATCOM is paramount importance as it allows the STATCOM to provide sufficient reactive power during transient and other power network disturbances. The DC capacitance of the STATCOM can be determined with following analytical equation [54].

$$C_{dc} = \frac{3 V_{ac} I_{SC} t}{[V_{dc}]^2 - [0.05 \times V_{dc}]^2} = \frac{3 \times \left(2500/\sqrt{3}\right) \times 3464.10 \times 375 e^{-6}}{4000^2 - 3800^2} = 3599.76\mu\text{F} \tag{4.21}$$

Where, the response time $t = 375\mu\text{s}$ and DC link voltage dip is 5% of rated DC link voltage. Therefore, DC link voltage may vary in between 4000V to 3800V. In order to avoid any DC side resonance, it is wise to choose a proper capacitance value [38]. In this work, therefore, the capacitance value is chosen as $3600\mu\text{F}$.

4.7 System configuration

In this work, a fixed-speed wind farm is considered as shown in Figure 4.8 which consists of twenty four 1.5MW rated fixed-speed SCIGs and thus 36MW wind farm has been connected to 120kV grid. The stator winding of each generator is connected at the point-of-common-coupling (PCC) through a step-up transformer (0.69/25kV) which thereafter, another step-up transformer (25/250kV) is connected at the PCC which helps in exporting power to the 120kV grid through a transmission line. The power factor correction capacitors are connected to the low voltage terminal of the each wind generators. Under normal operating condition, these capacitors provide required amount of reactive power to the FSIGs. But, these devices fail to support reactive power demanded by the FSIGs under severe faults conditions as discussed earlier. Therefore, to supply the adequate reactive power and voltage support at the PCC under fault conditions, the STATCOM has been employed and connected at the 25kV bus. The design parameters of the generator and wind turbine are presented in Appendix.

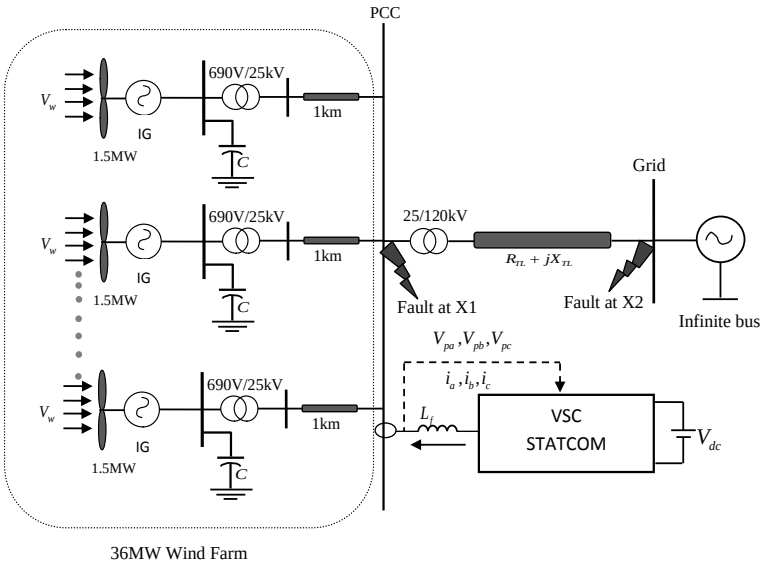

Figure 4.8: Configuration of the studied system

4.8 Results and Discussions

In order to investigate the fault ride through impact on the stability of fixed-speed wind farm using STATCOM, two cases (case 1: Fault location and Case 2: Fault duration) have been considered with different types of faults on the connected transmission line.

4.8.1 Fault location

Two fault locations (X1 and X2) have been defined on the studied system as shown in Figure 4.8 in which X1 is close to PCC of the wind farm whereas, another i.e. X2 is at the far end of the line. To analyze the effect of fault locations on the stability of wind farm, different types of faults have been considered, with and without considering STATCOM at the PCC.

4.8.1.1 Single line-to-ground (LG) fault

When a single line-to-ground fault occurs at the locations X1 and X2 without STATCOM, the variation of PCC voltage, active and reactive power transfer of wind farm to the grid are as shown in Figure 4.9(a), (b) and (c), respectively. During the fault, PCC voltage drops to 0.7621p.u when the fault occurs at X1 and drops to 0.7925p.u, when the fault occurs at X2. Also, the wind farm total active power exported to the grid decreases to 32.5MW when the fault occurs at X1 and to 33.01MW, when the fault occurs at X2. After the fault has cleared, the maximum amount of reactive power absorbed by the wind farm is 6.812Mvar for the fault at X1, whereas it is 6.612Mvar for fault at X2.

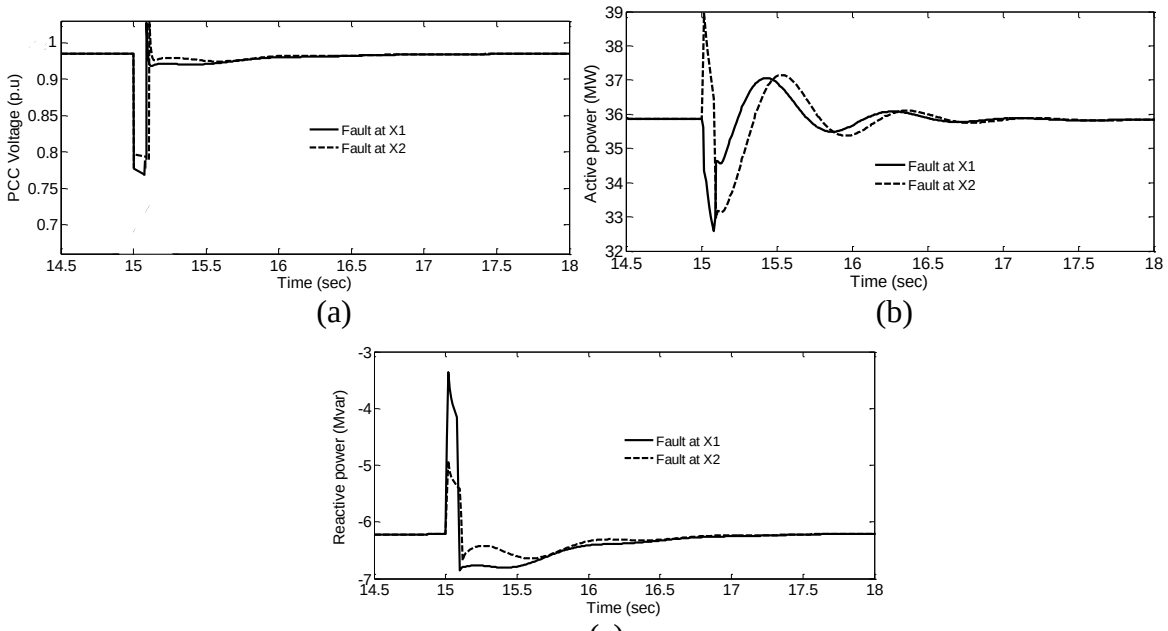

Figure 4.9: Single line-to-ground fault at different fault locations X1 and X2-without STATCOM: a) PCC voltage; b) Active power; c) Reactive power

Similarly, Figure 4.10(a)-(c) show the responses of the system when it is subjected to LG fault on the locations X1 and X2 with STATCOM. Figure 4.10(a) shows the PCC voltage, during the fault period, it drops to 0.8201p.u in when the fault occurs at X1, and to 0.8523p.u when the fault occurs at X2. Also, the wind farm total active power exported to the grid shown in Figure 4.10(b) decreases to 33.65MW when the fault occurs at X1, and to 33.86MW

when the same fault occurs at the location X2. After the fault cleared, the maximum amount of reactive power absorbed by the wind farm for different locations X1 and X2, respectively, are 4.351Mvar and 4.081Mvar as depicted in Figure 4.10(c).

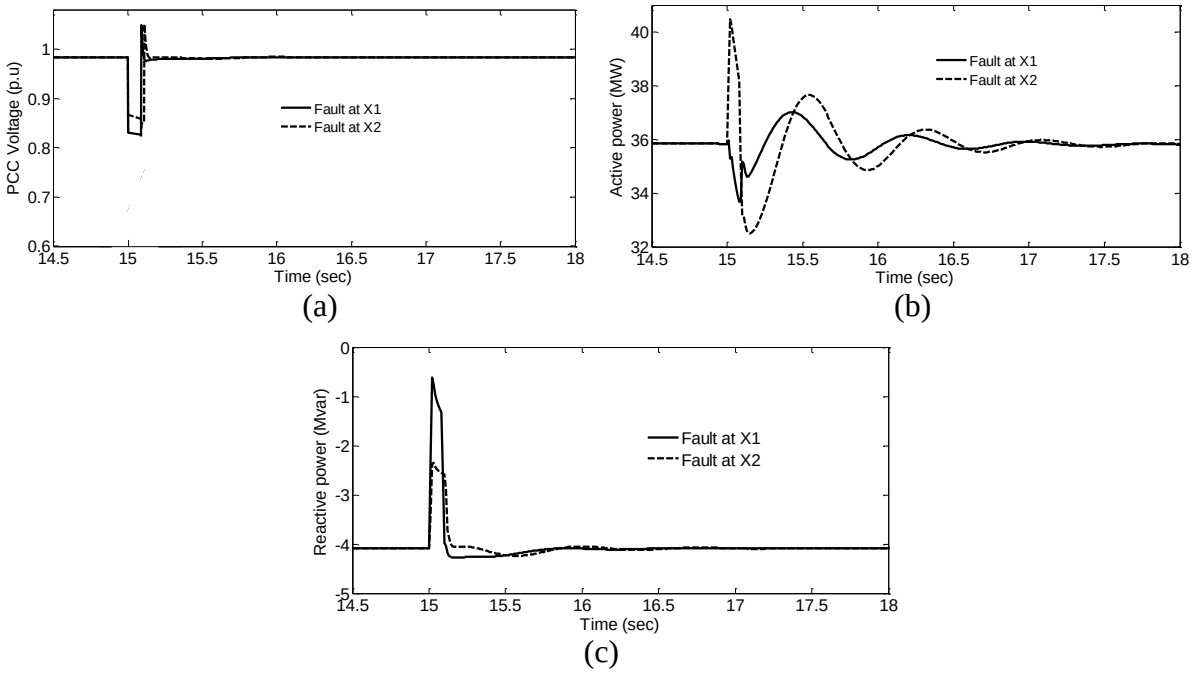

Figure 4.10: Single line-to-ground fault at different fault locations X1 and X2-with STATCOM: a) PCC voltage; b) Active power; c) Reactive power

It may, therefore, concluded that the STATCOM placed at the PCC arrests the fall in the PCC voltage and helps in faster restoration, thereby it results in increased amount of real power transfer to the grid and decreased amount of reactive power drawn from the grid by supplying local reactive support at the PCC itself.

4.8.1.2 Double-line-to-ground (LLG) fault

In this case instead of LG fault, an LLG fault is considered at the same locations X1 and X2 and the PCC voltage, active and reactive power (without STATCOM) measured are as shown in the Figure 4.11(a)-(c). As observed from Figure 4.11(a), the PCC voltage drops to 0.4801p.u during the fault when the fault location is X1, whereas it drops to 0.5521p.u when fault occurs at X2. The active power supply to the grid is reduced to 16.20MW when the fault location is at X1, and to 19.MW when the fault occurs at X2. Similarly, the maximum reactive power consumption of wind farm increases to 9.52Mvar and 9.451Mvar respectively, for the fault locations X1 and X2.

In the same way, Figure 4.12(a)-(c) show the variations of system parameters with STATCOM subjected to LLG fault at X1 and X2. During the fault, the PCC voltage now

decreases to 0.5410p.u and 0.5981p.u; when the fault occurs at X1 and X2, respectively as opposed to 0.4801p.u. and 0.5521p.u (see Figure 4.11(a)) respectively when STATCOM was not present. Similarly, the active power transferred to the power network is reduced to 16.532MW only when the fault initiated at X1, and reduced to 22.13MW when the fault occurs at X2. The amount of reactive power absorption by the wind farm is 5.98Mvar and 5.723Mvar; respectively, when the fault occurs at X1 and X2.

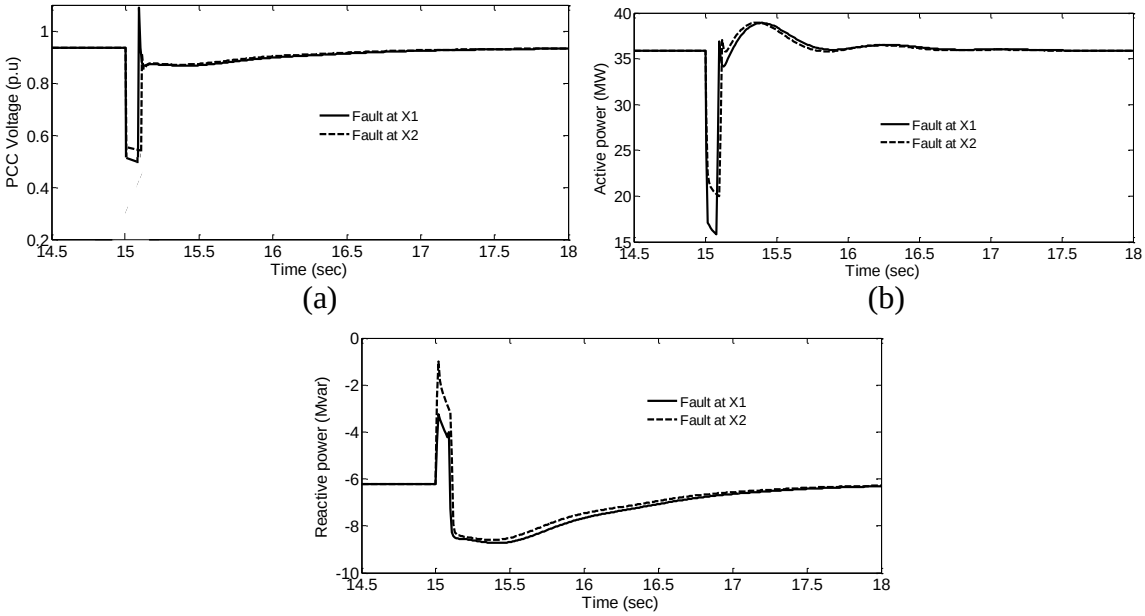

Figure 4.11: Double Line-to-ground fault at different fault locations X1 and X2-without STATCOM: a) PCC voltage; b) Active power; c) Reactive power

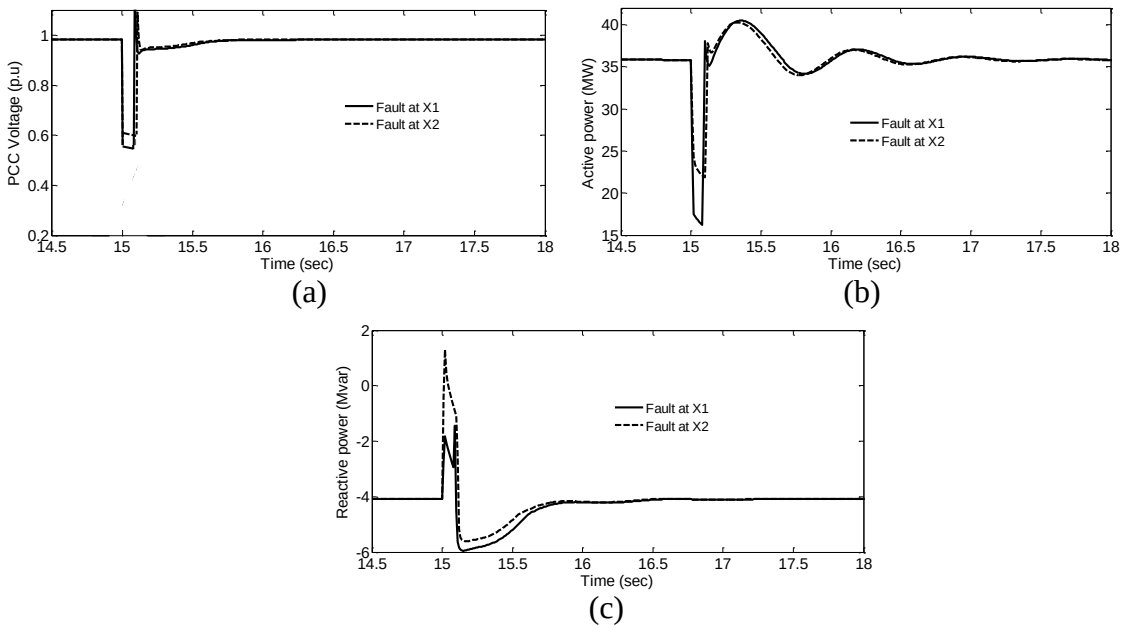

Figure 4.12: Double Line-to-ground fault at different fault locations X1 and X2-with STATCOM: a) PCC voltage; b) Active power; c) Reactive power

Again in case of LLG faults too, the STATCOM placed at the PCC arrests the fall in the PCC voltage and helps in faster restoration, resulting in the increased amount of real power transferred to the grid and ample reduction in the reactive power drawn from the grid.

4.8.1.3 Three line-to-ground (LLLG) fault

Since a three-phase fault is the most severe fault among all, a LLLG fault as considered again at locations X1 and X2 and results shown in Figure 4.13(a)-(c) reveal the variations in voltage, active and reactive power of the studied system (without STATCOM). Now, during the fault period, the PCC voltage and active power are reduced zero when fault occurs at X1; while voltage reduces to 0.2050p.u and active power is zero again when the fault occurs at X2. The maximum amount of reactive power consumption by the wind farm is 12.85Mvar when the fault initiated at X1, and 9.85Mvar when the fault occurs at X2. It is clear that when the LLLG fault occurs at X1, the system parameters failed to return to their post-fault condition; whereas, if the fault occurs at X2, all the responses are return back to their post-fault condition.

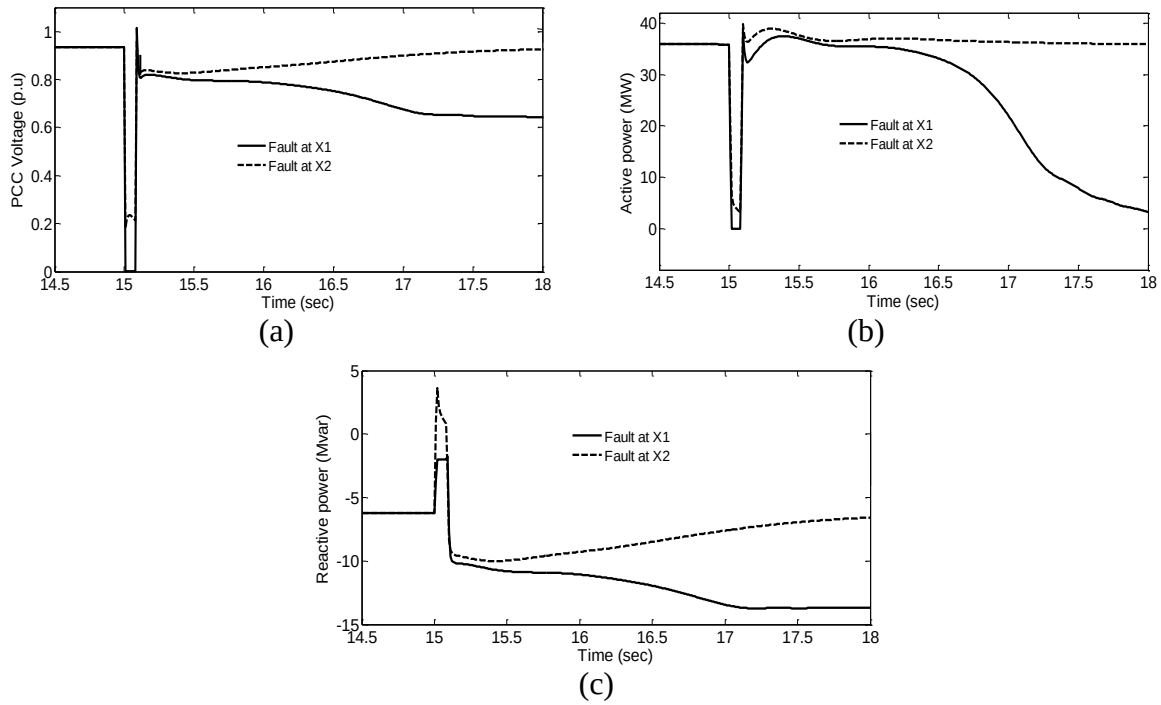

Figure 4.13: Three Line-to-ground fault at different fault locations X1 and X2-without STATCOM: a) PCC voltage; b) Active power; c) Reactive power

Figure 4.14(a), (b) and (c) show the effect of different fault locations on the system with STATCOM connected when the system is subjected to LLLG fault at X1 and X2. It is clear from Figure 4.14(a) that during the LLLG fault, the voltage becomes zero when the fault

initiates at X1 whereas, it is 0.2355p.u when the fault occurs at X2. Also, the active power injected into the grid becomes zero when the fault occurs at X1, and decreases to 4.5MW if the same fault occurs at X2 (during fault). After the fault cleared, the maximum amount of reactive power absorbed is 8.32Mvar and 7.232Mvar respectively; when the fault occurs at X1 and X2. With the STATCOM connection, all the responses returned back to their post-fault conditions and hence, wind farm stays connected to the grid. It is also observed that during the low voltage period a small amount of the active power can be exported to the grid when the fault occurs at X2.

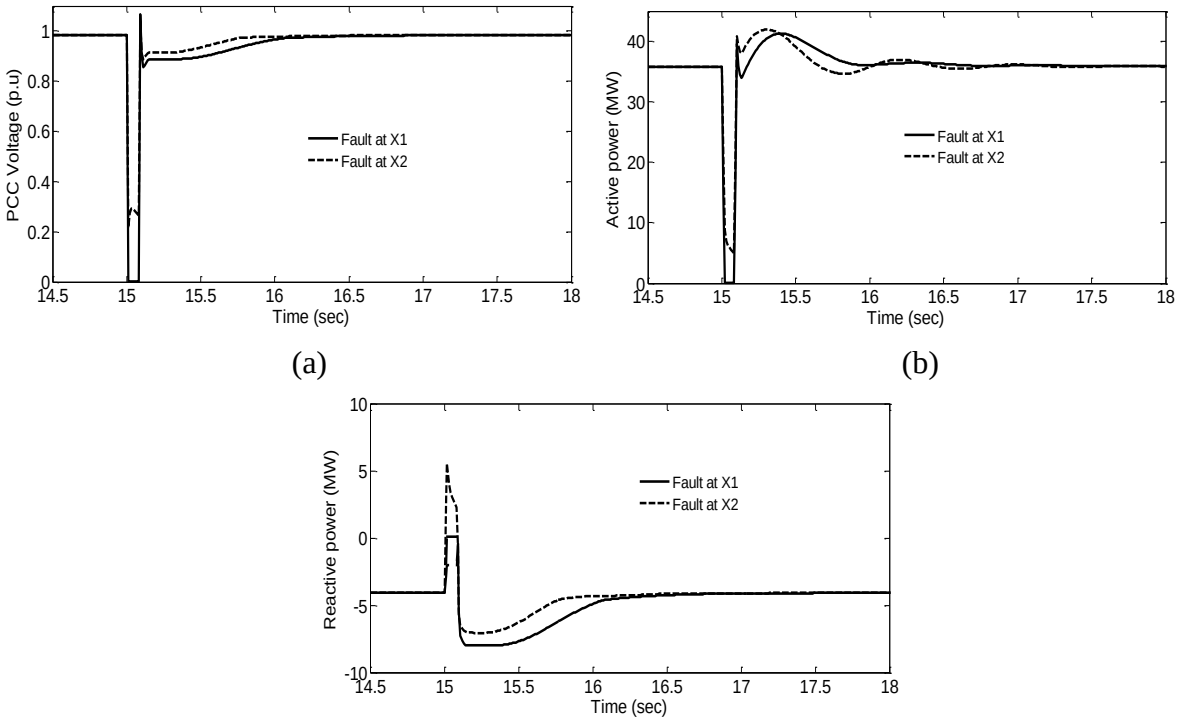

Figure 4.14: Three Line-to-ground fault at different fault locations X1 and X2-with STATCOM: a) PCC voltage; b) Active power; c) Reactive power

Table 4.1 shows the results comparison of impact of different fault locations on the wind farm stability (with and without STATCOM) subjected to various types of faults. It is observed from the Table 4.1, as the fault location distance increases it effect on the wind farm being reduces. The three lines to ground fault is more severe than other faults, since in which electrical torque reduces to zero as result active power become zero, consequently, the voltage at the wind farm decreases to zero. If this condition present for a long time then wind farm would be disconnected from the grid. However, the STATCOM can improve the low-voltage-ride through capability of the wind farm as shown in Figure 4.14(a).

Table 4.1: For different fault locations: variations of system parameters with different types of fault with and without STATCOM

Type of fault	Fault location at X1			Fault location at X2		
	PCC Voltage (p.u)	Active power (MW)	Reactive power (Mvar)	PCC Voltage (p.u)	Active power (MW)	Reactive power (Mvar)
LG Fault without STATCOM	0.7621	32.5	6.812	0.7925	33.01	6.612
LG Fault with STATCOM	0.8201	33.65	4.351	0.8523	33.86	4.081
LLG Fault without STATCOM	0.4801	16.20	9.52	0.5521	19.8	9.451
LLG Fault with STATCOM	0.5410	16.532	5.98	0.5981	22.13	5.723
LLLG Fault without STATCOM	0	0	12.85	0.2050	3.211	9.85
LLLG Fault with STATCOM	0	0	8.32	0.2355	4.5	7.232

4.8.2 Fault duration

In this section, in order to analyse the impact of fault-ride-through capability (FRT) of the wind farm on its stability, different fault types of faults are considered at the same location X1 on the transmission line but with different time durations, with and without STATCOM connected at the PCC.

4.8.2.1 Single line-to-ground (LG) fault

The behaviour of PCC voltage, active and reactive power of employed system is shown in Figure 4.15(a)-(c) subjected to LG fault without STATCOM. During the fault, the voltage reduced to 0.7621p.u for the fault durations 100ms and to 0.7316p.u when the fault remains for longer duration i.e. 150ms. Furthermore, the active power supplied by the wind farm to the grid is decreased to 32.5MW when the fault exists for 100ms whereas it comes down to 31.5MW when the fault occurs for 150ms. After the fault cleared, the amount of reactive

power absorbed by the FSIG-wind farm is 6.812Mvar for the fault duration 100ms, and 7.251Mvar when the fault occurs for duration 150ms.

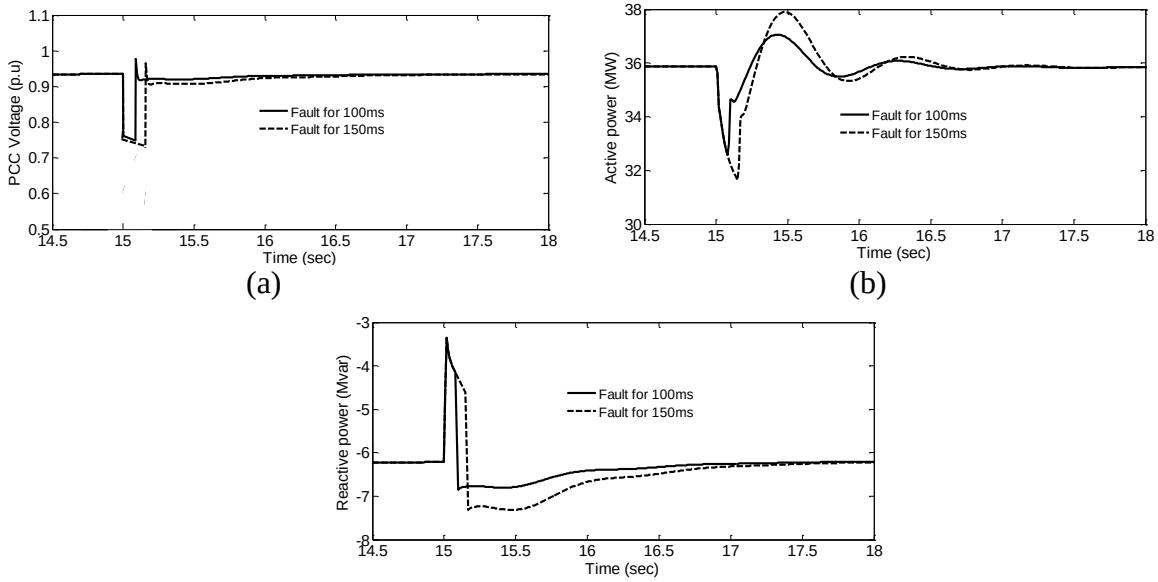

Figure 4.15: Single line-to-ground fault at different fault durations 100ms and 150ms-without STATCOM: a) PCC voltage; b) Active power; c) Reactive power

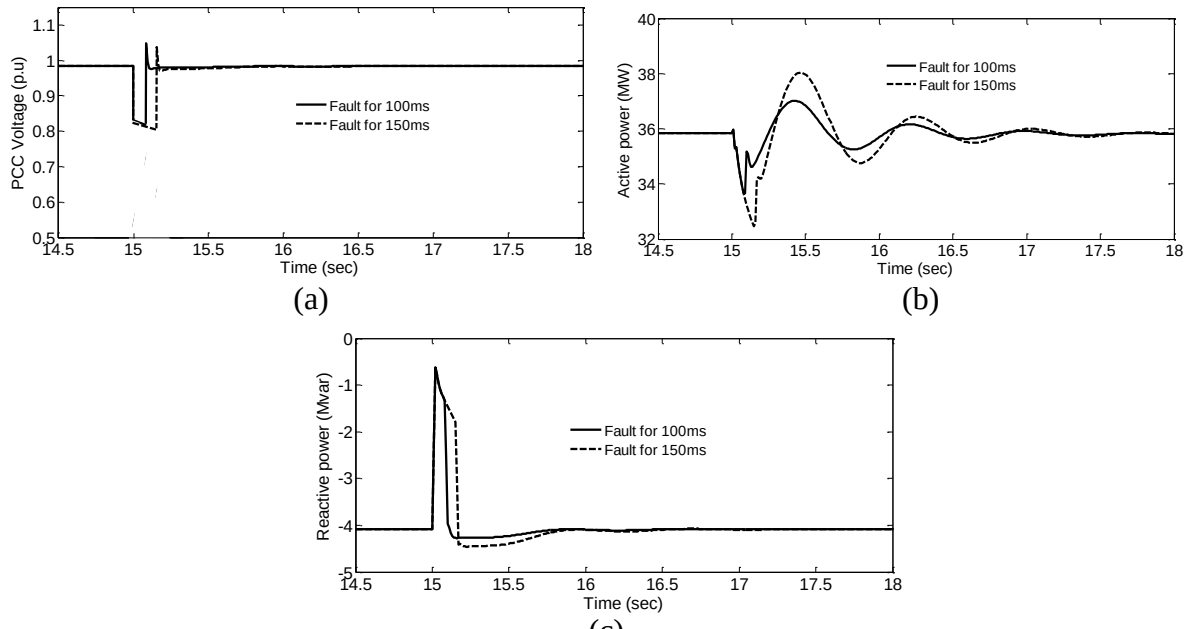

Figure 4.16: Single line-to-ground fault at different fault durations 100ms and 150ms-with STATCOM: a) PCC voltage; b) Active power; c) Reactive power

Figure 4.16(a), (b) and (c) show the variation of PCC voltage, active and reactive power of the studied system subjected to LG fault with STATCOM. During the fault, the voltage at the PCC becomes 0.8201p.u and 0.8102 respectively, for fault durations of 100ms and 150ms. Also, the active power exported to the grid is reduced to 33.65MW and 32.2MW when the fault exists for 100ms and 150ms, respectively. The reactive power consumption increases to 4.351Mvar and 4.489Mvar respectively, when the faults initiated for 100ms and 150ms. It

clears that in all conditions the wind farm stay connected to the grid when the line-to-ground fault occurs. However, different fault time duration with STATCOM has produced improved voltage, active power and reactive power consumption by IG as compared to without STATCOM (see Figure 4.15 and Figure 4.16).

4.8.2.2 Double line-to-ground (LLG) fault

Figure 4.17(a)-(c) show the effect of fault durations on the voltage, active and reactive power of studied system subjected to LLG fault without STATCOM. During the fault time, the PCC voltage depressed to 0.4801p.u and 0.4793p.u respectively, when the fault durations of 100ms and 125ms are applied. Also, the wind farm active power transferred to grid has dropped to 16.20MW when the fault duration of 100ms applied, and it dropped to 12.5MW when the fault time period increased to 125ms. The reactive power absorbed by the wind farm after the fault cleared are 9.52Mvar and 14Mvar respectively; for the fault durations 100ms and 125ms. For a given LLG fault, the wind farm stay connected to the grid for the fault duration of 100ms, but it disconnected when the fault duration exists for 125ms. It is clear that even for LLG fault if the fault duration increases the wind farm fails to recover its post-fault state results in may be disconnected from grid.

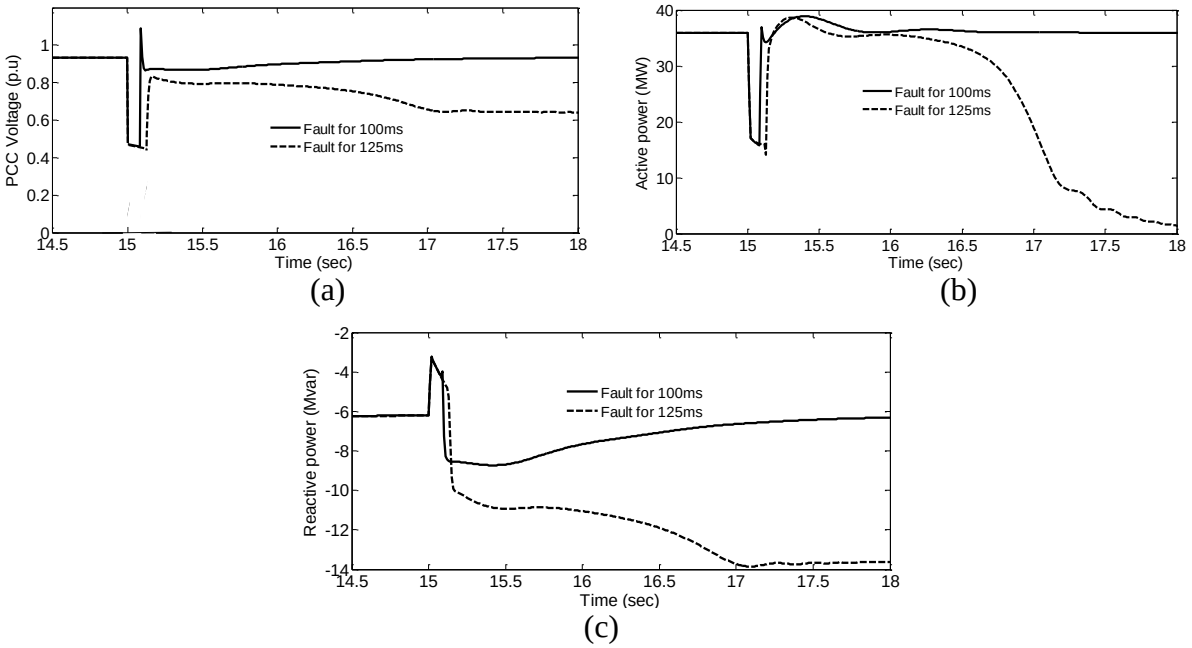

Figure 4.17: Double line-to-ground fault at different fault durations 100ms and 125ms-without STATCOM: a) PCC voltage; b) Active power; c) Reactive power

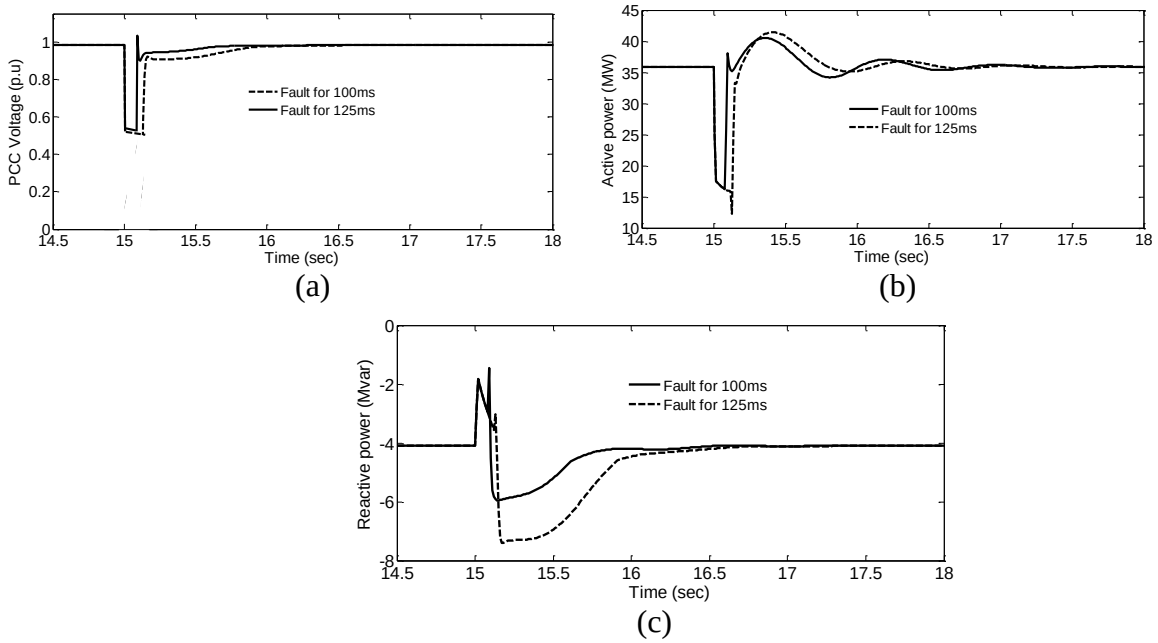

Figure 4.18: Double line-to-ground fault at different fault durations 100ms and 125ms-with STATCOM: a) PCC voltage; b) Active power; c) Reactive power

Similarly, Figure 4.18(a)-(c) show the responses of wind farm with STATCOM for different fault time durations when it subjected to LLG fault. During the fault, the PCC voltage shown in Figure 4.18(a) reduced to 0.5410p.u and 0.5123p.u for the fault durations 100ms and 125ms, respectively. Also the case, where the wind farm generated active power exported to grid decreases to 16.532MW and 12.85MW when the fault durations exist for 100ms and 125ms, respectively. The maximum amount of reactive power absorbed by the wind farm after the fault cleared is 5.98Mvar when the fault duration occurs for 100ms, whereas it 7.58Mvar when the fault exist for 125ms. In this condition when the STATCOM included, the wind farm stability is improved and, therefore, it stay connected to the grid.

4.8.2.3 Three line-to-ground (LLLG) fault

The variations in PCC voltage, active and reactive power profiles of the studied system are as shown in Figure 4.19(a)-(c) without STATCOM, if the fault durations have been considered for 80ms and 100ms, subjected to LLLG fault. During the fault, voltage and active power becomes zero for both cases (80ms and 100ms). After the fault cleared, the maximum reactive power absorption by the wind farm is 9.75Mvar and 12.85Mvar respectively, for the fault durations 80ms and 100ms. In condition where the fault duration occurs for 80ms the wind farm remains stay connected to the grid even STATCOM not been incorporated. But, when the fault time duration of 100ms is tested for which the wind farm fails to recover its steady-state behaviour and may disconnected from the grid.

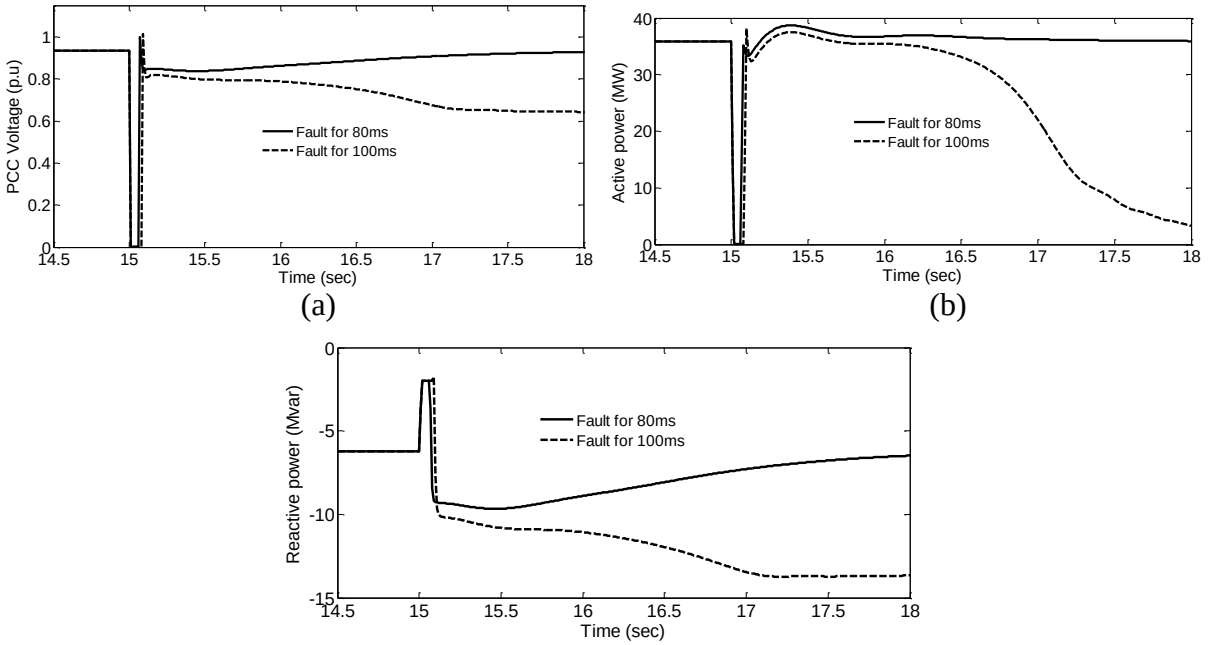

Figure 4.19: Three line-to-ground fault at different fault durations 80ms and 100ms-without STATCOM: a) PCC voltage; b) Active power; c) Reactive power

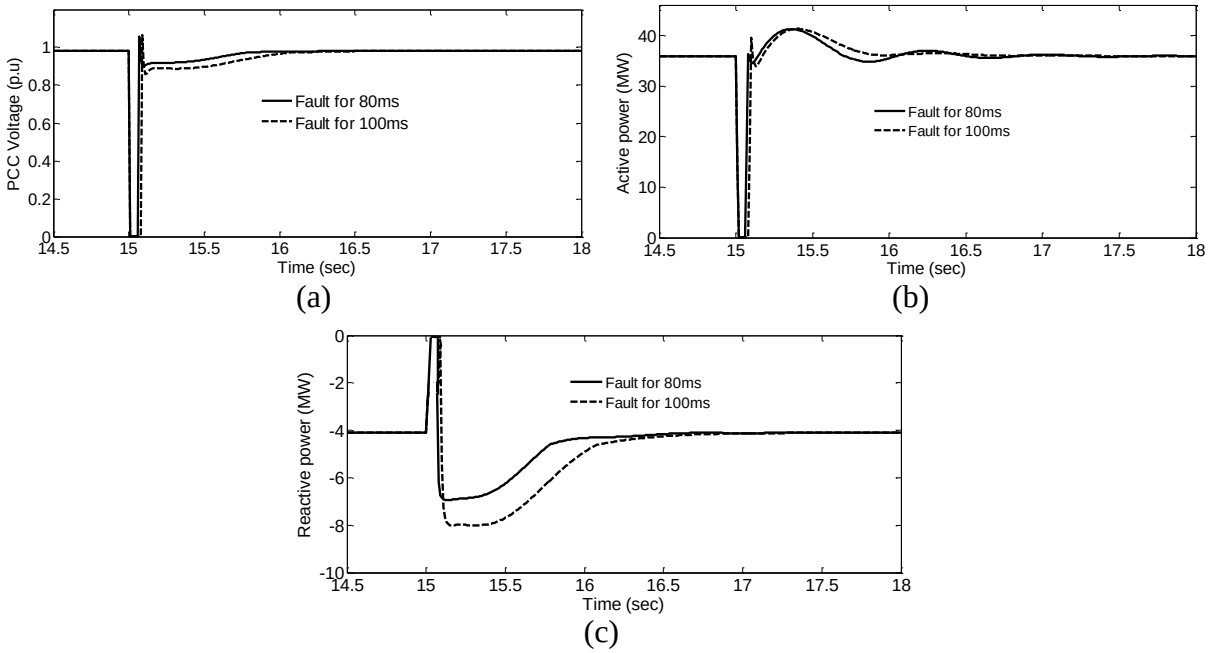

Figure 4.20: Three line-to-ground fault at different fault durations 80ms and 100ms-with STATCOM: a) PCC voltage; b) Active power; c) Reactive power

Similar analysis also can be done from the Figure 4.20(a)-(c), where it obtained the results such as PCC voltage, active and reactive power variations with STATCOM connected. During the fault, the active power and voltage at the PCC becomes zero for both fault durations. After the fault cleared, the amount of reactive consumed by the wind farm respectively, 6.852Mvar and 8.32Mvar for the fault durations 80ms and 100ms. In both cases (80ms and 100ms) wind farm maintaining good stability with STATCOM connected.

Table 4.2 shows the effect of fault durations on the system stability with and without STATCOM under different fault conditions. In case of LG fault with 100ms of fault duration, the active power and PCC voltage are become 32.5MW and 0.7621p.u respectively, without STATCOM, whereas with STATCOM connected the active power and PCC voltage are improved to 33.65MW and 0.8201p.u, respectively. After the fault cleared, the amount of reactive consumed by the wind farm is 6.812Mvar without STATCOM and it has improved to 4.351Mvar with STATCOM connected. Similar analysis has done for all types of fault with different fault time durations and with and without STATCOM connected, and the results are presented in Table 4.2. It is also noticed from the Table 4.2, as fault time duration increases it effect the stability of wind farm more severe as a results, it may disconnect from the power grid if compensating devices such as STATCOM not present in case of fixed speed wind farm.

Table 4.2: For different fault durations: variations of system parameters with different types of fault with and without STATCOM

Type of fault	Fault duration of 100ms			Fault duration of 150ms		
	PCC Voltage (p.u)	Active power (MW)	Reactive power (Mvar)	PCC Voltage (p.u)	Active power (MW)	Reactive power (Mvar)
LG Fault without STATCOM	0.7621	32.5	6.812	0.7313	31.5	7.251
LG Fault with STATCOM	0.8201	33.65	4.351	0.8102	32.2	4.489
	Fault duration of 100ms			Fault duration of 125ms		
LLG Fault without STATCOM	0.4801	16.20	9.52	0.4793	12.5	14
LLG Fault with STATCOM	0.5410	16.532	5.98	0.5123	12.85	7.58
	Fault duration of 80ms			Fault duration of 100ms		
LLLG Fault without STATCOM	0	0	9.75	0	0	12.85
LLLG Fault with STATCOM	0	0	6.852	0	0	8.32

4.9 Type-2 fuzzy logic based damping controller for STATCOM

Induction generator (IG) type wind farms are extremely sensitive to the grid faults as their stator windings are directly connected to the grid, results in wind power fluctuations. When delivering large amount of power to the grid inherent wind power fluctuations have adverse impact on the power quality of the power system to which they are connected. Several research works have proposed STATCOM with damping controller to reduce the negative impact of wind farms on the power system, where the damping controller is designed using different control techniques, however, recently employed methods are such as fuzzy neural [124], fuzzy [169] and hybrid PID plus fuzzy [193] as they exhibit superior performance. Though, these intelligent techniques showing better results, but due to inherent characteristics of uncertainties in MFs and rules fuzzy technique (type-1 FLC) is very limiting.

This section of thesis, therefore, proposed an interval type-2 FLC based damping controller for STATCOM to achieve best damping characteristics and thus improve the performance of the wind power system very effectively by overcoming uncertainties in rules and MFs.

4.9.1 Configuration of the system

To evaluate the proposed control technique for the STATCOM equipped with damping controller, a typical wind integrated power system is considered as shown in Figure 4.21. A 36MW fixed speed wind farm (consisting of twenty four 1.5MW rated wind turbines) is exporting power to the grid. A synchronous generator (SG) of 100 MVA is assumed to be connected to the PCC through a transformer (11/25kV). The design parameters and modelling of the synchronous generators is provided in Appendix. A STATCOM which is developed in the previous section has employed and connected to the point-of-common coupling to provide the necessary amount reactive power to the system. However, this STATCOM now possess a damping controller in order to improve the damping characteristics of the wind integrated power system subjected to network disturbances.

4.9.2 STATCOM with damping controller

The control block diagram of damping controller with STATCOM control scheme is shown in Figure 4.22. Here, STATCOM damping controller utilizes synchronous generator rotor speed deviation (difference between measured SG speed and reference SG speed) as feedback signal to damping controller since it is easier to obtain in practice by measurement

and analysis. The structure of the proposed interval type-2 FLC based damping controller is shown in

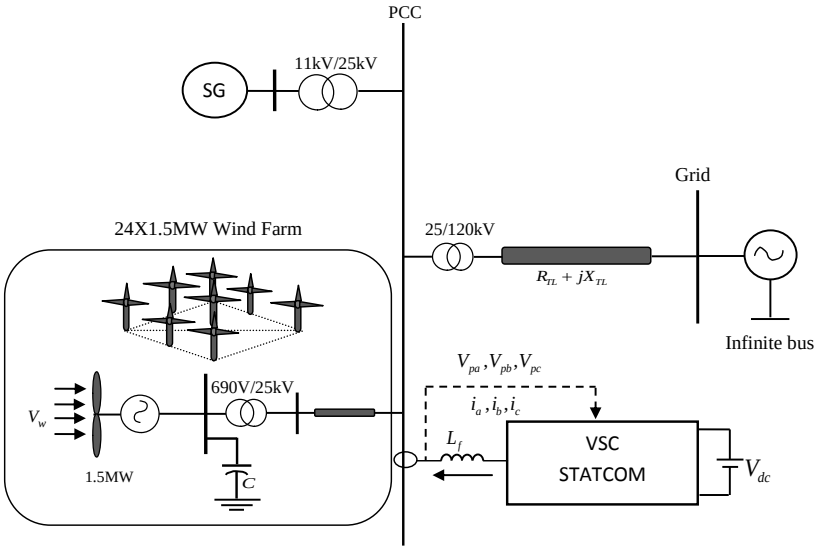

Figure 4.21: Studied wind farm integrated power system

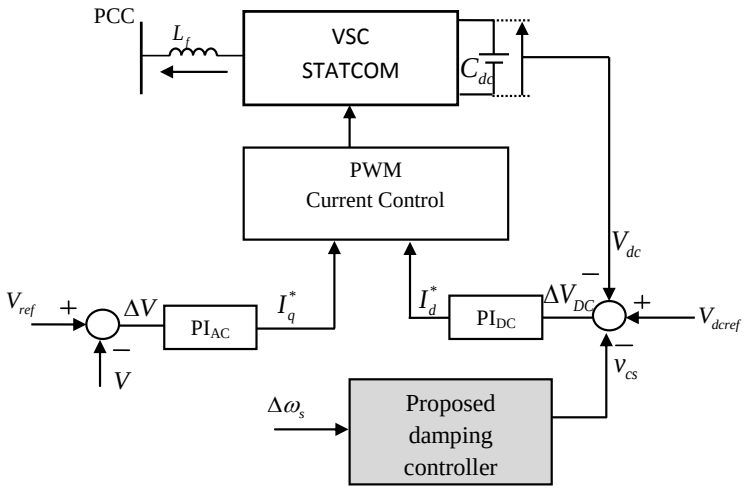

Figure 4.22: Control block diagram of STATCOM with damping controller

Figure 4.23. The deviation in SG rotor speed signal is given as input to the Type-2 fuzzy damping controller, where initially it passes through the washout filter in order to washout (reject) steady-state components while passing transient components of $\Delta\omega_s$. Later on, it is divided in to two paths: x_1-proportional path and x_2-integral path. Moreover, two input gains K_e and K_d are incorporated to make $\varepsilon = x_1 K_e$ and $c\varepsilon = x_2 K_d$ usually within a proper range of [-1, 1] for fuzzifier design. Another gain K_u is also employed at the output side of the type-2 fuzzy controller where the type-2 fuzzy logic controller computes the proper output signal v_{cs} through the defuzzification technique. This output signal applied to the STATCOM

for damping oscillation control. K_e, K_d and K_u are the gains of the controller which are chosen based on the expert knowledge and experience so as to get satisfactory performance of the type-2 fuzzy controller.

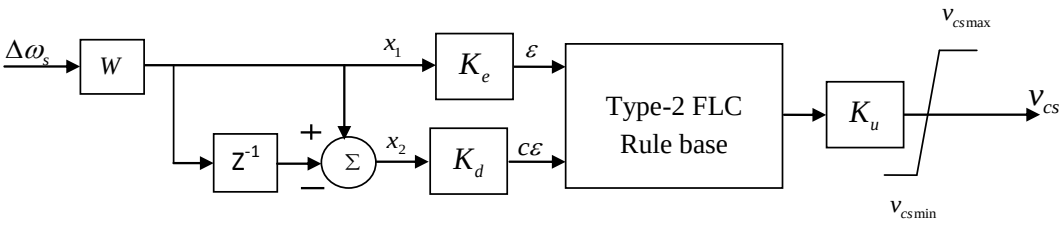

Figure 4.23: Proposed Type-2 fuzzy logic based damping controller

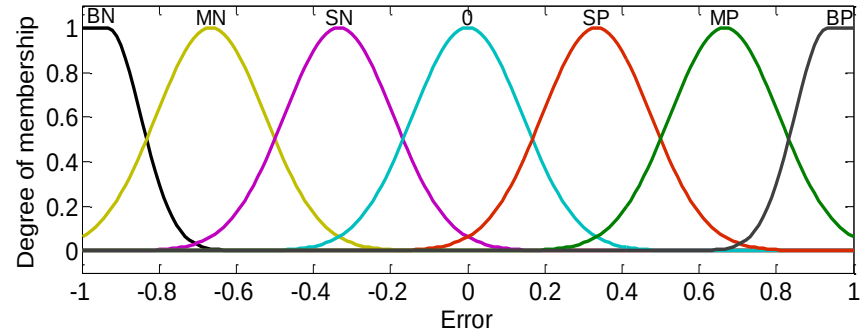

(a)

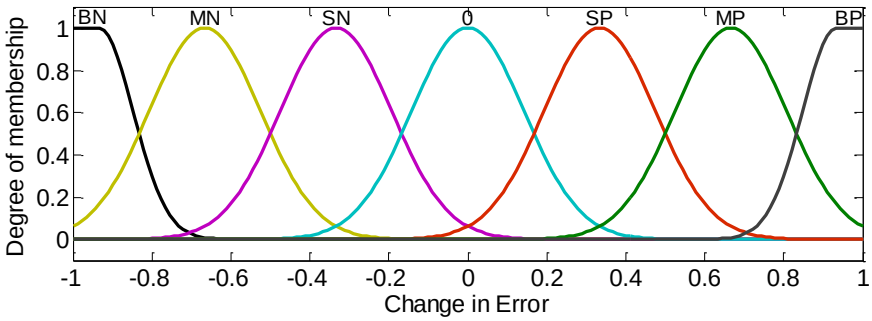

(b)

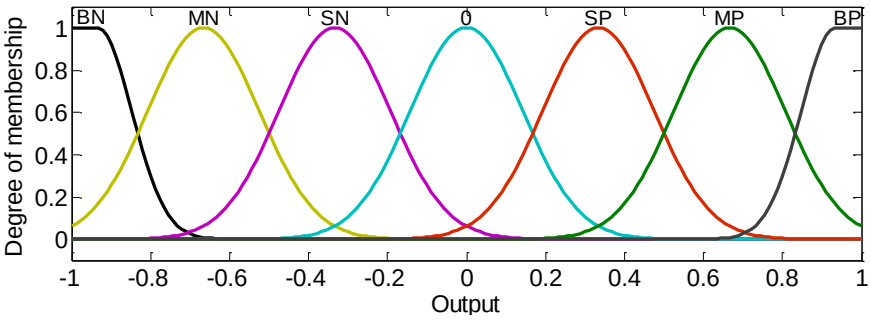

(c)

Figure 4.24: MFs for Type-1 FLC (a) Input1 (b) Input 2 (c) Output

For the fuzzy based damping controller, the two inputs error ($\mathcal{E}$) and change in error ($c\mathcal{E}$) are fuzzified using seven Gaussian membership functions as it shows better compensation capabilities. The Gaussian membership function is also used to defuzzify the output fuzzy sets. The fuzzy sets for inputs and output are defined as: Big Negative (BN), Medium Negative (MN), Small Negative (SN), Zero (0), Small Positive (SP), Medium Positive (MP), and Big Positive (BP) and used for the type-1 and type-2 FLCs are shown in Figure 4.24 and Figure 4.25, respectively. The maximum and minimum values of the universe of discourse for all inputs and outputs are -1 to +1. The fuzzy mapping of input variable to output is formed with help of the IF-THEN rules framed as:

IF: $\mathcal{E}$ is A_i and $c\mathcal{E}$ is B_i THEN $v_{cs} = C_i$

Where $\mathcal{E}$ and $c\mathcal{E}$ are inputs and A_i and B_i are the fuzzy sets, C_i is the output within the fuzzy range, v_{cs} is designed parameter for the output of fuzzy. Similarly, 49 rules are formed as shown in Table 4.3.

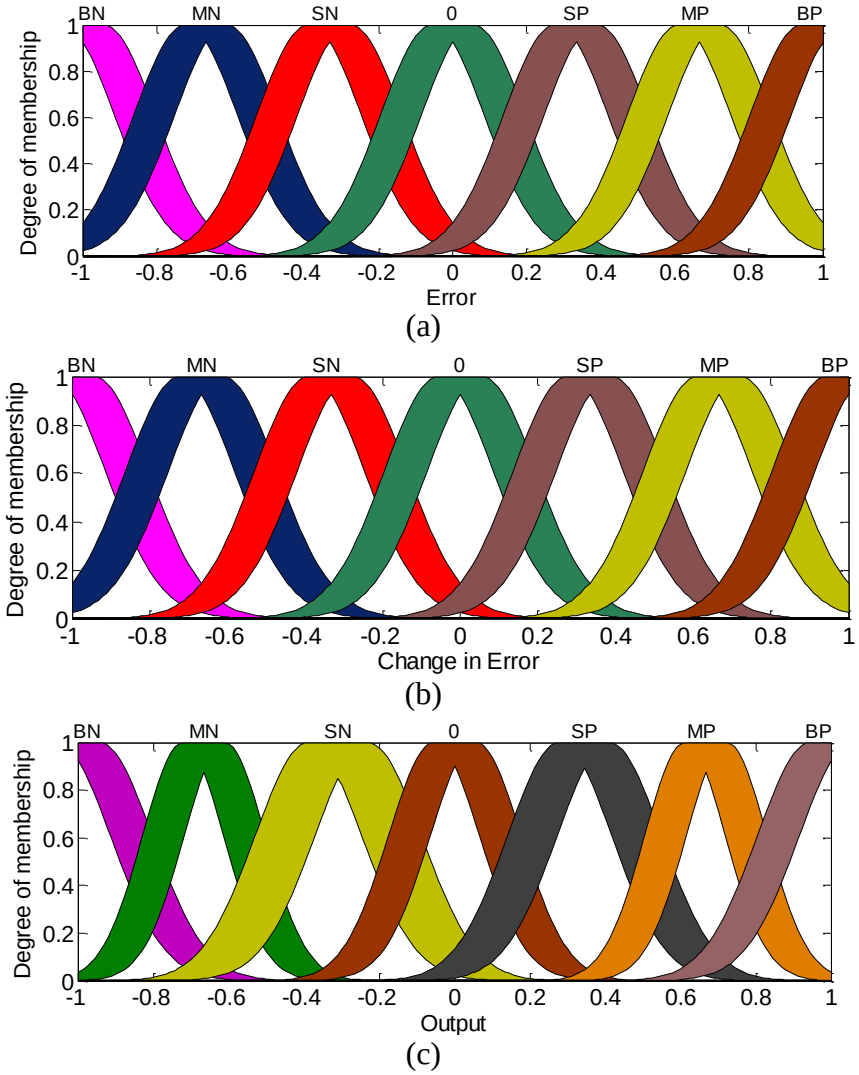

Figure 4.25: MFs for Type-2 FLC (a) Input1 (b) Input 2 (c) Output

Table 4.3: Rule base table for v_{cs}

Change in Error ($\mathcal{CE}$)	Error ($\mathcal{E}$)						
	BN	MN	SN	0	SP	MP	BP
BP	0	SP	MP	BP	BP	BP	BP
MP	SN	0	SP	MP	BP	BP	BP
SP	MN	SN	0	SP	MP	BP	BP
0	BN	MN	SN	0	SP	MP	BP
SN	BN	BN	MN	SN	0	SP	MP
MN	BN	BN	BN	MN	SN	0	SP
BN	BN	BN	BN	BN	MN	SN	0

4.9.3 Simulation Results

To investigate the contribution of the proposed damping controller, this section uses the nonlinear simulation test system which is shown in Figure 4.21. Three cases have been considered to study the effectiveness of the type-1 and type-2 FLC based damping controllers as follows:

Case 1: Three-line-to-ground fault (LLG)

Case 2: Two-line-to-ground fault (LLG)

Case 3: Single-line-to=ground fault (LG)

In all the cases the faults have been occurs at t=10sec and cleared at t=10.05sec. The operating wind speed is assumed to be constant at 14m/sec. The simulation results of studied system are obtained for three different scenarios such as STATCOM-without damping

controller, STATCOM with type-1 FLC based damping controller and STATCOM with type-2 FLC based damping controller.

Figure 4.26(a)-(f) shows the wind integrated power system behavior under the three phase short circuit fault (case 1). This figure plots the comparative transient responses of the system with STATCOM-without damping controller (gray lines), STATCOM-with designed type-1 FLC damping controller (red lines) and STATCOM-with proposed type-2 FLC damping controller (black lines). The real power oscillation in wind farm is shown in Figure 4.26(c), the STATCOM with proposed type-2 FLC based damping controller offers better damping effect and quickly return to steady state around 0.5sec. The dynamic response of the SG and IG rotor speed are shown in Figure 4.26(b) and (d), respectively. It can found that the proposed controller has faster convergence rate than other scenarios and recover more quickly to steady state value. Figure 4.26(a) shows the rotor angle of the SG where proposed controller exhibits better damping results than STATCOM-without damping controller and with type-1 FLC based damping controller. This type of fault also leads to fluctuations in voltage as shown in Figure 4.26(e), thus voltage stability is also required. Figure 4.26(e) shows that STATCOM with type-2 FLC based damping controller improve the transient stability and effective voltage recovery is achieved. The reactive power generation of the STATCOM without damping controller and with damping controller (designed with type-1 and type-2 FLCs) are shown in Figure 4.26(f). The absolute maximum deviations indices for all the quantities such as SG rotor-angle, SG rotor-speed, WF active-power and WF rotor-speed of the studied system are listed in Table 4.4. It is observed from the table that the type-2 FLC based damping controller showed reduced deviations due to LLLG fault as compared to the other two scenarios (without damping controller and type-1 FLC controller).

Figure 4.27(a)-(f) shows the transient behaviour of the studied system with double line to ground fault (case 2). Though, this type of fault is less severe compared to three phase short circuit faults, it has negative impact on the system. From the simulation results it is observed that STATCOM with external damping controller designed using type-2 FLC offers better damping effect and fast convergence rate than other two scenarios. Table 4.5 provided the maximum parameters deviation indices for all types of scenarios. It showed that proposed damping controller exhibits lesser parameters deviations compared to without and with type-1 FLC damping controllers.

The system transient behaviour with single to ground fault (case 3) with different scenarios is shown in Figure 4.28(a)-(f). Though, this type of fault is lesser severe compared to double line to ground and three line to ground faults, but it is most frequently occurs and therefore, need to investigate its impact on the system. From the simulation results it is

examined that the fluctuations occur due to LG fault are effectively damped out by the proposed controller. The maximum deviation of the system parameters with three different scenarios are incorporated in the Table 4.6. In this case as well proposed controller offers lesser deviations in the parameters.

Figure 4.29(a) and (b) shows the control surfaces formed by the Type-1 and Type-2 FLCs, respectively. It is observed from Figure 4.29(b) that as its control surface is formed with large number of embedded Type-1 FSs, the proposed Type-2 controller surface is very smooth as compared to Type-1 FLC shown in Figure 4.29(a). This smooth surface is less sensitive to disturbances and therefore, its effect is clearly visible on the responses of the studied system as shown in Figure 4.26, Figure 4.27 and Figure 4.28.

4.9.3.1 Case 1: Three-line-to-ground fault (LLG)

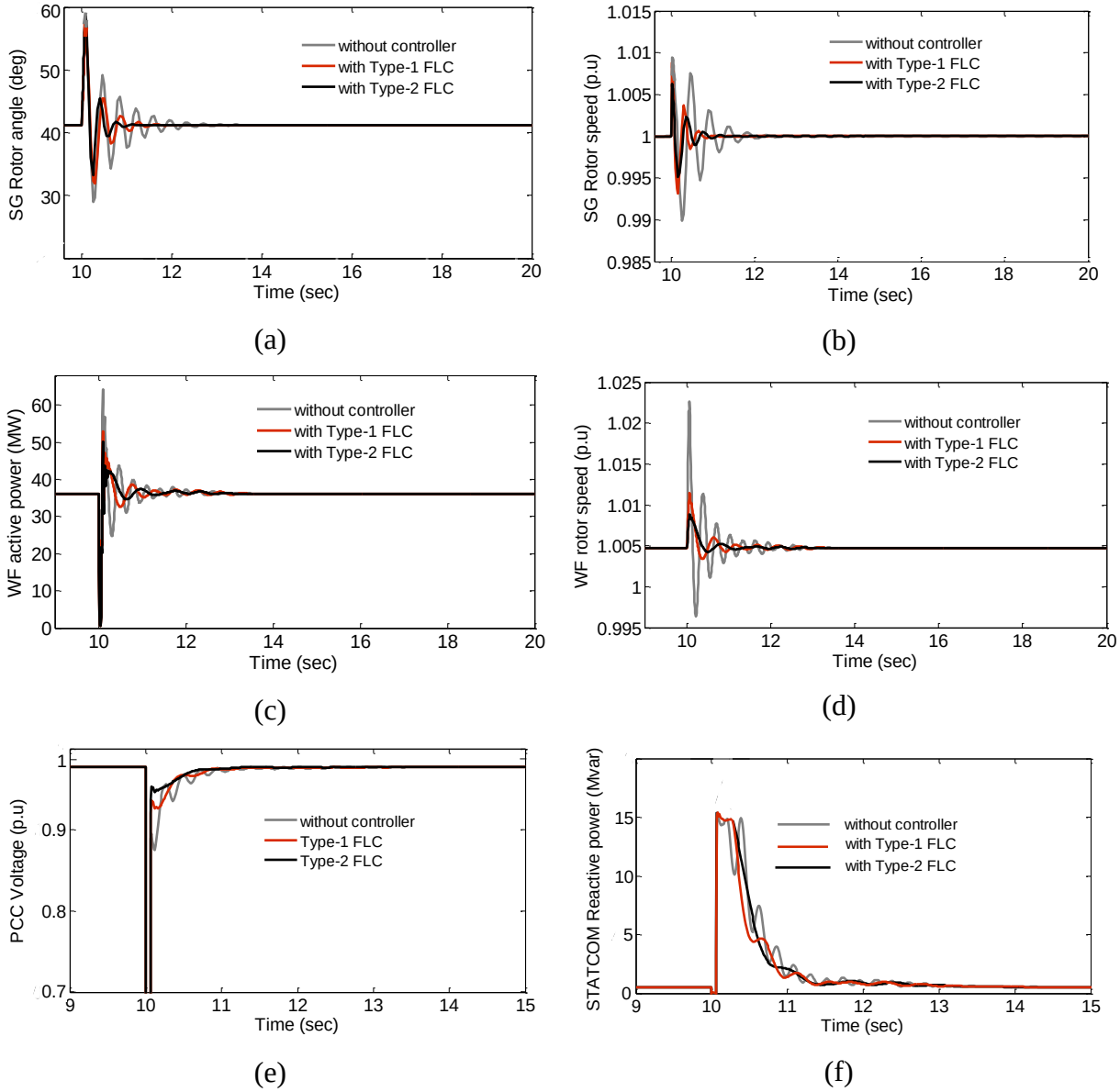

Figure 4.26: Responses of the studied system under three-line-to-ground fault (a) SG rotor angle (b) SG rotor speed (c) Wind farm active power (d) Wind farm generator rotor speed (e) Voltage at the PCC (f) Reactive power supplied by the STATCOM

Table 4.4: Maximum deviation in the quantities of the studied system under the 3LG fault disturbance

Quantities	Studied system without Damping controller	Studied system with Type-1 FLC Damping controller	**Studied system with Type-2 FLC Damping controller**
SG rotor angle	3.9514	3.9016	**3.8801**
SG rotor speed	0.0021	0.0013	**0.0011**
WF Active power	4.1618	4.1204	**4.1003**
WF rotor speed	0.0028	0.0017	**0.0014**

4.9.3.2 Case 2: Two-line-to-ground fault (LLG)

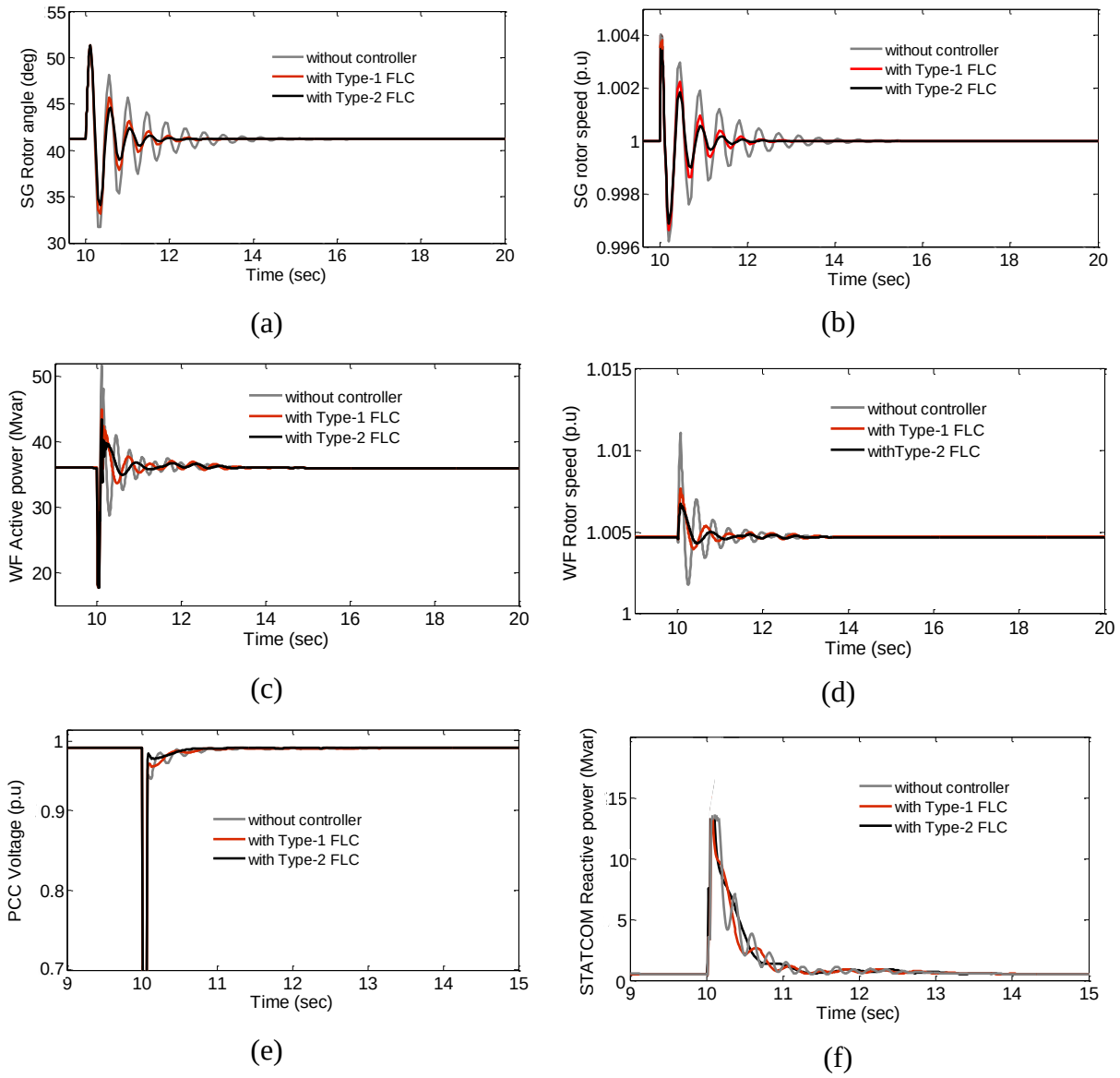

Figure 4.27: Responses of the studied system under two-line-to-ground fault (a) SG rotor angle (b) SG rotor speed (c) Wind farm active power (d) Wind farm generator rotor speed (e) Voltage at the PCC (f) Reactive power supplied by the STATCOM

Table 4.5: Maximum deviation in the quantities of the studied system under the 2LG fault disturbance

Quantities	Studied system without Damping controller	Studied system with Type-1 FLC Damping controller	**Studied system with Type-2 FLC Damping controller**
SG rotor angle	3.5853	3.5058	**3.3811**
SG rotor speed	0.0019	0.0013	**0.0009**
WF Active power	3.7957	3.7274	**3.5810**
WF rotor speed	0.0026	0.0014	**0.0012**

4.9.3.3 Case 3: Single-line-to=ground fault (LG)

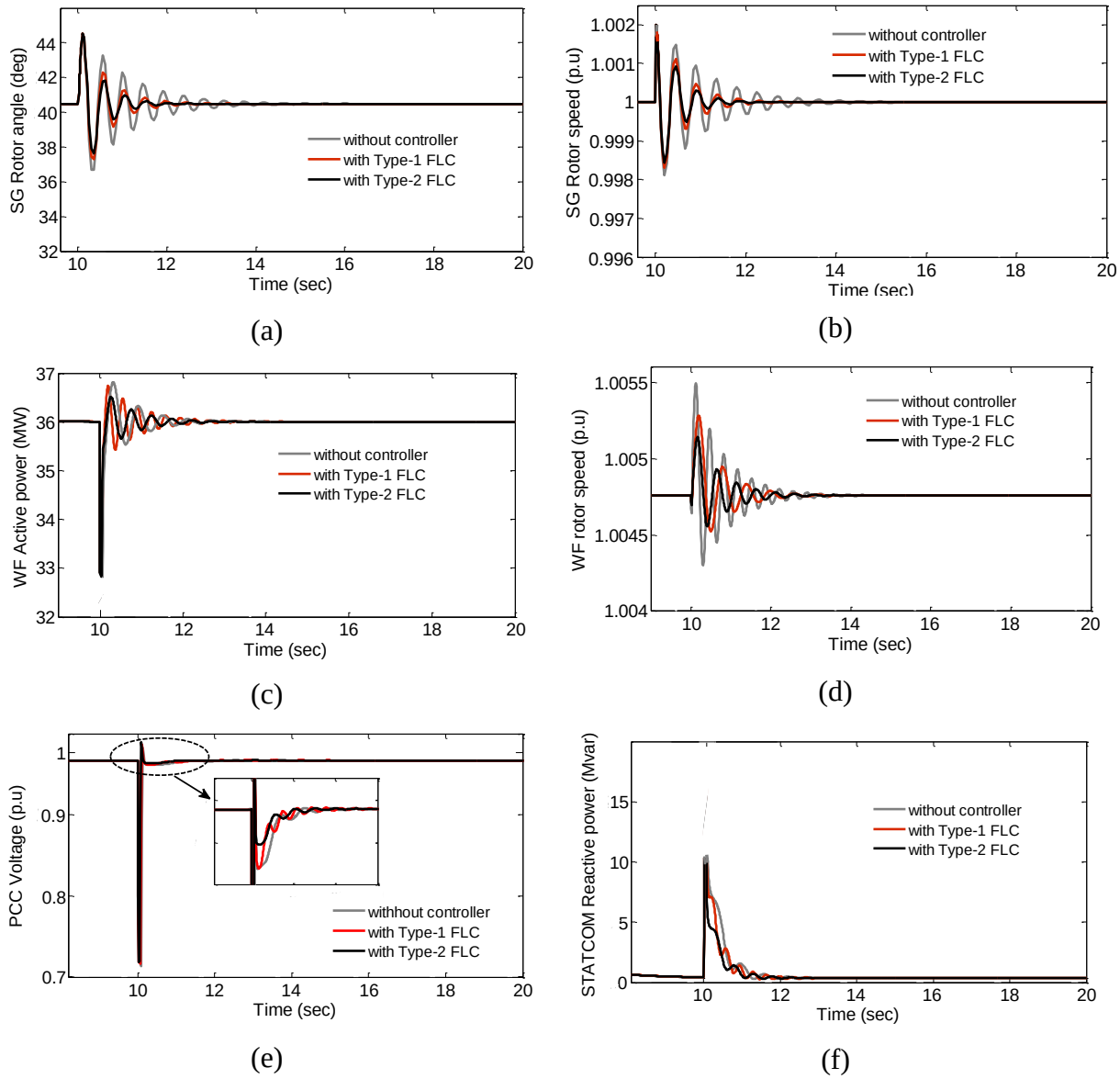

Figure 4.28: Responses of the studied system under single-line-to-ground fault (a) SG rotor angle (b) SG rotor speed (c) Wind farm active power (d) Wind farm generator rotor speed (e) Voltage at the PCC (f) Reactive power supplied by the STATCOM

Table 4.6: Maximum deviation in the quantities of the studied system under the LG fault disturbance

Quantities	Studied system without Damping controller	Studied system with Type-1 FLC Damping controller	**Studied system with Type-2 FLC Damping controller**
SG rotor angle	2.2851	2.2053	**2.0811**
SG rotor speed	0.0007	0.00055	**0.00043**
WF Active power	3.5847	3.5629	**3.5412**
WF rotor speed	0.0014	0.0008	**0.0003**

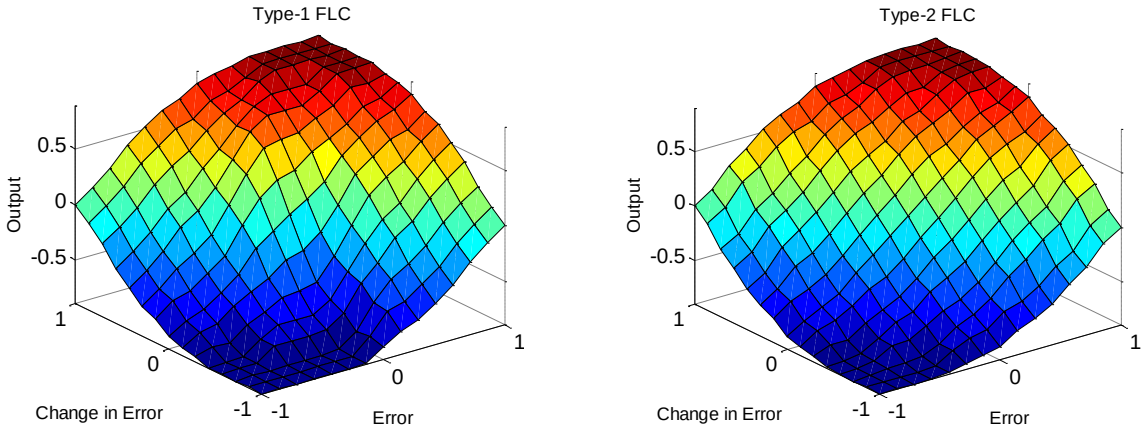

(a) (b)

Figure 4.29: Control surfaces (a) Type-1 FLC (b) Type-2 FLC

4.10 Conclusions

Concern to global warming effect with non-renewable energy sources and with ever increasing demand of electricity, it has become an absolute necessity to integrate the wind energy systems in the grid, for which a complete and detailed study of wind farm is required, in which simulation studies under various operating conditions expected (such as different type of faults, fault locations and durations) are highly needed to prevent any harmful impact of the wind farm to the grid where it is connected. In this chapter, a system which consists of 36MW wind farm exporting power to 120kV grid has been employed to study the impact of fault locations and durations on it, when it subjected to different types of faults. The system parameters such as PCC voltage, active and reactive powers are monitored during and after faults. Two different fault locations X1 and X2 are considered to study the impact of fault locations on the system. It observed, for both locations (X1 and X2) due to occurrence of faults (LG and LLG) the wind farm has an ability to stay connected to the system with and without STATCOM. Similarly, in case of LLLG fault the wind farm has remains connected to the system when the fault location is at X2 (with or without STATCOM). But, the wind farm become unstable if LLLG fault occurs at X1 without STATCOM, whereas it return back to stable-state and stay connected to the grid, if the STATCOM is connected at the PCC.

On investigating the effect of fault time durations, the wind farm remains stay connected to the grid when the LG fault occurs for durations of 100ms and 150ms, with and without STATCOM. In case of LLG fault, wind farm has stay connected to the system for fault duration of 100ms with and without STATCOM. But, for the same fault (LLG), if fault duration of 125ms then wind farm returns back to its stable-state, if STATCOM is connected.

Similar analysis was also done for LLLG fault, with duration of 80ms, the wind farm remains in stable-state with and without STATCOM. Whereas it occurs for duration of 100ms the wind farm becomes unstable without STATCOM, and when the STATCOM is employed then wind farm return back its stable state and stay connected to the grid.

Furthermore, this chapter also investigated STATCOM with type-2 fuzzy logic based damping controller for stability improvement of wind integrated power system. The STATCOM equipped with the proposed damping controller suppressed the inherent fluctuations of the studied system and thus enhance the stability of the system under different disturbances such as LLLG, LLG and LG faults. To examine the effectiveness of the proposed damping controller, simulation results are obtained for three different scenarios. From the simulation results, it can be concluded that STATCOM with type-2 FLC based damping controller offered best damping characteristics to improve the performance of the studied system under different fault conditions.

CHAPTER 5: PERFORMANCE IMPROVEMENT OF A FIXED SPEED WIND FARM USING UVPC STRATEGY

5.1 Introduction

In order to keep the acceptable and reliable operation of power system, the grid engineers are setting new grid code requirements for the wind plants. One of the relevant grid code requirements is low-voltage-ride -through (LVRT) capability of wind generators. Figure 1.11 represents the Germany grid code, the admissible operating point of a wind farm during the grid fault and subsequent voltage recovery as function of the time. The STATCOM is a common solution for LVRT problem in the fixed-speed wind farm. However, STATCOM alone may not guarantee grid code compliance [134], which provides the scope for further investigation of STATCOM with adequate control strategy in order to fulfil the LVRT grid code requirement.

Moreover, fixed speed WES output power and generator terminal voltage fluctuates with wind speed variation resulting in problem of frequency stability and voltage flickering (power quality issue). However, the main purpose of STATCOM connected to the wind farm is to improve the voltage stability and thus enhances the fault-ride through capability. In addition, it is well suited for reduction of voltage fluctuations at the generator terminal due to wind speed variations results in voltage flicker mitigation. As the STATCOM operates in lagging and leading modes, its role in the wind power system is limited to reactive power support. Therefore, the wind generator output power fluctuations due to wind speed variations cannot be smoothened out using STATCOM alone. Thus, it is also needed to investigate and develop an appropriate control strategy to smoothen out the generator output power as well as terminal voltage regulation subjected to below rated wind speed variation.

The contribution of this chapter: This chapter proposes a Unified Voltage and Pitch angle Control (UVPC) strategy for fixed speed wind farm. The focus put on guaranteeing the LVRT grid code requirement when the wind farm subjected to severe faults. The UVPC consist of STATCOM voltage control loops with adequate pitch angle control loops which are coordinated to enhance the low-voltage ride-through capability of the wind generators thereby, complying the LVRT grid code requirement as desired by the Germany grid code. Different scenarios such as system without STATCOM and pitch-angle controller, with STATCOM only, and system with STATCOM and pitch-angle control (i.e. UVPC) are simulated. The simulation results show that the adoption of STATCOM and pitch angle

controller fulfilling the LVRT grid code requirement to ensure the continuous operation of wind turbines. Furthermore, a concept of critical clearing time (CCT) is discussed and its utility has been emphasized. Calculations, simulations and measurements provide how the increased STATCOM rating can offer an enhanced stability margin.

Moreover, UVPC strategy is also employed and investigated for output power smoothing and terminal voltage regulation of a fixed speed wind generator, subjected to below-rated wind speed variations. Different scenarios as mentioned above are considered to evaluate the effectiveness of the proposed strategy. Simulation results clearly show that the proposed UVPC effectively smoothens out the generator output power and also regulates the terminal voltage at constant magnitude.

The pitch angle control loop of UVPC has been designed using type-2 fuzzy logic controller as it is very efficient in handling uncertainties in membership functions and rules than their traditional fuzzy logic counterparts and thus, offers robust performance.

5.2 Enhancement of LVRT capability of a fixed speed wind farm

In this section, first of all, the STATCOM control and pitch angle control schemes are discussed and thereafter proposed UVPC scheme which combines both control schemes is elaborated.

5.2.1 The STATCOM control scheme

The STATCOM which is employed here is already discussed in the chapter 4 in detail. Figure 5.1 depicts the STATCOM operating logic/flow chart. During a fault, there is a sudden dip in the voltage at the PCC and if it is below the threshold voltage (below 90 percentage of nominal voltage), the STATCOM injects the sufficient amount of reactive power to recover the PCC voltage. Besides this, under normal operation, it can compensate or inject quadratic current at the PCC according to the system operating condition to maintain the voltage within prescribed limits.

5.2.2 Pitch angle control scheme

The main purpose of the pitch angle controller is to maintain the output power of the wind generator at rated value when the wind speed exceeds the rated speed. In addition, it can also improve the transient stability of the wind turbine generator. Specially, for improving the fault-ride-through (FRT) capability of wind generators, the pitch-angle is modified with the help of pitch angle controller as shown in Figure 5.2(a) based on generator rotor speed, and explained in section 0 of chapter 3 in detailed. The inputs to the pitch angle controller are

generator rotor speed (ω_r) and the reference rotor speed (ω_r^{REF}). The resulting error (ε) passes through the controller $C(s)$ and thus, can improve the transient stability.

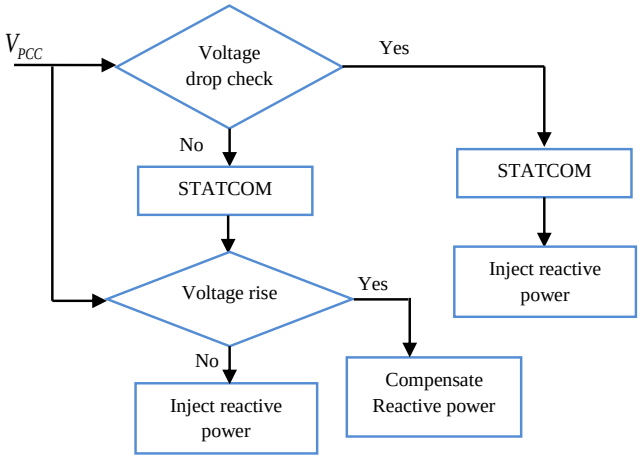

Figure 5.1: STATCOM control strategy Flow chart

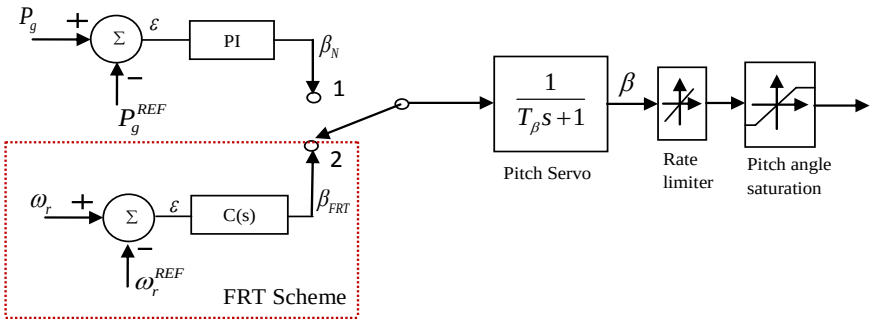

(a)

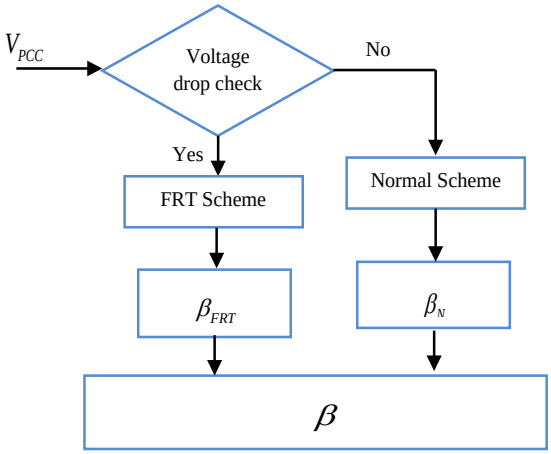

(b)

Figure 5.2: Pitch angle controller strategy: (a) Pitch angle control, (b) Flow chart.

The operating modes (for normal and fault-ride-through operations) of the controller can be determined using selection switch as shown in Figure 5.2(b). If the system voltage goes below

threshold (i.e below 90 percentage of nominal voltage) due to severe network faults, the switch connects to position ‘2’ and fault ride through (FRT) scheme of pitch angle controller (dotted box in Figure 5.2(b)) is activated which generates the pitch angle accordingly to reduce the mechanical torque for preventing generator rotor from over speeding and transient voltage instability. Under normal operating condition, the switch move from ‘2’ to ‘1’ position for activating normal pitch-angle control scheme.

5.2.3 The proposed UVPC scheme

Figure 5.3 depicts a proposed unified control scheme (big dotted box) comprising of pitch angle and voltage control loops. During the disturbances, the STATCOM voltage control loops especially, AC voltage controller provides reactive power compensation whereas, the FRT pitch-angle control loop prevents the rotor acceleration by reducing the mechanical torque. Therefore, using UVPC coordination control strategy reactive current injected has been controlled through pitch angle and STATCOM, which enhances the low-voltage-ride-through capability of the fixed speed wind farm.

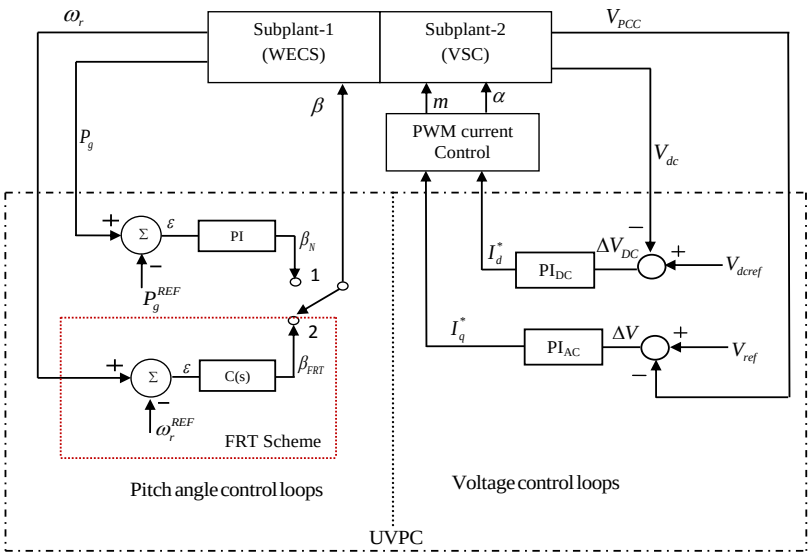

Figure 5.3: Block diagram of proposed UVPC

The major features of the UVPC can be summarized as:

1) As voltage restoration is essential for the fault-ride-through of a wind generator during faults, it is achieved by injecting quadratic current determined by AC voltage control loop, into the system.
2) For the severe faults, the fault-ride-through (FRT) scheme of pitch-angle-control loop limits the rotor from over speeding by reducing the wind turbine mechanical power through a suitable pitch angle generation. As a result, the AC voltage control loop can more effectively restore the PCC voltage to satisfy the grid code compliances.

3) After the fault has been cleared (i.e. during normal operating condition), AC voltage control loop can effectively regulate the bus voltage fluctuations. Thus, the active power imbalance of the IG is minimized and the mechanical power and the rotor speed can be more effectively controlled by pitch-angle control with the help of normal pitch-angle-controller.

5.2.4 Coordination of STATCOM and pitch angle flow chart

The flowchart for simultaneous control of pitch angle and STATCOM (i.e. UVPC) is as shown in Figure 5.4. The steps of UVPC coordination control algorithm are as follows:

Step 1: From the simulation of faulted system, the value of PCC voltage (V_{PCC}) is determined and checked whether, there exists a severe voltage depression i.e less than nominal operating voltage (V_N).

Step 2: If the condition ($V_{PCC} < 0.9V_N$) is satisfied (especially in case of transient faults), both AC voltage control loop of STATCOM as well as FRT scheme of pitch-angle control loop are activated. The output (I_q^*) of voltage controller ($\mathrm{PI_{AC}}$) determines the amount of reactive power injected into the system, at the same time, the error (ε) in generator rotor speed passes through the controller $C(s)$ which generates an appropriate pitch-angle (β_{FRT}) to reduce the mechanical torque.

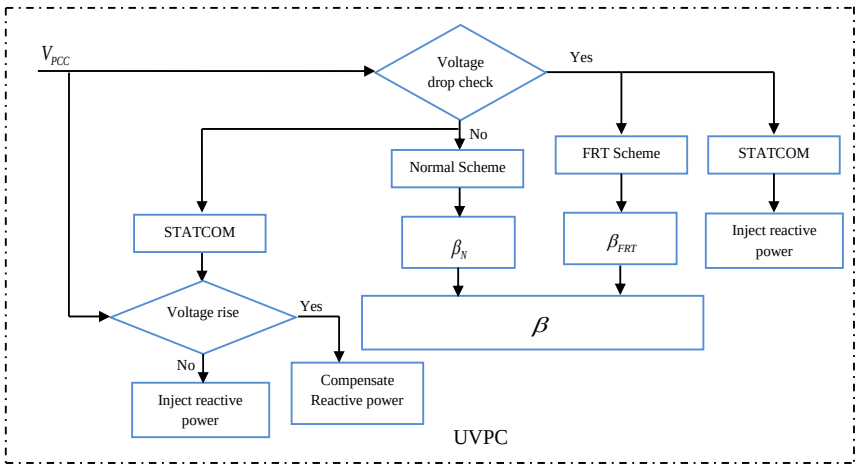

Figure 5.4: Coordination cycle of UVPC

Step 3: If the condition ($V_{PCC} < 0.9V_N$) is not satisfied i.e. during normal operating condition, if the system voltage and active power fluctuates due to normal disturbances (not severe). In that case, normal pitch-angle control loop determines the pitch angle (β_N)

to control the mechanical power thereby, reducing the oscillations in the active power. Meanwhile, AC voltage control loop also regulate the voltage at the PCC by injecting/absorbing the necessary reactive power by an appropriate output (I_q^*) through controller ($\mathrm{PI}_{\mathrm{AC}}$).

In order to achieve the successful LVRT capability and transient stability enhancement of the wind farm, the pitch angle and voltage control loops of UVPC need to be designed with an effective control method. The STATCOM voltage control and normal pitch-angle loops are designed using conventional PI controller technique, offering satisfactory performance. But, PI controller is not a good choice in fault-ride-through (FRT) scheme of pitch-angle control loop, as the controller is required to generate a desired pitch-angle command (β_{FRT}) so that the mechanical power can be reduced in a very efficient manner to limit rotor speed. Therefore, fuzzy logic controller (Type-1) is the best choice for FRT scheme of pitch-angle controller [36]. However, once the membership functions are defined for designing the controller, the uncertainties in membership functions (MFs) cannot be incorporated, thereafter. This may degrade the controller performance especially, when the wind farm is subjected to severe disturbances. In such conditions, an advanced Type-2 fuzzy logic controller is a better choice in comparison of their traditional fuzzy logic counterpart (Type-1). The following subsections, therefore, discuss the designing of the interval Type-2 FLC for the FRT scheme of pitch-angle controller.

5.2.5 Pitch angle controller design using type-2 FLC

To achieve fast and accurate mechanical torque control during the network disturbances, the FRT scheme of the pitch angle controller which shown in Figure 5.3 is designed using type-2 fuzzy logic controller and the proposed structure is as shown in Figure 5.5.

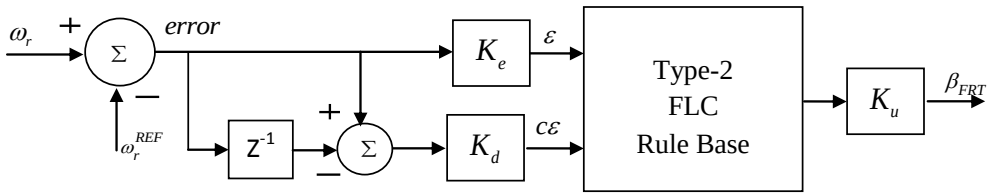

Figure 5.5: Proposed structure of type-2 FLC for FRT scheme of UVPC

Here, the controller gains K_e and K_d are used as a scaling gains for input signals whereas, K_u is used for scaling the output signal. These scaling gains can be variables or constants.

During the FLC design, these can play an important role to achieve suitable steady-state and transient-state responses. In this work these gains are considered to be constant.

In general as fuzzy type controllers did not handle the crisp input signals, but they needs to be defined in fuzzy terms. Therefore, the crisp input signals must be described in terms of fuzzy membership sets. The triangular membership functions (MFs) employed for design the input as well as output variables of Type-2 FLCs are depicted in Figure 5.6. Seven fuzzy sets for rotor speed error ($\mathcal{E}$) are defined and as: XLP(Extra Large Positive), LP(Large Positive), MP(Medium Positive), SP(Small Positive), XSP(Extra Small Positive), ZE (Zero) and N(Negative). Similarly, with expert knowledge for the change-in-rotor speed error ($\mathcal{CE}$) five fuzzy sets are chosen as: ZE (Zero), NB (Negative Big), PB (Positive Big), NS (Negative Small), and PS (Positive Small). Finally, to generate appropriate output pitch-angle, six membership functions are defined and notation as XL (Extra Large), L (Large), M (Medium), S (Small), XS (Extra Small) and ZE (Zero). Total, 35 inference rules were defined for all input-output MFs as shown in Table 5.1.

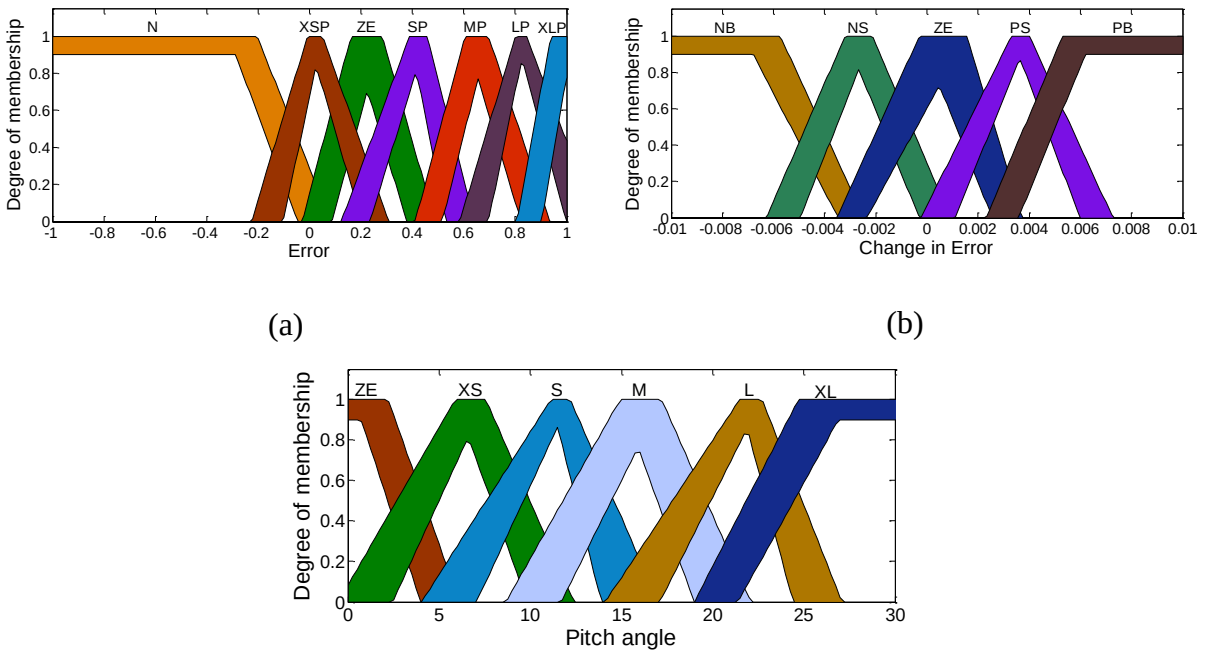

(a) (b)

(c)

Figure 5.6: Type-2 FLC Membership functions (a) Error (b) Change in Error (c) Pitch angle

Table 5.1: Fuzzy rules table for pitch angle generation

Change in Error ($c\varepsilon$)	Error (ε)						
	N	ZE	XSP	SP	MP	LP	XLP
NB	ZE	ZE	ZE	XS	S	M	L
NS	ZE	ZE	XS	S	M	L	XL
ZE	ZE	ZE	XS	S	M	L	XL
PS	ZE	ZE	XS	S	M	L	XL
PB	ZE	ZE	S	M	L	XL	XL

5.2.6 Employed system configuration

To evaluate the proposed UVPC control strategy, a typical power system is considered as shown in Figure 5.7. In this, 36MW of wind farm is considered (which consists of twenty four 1.5MW induction generators equipped with fixed speed wind turbines) connected to the 120kV grid. Each induction generator works at the rated operating point and supply 1.5MW of active power. The stator winding of the each induction generator is connected to the point-of-common-coupling (PCC) through a step-up transformer (0.69/25kV) which exports power to the 120kV grid through another step-up transformer T (25/120kV) and a transmission line. The employed STATCOM is connected to the 25kV bus (i.e PCC).

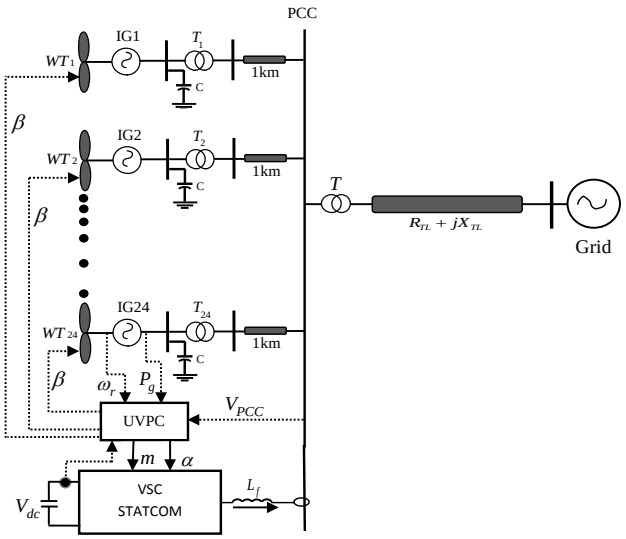

Figure 5.7: Block diagram of typical FSIG based studied wind farm

The addition of STATCOM with appropriate control strategy is expected to increase the stability margin as well as LVRT capability of the wind turbine. Therefore, in this work UVPC strategy has been proposed to control both mechanical torque (resulting in rotor speed control) and reactive power (resulting in voltage control) of wind energy system using pitch angle controller and STATCOM, respectively.

5.2.7 Results and Discussions

In order to observe the LVRT capability improved by the proposed UVPC, a solid three-phase-fault (with duration of 150ms) is applied at the PCC of the wind farm in the test system (as shown in Figure 5.7) at t=10s. To evaluate the effectiveness of UVPC strategy, three cases are considered: (1) System without STATCOM and pitch-angle controller (2) System with STATCOM only and (3) System with STATCOM as well as pitch-angle control (i.e. UVPC). The results are as follows:

5.2.7.1 Case 1: Without STATCOM and pitch-angle controller

In this case, the wind power system is considered (without STATCOM and pitch angle control) which is subjected to a three-phase fault at the PCC, for duration of 150ms at time t=10s. Figure 5.8(a)-(e) shows the various responses of the system.

It is observed that when the fault occurs, the electrical torque of the generator reduces drastically whereas the mechanical-input torque remains constant as shown in Figure 5.8(a), due to this difference between the electrical and mechanical torque, the generator rotor speed starts increasing (as governed by the equation (3.16)) as shown in Figure 5.8(b). Since the electrical torque decreases due to fault, the real power output of the generator also reduces accordingly as shown in Figure 5.8(c). Thereafter, it reduces to zero at 13s and becomes negative, resulting in the motoring action of the FSIG which can damage the turbine blades, if the protection system does not used. As observed from Figure 5.8(d), before the fault (under normal operating condition) FSIG draws around 5Mvar from the grid. After the fault is cleared, the induction generator absorbs a large amount of reactive power, impeding the voltage restoration at PCC. But, due to lack of quick reactive power supply, the PCC voltage cannot be fully retrieved (not able to recover upto 90%) as shown in Figure 5.8(e). Consequently, it increases rotor speed further as shown in Figure 5.8(b), and wind farm even consumes large amount of reactive power (around 22Mvar) as shown in Figure 5.8(d). This process may lead to power system instability, and therefore, FSIG may be tripped off from the grid by the over-speed protection. Under this condition, the FSIG does not possess sufficient

ride-through capability on its own and therefore, installation of STATCOM may be justified at the PCC to improve its ride-through capability.

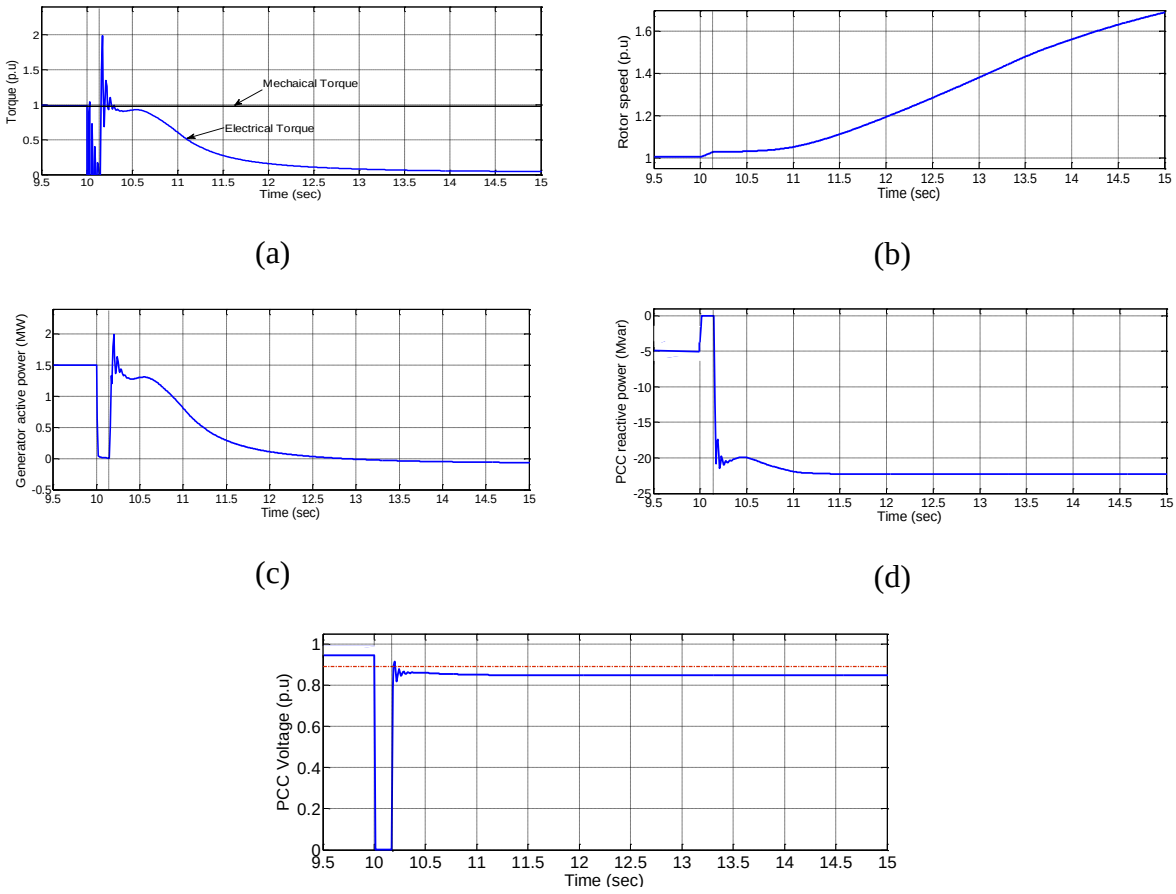

Figure 5.8: Simulation results without STATCOM and pitch angle controller: (a) Electrical and mechanical torques of the generator; (b) Generator rotor speed; (c) Generator active power; (d) Reactive power at the PCC; (e) Voltage at the PCC

5.2.7.2 Case 2: System with STATCOM

As discussed above, in order to improve system stability, a reactive power compensator (i.e. STATCOM) is installed at the PCC and considering the same solid three phase fault as before. The system responses obtained are as shown in Figure 5.9(a)-(f).

It is observed from Figure 5.9(a) that as the fault occurs at 10s, the electrical torque reduced to zero and the mechanical torque remains (assumed as constant) exist, and therefore, the rotor speed of FSIG increases as shown in Figure 5.9(b). After the fault is cleared, the STATCOM prevents the electrical torque loss, by injecting sufficient amount of reactive power to the system. Consequently, the FSIG rotor speed start decreases and returns back to

its initial value as shown in Figure 5.9(b). On comparing Figure 5.9(a) and (c), the real power supplied by FSIG varies exactly similar to its electrical torque.

Regarding the reactive power consumption of the FSIG during normal operating condition, it is drawing 4Mvar from the grid whereas the rest i.e. 1Mvar is being supplied by the STATCOM. Just after the fault clearance, FSIG withdraws almost 20Mvar from the grid but due to the corrective action taken by the STATCOM which suddenly pumps about 15Mvar into PCC, the amount of reactive power drawn from the grid starts reducing. However due to the fault clearance, the grid itself is able to recover the PCC voltage and therefore, the reactive power supplied by STATCOM goes on reducing as observed from Figure 5.9(d) and (f). The simultaneous reactive support from the grid and the STATCOM restores the PCC voltage to its nominal value after 13s as shown in Figure 5.9(e).

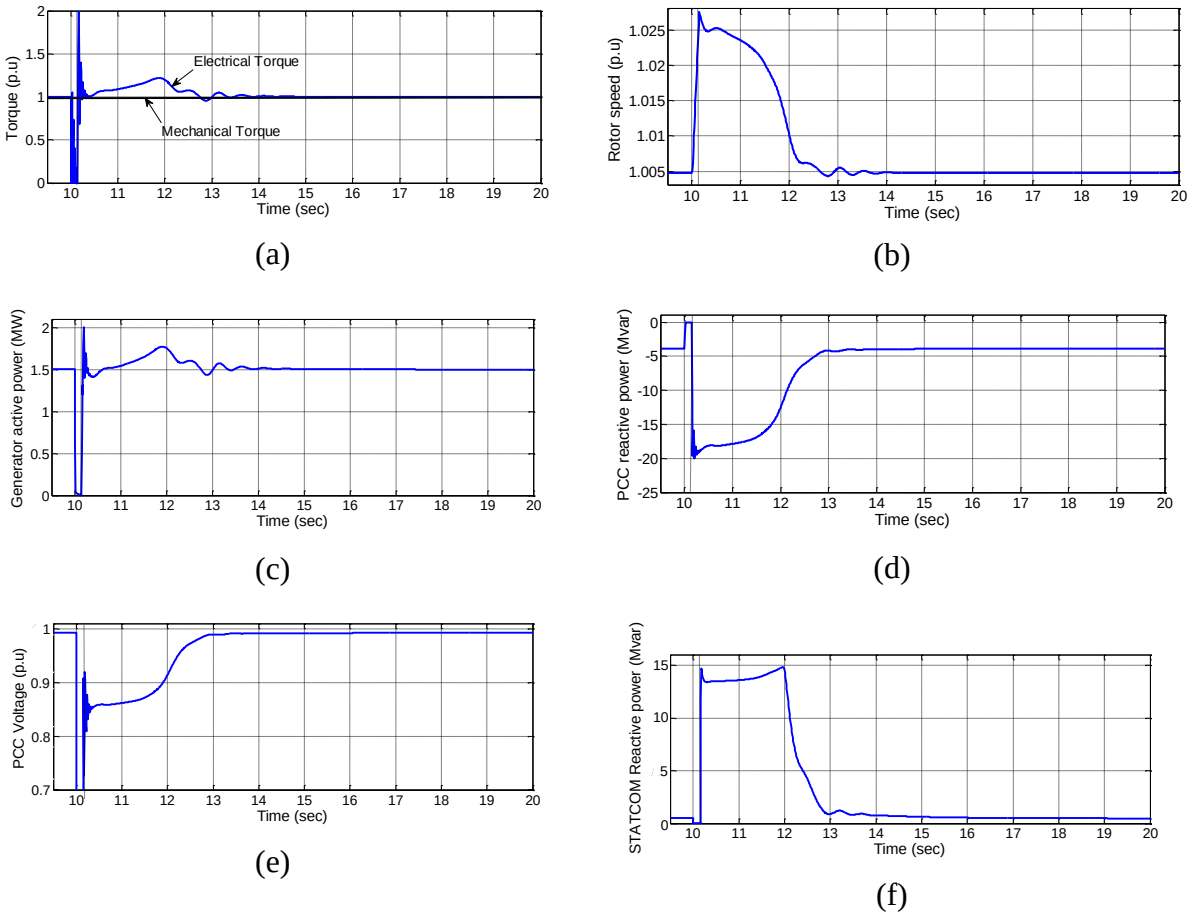

Figure 5.9: Simulation results with STATCOM: (a) Electrical and mechanical torques of the generator; (b) Generator rotor speed; (c) Generator active power; (d) Reactive power at the PCC; (e) Voltage at the PCC; (f) STATCOM reactive power injection

However, the voltage at PCC recovers to about 0.85p.u just after the fault clearance. But, it takes time duration of 1.9s to recover the voltage upto 0.9p.u from the fault occurrence time, which does not meet the grid code requirement (see Figure 1.11). Therefore,

STATCOM employment is able to improve the low voltage ride-through capability of the FSIG to some extent but, alone is not sufficient to meet the grid code requirement which provides the scope for further improvement of LVRT capability with the help of pitch-angle control of wind turbine as discussed earlier. Moreover as observed from Figure 5.9(b) and (c), rotor speed and active power are not free from the oscillations, resulting in grid frequency variation (especially in case, large wind farms are connected to power system networks). These oscillations also can be damped with the help of pitch-angle controller.

5.2.7.3 Case 3: System with STATCOM and pitch-angle control (i.e UVPC)

As explained earlier, in order to further improve the LVRT capability of the wind farm, UVPC control strategy is used through which, a simultaneous control of STATCOM and pitch-angle control is achieved. During the network disturbances, the proposed strategy injects the justified amount of reactive power as required during rotor acceleration. Besides, it can vary the mechanical torque by changing the pitch (rotor blade) angle of the wind turbine. The simulation results obtained by employing the proposed UVPC strategy to the system are as shown in Figure 5.10(a)-(h).

It is observed from Figure 5.10(a) that during the fault, the pitch-angle control (as shown in Figure 5.10(g)) helps in reducing the mechanical torque, which allows the rotor speed to reach only about 1.025p.u as shown in Figure 5.10(f) but earlier, it was able to go beyond 1.025p.u (see Figure 5.9(b)). As a result, the 0.9p.u of PCC voltage recovery has been achieved with time duration of 1.4s as shown in Figure 5.10(e) and satisfying the grid code compliance (see Figure 1.11), as compared to the previous case where voltage recovery of 0.9p.u is achieved with time duration of 1.9s. Therefore, the addition of STATCOM with pitch angle control (UVPC) is able to satisfy the grid code requirements as desired by Germany LVRT grid code.

After the voltage recover (0.9p.u), the pitch-angle control increases the mechanical torque which causes rotor speed to reduce and regain its initial value within 12s whereas it was taking about 14s earlier (see Figure 5.9(b)). In addition, the pitch-angle control is able to reduce the oscillations in the rotor speed. Similarly, if compare Figure 5.9(a) and(c) with Figure 5.10(b) and (c) respectively, there is no major difference but the pitch-angle control is effective in decreasing the oscillations in lesser time.

On comparing Figure 5.10(d) with Figure 5.9(d), it is observed that the pitch-angle control also contributes in reducing the reactive power drawn by the FSIG from the grid (after the fault clearance) from 20Mvar to 16Mvar. Even the reactive power contribution from the STATCOM (as shown in Figure 5.9(f) and Figure 5.10(h)) reduce from about 15Mvar to

13Mvar and its duration also get reduced from 12s to 11.5s, which indicates that pitch-angle control helps in reducing the size of STATCOM to be installed too.

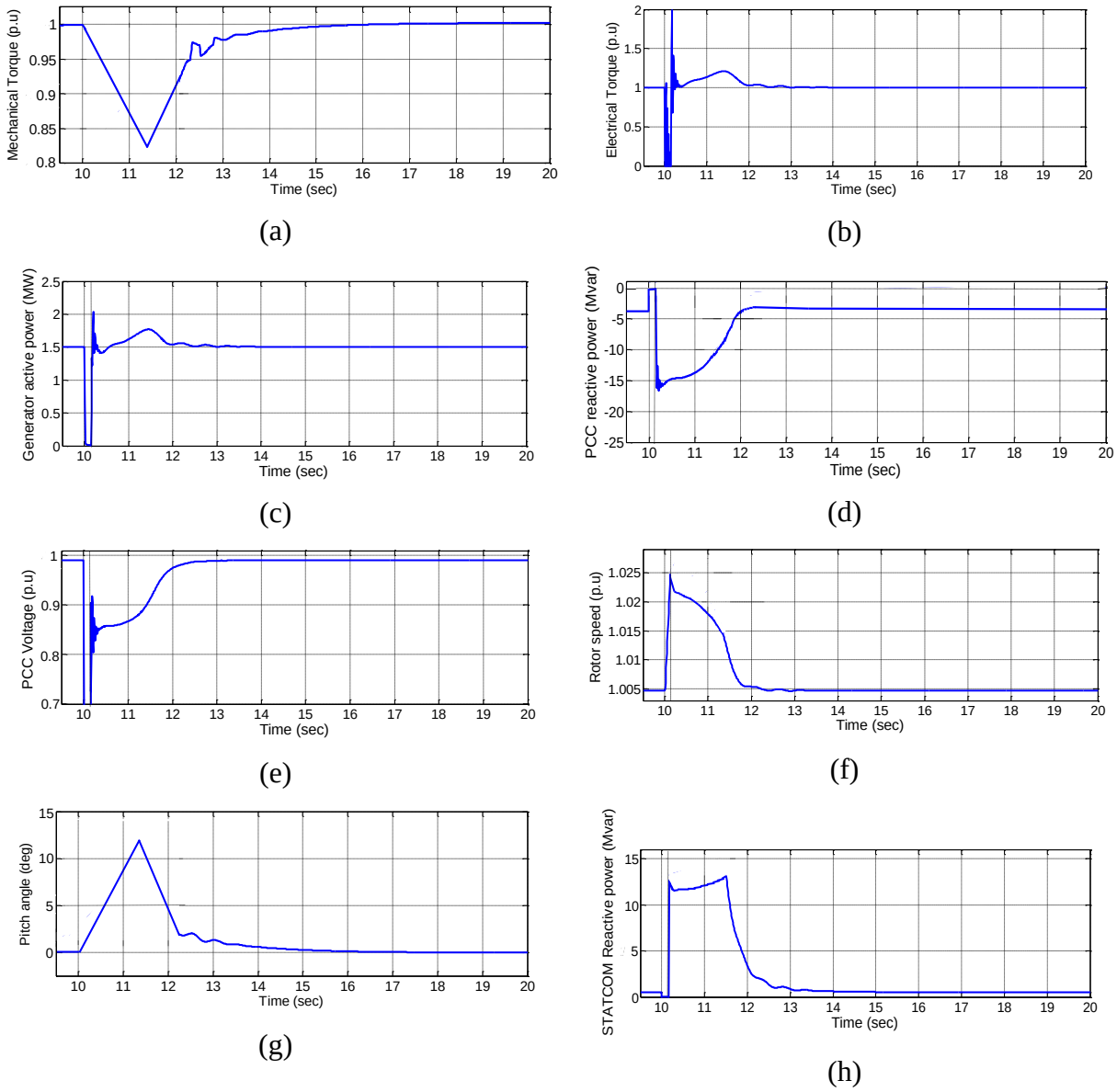

Figure 5.10: Simulation results with UVPC strategy: (a) Mechanical torque of the generator; (b) Electrical torque of the generator; (c) Generator active power; (d) Reactive power at the PCC; (e) Voltage at the PCC; (f) Generator rotor speed (g) Pitch-angle of the wind turbine (h) STATCOM reactive power injection

The performance of the UVPC is also compared with respect to critical clearing time (CCT). For a given system, it is essential to find the maximum value of CCT (maximum fault duration) for which system remains in stable state. In this work, CCT value is determined from the simulation in which, it is obtained by increasing the fault time interval for the same fault, until the system loses its stability. For example, simulation results in Figure 5.11 shows the rotor speed of the FSIG subjected to different faults durations with UVPC. The solid line

represents rotor speed variation for 0.15s fault and dotted line shows rotor speed variation for the maximum fault duration of 0.452s. Since the CCT is increased, UVPC is able to increase the stability of the wind farm system.

In order to further investigate the applicability of the proposed UVPC controller, different STATCOM capacities are considered. Table 5.2 shows the controllers' performance comparison in terms of CCT with different STATCOM capacities. The CCT of the system with a 15Mvar STATCOM is 0.452s with UVPC strategy, compared with 0.445s with STATCOM alone. Similar results are also obtained with 20 and 25Mvar STATCOM. This shows that the proposed UVPC can provide increased CCT, which consequently enhances the LVRT capability. The graphical representation of STATCOM capacity verses CCT with different control approaches are as shown in Figure 5.12. It is observed from this figure that for suppose maintaining the stability against 0.5s fault duration (CCT), the required STATCOM capacity with UVPC controller is 18.9Mvar comparison to 19.7Mvar without UVPC controller which is an economical benefit.

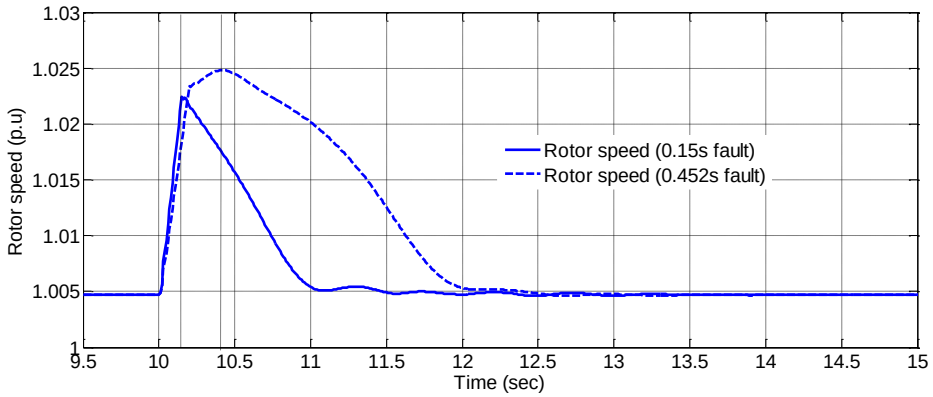

Figure 5.11: Rotor speed of generator with UVPC under different faults interval

Table 5.2: Performance comparison

STATCOM capacity (Mvar)	CCT(s) for the system with STATCOM	CCT(s) for the system with UVPC
15	0.445	0.452
20	0.503	0.513
25	0.521	0.543

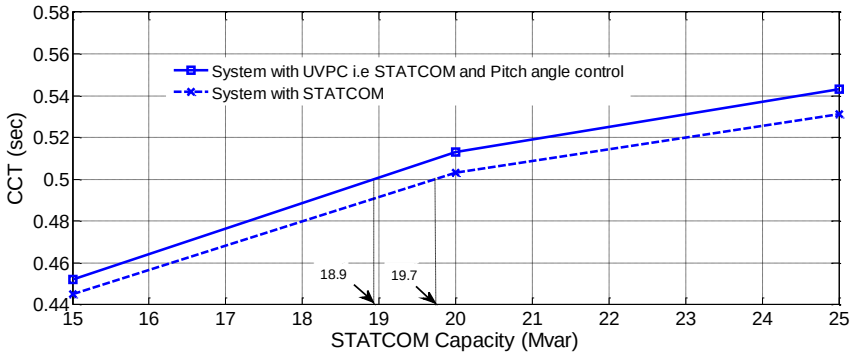

Figure 5.12: System CCT characteristics in terms of STATCOM capacity

5.3 Output power smoothing and voltage regulation of a fixed speed wind farm

In the above section 5.2, a simultaneous control of STATCOM and pitch angle control is used in order to enhance the wind farm low voltage ride through capability when it subjected to network faults. The idea of mixing electrical and mechanical parts seems to be interesting but, it has not been explored in respect of wind speed variations, due to which the output power and voltage of the wind generator fluctuate. It is becoming more concern as the wind generator installations are increasing in number. However, the installation of STATCOM can regulate the generator terminal voltage with varying wind speed irrespective of the wind speed regions (above or below rated). The pitch angle controller limits the aerodynamic power at its rated level only when the wind speed surpasses above rated. But in below-rated wind speed (partial load region), there is no role of the pitch angle control system to control the active power (in this region the maximum power extraction is allowed). As a result, any variation in the wind speed causes fluctuations in output power. Therefore, a typical pitch angle control strategy is developed by introducing exponential moving average (EMA) concept from which, the controller reference power (signal) can be set for below-rated wind speed. As a result, the employed pitch angle controller together with STATCOM named as unified voltage and pitch angle controller (UVPC), involved with an objective of power smoothing and terminal voltage regulation of a wind generator, subjected to below-rated wind speed variations is achieved.

5.3.1 The employed STATCOM Control Scheme

The STATCOM control scheme employed here is already discussed in the section 4.5 of chapter 4.

5.3.2 Pitch angle control scheme

The typical pitch angle controller scheme employed here is already discussed in detailed in the section 3.7 of chapter 3.

5.3.3 UVPC control scheme

The reactive power compensator like STATCOM is installed at the wind farm connection point can supply the amount of reactive power to the wind generator resulting in voltage regulation subjected to above/below rated wind speed disturbances. In the same trend, the pitch angle controller which is discussed in section 3.7 of chapter 3 can control the mechanical torque of the generator and thus, can smooth the generator output power under below-rated wind speed variations.

In this study, therefore, simultaneous control of STATCOM and pitch angle controller are employed to smoothing the voltage and output power fluctuations of the wind generator subjected to below-rated wind speed disturbances. Figure 5.13 shows a proposed UVPC control scheme (dotted box) comprising pitch angle and voltage control loops. During the wind speed disturbances, the UVPC voltage control loops especially AC voltage controller generate a proper quadratic current command (I_q^*) which decide the amount of reactive power to be compensated by STATCOM. Besides, the pitch angle control loop of UVPC can smooth the active power of generator by controlling the mechanical torque through suitable pitch angle generation.

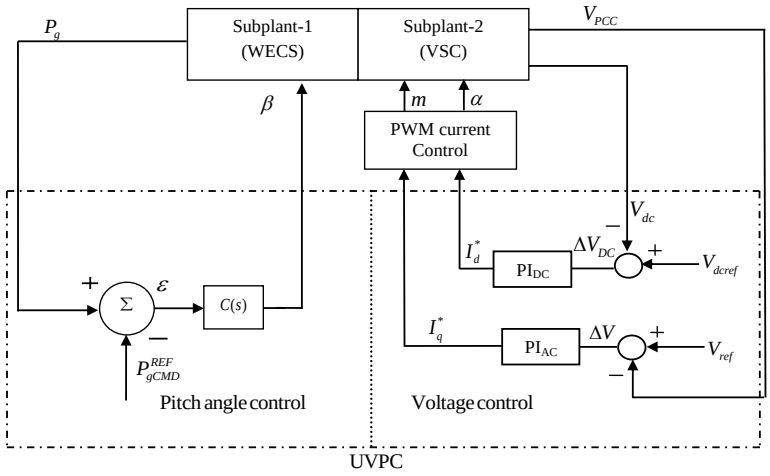

Figure 5.13: Block diagram of proposed UVPC

In order to achieve the successful reduction in power fluctuations and voltage regulation, the pitch angle and voltage controllers of UVPC need to be designed with an effective control technique. However, the STATCOM voltage control loops designed by using conventional PI

controller offered satisfactory performance, but in pitch angle control loop the PI controller design is not a good choice as the controller required to work under below-rated wind speed variations. In this trend, an advanced type-2 fuzzy logic controller is the best choice than their traditional fuzzy logic counterpart, as it can handle higher uncertainty levels. The following subsections discuss the designing part of the interval type-2 FLC for the pitch angle controller.

5.3.4 Pitch angle controller design using type-2 FLC

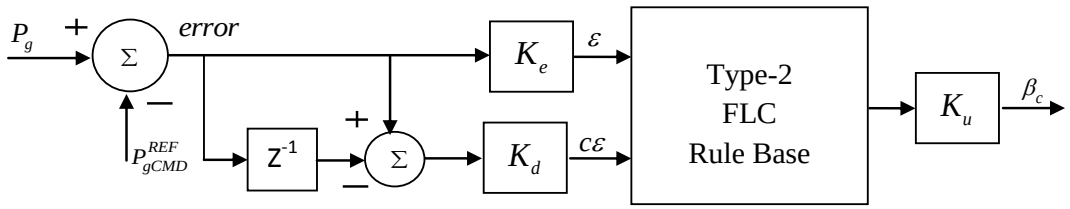

Figure 5.14: Structure of type-2 FLC based pitch angle controller

The controller gains K_e and K_d are used as a scaling gains for input and K_u for the output signals. In this work these gains considered to be constant and chosen as $K_e = 1$ $K_d = 100$ and $K_u = 10$.

The difference between P_g and P_{gCMD}^{REF} goes through the Type-2 FLC as an error (ε) and change in error ($c\varepsilon$) signals which are fuzzified by employing seven triangular linguistic variables MFs. Notation for the fuzzy sets as: NL (Negative Large), NM (Negative Medium), NS (Negative Small), ZR (Zero), PS (Positive Small), PM (Positive Medium), PL and (Positive Large). The designed MFs of type-2 FLCs are shown in Figure 5.15. For all the inputs and outputs, the universe of discourse is chosen as [-1, +1]. After the successful design of degree of membership type-2-fuzzy sets, the rules that are dealing with the control problem need to be defined. These rules define what actions are to be taken for all conceivable combinations of membership. The Total, 49 rules have been defined for all input-output MFs as shown in Table 5.3.

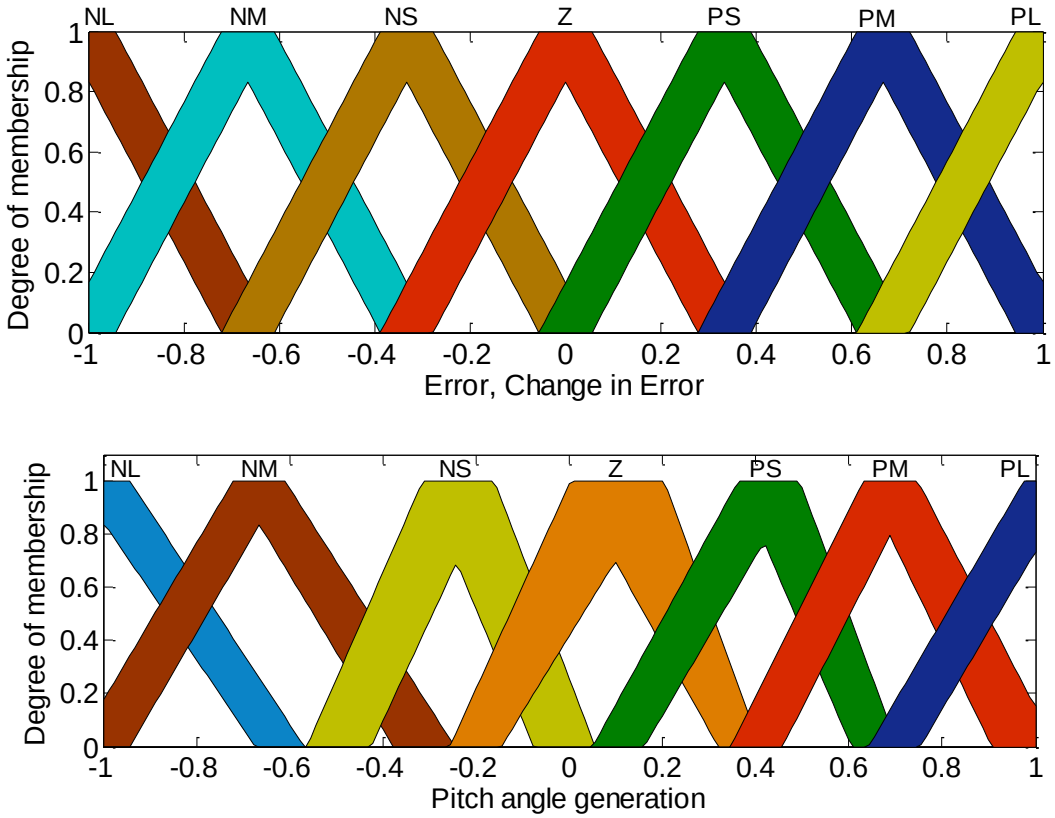

Figure 5.15: Type-2 FLC designed membership function

Table 5.3: Controller rules

Change in Error ($c\varepsilon$)	Error (ε)						
	NL	NM	NS	Z	PS	PM	PL
NL	NL	NL	NL	NL	NM	NS	Z
NM	NL	NL	NL	NL	NS	Z	PS
NS	NL	NL	NM	NM	Z	PS	PM
Z	NL	NM	NS	Z	PS	PM	PL
PS	NM	NS	Z	PM	PM	PL	PL
PM	NS	Z	PS	PM	PL	PL	PL
PL	Z	PS	PM	PL	PL	PL	PL

5.3.5 Employed system configuration

The employed and simulated system for this work is as shown in Figure 5.7.

5.3.6 Results and discussions

In order to observe the power smoothing and voltage regulation capability contributed by the proposed UVPC strategy, three different cases have been considered as case 1: System without compensation (i.e without STATCOM and pitch angle controller), case 2: System with STATCOM, and case 3: System with STATCOM and pitch angle control i.e UVPC. The Figure 5.16 shows the employed below-rated wind speed data for the simulation study.

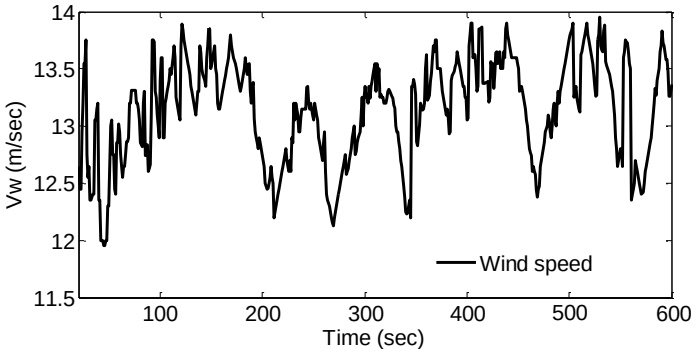

Figure 5.16: Wind speed profile

5.3.6.1 Case 1: System without compensation

In this case, the wind power system without compensation (i.e without STATCOM and pitch angle control) has been considered and subjected to below-rated wind speed variations as shown in Figure 5.16. The responses of the generator voltage, active power, and rotor speed are as shown in Figure 5.17(a-(c).

Figure 5.17(a) represents the magnitude of the generator terminal voltage obtained without STATCOM. It is clear that the generator voltage fluctuates significantly as there is no dynamic reactive power compensation. Thus, it leads to voltage fluctuations at the PCC in a reasonable range resulting in flicker problems. Therefore, it (voltage flicker) is a major limiting factor with the connection of the wind turbines into weak grids, where the wind penetration level is very high.

Since there is no pitch angle generation (without pitch angle controller) which ensures no point of limiting the rotor speed as shown in Figure 5.17(c) and the wind turbine operates with its maximum possible efficiency. As a result, the generator active power followed the wind speed disturbances and exhibits huge fluctuations as shown Figure 5.17(b). If a large number

of wind farms were realized and connected to power system networks, it leads to grid frequency problems.

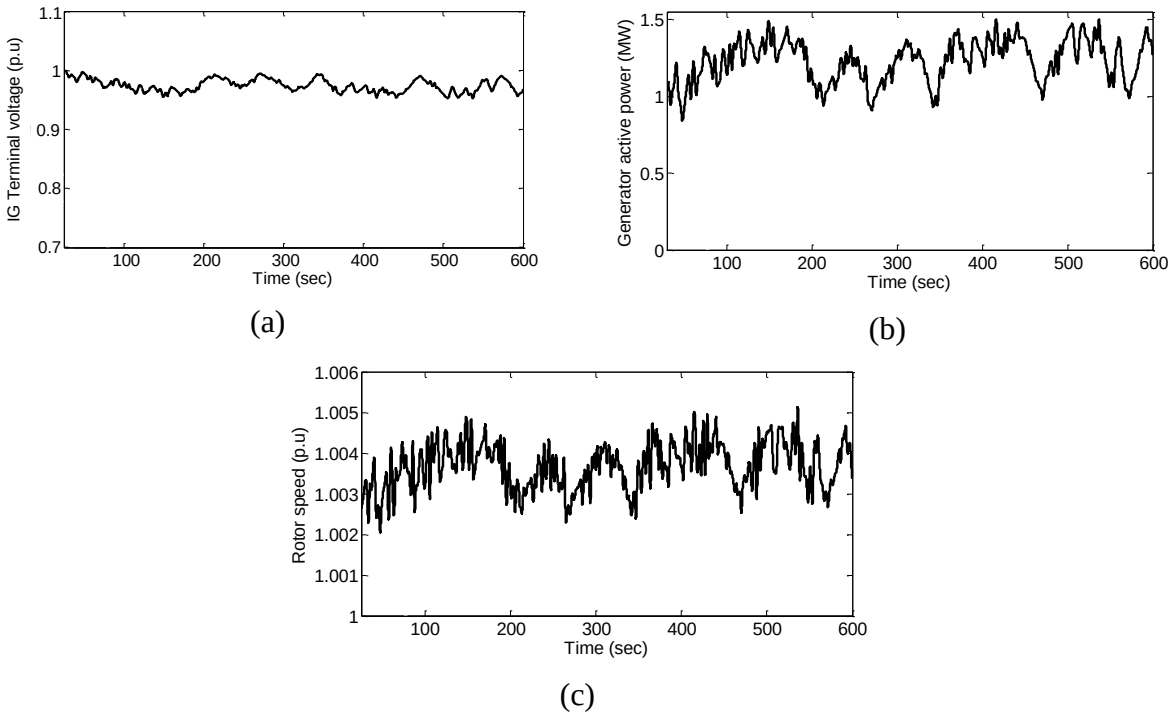

Figure 5.17: Dynamic response of the system without compensation subjected to below-rated wind speed: (a) Generator terminal voltage; (b) Generator output power; (c) Generator rotor speed

5.3.6.2 Case 2: System with STATCOM

In this case, the STATCOM has employed and connected to the PCC point from where studied wind power system is integrated (see Figure 5.7). The dynamic responses of the system, subjected to below-rated wind speed variations are as shown in Figure 5.18(a)-(c). Since the STATCOM provides dynamic reactive power compensation, the voltage fluctuations caused by the wind speed variations were regulated as shown in Figure 5.18(a). Thus, it mitigates the voltage flicker occurred in the wind farm for a smooth grid interaction.

Although, the STATCOM improves the voltage fluctuations due to wind speed variations by controlling the reactive power, but it does not have a capability to control the active power. As a result, the generator output power follows the wind speed variations as no pitch angle controller was employed and exhibits fluctuations as shown in Figure 5.18(b). And thus, the consequence of power fluctuations leads to network frequency stability problems. Figure 5.18(c) shows the amount of reactive power compensation provided by the STATCOM to regulate the generator terminal voltage.

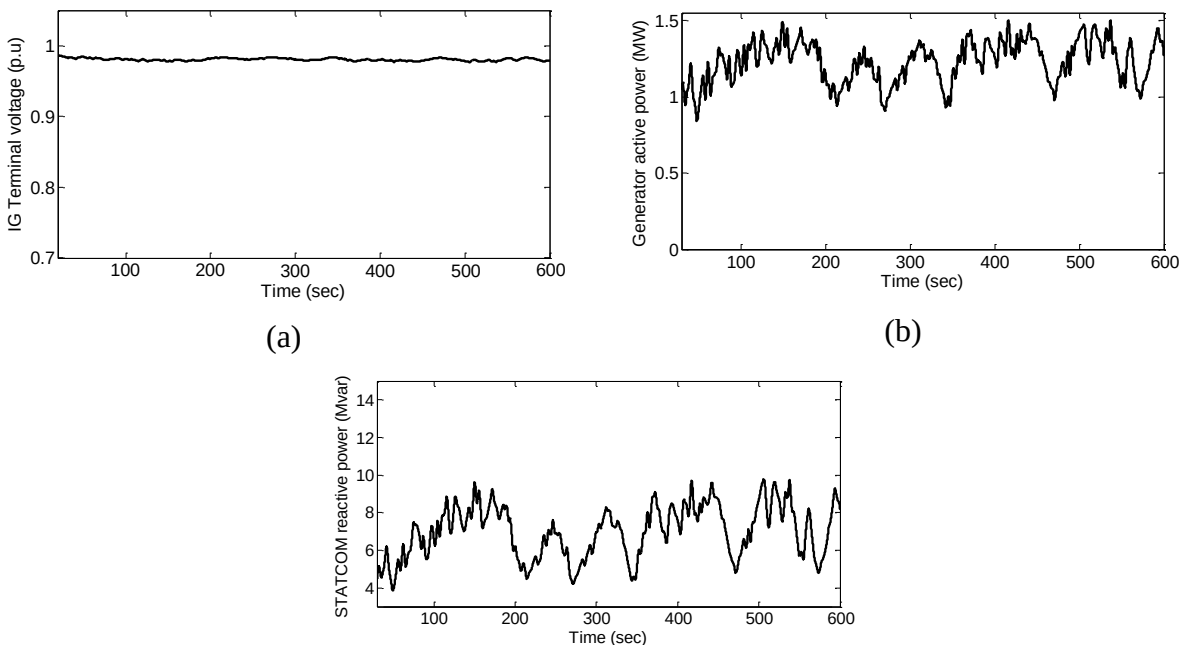

Figure 5.18: Dynamic response of the system with STATCOM subjected to below-rated wind speed: (a) Generator terminal voltage; (b) Generator output power; (c) STATCOM reactive power compensation

5.3.6.3 Case 3: System with STATCOM and pitch angle control (i.e with UVPC)

In this case, a control strategy (UVPC) has employed through which a simultaneous control of STATCOM reactive current and pitch angle were achieved. In addition, to compensate reactive power required during wind speed disturbances, the proposed strategy can control the mechanical torque by changing the rotor blade angle of the wind turbine resulting active power control. The simulation results obtained with proposed UVPC are as shown in Figure 5.19(a)-(d).

As it discussed earlier, to smooth the output power fluctuations under below-rated wind speed, first it is required to determine the output command power (P_{gCMD}^{REF}) and thereafter, fuzzy logic approach (type-2 FLC) has been implemented to smoothen out power fluctuations. From Figure 5.19(b), it is observed that the active power output of the wind energy system follows the reference command power and real power fluctuations are being smoothened out more effectively compared to the previous case (see Figure 5.18(b)). The pitch angle profile generated by the pitch angle controller for output power smoothing is as shown in Figure 5.19(d). The Figure 5.19(a) shows the generator voltage regulation achieved with STATCOM reactive power control. The reactive power compensation provided by the STACOM is shown

in Figure 5.19(c). By observing the results, it is clear that by employing UVPC strategy, simultaneous control of STATCOM and pitch angle is achieved which leads to reduction in fluctuations in generator voltage and active power. Moreover, by employing this control strategy the maximum amount of reactive power required for compensation using STATCOM is around 7.5Mvar, whereas only with STATCOM (case 2) the amount of reactive power required is around10Mvar (see Figure 5.18(c)). Thus, for a given operating condition, the proposed strategy can reduce the amount of reactive power supplied by the STATCOM.

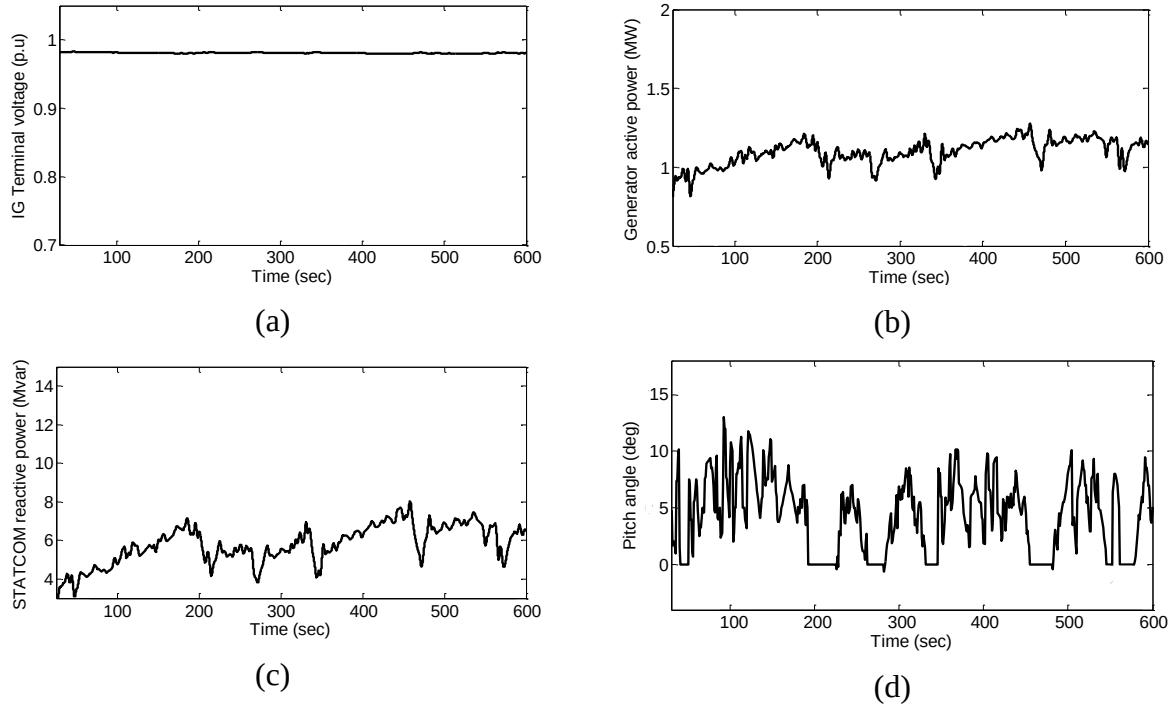

Figure 5.19: Dynamic response of the system with STATCOM and pitch angle control i.e UVPC subjected to below-rated wind speed: (a) Generator terminal voltage; (b) Generator output power; (c) STATCOM reactive power compensation; (d) Pitch angle

5.3.6.4 Performance indices

Figure 5.20(a) shows the output power comparison of without UVPC (i.e case 1) and with UVPC (i.e case 3). It is clearly noticed from the figure that the better real output power smoothing has been achieved with proposed UVPC strategy. The Figure 5.20(b) shows that the power smoothing function (performance index) obtained using equation (3.27) with and without UVPC. The proposed method has smaller magnitude for performance index as compared to without UVPC throughout the wind speed pattern considered.

Using equation (3.28), the maximum energy output of WES obtained over the wind speed disturbance was also determined considering case 1 (without UVPC) and case 3(with UVPC) but one at a time. The plot is as shown in Figure 5.20(c). The maximum energy has been obtained without UVPC as there is no pitch angle generation (it remains fixed at zero

degrees). But with UVPC, there is a drop in the output power due to pitch angle generation. However, the purpose of this work is to IG terminal voltage regulation and smoothing the output power and thus drop cannot be avoided.

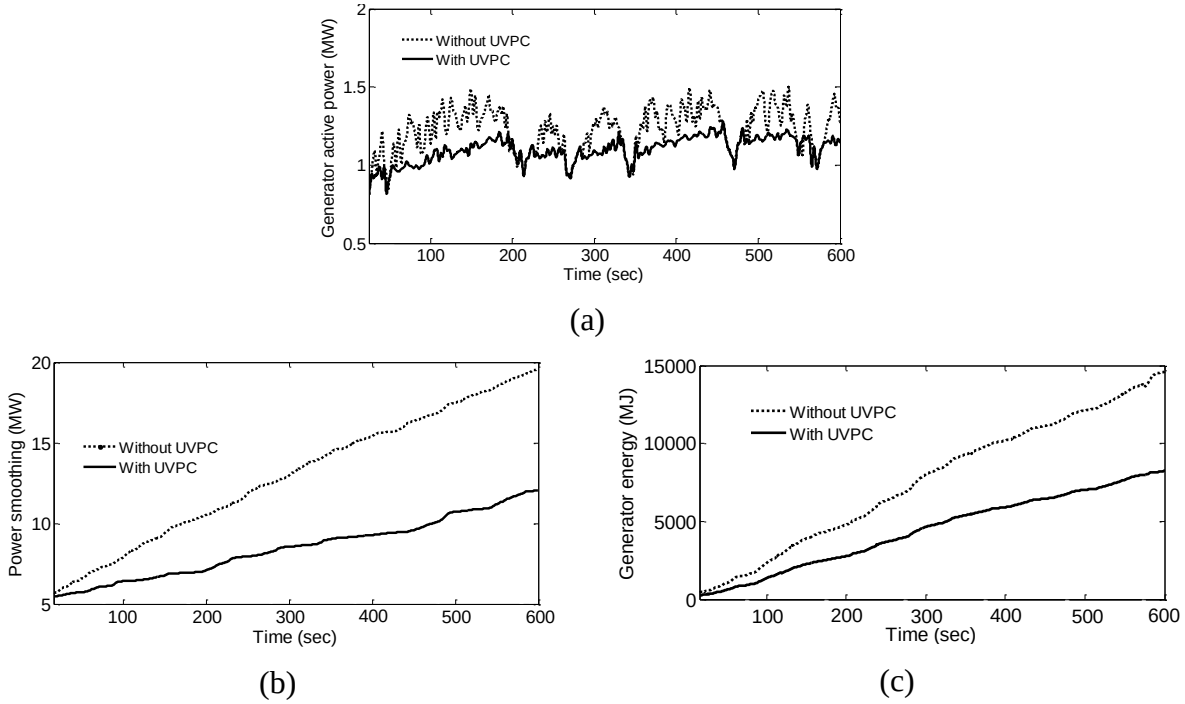

Figure 5.20: Performance comparison of system without UVPC and with UVPC: (a) Generator active power; (b) Generator output power smoothing function; (c) Maximum energy function

Similarly, the voltage regulation function (performance index) for the wind generator can also express as equation (5.1). And the corresponding regulation function outcome, with and without UVPC is as shown in Figure 5.21. It indicates that the voltage regulation function with UVPC possesses smaller magnitude compared to without UVPC throughout the simulation and hence, provides good constant voltage magnitude.

$$V_{reg} = \int_0^T \left| \frac{dV_g(t)}{dt} \right| dt \tag{5.1}$$

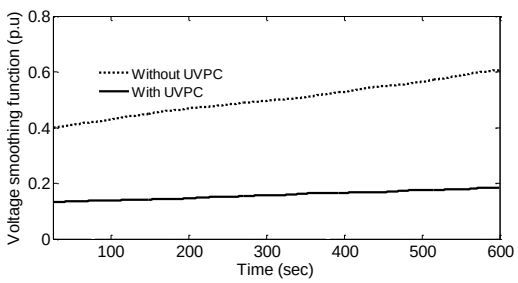

Figure 5.21: Generator terminal voltage regulation function

5.4 Conclusions

In this work, UVPC control strategy is proposed to guarantee satisfying the LVRT grid code requirement as well as effective output power smoothing and generator terminal voltage regulation for fixed speed wind farm subjected to transient fault and wind speed variations, respectively. The UVPC strategy consists of STATCOM control loops in combination with adequate pitch angle control. The pitch angle control loop employed in UVPC strategy is designed using interval type-2 fuzzy logic technique as it exhibits robust performance than any other controllers.

In this regard, static synchronous compensator (STATCOM) provides dynamic reactive power support to assist the fixed-speed induction generator for voltage restoration. Besides, the pitch-angle controller of constant speed wind turbines can effectively reduce the wind turbine mechanical power, preventing the wind generator from over-speeding. Therefore, using STATCOM in combination with pitch angle control, named as unified voltage and pitch-angle (UVPC) control strategy, enhances the LVRT capability of the fixed speed wind farm as well fulfilling the grid code requirement when it subjected to severe faults. In addition, the proposed UVPC helps in reducing the size of the STATCOM to be installed for improving the LVRT of such wind farms.

Furthermore, UVPC strategy is also implemented and investigated for output power smoothing and terminal voltage regulation of generator subjected to below-rated wind speed variations. It is seen from the simulation results that the voltage fluctuations are drastically reduced thereby improve the power quality of the system. As the effective output power smoothing achieved with proposed UVPC scheme, the system frequency affected by power fluctuations can also controlled within the acceptable limit. It is also noticed from the simulation results that by employing pitch angle controller and STATCOM (case 3), the maximum amount of reactive power required to regulate the generator voltage is around 7.5Mvar, whereas only with STATCOM (case 2) the amount of reactive power required is around 10Mvar. It reveals that with pitch angle controller, the capacity of the STATCOM can be minimized. Moreover, if the power storage systems are employed to minimize the power fluctuations by including this type of pitch angle controller, then size of power storage system capacity can also be minimized.

CHAPTER 6: STABILITY ENHANCEMENT OF VARIABLE SPEED WIND ENERGY SYSTEM

6.1 Introduction

Until the year 2000s, the fixed speed wind energy systems dominated the market, and still exist with a significant amount in the global wind turbine population. However, recently variable speed WESs draws an attention of power system engineers due to their advantages. The variable speed wind energy system incorporates the power electronics converter [120] thereby it can achieve independent control of active and reactive power. Among the many variable concepts Doubly-fed Induction Generator (DFIG) based variable speed WES have become most popular, since converter rating can be kept fairly low (approximately 25%-30% of the total machine power). Currently, DFIG based WES occupies close to 50% among the total wind power generation. However, DFIG is very sensitive to the voltage variations in the grid, which poses limitations for wind energy system during the grid interaction. When the penetration levels of these WES are very high, the large voltage drop occurs during the network disturbances such as short circuit faults, which may trigger a sequence of other events in the power network. Handling the disturbances which deteriorates the stability of DFIG is a major challenge to make it complaint with the modern grid code requirement. Therefore, there is need to look for a robust control strategy for DFIG based WES, which provides better stability performance thus offers effective grid interaction operation.

The contribution of this chapter: In this chapter, an advanced interval type-2 fuzzy logic-proportional integral (PI) controller has been proposed for torque and voltage control loops of rotor side converter of DFIG. The gains of PI controller are determined and tuned by interval type-2 fuzzy logic method according to system operating condition. Thus, the adaptive nature of type-2 fuzzy logic and robust nature of PI controller are combined eventually, which exhibits good steady state and dynamic responses. The performance of the proposed controller has been evaluated for different operating conditions of DFIG such as severe fault and voltage sag with reference to varying wind speed. Real time simulations are developed for DFIG based WES to validate the proposed controller using the OPAL-RT digital simulator. The performance of the proposed controller is examined through a comparative analysis with its traditional fuzzy logic-PI counterpart. The transient analysis of DFIG with interval type-2 fuzzy-PI shows the improved results subjected to three-phase fault and voltage sag as desired by the grid codes.

6.2 Maximum-Power-Point-Tracking (MPPT)

The extracted mechanical power from the rotor of a wind turbine of variable speed wind energy system can be written as:

$$P_m = \frac{1}{2}\rho A_r C_p(\lambda,\beta)V_w^{\,3} \tag{6.1}$$

where, V_w is wind speed [m/s], $A_r = \pi R^2$ is the rotor swept area [$m^{2]}$, R is the radius of the blade [m], ρ is air density [kg/m^3], and C_p is the power coefficient which depends upon the ratio of blade pitch-angle (β) and rotor-tip speed (λ). For the commercial wind turbines, manufactures were not ready to provide the information regarding power coefficient. As a result, different mathematical approximations were derived and several appropriate equations that have been developed to describe the power coefficient. The mathematical equation of power coefficient (C_p) used in this study is as follows [3]:

$$C_p(\lambda,\beta) = c_1\left(c_2/\lambda_i - c_3\beta - c_4\right)e^{-c_5/\lambda_i} + c_6\lambda \tag{6.2}$$

where

$$\frac{1}{\lambda_i} = \frac{1}{\lambda + 0.008\beta} - \frac{0.035}{\beta^3 + 1} \tag{6.3}$$

The maximum power extraction at each wind speed of a typical wind turbine characteristic is shown in Figure 6.1(a). The speed control of DFIG can be achieved by driving the generator rotor speed along with optimum power-speed characteristic where the power coefficient kept at maximum at each wind speed. The complete generator toque-speed characteristic is as shown in Figure 6.1(b). The generator operates at almost constant rotational speed for very low wind speed (see points A to B). The maximum energy can be extracted from the turbine during low to medium wind speeds (see points B to C). The rotational speed is also often limited by aerodynamic noise constraints, at which point the controller allows the torque to increase, at essentially constant speed (C to D) until rated torque. If wind speed increases further the torque follows the point D to E, where the electromagnetic toque is constant. When the turbine characteristic reaches to point E, pitch angle controller takes over from the torque control to limit the aerodynamic power. Therefore, for high wind speeds the pitch angle controller regulates the generator output power, until its shutdown limit is reached.

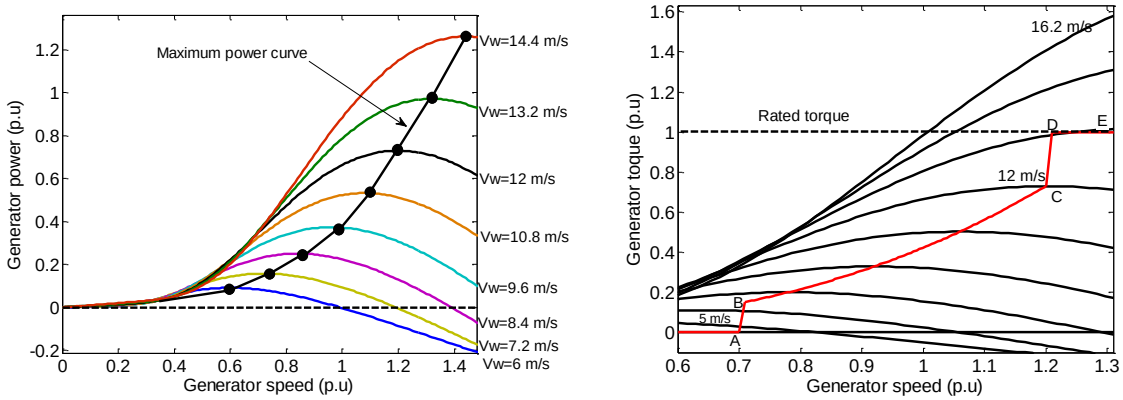

(a) (b)

Figure 6.1: Wind turbine maximum power extraction characteristic: (a) Generator power versus rotor speed curve; (c) Generator toque versus rotor speed curve

6.3 DFIG modelling

The DFIG is being represented by its steady-state equivalent circuit with injected rotor voltage as shown in Figure 6.2. In this figure, V_R and V_S are rotor and stator voltages respectively, I_R and I_S are rotor and stator currents, I_M is exciting current of the DFIG, R_R and R_S are the rotor and stator resistance, respectively and S is the slip. X_S, X_R and X_M are respectively, stator, rotor and magnetizing reactance. Figure 6.2 further simplified by transferring the magnetizing branch to the terminal side as shown in Figure 6.3 [160].

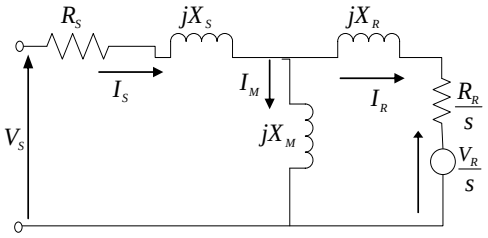

Figure 6.2: Electrical equivalent of DFIG with injected rotor voltage

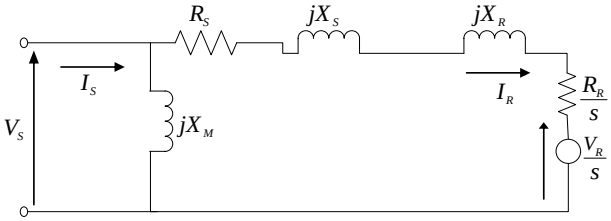

Figure 6.3: Simplified equivalent of DFIG

From the Figure 6.3, the rotor current can be determined as:

$$I_R = \frac{V_S - \left(\frac{V_R}{S}\right)}{\left(R_S + \frac{R_R}{S}\right) + J\left(X_S + X_R\right)} \tag{6.4}$$

The rotor active power (supplied or absorbed by controllable source injecting voltage into rotor circuit) calculated as:

$$P_R = \frac{V_R}{s} I_R \cos\theta \tag{6.5}$$

By neglecting the stator and rotor loss stator active power P_S can be expressed as

$$P_S = P_m - P_R \tag{6.6}$$

Finally the total power delivered to the grid can be obtained as

$$\boldsymbol{P_g = P_S + P_R} \tag{6.7}$$

6.3.1 Operating modes of DFIG

DFIG based WES can be operated in two modes of operation with respect to the rotor speed: (1) If the generator rotor rotates with above synchronous speed called as super-synchronous mode of operation and,

2) If the generator operated with below synchronous speed called as sub-synchronous mode of operation.

Figure 6.4 depicts the power flow diagram of a DFIG based wind energy system. Depending of the slip convention (negative or positive), the rotor circuit can deliver or receive power to or from the grid. In the super-synchronous mode of operation, the mechanical power $|P_m|$ is transferred to the grid through rotor and stator circuits. The stator power $|P_S|$ is directly deliver to the grid, whereas the rotor power $|P_R|$ is transferred to the grid through a power electronic converter incorporated in the rotor circuit. By neglecting converter and generator losses, the power transferred to the grid $|P_g|$ is equal to mechanical power $|P_m|$ of the generator, as shown in Figure 6.4(a).

Figure 6.4(b) illustrates the power flow process of the DFIG when it operated in sub-synchronous mode. Here, the rotor receives the power from the grid. Both mechanical and

rotor power are transferred to the grid via stator. Although, the stator power $|P_S|$ is sum of mechanical and rotor power $|P_m|+|P_R|$, it will not exceed its power rating since in this mode of operation, the mechanical power is lower than that of super-synchronous mode of operation.

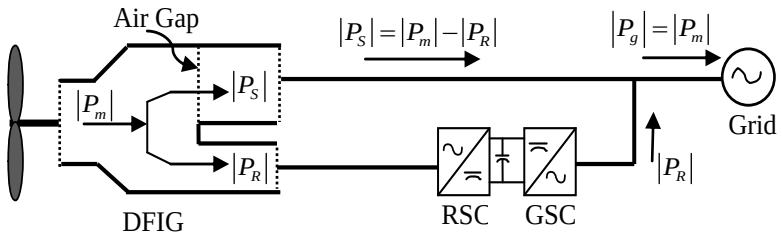

(a)Super-synchronous mode

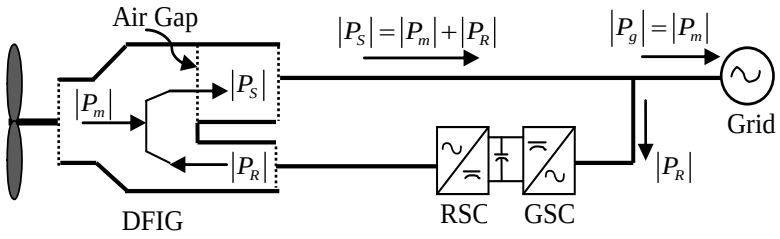

(b) Sub- synchronous mode

Figure 6.4: DFIG power flow diagram: (a) Super-synchronous mode (b) Sub- synchronous mode

6.3.2 The d-q reference frame of induction generator

The a-b-c reference frame of induction generator is transformed into the *d-q* axis reference frame and described as [3].

Stator equations

$$\begin{aligned} v_{ds} &= -R_S i_{ds} - \omega_s \varphi_{qs} + \frac{1}{\omega_b}\frac{d\varphi_{ds}}{dt} \\ v_{qs} &= -R_S i_{qs} + \omega_s \varphi_{ds} + \frac{1}{\omega_b}\frac{d\varphi_{qs}}{dt} \end{aligned} \tag{6.8}$$

Rotor equations

$$\begin{aligned} v_{dr} &= R_R i_{dr} - s\omega_s \varphi_{qr} + \frac{1}{\omega_b}\frac{d\varphi_{dr}}{dt} \\ v_{qr} &= R_R i_{qr} + s\omega_s \varphi_{dr} + \frac{1}{\omega_b}\frac{d\varphi_{qr}}{dt} \end{aligned} \tag{6.9}$$

The flux linkages can be calculated as:

$$\begin{aligned}\varphi_{ds} &= X_M i_{dr} - i_{ds} X_{SS} \\ \varphi_{qs} &= X_M i_{qr} - i_{qs} X_{SS} \\ \varphi_{dr} &= -X_M i_{ds} + i_{dr} X_{RR} \\ \varphi_{qr} &= -X_M i_{qs} + i_{qr} X_{RR}\end{aligned} \tag{6.10}$$

The electromagnetic torque is expressed as:

$$T_e = X_M \left(i_{dr} i_{qs} - i_{qr} i_{ds} \right) \tag{6.11}$$

The mathematical equation for one mass model is given by

$$\frac{d\omega_r}{dt} = \frac{1}{2H}(T_m - T_e) \tag{6.12}$$

where, H is the equivalent inertia constant of both induction generator rotor and wind turbine.

6.4 DFIG control strategies

The objective of this work is to improving the dynamic performance of DFIG using torque and voltage control loop of RSC converter. Therefore, only the control of RSC is discussed in detailed. The most popular control scheme employed for DFIG is PV*dq* [9], in which the rotor current is decomposed into two orthogonal components along *d* and *q* axis. The *d*-axis component of current employed to regulate the power factor or terminal voltage of DFIG, whereas *q*-axis component of current used to regulate the torque.

6.4.1 Torque control scheme

The purpose of torque control scheme is to regulate the electromagnetic torque of the generator with wind speed variations and drive the system towards its operating reference point. For a given rotor speed (ω_r) measurement, the optimal torque (T_{op}) is obtained by use of wind turbine characteristics as shown in Figure 6.1(b). By making use of determined T_{op}, a reference rotor current ($i_{qr,ref}$) is computed. Finally, the required rotor voltage (v_{qr}) for operating DFIG at the optimal torque is obtained through a summation of the compensation term and the term ($v_{qr}^{'}$) computed by PI_1 controller.

By neglecting the stator transients and rotor resistances from equation (6.8) and use of φ_{ds} and φ_{qs} from equation (6.10) into (6.8), the *d* and *q* axis stator voltages are:

$$v_{ds} = -\omega_s \left(X_M i_{qr} - X_{SS} i_{qs} \right) \tag{6.13}$$

$$v_{qs} = \omega_s \left(X_M i_{dr} - X_{SS} i_{ds} \right) \tag{6.14}$$

By using equations (6.13) and (6.14), the *d* and *q* axis stator currents can be obtained as:

$$i_{qs} = \frac{X_M}{X_{SS}} i_{qr} + \frac{1}{\omega_s X_{SS}} v_{ds} \tag{6.15}$$

$$i_{ds} = \frac{X_M}{X_{SS}} i_{dr} - \frac{1}{\omega_s X_{SS}} v_{qs} \tag{6.16}$$

This study employs stator flux oriented reference frame, therefore stator voltage $v_{ds} = 0$ then the resultant expression from equation (6.15) as:

$$i_{qs} = \frac{X_M}{X_{SS}} i_{qr} \tag{6.17}$$

By substituting equations (6.16) and (6.17) in equation (6.11), the electromagnetic torque can be derived as:

$$T_e = X_M \left(i_{dr} \left(\frac{X_M}{X_{SS}} i_{qr} \right) - i_{qr} \left(\frac{X_M}{X_{SS}} i_{dr} - \frac{1}{\omega_s X_{SS}} v_{qs} \right) \right) \tag{6.18}$$

The reference *q*-axis rotor current that can be obtained with help of optimal torque/reference set point torque is as:

$$i_{qr,ref} = \frac{\omega_s X_{SS}}{X_M V_{qs}} T_{op} \tag{6.19}$$

After neglecting the transient term from equation (6.9), using φ_{dr} from equation (6.10) and i_{ds} from equation (6.16), the final equation of *q*-axis rotor voltage can be obtained as:

$$v_{qr} = R_R i_{qr} + s\omega_s \left(X_{RR} - \frac{X_M^2}{X_{SS}} \right) i_{dr} - \frac{X_M}{\omega_s X_{SS}} v_{qs} \tag{6.20}$$

From the above equation, the second and third terms on right hand side denotes compensation term.

The complete torque control scheme of RSC is shown in Figure 6.5. The rotor current i_{qr} and reference rotor current $i_{qr,ref}$ forms the error signal ε which is processed through PI_1 controller to generate rotor voltage ($v_{qr}^{'}$). Finally, *q*-axis rotor voltage is obtained by adding compensation term to the PI_1 controller output. This minimize the cross coupling between torque and voltage control loops.

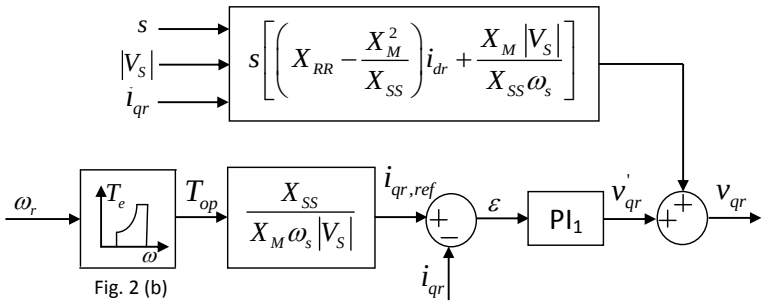

Figure 6.5: Torque control strategy of DFIG

6.4.2 Voltage control scheme

The power factor control or terminal voltage of DFIG can be achieved through the RSC. Although, GSC can be employed to inject reactive power injection, for DFIG voltage control RSC is likely to be preferred. The terminal voltage will decrease or increase with change in reactive power to the grid. In this condition, the voltage controller should fulfil the following requirements: (i) If the voltage is too high or too low compared with reference value, the *d*-axis rotor current ($i_{dr,ref}$) should be adjusted accordingly which can be achieved by adjusting the control gain K_{VC} and (ii) the reactive power consumption by the DFIG should be compensated. The rotor *d*-axis voltage (v_{dr}) is obtained through PI_2 controller output minus compensation term. The complete block diagram of DFIG voltage control scheme is as shown in Figure 6.6.

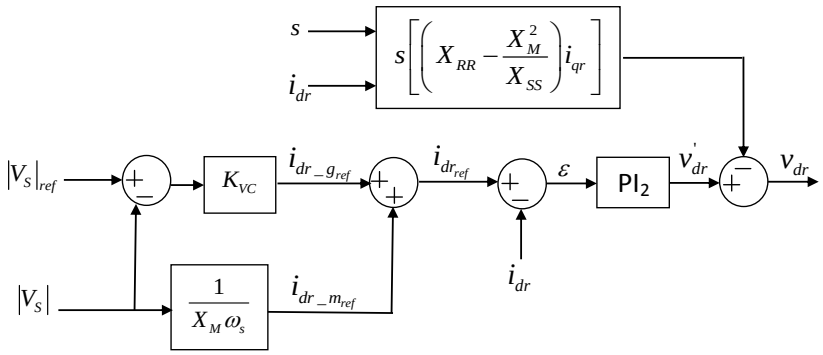

Figure 6.6: Voltage control scheme of DFIG

The controllers PI_1 and PI_2 of torque and voltage control schemes, respectively, are chosen as symmetric [50, 160]. Therefore, the gains can be considered as:

$$\begin{cases} K_{P1} = K_{P2} = K_P \\ K_{I1} = K_{I2} = K_I \end{cases} \tag{6.21}$$

6.5 Proposed type-2 fuzzy-PI controller for RSC control scheme

As the wind speed and grid conditions are variable, the adaptive controlled converter (for RSC) is important for DFIG to fulfil the grid code requirements. In this work a Type-2 FLC-PI controller is proposed for torque and voltage control schemes of RSC. Type-2 fuzzy-PI controller can be achieved by combining Type-2 FLC which is adaptive and PI controller results in superior dynamic and steady state response from the system. Here, proportional and integral gains of PI controller are adjustable and they are computed by Type-2 FLC approach according to the system operating condition changes. Thus, it achieves the adaptive structure required for RSC converter for smooth interaction of DFIG with the grid. Figure 6.7(a) and (b) depicts the torque and voltage control strategies of RSC respectively, designed with Type-2 fuzzy-PI controllers. Moreover, the control gain K_{VC} (shown in Figure 6.7(b)) is also tuned using Type-2 fuzzy logic method because by adjusting the *d*-axis rotor current ($i_{dr,ref}$), voltage regulation can be achieved.

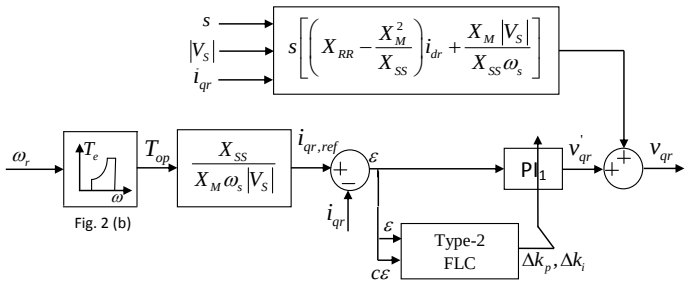

(a)

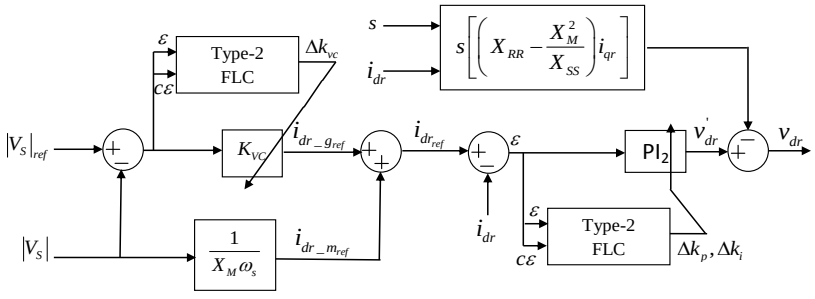

(b)

Figure 6.7: Proposed Type-2 FLC-PI controlled RSC schemes: (a) Torque control (b) Voltage control

6.6 Design of adaptive type-2 fuzzy-PI controller

This approach employs the type-2 fuzzy logic rules to determine the control gains (K_P , K_I and K_{VC}) of RSC schemes. The range of each parameter was computed by observations from various simulation results. The range of parameters obtained for this study are $\left[K_{P\min}, K_{P\max}\right] = K_P \in \left[0.1,1\right], \left[K_{I\min}, K_{I\max}\right] = \left[5,12\right]$, and $\left[K_{VC\min}, K_{VC\max}\right] = \left[2,9\right]$. Therefore, they can be calibrated into the range between zero and one as follows:

$$\Delta k_p = \frac{K_P - K_{P\min}}{K_{P\max} - K_{P\min}} = \frac{K_P - 0.1}{1 - 0.1},\ K_P = 0.9\Delta k_p + 0.1 \tag{6.22}$$

$$\Delta k_i = \frac{K_I - K_{I\min}}{K_{I\max} - K_{I\min}} = \frac{K_I - 5}{12 - 5},\ K_I = 7\Delta k_p + 5 \tag{6.23}$$

$$\Delta k_{vc} = \frac{K_{VC} - K_{VC\min}}{K_{VC\max} - K_{VC\min}} = \frac{K_{VC} - 2}{9 - 2},\ K_{VC} = 7\Delta k_p + 2 \tag{6.24}$$

For the fuzzy methods, input, output and fuzzy membership functions are defined based on experts' knowledge and experience. Similar rules and membership functions have been considered for both Type-1 and Type-2 FLCs and therefore linguistic variables of input and output are as shown in Figure 6.8 and Figure 6.9, respectively. The schematic diagrams of proposed Type-2 FLC are shown in Figure 6.7(a) and (b). In this work, error ($\mathcal{E}$) and change in error ($\mathcal{CE}$) are defined as input variable to the Type-2 FLCs. The input error signals are fuzzified using five triangular memberships functions and defined as: LN-Large Negative, N-Negative, Z-Zero, P-Positive, LP-Large Positive. Most of researchers choose the MFs with equal span and equal width of FOU which do not offer best performance. In this work, by varying the FOU in an appropriate way the optimal performance of the system is achieved from various simulation results. The universe of discourse for error and change in error are obtained in between the +1 to -1. Similarly, the output of fuzzy type's controller are defined with five triangular membership functions and donated as: XLP-Extra Large Positive, LP-Large Positive, MP-Medium Positive, SP-Small Positive, and XSP-Extra Small Positive.

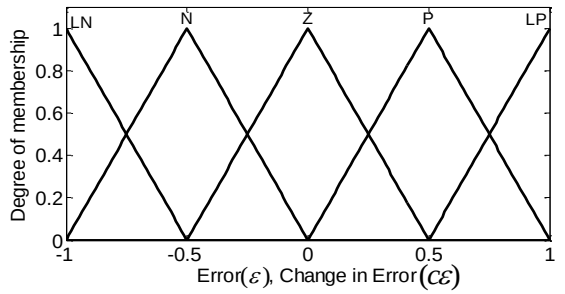

(a)

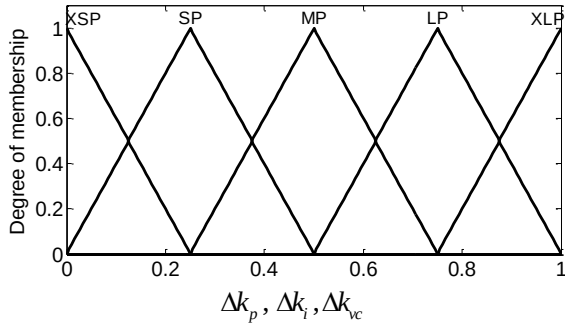

(b)

Figure 6.8: MFs of Type-1 FLC: (a) Inputs (b) Outputs

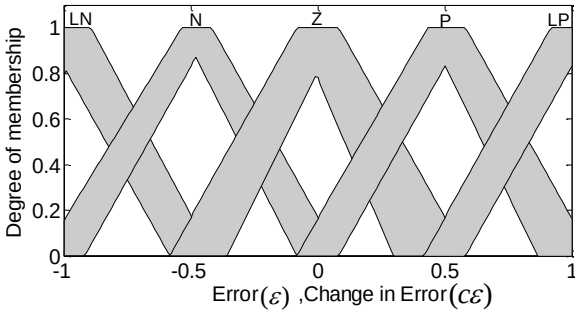

(a)

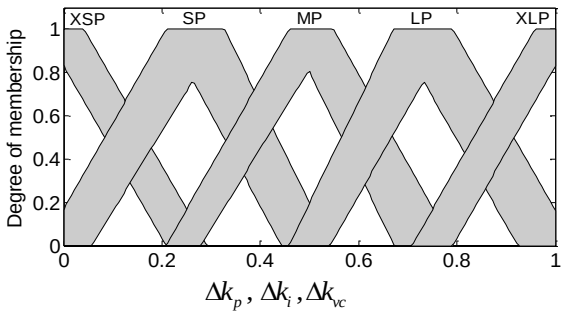

(b)

Figure 6.9: MFs of Type-2 FLC: (a) Inputs (b) Outputs

The major function in the inference engine is the rules' implementation, aggregation and Type reduction. In this work, with help of an expert' knowledge and experience, a control strategy is framed as a set of IF-THEN rules and are containing two antecedences and one consequence, expressed as:

IF ($\mathcal{E}$ is x_1) and ($c\mathcal{E}$ is y_1) THEN ($_{\Delta k_p}$ is w_1)

Similarly, 25 rules have been defined for output variables Δk_p, Δk_i and Δk_{vc} respectively, in Table 6.1, Table 6.2 and Table 6.3. In the Type-2 FLCs, the union and intersection functions are defined by join and meet operations to map the input and output sets with fired rules. Therefore, the inference engine utilizes respectively, min-method and max-method for meet and join operations. However, due to computational limitations the output of inference engine cannot be converted directly to crisp value as discussed in Chapter 2. Thus, type reduction (TR) method has been suggested in the type-2 FLC system to obtain type-1 fuzzy sets from type-2 output fuzzy sets, and later the normal defuzzification techniques can be applied. Height, center-of-sets, center-of-sums and modified-height are the most accepted TR methods, in which centroids of the embedded type-2 sets are calculated. In the present work 'height' TR method has been used for the calculation of the centroid of type-2 FLCs as it involves much lesser computations as compared to other methods [73].

Table 6.1: Tuning rules for Δk_p

Change in Error ($c\varepsilon$)	Error (ε)				
	LN	N	Z	P	LP
LN	XSP	XSP	XSP	SP	MP
N	XSP	SP	SP	SP	MP
Z	XSP	SP	MP	LP	XLP
P	MP	LP	LP	LP	XLP
LP	MP	LP	XLP	XLP	XLP

Table 6.2: Tuning rules for Δk_i

Change in Error ($c\varepsilon$)	Error (ε)				
	LN	N	Z	P	LP
LN	XLP	XLP	XLP	SP	XSP
N	XLP	LP	LP	MP	XSP
Z	LP	LP	MP	SP	XSP
P	MP	LP	SP	SP	XSP
LP	MP	SP	XSP	XSP	XSP

Table 6.3: Tuning rules for Δk_{vc}

Change in Error ($c\varepsilon$)	Error (ε)				
	LN	N	Z	P	LP
LN	XSP	XSP	XSP	SP	MP
N	XSP	SP	SP	SP	MP
Z	XSP	SP	MP	LP	XLP
P	MP	LP	LP	LP	XLP
LP	MP	LP	XLP	XLP	XLP

The common defuzzification methods used for the Type-2 FLC are the first (or last) of maxima, centroid-of-area and mean-of-max methods. In this study, centroid-of-area method has been utilized which is the most reasonable and popular method among the others. The centroid of the Type-2 fuzzy set is the collection of centroids of all of its embedded sets. The defuzzification method converts the output fuzzy to crisp value.

6.7 Employed system configuration

Figure 6.10 shows the schematic diagram of vector controlled DFIG connected to an infinite bus through transformers. Simulation data used for this system is provided in the Appendix. The DFIG rotor circuit is connected to the grid through back to back connected power electronic converters, while the stator circuit is directly connected to the power grid. Due to their connection positions, they are named as grid side converter (GSC) and rotor-side converter (RSC). The RSC controls the electromagnetic toque by controlling the injected rotor current, which must follow the reference speed provided by the control system. Addition, it can offer reactive power control and power factor or voltage control of the system. This ensures the variable speed operation of DFIG with maximum power point tracking characteristics. Regarding GSC, this is connected to the power grid through a filter and used

to control dc-link voltage and reactive power exchange with the grid. During the transient operating condition of DFIG, GSC may offer additional voltage support capabilities as RSC provide reactive power control.

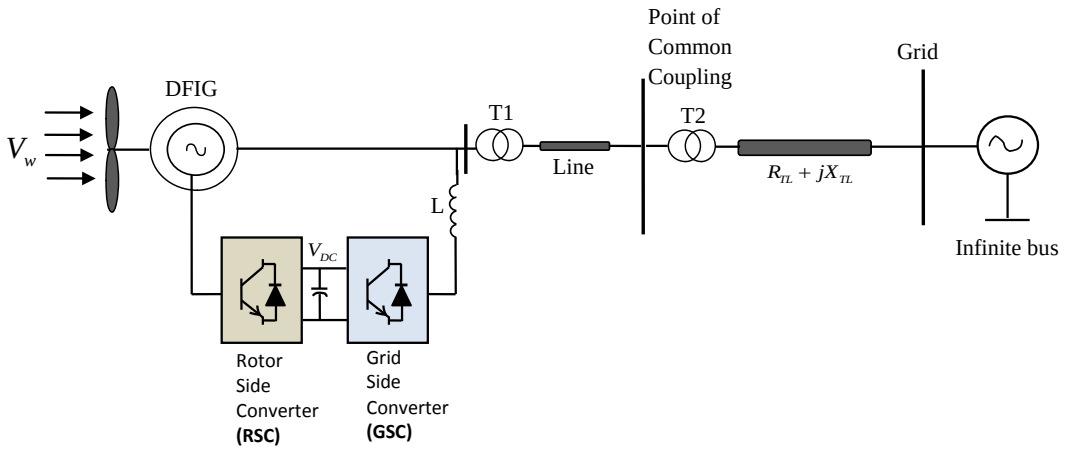

Figure 6.10: One line diagram of DFIG integrated with power network

The major advantage of DFIG is that it has decoupled active and reactive power control by making use of different control strategies for rotor side and grid side converters. With this feature, DFIG has the various controls namely P_{ref} (maintain the maximum power tracking), V_{sref} (stator terminal voltage), V_{dcref} (dc voltage level), and Q_{cref} (GSC reactive power level).

6.8 Real time(RT) simulation

In this work, to study the performance of the WES system shown in Figure 6.10:, a real time digital simulation using RT-Lab software package is used. RT-Lab is fully integrated with MATLAB^{TM}/Simulink and therefore, it uses MATLAB^{TM}/Simulink as a front-end interface for editing graphic models in block diagram format, which are later used by RT-Simulator. Real time is achieved by running on separate processors (targets) and in parallel, each part of the system (the sub-systems).

The WES as shown in Figure 6.10 is divided into two subsystems as shown in Figure 6.11. For the real time simulation, the model is built in Simulink with Sim-power system and Artemis blocks. The console subsystem denoted as SC_Console which contains parameters accessing and displaying blocks, runs on the host PC, which can receive simulation results and display through the scope. Another subsystem is a computing subsystem named as SM_Master which contains all the calculation blocks (studied WES). This subsystem runs on the target machine with real time condition. The simulation time step fixed as $50\mu s$ for both

real time simulation and simulation in simulink. A detailed explanation about OPAL-RT has been provided Appendix.

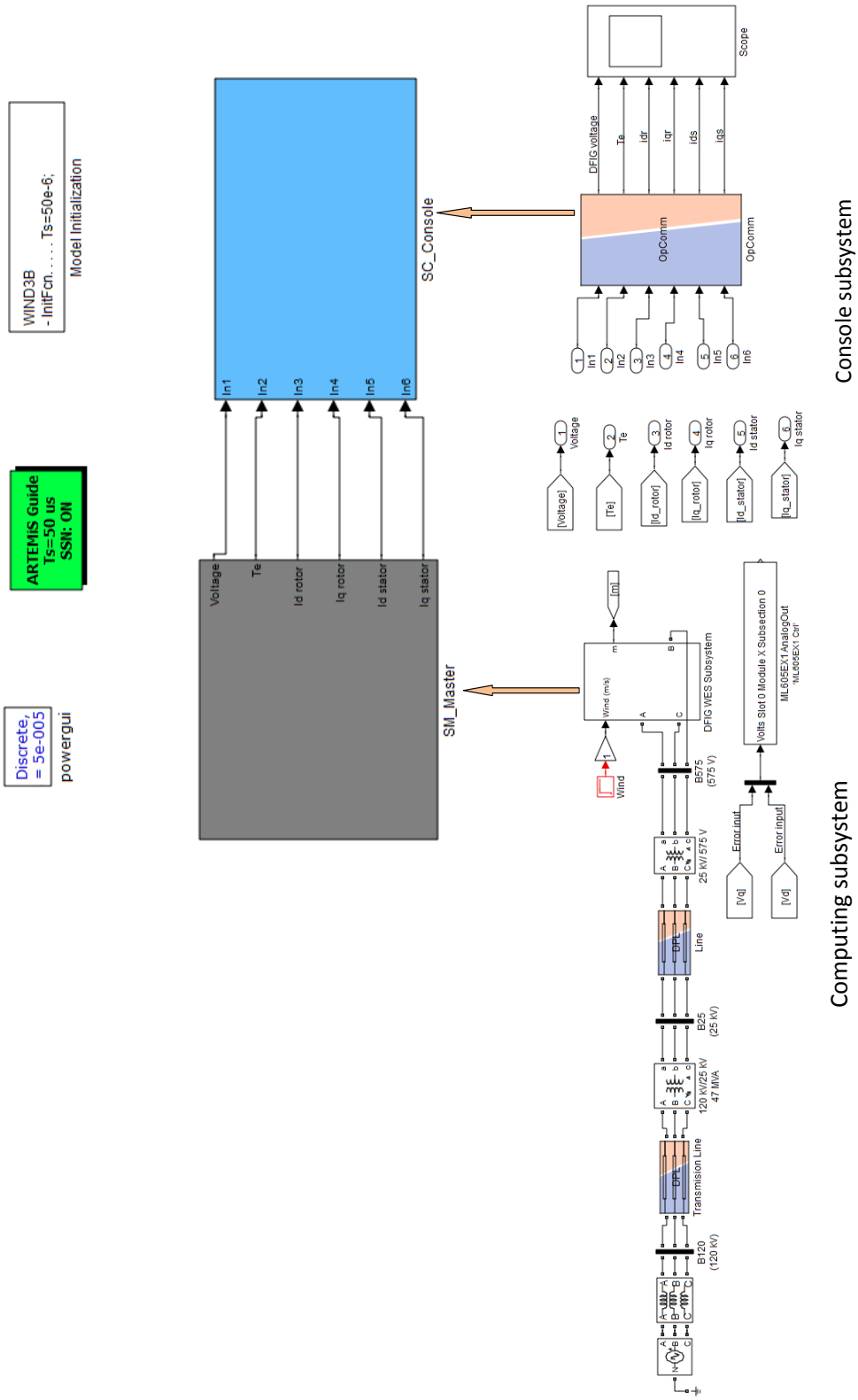

Figure 6.11: Distributed model of the DFIG based WES for real time simulation

The real time digital simulation laboratory setup is as shown in Figure 6.12; The simulator employed here is OP5600 with one processor and four 3.33-GHz dedicated cores to perform parallel computations. The work station computer (Host-PC) executes the WES model and interacts with the real time digital simulator (RTDS) to produce the results of real time simulation. Real time simulation results were observed through the Opcomm block. The digital oscilloscope is also employed to observe the real time results of controller error inputs.

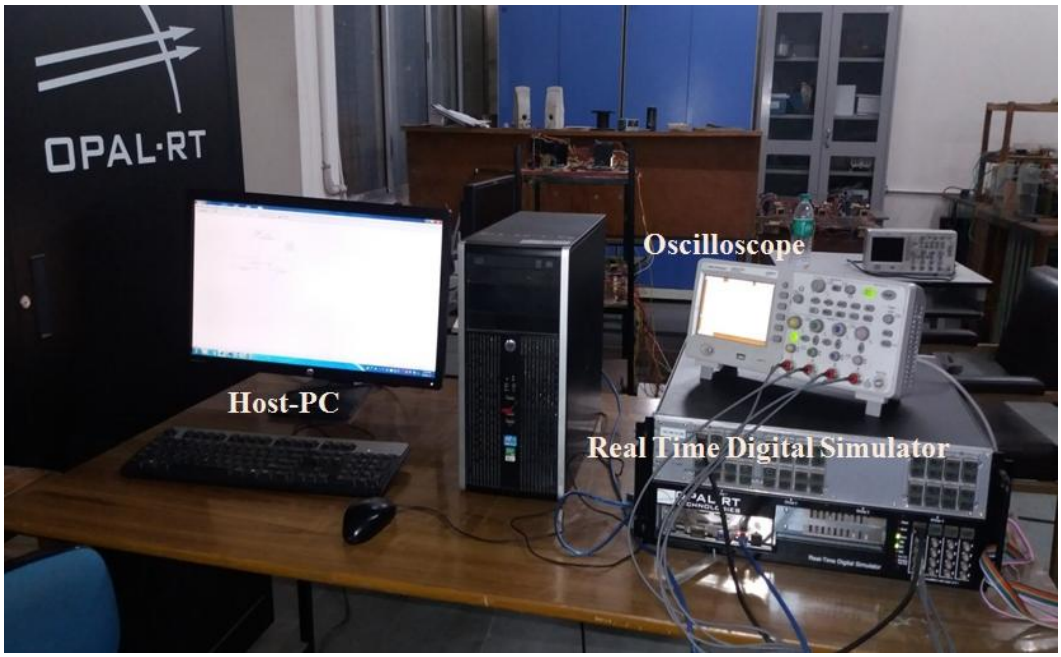

Figure 6.12: Real time digital simulator laboratory setup

6.9 Results and Discussions

As the penetration of wind energy systems in power network increasing in number, the performance of wind turbines subjected to severe faults, voltage sag and other disturbances are becomes important, especially the wind energy systems equipped with power electronic converters. The severe disturbances (transient faults and voltage sag) results in DFIG rotor current to increase, which may damage the RSC. Due to large rotor current and oscillations occurring in torque due to faults are harmful to the DFIG equipped wind turbines. In these conditions, either the DFIG may be disconnected from the grid or by using crowbar resistors, RSC must be deactivated. A sudden loss of wind power will results in considerable amount of rate of change of frequency in the electrical system. In addition, when the RSC deactivated

using crowbar resistor, DFIG will behaves like squirrel cage induction generator and absorbs huge amount of reactive power which causes the voltage instability issues. Thus, it is required that wind turbine must be stay connected and actively involved in maintaining system stability during and after the disturbances. The low voltage ride through ability is the ability of the wind turbines systems must be stay connected to the grid throughout the faults and voltage dips [45, 119]. Most of the countries nowadays enforce their grid codes for LVRT capability to the wind generation systems in order to ensure the power system security.

In order to observe the transient performance contributed by the proposed type-2 FLC-PI controller, a test system employed has been shown in Figure 6.10. The RSC control strategies of DFIG have been designed with type-1 FLC-PI and type-2 FLC-PI for comparative analysis. The transient behavior of the DFIG is investigated with both controllers for the subsequent rotor speeds taking into account and the following three cases are considered.

(a) Case A: Rotor speed =0.8p.u

(b) Case B: Rotor speed=1.1p.u

(c) Case C: Rotor speed =1.29p.u

6.9.1 Three phase fault

The transient behavior of the DFIG has been analyzed by applying three phase short circuit fault at the PCC point. The fault is initiated at 25s for duration of 150ms and later normal operation is restored. The steady state behavior of the DFIG terminal voltage, electrical torque (T_e), rotor currents (i_{dr}, i_{qr}) and stator currents (i_{ds}, i_{qs}) have been obtained. Therefore, the comparative analysis of transient performance of the system with type-1 FLC-PI and type-2 FLC-PI controllers for different rotor speed variations are as shown in from Figure 6.13 to Figure 6.15.

Figure 6.13(a)-(f) shows the various parameters of the DFIG with rotor speed of 0.8p.u and subjected to three phase short circuit fault. Figure 6.13(a) represents the terminal voltage where sudden loss of voltage occurs from 25s to 25.15s due to fault. The electrical torque of the DFIG is as shown in Figure 6.13 (b). Figure 6.13(c) and (d) represent the d-axis and q-axis rotor current of DFIG, respectively, initially rotor currents are at their settled value but when fault is occurs, these parameters are oscillate and return back to steady-state value after some time. However, in comparison of type-1 FLC-PI and type-2 FLC-PI controllers, the d-axis and q-axis rotor current of DFIG shows better results with proposed controller design. Similar

analysis also obtained for d-axis and q-axis stator currents of DFIG respectively, as shown in Figure 6.13(e) and (f).

Figure 6.14(a)-(f) shows all the parameters behavior of the DFIG system with rotor speed of 1.21p.u with severe fault initiated. Figure 6.14 (b) depicts the electrical torque response of the DFIG as it observed that the oscillations are effectively suppressed with type-2 FLC-PI than that of type-1 FLC-PI counterparts. Figure 6.14 (c) and (d) show respectively, d-axis and q-axis rotor current of DFIG. Moreover, Figure 6.14 (e) and (f) denote DFIG stator currents in

6.9.1.1 Case A: Rotor speed=0.8p.u

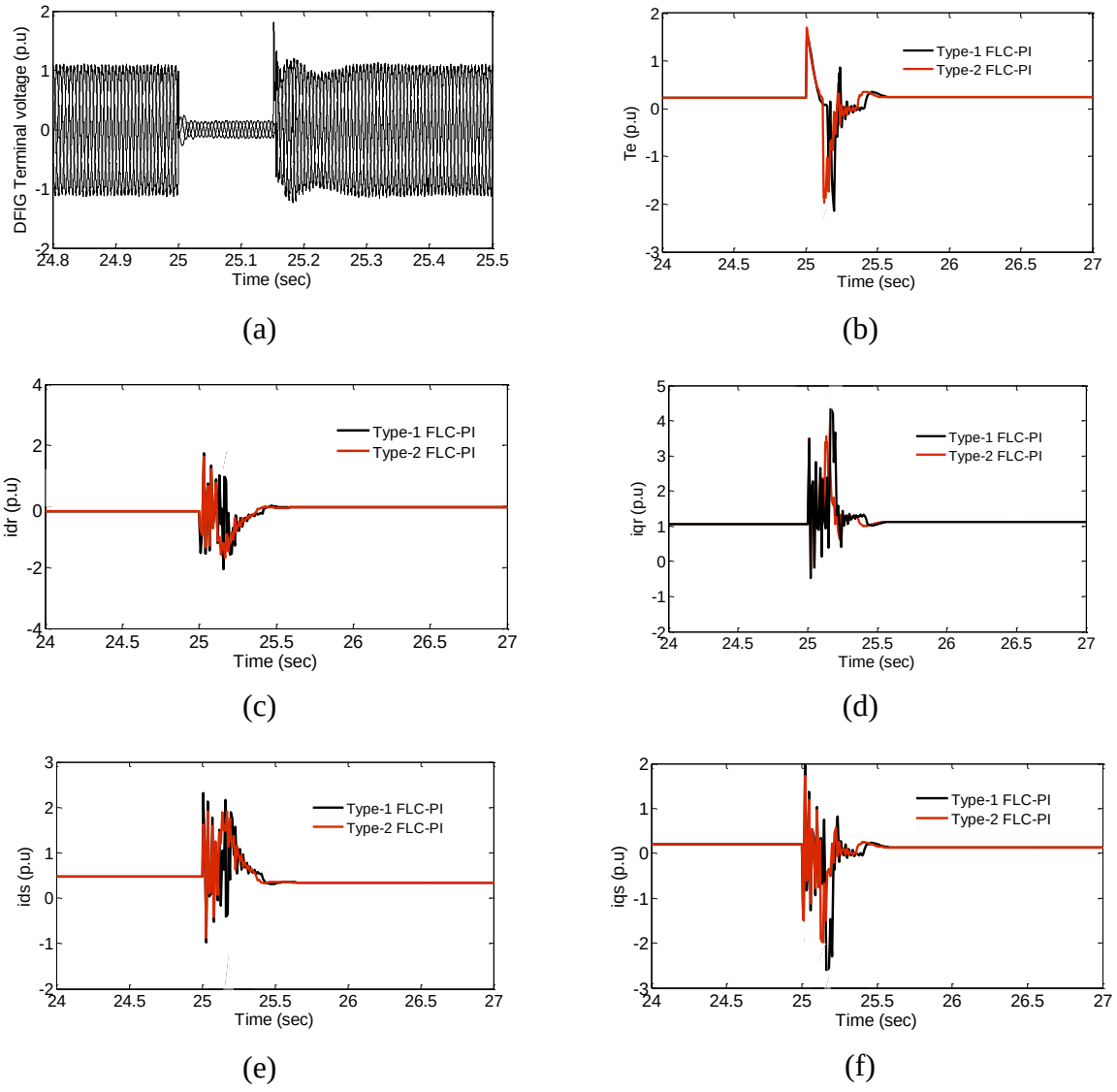

Figure 6.13: Three phase short circuit fault: (a) DFIG terminal voltage (b) Mechanical torque (c) *d*-axis rotor current (d) *q*-axis rotor current (e) *d*-axis stator current (f) *q*-axis stator current.

d-axis and q-axis, respectively. As the fault is suddenly occurred, all these parameters of DFIG experienced significant oscillations in their responses. However, in all the responses of DFIG the type-2 FLC-PI controller shows better results in comparison to type-1 FLC-PI.

6.9.1.2 Case B: Rotor speed=1.21p.u

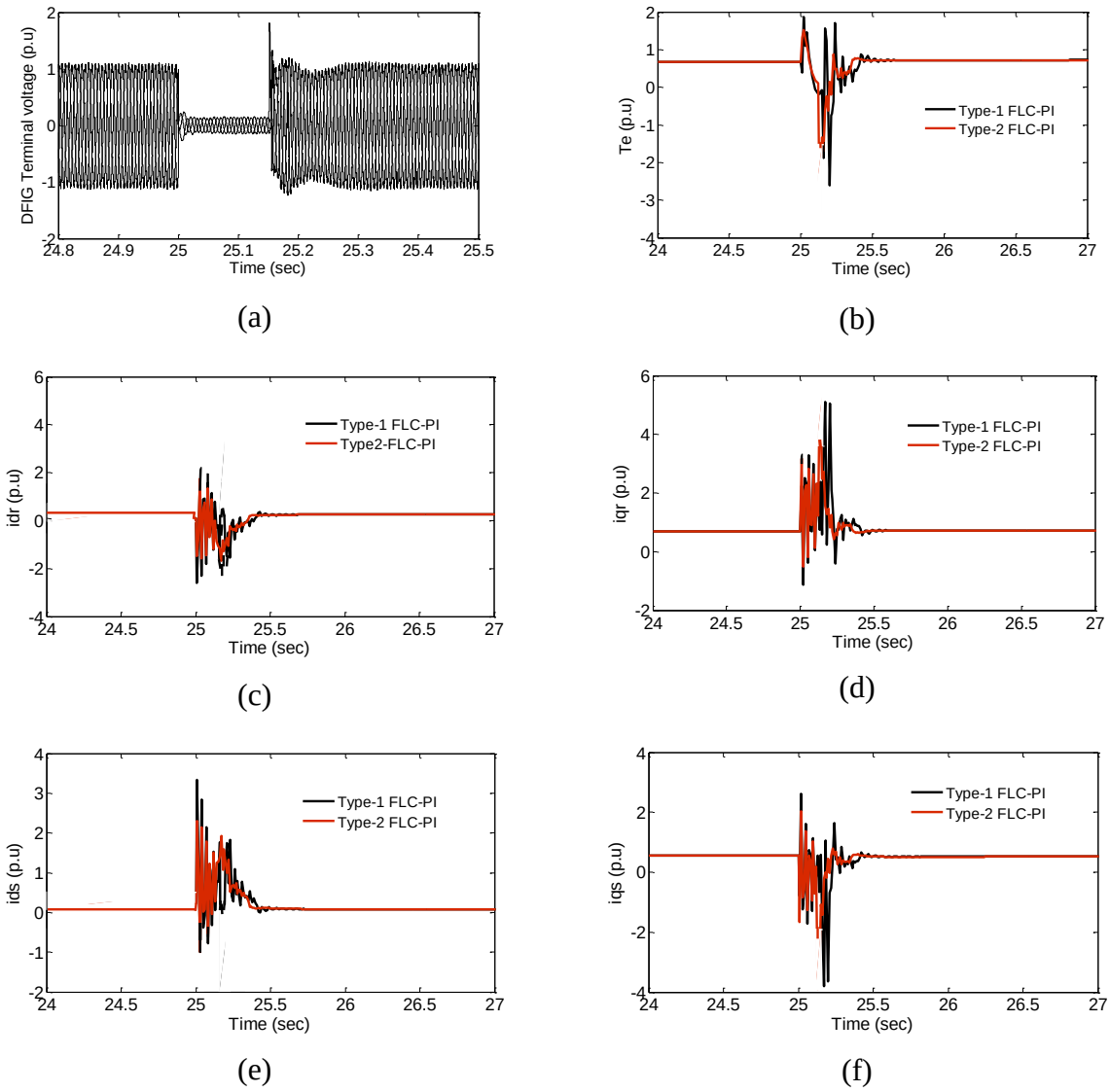

Figure 6.14: Three phase short circuit fault: (a) DFIG terminal voltage (b) Mechanical torque (c) *d*-axis rotor current (d) *q*-axis rotor current (e) *d*-axis stator current (f) *q*-axis stator current.

Figure 6.15(a)-(f) shows parameters of DFIG respectively, DFIG terminal voltage, electrical torque, d-axis rotor current, q-axis rotor current, d-axis stator current, and q-axis stator current with rotor speed of 1.29p.u. All the parameters are at their initial settled value before the occurrence of the fault. As the fault is initiated suddenly, all the parameters of DFIG experienced significant excursions in transient response. The designed controllers limit the peak values in these transients and suppress them very quickly to their normal position. Later on, system comeback to its normal position as quickly as the fault is removed. It is clearly observed from the results that the adaptive type-2 FLC-PI approach offers better

transient response as compared to type-1 FLC-PI. Therefore, the proposed control design meets the grid code requirement very effectively.

6.9.1.3 Case C: Rotor speed=1.29p.u

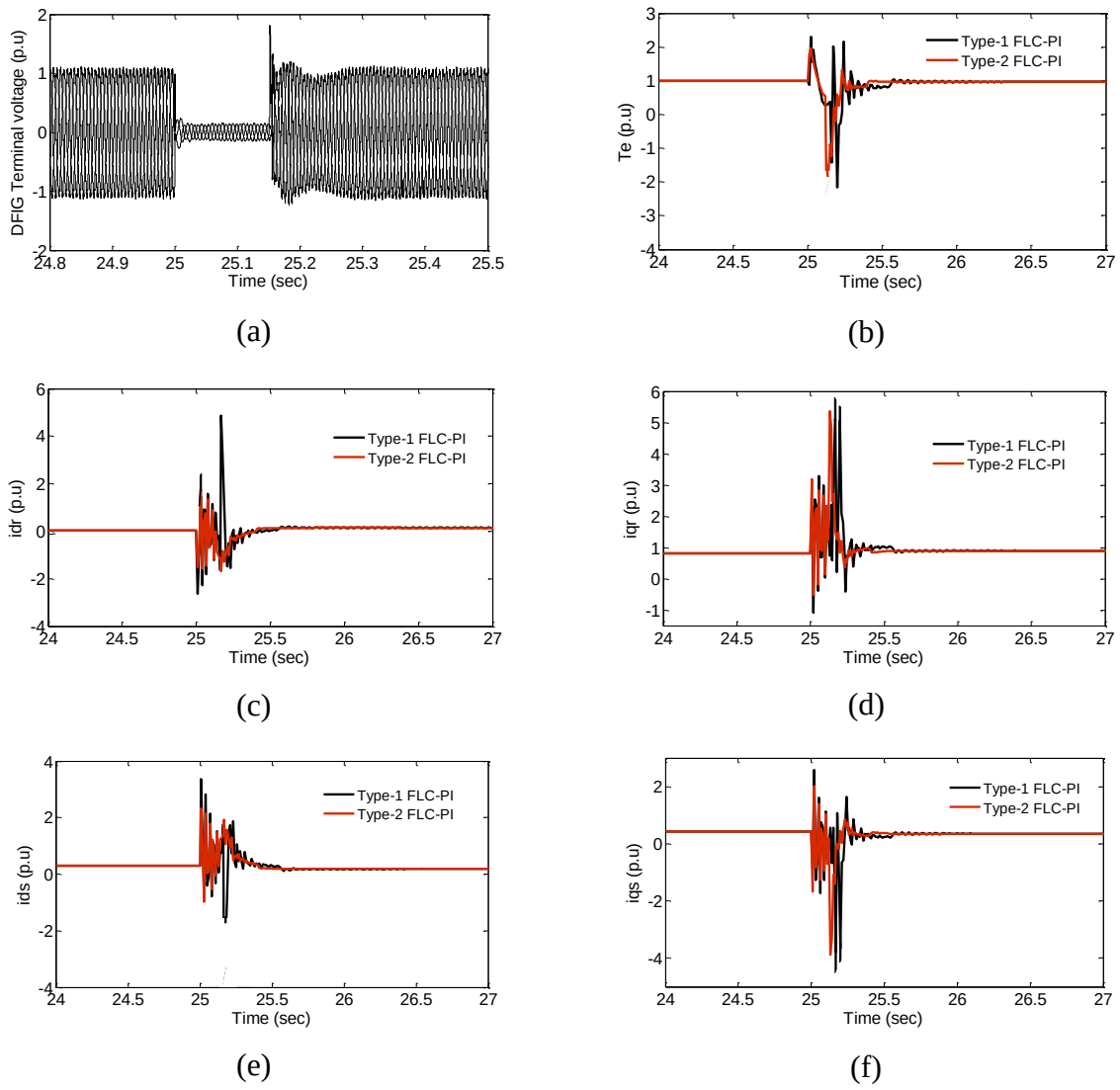

Figure 6.15: Three phase short circuit fault: (a) DFIG terminal voltage (b) Mechanical torque (c) *d*-axis rotor current (d) *q*-axis rotor current (e) *d*-axis stator current (f) *q*-axis stator current

6.9.2 Voltage sag

As per the LVRT capability stated in grid codes, wind turbine generators to be able to operate at reduced voltage for few hundreds of mille seconds to several seconds. The grid-code requirement specified by the TSO UK [45, 119] according this, the wind turbines should ride-through a 50% of fault for 710ms. This condition is established by reducing DFIG terminal voltage by 50% for 710ms.

6.9.2.1 Case A: Rotor speed =0.8p.u

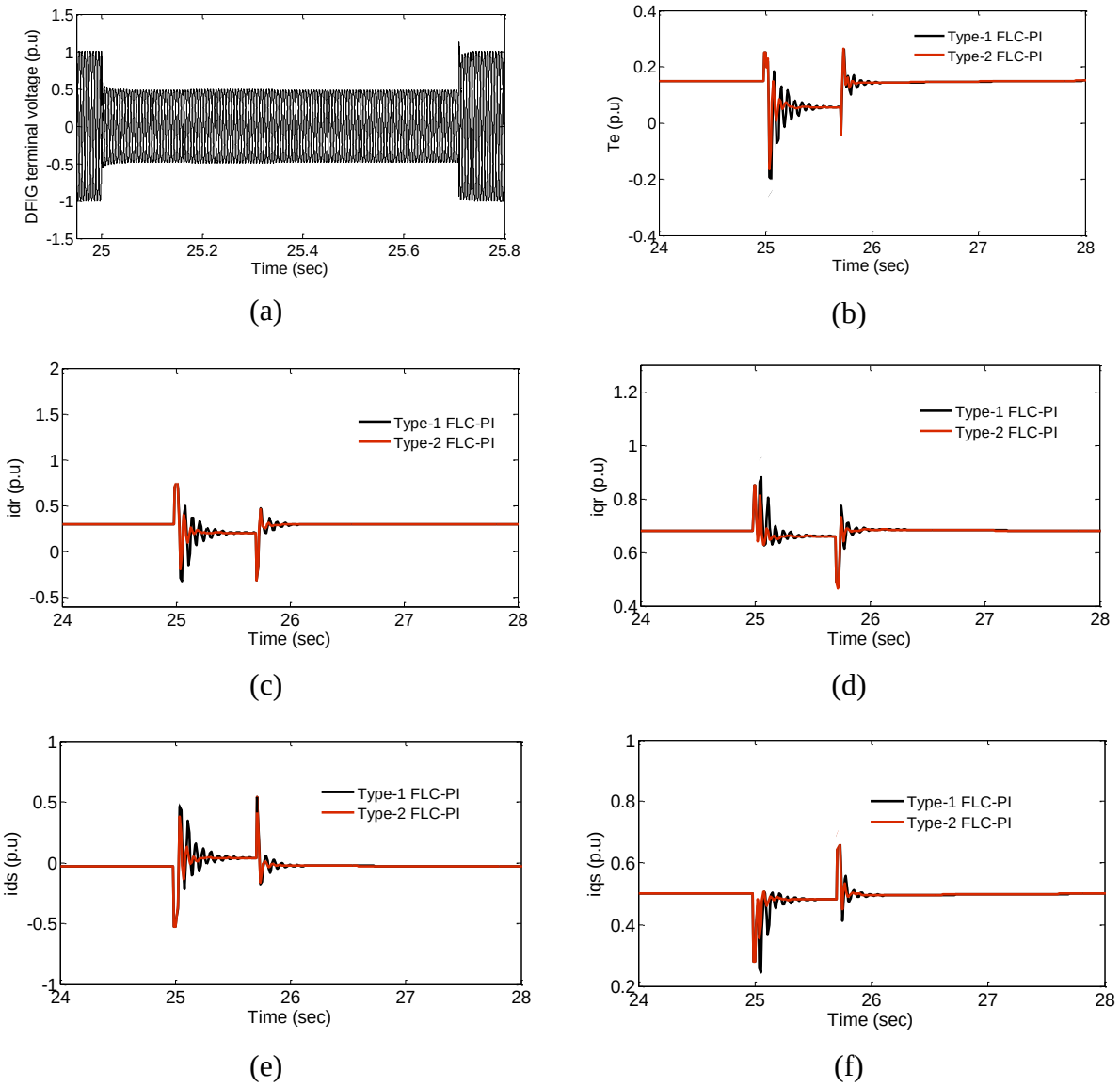

Figure 6.16: Voltage sag for 710ms: (a) DFIG terminal voltage (b) Mechanical torque (c) *d*-axis rotor current (d) *q*-axis rotor current (e) *d*-axis stator current (f) *q*-axis stator current

Figure 6.16 (a)-(f) shows all the parameters behavior of the DFIG system with rotor speed of 0.8p.u and subjected to 50% of voltage sag. Figure 6.16 (a) shows the terminal voltage of DFIG where the voltage sag of 50% initiated from 25s to 25.71s. Figure 6.16 (b) depicts the electrical torque response of the DFIG, as it observed that oscillations are effectively suppressed with type-2 FLC-PI than that of type-1 FLC-PI counterparts due to sudden voltage dip. Figure 6.16(c) and (d) show respectively, d-axis and q-axis rotor current of DFIG. Moreover, Figure 6.16(e) and (f) denote DFIG stator currents in d-axis and q-axis, respectively. As the voltage sag is suddenly occurred, all these parameters of DFIG

experienced significant oscillations in their responses. However, in all the responses of DFIG the type-2 FLC-PI controller shows better results in comparison to type-1 FLC-PI.

Similarly, the comparative analysis of the system with type-1 FLC-PI and type-2 FLC-PI controllers for rotor speed variations of 1.21p.u and 1.29p.u are as shown Figure 6.17(a)-(f) and Figure 6.18(a)-(f), respectively. It clearly observed from the results that the proposed adaptive type-2 FLC-PI controller exhibits superior steady state response for the voltage sag consideration as compared to type-1 FLC-PI counterparts.

6.9.2.2 Case B: Rotor speed =1.21p.u

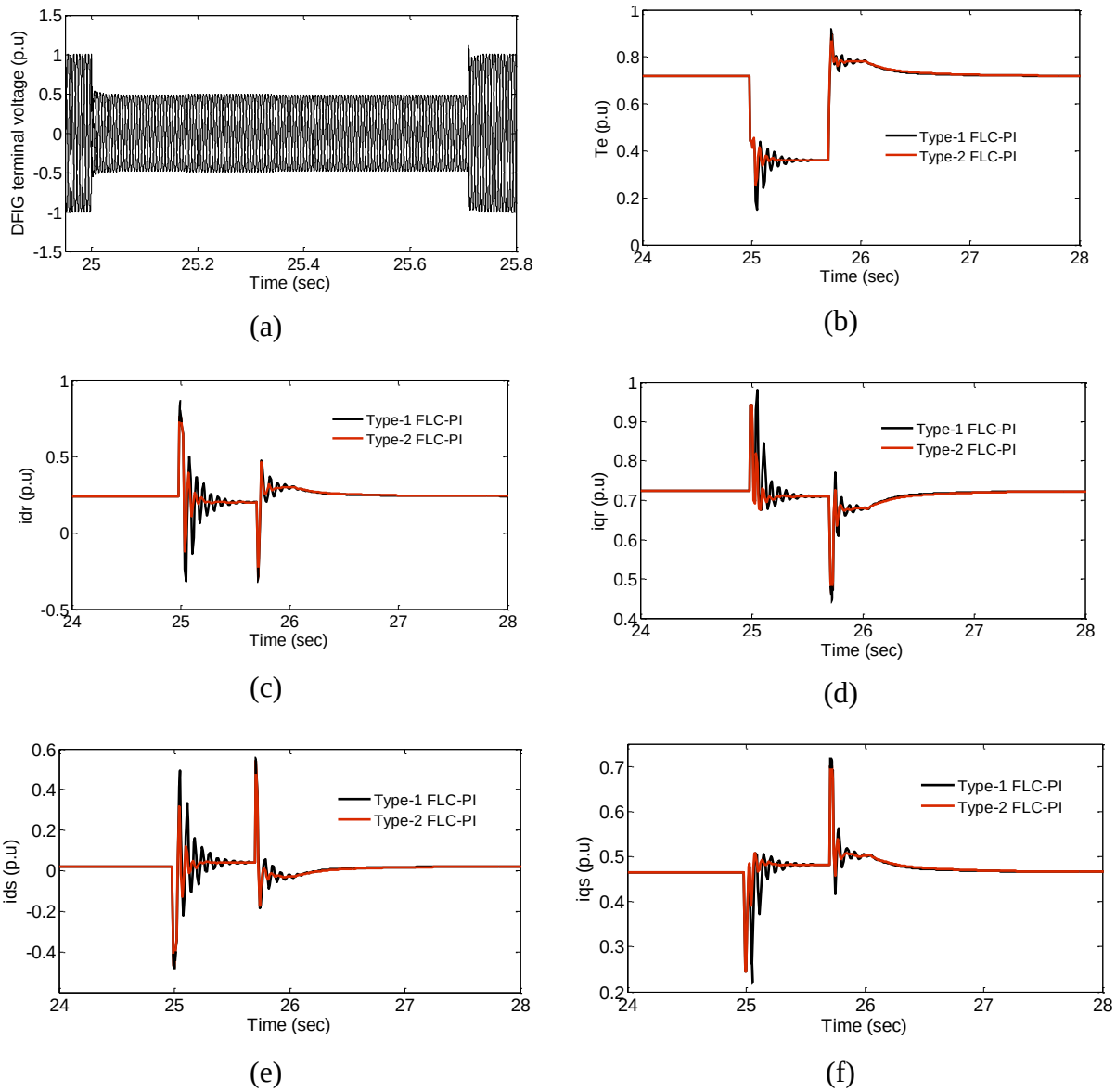

Figure 6.17: Voltage sag for 710ms: (a) DFIG terminal voltage (b) Mechanical torque (c) *d*-axis rotor current (d) *q*-axis rotor current (e) *d*-axis stator current (f) *q*-axis stator current

6.9.2.3 Case C: Rotor speed=1.29p.u

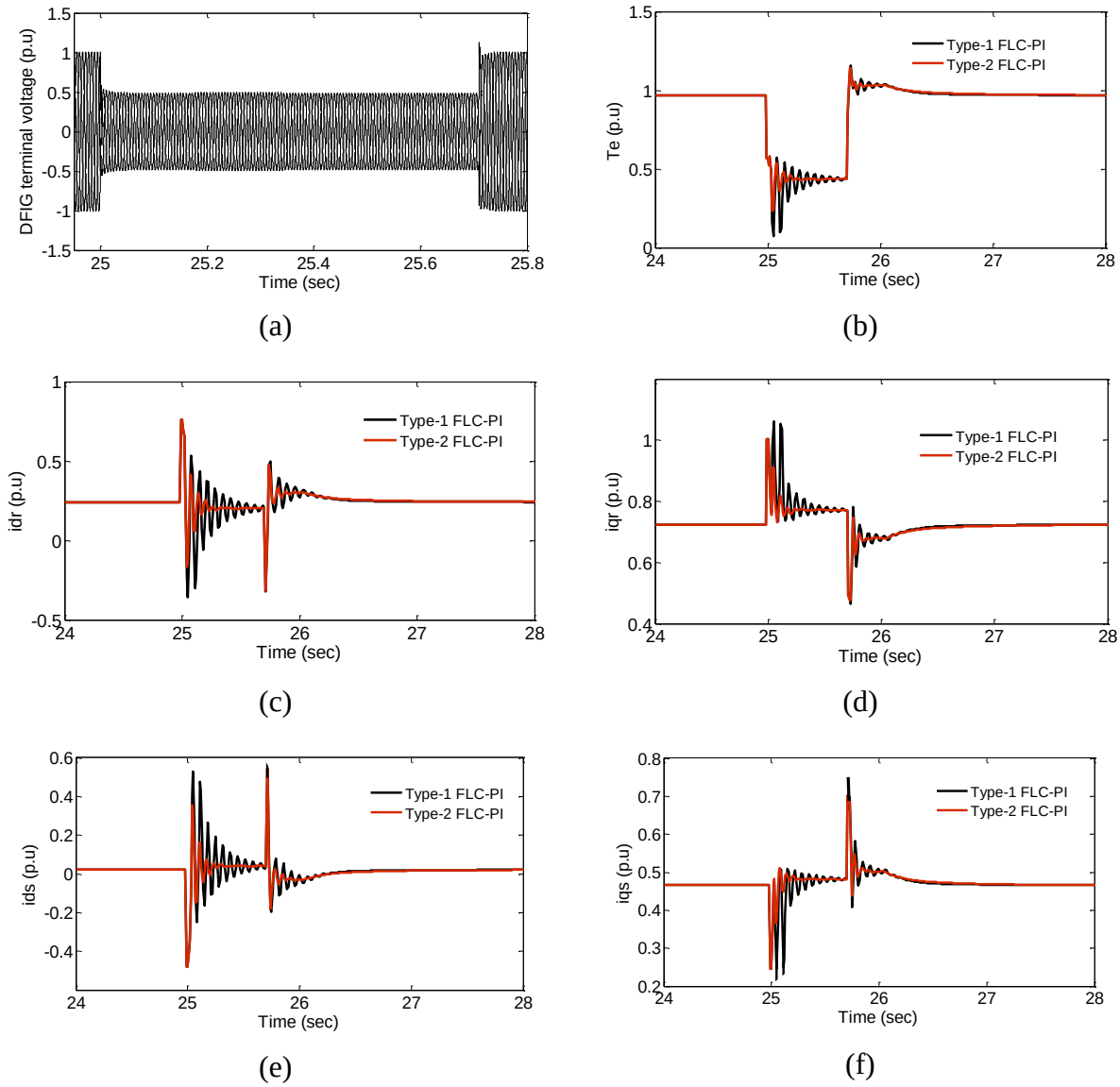

Figure 6.18: Voltage sag for 710ms: (a) DFIG terminal voltage (b) Mechanical torque (c) *d*-axis rotor current (d) *q*-axis rotor current (e) *d*-axis stator current (f) *q*-axis stator current

The controllers error input are also observed in the digital oscilloscope as shown in Figure 6.19 and Figure 6.20 respectively, for type-1 FLC-PI and type-2 FLC-PI. Figure 6.19(a) shows the torque controller error input and Figure 6.19(b) illustrates the voltage controller error input for type-1 FLC-PI, whereas Figure 6.20(a) and (b) repeat same but with type-2 FLC-PI. It is observed that controller error increases at the time of fault in order to bring the generator parameters to their normal value. Moreover, the error signal generated by the proposed method lasts few seconds as compared to that of type-1 FLC-PI. As a result, the proposed type-2 FLC-PI is able to improve the performance of the wind generator during disturbances very effectively.

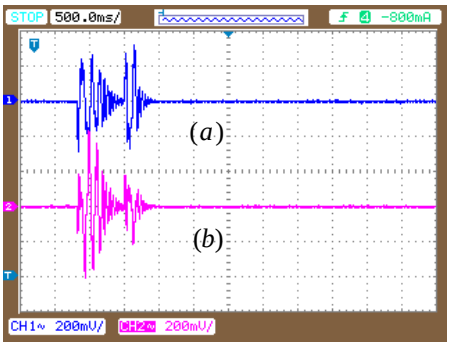

Figure 6.19: Error input of type-1 FLC-PI: (a) Torque controller (b) Voltage controller

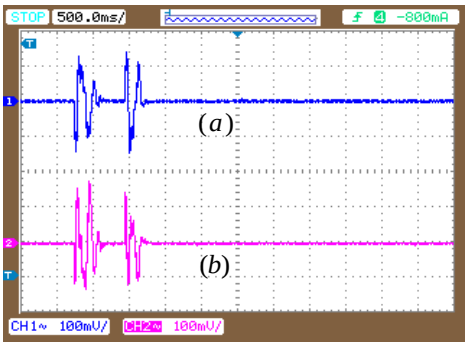

Figure 6.20: Error input of type-2 FLC-PI: (a) Torque controller (b) Voltage controller

6.10 Conclusions

In this chapter, an interval type-2 fuzzy-PI is proposed and implemented for RSC of DFIG. The gains of PI controller were determined by the type-2 fuzzy logic method according to the changes in system operating condition. Thus, an adaptive structure, which is important for DFIG rotor side converter control is obtained. To validate the proposed control method, real time simulations are developed for studied system using digital real-time simulator of OPAL-RT platform. The performance of the proposed approach has been investigated for different operating conditions of DFIG such as severe fault and voltage sag with reference to varying wind speed. The results of type-2 FLC-PI are compared with that of type-1 FLC-PI controller, one at a time. It is observed from simulation results that the proposed controller offers better performance than its type-1 fuzzy-PI counterpart. Finally, it concluded that the adaptive nature of proposed type-2FLC-PI controller played vital role to enhance the LVRT capability of DFIG.

CHAPTER 7: CONCLUSIONS AND FUTURE SCOPE

7.1 Conclusions

The work presented in this thesis mainly focused on controller design and control strategies to improve the performance of the wind energy systems (fixed speed and variable speed) subjected to the grid integrated issues such as varying wind speed, transient fault and grid code requirements. A special focus on interval type-2 fuzzy logic method is concentrated as it addresses the issues related to uncertainties in the membership functions and rules thus, counter the effects of nonlinearities in the model and uncertainties in the operating conditions of the WESs.

An effort has been made to design the type-2 fuzzy logic controller by exploring the properties of interval type-2 fuzzy sets, for pitch angle controller of fixed speed WES, damping controller of fixed speed wind farm and RSC controllers of the variable speed WES. Furthermore, the proposed control technique is also validated by developing the real time simulations using OPAL-RT technology RTDS simulator for power smoothing of WES using pitch angle controller; and torque and voltage control of rotor side converter of DFIG.

The following conclusions are drawn on the accomplishments of this thesis:

- In this work the electrical equivalent circuit of the IG from the PCC has derived and mathematical relation between the pitch angle, rotor speed, mechanical and electrical torques were obtained and some key factors that may affect the transient stability of the fixed-speed IG has been investigated using analytical approach. This type of investigation is very important in order to expand the operating limitations of the wind turbine driven IG under the severe faults to guarantee the wind farm connection to the grid.
- A typical pitch angle controller is developed which works well in power control mode to regulate the IG output power subjected to varying wind speed and, in speed control mode to enhance the transient stability during network fault. This type of pitch angle configuration with well designed (using Type-2 FLC) controller is an effective solution for WES transient stability enhancement as well as output power regulation. A grid connected fixed speed WES model is implemented in MATLLAB^{TM}/Simulink platform and a type-2 FLC is designed for the pitch angle controller of WES and tested for frequently varying wind speed and network faults.
- In the section 3.7, an interval Type-2 FLC based pitch-angle controller is proposed for smoothening out the output power fluctuations of a wind energy system. At first,

command reference power based on EMA concept is obtained and then interval Type-2 FLC is implemented to follow the reference command power more effectively. To validate the proposed technique, the system designed in MATLAB^{TM}/Simulink was exported to RT-lab via RTW for real time simulation. Real time digital simulator is a suitable platform for real time analysis of renewable energy resources for controller prototyping, real time simulations and hardware in loop tests. Two different types of wind speed patterns are employed to study the effectiveness of the proposed controller. The results show the pitch-angle controller with Type-2 FLC offer better performance in smoothing the output power of WES than PI and Type-1 FLC. To estimate the smoothing level of proposed controller, power smoothing function has been incorporated as performance index.

- Taking into consideration of the restraints due to the limited non-renewable energy sources and with the ever increasing demand of electricity, it has become an absolute necessity to integrate the wind energy systems in the grid, for which a complete and detailed study of wind farm is required, in which, simulation studies under various expected operating conditions (such as different type of faults, fault locations and durations) are highly needed to prevent any harmful impact of the wind farm to the grid. Therefore, in this work, a system consists of 36MW fixed speed wind farm exporting power to 120kV grid has been designed using MATLAB^{TM}/Simulink. As a preliminary study, it investigates the impact of fault ride through on the stability of the fixed speed wind farm connected to power grid. The effect of fault locations and fault time durations on stability of fixed speed wind farm, subjected to different types of faults were studied. Moreover, a STATCOM is included to investigate its effect on the system stability during different fault durations and locations. The system parameters such as PCC voltage, active and reactive powers are monitored in steady-state as well as fault conditions. Later on, we investigated STATCOM with type-2 fuzzy logic based damping controller design for stability improvement of wind integrated power system. The STATCOM with proposed damping controller suppresses the inherent power fluctuations of the studied system and thus enhance the stability of the system subjected to disturbances. Different scenarios have been considered to demonstrate the effectiveness of the proposed controller.
- This work also investigates the role of control system based on simultaneous control of STATCOM reactive power and pitch angle control rotor blades. Therefore, in this thesis, unified voltage and pitch-angle (UVPC) control strategy has been proposed through which the simultaneous control of STATCOM and pitch-angle control has been achieved in order to guarantee the compliances of the grid code requirement as well as enhance the

LVRT capability of the fixed speed wind farm. A coordinated control algorithm is implemented for successful control of STATCOM in combination with pitch angle controller. The FRT scheme of pitch-angle controller has been designed using type-2 fuzzy logic technique as it is capable of effectively stabilizing generator rotor speed than their traditional fuzzy logic counterpart. The simulation results show that the simultaneous control of STATCOM and pitch-angle control improve the LVRT capability of the FSIG wind farm and improving the stability margin of rotor speed of the generator. Moreover, the proposed UVPC helps in reducing the size of the STATCOM to be installed for improving the LVRT of such wind farms.

- Another contribution is that by using UVPC, effective generator output power smoothing and voltage regulation is achieved. A typical pitch angle control approach has been incorporated which works under below-rated wind speed. Moreover, an interval type-2 fuzzy logic technique has employed to design the pitch angle controller, as it is more suitable than their traditional fuzzy logic counterpart. Therefore, a new type of pitch angle controller and STATCOM (termed as UVPC) can smoothen out the generator active power as well as regulate the generator terminal voltage to a constant magnitude whenever wind farm is subjected to below-rated wind speed variations.
- An interval type-2 fuzzy-PI based adaptive technique is proposed for torque and voltage controllers of RSC of variable speed WES. The gains of PI controller were determined by using type-2 fuzzy logic method according to the system operating condition changes. Thus, an adaptive structure which is important for DFIG rotor side converter control is obtained. A 1.5MW DFIG model has been developed using MATLAB^{TM}/Simulink and then exported to OPAL-RT digital simulator for real time simulations. The performance of the proposed approach has been investigated for different operating conditions of DFIG such as severe fault, voltage sag with reference to varying wind speed. A comparative performance analysis is done with type-1 FLC-PI counterpart. The tracking performance of proposed controller is very effective, as a result, type-2 fuzzy-PI controlled RSC exhibits effective transient response and it is suitable for grid disturbances such as voltage sag and faults.
- The major part of this thesis incorporated an interval type-2 fuzzy logic method as the FLCs based on type-2 fuzzy sets have the potential to give better performance than the type-1 FLC with respect to uncertainty. Moreover, due to extra degree of freedom provided by the foot print of uncertainty (FOU), a smooth control surface can be generated that can enables the controller to handle system disturbances more effectively.

This special feature of type-2 FLC offers more robust performance than type-1 FLC counterpart.

7.2 Future Scope of the work

Research and development is a continuous process. For any research work carried out, there is always a better chance for improvement and many opportunities always remains opened for future work. As a result of investigation carried out in performance analysis of grid connected wind energy systems, the following aspects are identified for future scope of research.

- *Power system stabilization*:

Wind power generation slowly substituting the conventional power plants that commonly control and stabilize the power system. The increasing penetration of wind power system engaged in performing these tasks. The most common method employs to stabilize the power system using WES is pitch-angle controller. If the wind turbines are to take over such task, they need to be designed with an effective control technique to perform the power system stabilization. Therefore, future work can investigate further the type-2 FLC based pitch angle controller for power system stabilization by developing an appropriate IEEE standard wind integrated power system.

- *Improvement of micro-grid performance in islanding mode:*

In the present scenario, micro-grid is one of the alternatives for electricity generation and also contributes to emission reduction and mitigation of climate change. The micro-grid with renewable energy resources (wind and solar) encounter the challenges such as solar radiation and wind speed variation. As it discussed earlier, wind speed is an intermittent and stochastic in nature, any variation in wind speed will causes generator output power to fluctuate resulting in frequency fluctuations inside the micro-grid. During islanding mode this condition originates stability problems and provides poor power quality.

In our work, we have proposed type-2 fuzzy logic based pitch angle controller with EMA concept for smoothing the output power of WES where it is penetrated to the utility grid. Therefore, future work can be investigates the micro-grid stability problems due to wind speed variations by employing proposed concept to limit the frequency oscillations in acceptable range.

- *Economical benefit of ESS with EMA Concept:*

Although, the EMA incorporated pitch angle controller offers good smoothing in output power of wind generator, but considerable amount of drop in the output power cannot be avoided. If we concern with loss of generator output power, then energy storage system can solve the problem, however, it may need large energy storage capacity involving in

huge cost. The EMA based reference output power generated pitch angle controller can be adopted to make the ESS capacity comparatively small. Therefore, the ESS equipped with EMA pitch angle controller may be best suited for power smoothing wind turbine generator output power. However, this thesis does not incorporate the ESS for power smoothing therefore, ESS adopted with EMA reference command generated-pitch angle controller can be investigated for its applicability with optimal reference output power point.

Moreover, photovoltaic (PV) cell systems are also one of the most considerable renewable energy. The major dependency of them on irradiance of sun and temperature, these two factors are continuously varying and thus results in output power of PV cell with considerable amount of fluctuations which may also cause grid frequency and voltage fluctuations if they are connected in large number. Therefore, ESS equipped with EMA concept also can be investigated in the solar PV systems for its effective applicability.

- *Self tuning of FOU of type-2 FLC for more robust performance of an adaptive type-2 FLC-PI controller for renewable energy systems:*

It is observed from the chapter 2, the foot print of uncertainty (FOU) can be effect the control system performance. The FOU with equal width do not provide satisfactory results, therefore in our work we have varied the width of FOU systematically by observing its effect, on the oscillatory system parameters when subjected to the disturbances. This is however not an appropriate method to achieve the optimal width of the FOU. We need to develop an algorithm or optimal tuning method to compute the optimal width of FOU of type-2 memberships to get the more robust performance by considering sensitive parameters of the system. As the renewable energy resources such as wind and solar are highly uncertain can be effectively utilize this control approach.

BIBLIOGRAPHY

1. Abad, G., Lopez, J., and Rodriguez, M. (2011). *Doubly fed induction machine: modeling and control for wind energy generation applications*. Wiley-IEEE Press.
2. Abdel-Baqi, O., and Nasiri, A. (2011). Series Voltage Compensation for DFIG Wind Turbine Low-Voltage Ride-Through Solution. *IEEE Transactions on Energy Conversion*, 26(1): 272–280.
3. Ackerman, T. (2005). *Wind power in power system*. John Wiley & Sons. Ltd.
4. Ahshan, R., Iqbal, M. T., and Mann, G. K. (2008). Controller for a small induction-generator based wind-turbine. *Applied Energy*, *85*(4): 218–227.
5. Aisbett, J., and Rickard, J. T. (2014). Centroids of Type-1 and Type-2 Fuzzy Sets When Membership Functions Have Spikes. *IEEE Transactions on Fuzzy Systems*, 22(3): 685–692.
6. Ali, M. H., Murata, T., and Tamura, J. (2006). Minimization of fluctuations of line power and terminal voltage of wind generator by fuzzy logic-controlled SMES. *International Review of Electrical Engineering*, 1 (4): 559–566.
7. Ali, M. H., Tamura, J., and Wu, B. (2008). SMES strategy to minimize frequency fluctuations of wind generator system. *Proceedings of the 34th Annual Conference of the IEEE Industrial Electronics Society (IECON 2008*), Orlando, pages 3382–3387.
8. Ali, M. H. (2012). *Wind energy systems solution for power quality and stabilization*. CRC Press, Taylor and Francis Group, New York.
9. Anaya-Lara O., Jenkins, N., Ekanayake, J. B., Cartwright, P., Hughes, M. (2009). *Wind energy generation Modelling and control*. Wiley, Hoboken, NJ.
10. Anderson, P. M., and Bose, A. (1983). Stability simulation of wind turbine systems. *IEEE Transactions on Power Apparatus and Systems*, 102 (12): 3791–3795.
11. Arbi, J., Ghorbal, M. J. B., Slama-Belkhodja, I. (2009). Direct virtual torque control for doubly fed induction generator grid connection. *IEEE Transaction on Industrial Electronics*, 56(10): 4163–4173.
12. Arifujjaman, M., Iqbal, M. T., and Quaicoe, J. E. (2008). Energy capture by a small wind-energy conversion system. *Applied Energy*, *85*(1): 41–51.
13. Arifujjaman, M., Iqbal, M. T., and Quaicoe, J. E. (2009). Reliability analysis of grid connected small wind turbine power electronics. *Applied Energy*, *86*(9): 1617–1623.

14. Asuhaini, A. B., Zin, B. M., Pesaran, M. H. A., Khairuddin, A. B. (2013). An overview on doubly fed induction generators control and contributions to wind based electricity generation. *Renewable Sustainable Energy Reviews*, 27: 692–708.
15. Bansal, R. C., Kothari, D. P., and Bhatti, T. S. (2000). Some aspects of grid connected wind electric energy conversion systems, *NREC 2000: National Renewable Energy Convention* 2000, Allied publisher, pages 410–414.
16. Bansal, R. C., Bhatti, T. S., and Kothari, D. P. (2003). Bibliography on the application of induction generators in nonconventional energy systems. *IEEE Transactions on Energy Conversion*, *18*(3): 433–439.
17. Biglarbegian, M., Melek, W. W., and Mendel, J. M. (2011). Design of novel interval type-2 fuzzy controllers for modular and reconfigurable robots: Theory and experiments. IEEE Transactions Industrial Electronics, 58(4): 1371–1384.
18. Blaabjerg, F., and Chen, Z. (2006). *Power Electronics for Modern Wind Turbines*, Morgan & Claypool Publishers.
19. Blaabjerg, F., Iov, F., Kerekes, T., Teodorescu, R., and Ma, K. (2011). Power electronics - key technology for renewable energy systems. *2nd Power Electronics, Drive Systems and Technologies Conference*, Tehran, pages 445–466.
20. Bull, S.R. (2001). Renewable energy today and tomorrow: in *Proceedings of the IEEE*, 89 (8): 1216–1226.
21. Burnham, D., Santoso, S., and Muljadi, E. (2009). Variable Rotor-Resistance Control of Wind Turbine Generators. *In IEEE Power and Energy Society General Meeting (PES)*, pages 1–6.
22. Causebrook, A., Atkinson, D. J., and Jack, A. G. (2007). Fault ride-through of large wind farms using series dynamic braking resistors. *IEEE Transactions on Power Systems*, 22(3): 966–975.
23. Chen, W. L., and Hsu, Y. Y. (2008). Unified voltage and pitch angle controller for wind-driven induction generator system. *IEEE Transactions on Aerospace and Electronic Systems*, 44(3): 913–926.
24. Chen, S. Z., Cheung, N. C., Wong, K. C., and Wu, J. (2011). Integral variable structure direct torque control of doubly fed induction generator. *IET Renewable Power Generation*, 5(1): 18–25.
25. Chen, C.S. (2011). Supervisory interval type-2 TSK neural fuzzy network control for linear microstepping motor drives with uncertainty observer. *IEEE Trans. Power Electron*, 26(7): 2049–2064.

26. Chowdhury, M. A., Hosseinzadeh, N., and Shen, W. X. (2012). Smoothing wind power fluctuations by fuzzy logic pitch angle controller. *Renewable Energy*, 38(1): 224–233.
27. Jauch, C. (2016). Controls of a flywheel in a wind turbine rotor. *Wind Engineering*, *40*(2): 173–185.
28. Jauch, C., Cronin, T., Sorensen, P., and Jensen, B. B. (2007). A fuzzy logic pitch angle controller for power system stabilization. *Wind Energy*, *10*(1): 19–30.
29. Jauch, C., Islam, S. M., Sorensen, P., and Jensen, B. B. (2007). Design of a wind turbine pitch angle controller for power system stabilisation. *Renewable energy*, *32*(14): 2334–2349.
30. Darbyshire, J., & Nayar, C. V. (2007). Modelling, simulation and testing of grid connected small scale wind systems. In *Power Engineering Conference, AUPEC 2007. Australasian Universities*, pages 1–6.
31. Das, D., Haque, M. E., Chowdhury, M. M., Gargoom, A., Negnevitsky, M., and Muttaqi, K. M. (*2013*). A novel control scheme of NPC VSC based STATCOM to enhance the performance of wind farm with fixed and variable speed wind turbines. *IEEE Industry Applications Society Annual Meeting*, Lake Buena Vista, pages 1–8.
32. Devaraj, D., and Jeevajyothi, R. (2011). Impact of fixed and variable speed wind turbine systems on power system voltage stability enhancement. *IET Conference on Renewable Power Generation*, Edinburgh, pages. 1–9.
33. Doctor, F., Hagras, H., Roberts, D., and Callaghan, V. (2008). A type-2 fuzzy based system for handling the uncertainties in group decisions for ranking job applicants within human resources systems. *In Proceedings IEEE International Conference on Fuzzy Systems*, Hong Kong, pages 481–488.
34. Doostabad , H. H., Khalghani , M. R., and Khooban, M. H. (2016). A novel control system design to improve LVRT capability of fixed speed wind turbines using STATCOM in presence of voltage fault. *International journal of Electrical Power and Energy Systems*, 77: 280–286.
35. Duong, M. Q. Grimaccia, F. Leva , S. Mussetta M. and Ogliari, E. (2014). Pitch angle control using hybrid controller for all operating regions of SCIG wind turbine system. *Renewable Energy*, 70: 197–203.
36. Duong, M. Q., Grimaccia, F., Leva, S., Mussetta, M., and Le, K. H. (2015). Hybrid controller for transient stability in wind generators. *Clemson University Power Systems Conference (PSC)*, Clemson, pages 1–7.

37. Edrisian, A., Goudarzi, A., Davidson, I. E., Ahmadi, A., and Venayagamoorthy, G. K. (2015). Enhancing SCIG-based wind turbine generator performance through reactive power control. *Clemson University Power Systems Conference (PSC)*, Clemson, pages 1–8.
38. Ekanayake, J. B and Jenkins, N. (1999). Selection of passive elements for a three-level inverter based static synchronous compensator. *IEEE Transactions on Power Delivery*, 14(2): 655–661.
39. Fadaeinedjad, R., Moschopoulos, G., and Moallem, M. (2008). Using STATCOM to mitigate voltage fluctuations due to aerodynamic aspects of wind turbines. *IEEE Power Electronics Specialists Conference*, Rhodes, pages 3648–3654.
40. Flores, W. C., Mombello, E., Jardini, J. A., and Ratta, G. (2009). Fuzzy risk index for power transformer failures due to external short circuits. *Electric Power System Research*, 79(4): 539–549.
41. Freitas, W., Morelato, A., and Xu, W. (2004). Improvement of induction generator stability using braking resistors. *IEEE Transactions on Power Systems*, 19(2): 247–1249.
42. Garasi, P., Watanabe, M., and Mitani, Y. (2014). Power smoothing of wind turbine generator using Fuzzy-PI pitch angle controller. *Australasian Universities Power Engineering Conference (AUPEC)*, Perth, pages 1–5.
43. Ghazi, R., and Aliabadi, H. (2010). Stability improvement of wind farms with fixed-speed turbine generators using braking resistors. *45th International Universities Power Engineering Conference UPEC2010*, Wales, pages 1–5.
44. Greigarn, T., Garcia-Sanz, M. (2011). Control of Flywheel Energy Storage Systems for wind farm power fluctuation mitigation. *IEEE 2011 Energy Tech*, Cleveland, pages 1–6.
45. Grid Code—Extra High Voltage, Tennet TSO GmbH; 2010. <http://www.tennettso.de/site/binaries/content/assets/transparency/publications/gridconnection/tennetnar2010eng.pdf>.
46. Grilo, A. P., Mota, A., Mota, L. T. M., and Freitas, W. (2007). An analytical method for analysis of large-disturbance stability of induction generators. *Power System IEEE Transactions*, 22(4): 1861–1869.
47. GWEC, Global Wind Energy Council, http://gwec.net/global-figures/wind-in-numbers/ (Accessed on 25-1-2018).
48. Hagras, H. (2007). Type-2 FLCs: A New Generation of Fuzzy Controllers. *IEEE Computational Intelligence Magazine*, 2(1): 30–43.

49. Hagras, H., and Wagner, C. (2012). Towards the wide spread use of type-2 fuzzy logic systems in real world applications. *IEEE Computation Intelligent Magazine*, 7(3): 14–24.

50. Hamane, B., Doumbia, M. L., Bouhamida, M., and Benghanem, M. (2014). Control of wind turbine based on DFIG using Fuzzy-PI and Sliding Mode controllers. *9th International Conference on Ecological Vehicles and Renewable Energies (EVER)*, Monte-Carlo, pages 1–8.

51. Hansen, A. D., and Michalke, G. (2007). Fault ride-through capability of DFIG wind turbines. *Renewable Energy*, 32(9): 1594–1610.

52. Hazzab, A., Bousserhane, I. K., Zerbo, M., and Sicard, P. (2006). Real Time Implementation of Fuzzy Gain Scheduling of PI Controller for Induction Machine Control. *2nd International Conference on Information & Communication Technologies*, Damascus, pages 1416–1421.

53. Herman, P., Prasad, G., and McGinnity, T. (2005). Investigation of the type-2 fuzzy logic approach to classification in an EEG-based brain–computer interface. *In Proceeding IEEE International Conference Engineering in Medicine and Biology*, Shanghai, pages 5354–5357.

54. Hingorani, N. G., and Gyugyi, L. (2000). *Understanding FACTS: Concepts and Technology of Flexible AC Transmission Systems*, New York: IEEE Press.

55. Hisdal, E. (1981). The IF THEN ELSE statement and interval-valued fuzzy sets of higher type. *International journal of Man-Machine Studies*, 15(4): 385–455.

56. Holdsworth, L., Wu, X. G., Ekanayake, J. B., and Jenkins, N. (2003). Comparison of fixed speed and doubly-fed induction wind turbines during power system disturbances. *IEE Proceedings-Generation, Transmission and Distribution*, *150*(3): 343–352.

57. Hossain, M. J., Pota, H. R., and Ramos, R. A. (2011). Robust STATCOM control for stabilization of fixed-speed wind turbines during low voltages. *Renewable Energy*, 36 (11): 2897–2905.

58. Hsiao, M. Y., Li, T. H. S., Lee, J. Z., Chao, C. H., and Tsai, S. H. (2008). Design of interval type-2 fuzzy sliding mode controller. *Information Science*, 178(6): 1696–1716.

59. Hu, J., He, Y., and Xu, L. (2009). Improved control of DFIG systems during network unbalance using PI–R current regulators. *IEEE Transaction on Industrial Electronics*, 56(2): 439–451.

60. Islam, M. M., Islam, A., Shaikh, S. M., Sheikh, M. R. I. (2015). Stability enhancement of wind power system by using energy capacitor system. *International Conference on Electrical & Electronics Engineering*, Rajshahi, pages 85–88.
61. Jafarzadeh, S., Fadali, M. S., and Etezadi-Amoli, M. (2012). Fuzzy type-1 and type-2 TSK modeling with application to solar power prediction. *IEEE Power and Energy Society General Meeting*, San Diego, pages 1–6.
62. Jain, B., Jain, S., and Nema, R. K. (2014). Wavelet based Power Quality Monitoring in Grid Connected Wind Energy Conversion System. *International Journal of Computer Applications*, *98*(18): 9–15.
63. Jain, B., Jain, S., and Nema, R. K. (2015). Control strategies of grid interfaced wind energy conversion system: An overview. *Renewable and Sustainable Energy Reviews*, *47*: 983–996.
64. Jain, B., Singh, S., Jain, S., and Nema, R. K. (2015). Flexible mode control of grid connected wind energy conversion system using wavelet. *Journal of Energy*, 2015: 1–12.
65. Jalili-Marandi, V., Pak, L. F., and Dinavahi, V. (2010). Real-Time Simulation of Grid-Connected Wind Farms Using Physical Aggregation. *IEEE Transactions on Industrial Electronics*, 57(9): 3010–3021.
66. Jammeh, E., Fleury, M., and Ghanbari, M. (2008). Fuzzy logic congestion control of transcoded video streaming without packet loss feedback. *IEEE Transaction Circuits System Video Technology*, 18(3): 387–393.
67. Jammeh, E., Fleury, M., Wagner, C., Hagras, H., and Ghanbari, M. (2009). Interval type- 2 fuzzy logic congestion control for video streaming across IP networks. IEEE Transactions Fuzzy System, 17(5): 1123–1142.
68. Jiang, Q., and Wang, H. (2013). Two-time-scale coordination control for a battery energy storage system to mitigate wind power fluctuations. *IEEE Transactions Energy Conversion*, 28(1): 52–61.
69. Johnson, G. L. (2004). *Wind energy systems*, Manhattan: Prentice-Hall.
70. Kadri, M. B., and Khan, S. (2012). Fuzzy adaptive pitch controller of a wind turbine. *15th International Multitopic Conference (INMIC)*, Islamabad, pages105–110.
71. Kamel, R. A., Chaouachi, A., and Nagasaka, K. (2010). Wind power smoothing using fuzzy logic pitch controller and energy capacitor system for improvement Micro-Grid performance in islanding mode. *Energy*, 35(5): 2119–2129.
72. Kandel, A. (1992). *Fuzzy experts systems*, CRC Press, Inc.Boca Raton,FL.
73. *Karnik, N. N., and Mendel, J. M. (1999). Type-2 fuzzy logic systems. IEEE Transactions on Fuzzy, 7(6): pages 643–658.*

74. Khosravi, A., Nahavandi, S., and Creighton, D. (2011). Short term load forecasting using Interval Type-2 Fuzzy Logic Systems. *In Proceeding IEEE International Conference Fuzzy Systems*, Taipei, pages 502–508.
75. Kim, Y., Kang, M., Muljadi, E., Park, J. W., and Kang, Y. C. (2017). Power Smoothing of a Variable-Speed Wind Turbine Generator in Association with the Rotor-Speed-Dependent Gain. *IEEE Transactions on Sustainable Energy*, 8(3): 990–999.
76. Konara, K. M. S. Y., and Kolhe, M. L. (2015). Pitch controller modeling for wind turbine power regulation using feed forward control strategies. *IEEE PES Asia-Pacific Power and Energy Engineering Conf. (APPEEC)*, Brisbane, pages1–5.
77. Lee, C. C. (1990). Fuzzy logic in control systems: Fuzzy logic controller-Part 1. *IEEE Transactions on systems,Man and Cybernetics*, 20(2): 404–418.
78. Lee, C. C. (1990). Fuzzy logic in control systems: Fuzzy logic controller-Part 2. *IEEE Transactions on systems,Man and Cybernetics*, 20(2): 419–435.
79. Lee, C. S., Wang, M. H., and Hagras, H. (2010). A Type-2 Fuzzy Ontology and Its Application to Personal Diabetic-Diet Recommendation. In *IEEE Transactions on Fuzzy Systems*, 18(2): 374–395.
80. Liang, Q., and Mendel, J. M. (2000). Equalization of nonlinear time-varying channels using type-2 fuzzy adaptive filters. *IEEE Transactions on Fuzzy Systems*, 8(5): 551–563.
81. Liang, Q., and Mendel, J. M. (2000). Overcoming time-varying co-channel interference using type-2 fuzzy adaptive filters. *IEEE Transactions on Circuits and Systems II: Analog and Digital Signal Processing*, 47(12): 1419–1428.
82. Liang, Q., and Mendel, J. M. (2000). Interval type-2 fuzzy logic systems: theory and design. *IEEE Transactions on Fuzzy Systems*, 8(5): 535–550.
83. Lima, F. K. A., Luna, A., Rodriguez, P., Watanabe E. H., and Blaabjerg, F. (2010). Rotor Voltage Dynamics in the Doubly Fed Induction Generator during Grid Faults. *IEEE Transactions on Power Electronics*, 25 (1): 118–130.
84. Linda, O., Manic, M., Alves-Foss, J., and Vollmer, T. (2011). Towards resilient critical infrastructures: Application of type-2 fuzzy logic in embedded network security cyber sensor. 4th *International Symposium Resilient Control Systems*, Boise, pages 26–32.
85. Li, L., Lin, W. H., and Liu, H. (2006). Type-2 fuzzy logic approach for short-term traffic forecasting. *IEE Proceedings - Intelligent Transport Systems*, 153(1): 33–40.

86. Li, X. (2012). Fuzzy adaptive Kalman filter for wind power output smoothing with battery energy storage system. *IET Renewable Power Generation*, 6(5): 340–347.
87. Li, S., Yu, Z., Wang, X., and Su, X. (2016). The simulation of the wind power system vector control based on fuzzy PI. *Chinese Control and Decision Conference (CCDC)*, Yinchuan, pages 3114–3117.
88. Liu, F., and Mendel, J. M. (2008). Encoding Words into Interval Type-2 Fuzzy Sets Using an Interval Approach. In *IEEE Transactions on Fuzzy Systems*, 16(6): 1503–1521.
89. Luhana, P. P., and Shah, M. J. (2016). Stability improvement of fixed speed induction generator based wind farm using statcom for different types of fault. *International Conference on Electrical, Electronics, and Optimization Techniques (ICEEOT)*, Chennai, pages 943–949.
90. Luo, A., Tang, C., Shuai, Z., Tang, J., Xu, X. Y., and Chen, D. (2009). Fuzzy-PI-Based Direct-Output-Voltage Control Strategy for the STATCOM Used in Utility Distribution Systems. *IEEE Transactions on Industrial Electronics*, 56 (7):2401–2411.
91. Malla, S. G., and Bhende, C. N. (2014). Voltage Control of Stand-Alone Wind and Energy System. *Electrical Power and Energy Systems*, 56: 361–373.
92. Mansour, M., Mansouri, M. N., and Mimouni, M. F. (2011). Comparative study of fixed speed and variable speed wind generator with pitch angle control. *2011 International Conference on Communications, Computing and Control Applications (CCCA)*, Hammamet, pages 1–7.
93. Mamdani, E.M. (1976). Advances in the linguistic synthesis of fuzzy controllers. *International journal of Man-Machine Studies*, 8(6): 669–678.
94. Mamdani, E. M. (1977). Applications of fuzzy logic to approximate reasoning using linguistic synthesis. *IEEE Transactions on Computers*, 26(12): 1182–1191.
95. Martinez, R., Castillo, O., and Anguilar. L.T. (2009). Optimization of interval type-2 fuzzy logic controller for perturbed autonomous wheeled mobile robot using genetic algorithms. *Information Science*, 179(13): 2158–2174.
96. Mendel, J. M. (1999). Computing with words when words can mean different things to different people. *ICSC Congress Computat. Intell.: Methods Application, 3rd Annual. Symposium Fuzzy Logic Applications*, Rochester, pages 1–7.
97. Mendel, J. M. (1995). Fuzzy logic systems for engineering: A tutorial. *Proceeding IEEE*, 83(3):345–377.
98. Mendel, J. M., and John, R. I. B. (2002). Type-2 fuzzy sets made simple. *IEEE Transactions on Fuzzy Systems*, 10(2): 117–127.

99. Mendel, J. M. (2004). Computing derivatives in interval type-2 fuzzy logic systems. In *IEEE Transactions on Fuzzy Systems*, 12(1): 84–98.
100. Mendel, J. M., and John, R. I. B. (2006). Interval type-2 fuzzy logic systems made simple. *IEEE Transactions on Fuzzy System*, 10(2): 117–127.
101. Mendel, J. M., John, R. I., and Liu, F. (2006). Interval type-2 fuzzy logic systems made simple. IEEE Transaction Fuzzy System, 14(6): 808–821.
102. Mendez, G., Leduc-Lezama, L., Colas, R., Murillo-Perez, G., Ramirez-Cuellar, J., and Lopez, J. (2010). Modelling and control of coiling entry temperature using interval type-2 fuzzy logic systems. *Journal of Iron making Steelmaking*, 37(2): 126–134.
103. Mi, Y., Bao, X., Jiang, E., Deng, W., Li, J., Ren, L., and Wang, P. (2014).The pitch angle control of squirrel-cage induction generator wind power generation system using sliding mode control. *16thEuropean Conf. on Power Electronics and Applications*, Lappeenranta, pages 1–10.
104. Mi, Y., Bao, X., Yang, Y., Zhang, H., and Wang, P. (2014). The sliding mode pitch angle controller design for squirrel-cage induction generator wind power generation system. *33rd Chinese Control Conference*, Nanjing, pages 8113–8117.
105. Mikkili, S., and Panda, A. K. (2013). Types-1 and -2 fuzzy logic controllers-based shunt active filter I_d–I_q control strategy with different fuzzy membership functions for power quality improvement using RTDS hardware. *IET Power Electronics*, 6(4): 818–833.
106. Mikkili, S., Panda, A. K., and Prattipati, J. (2014). Review of Real-Time Simulator and the Steps Involved for Implementation of a Model from MATLAB/SIMULINK to Real-Time. *Journal of Institute Engineering India Ser. B*, 1–18.
107. Mizumoto, M., and Tanaka, K. (1976). Some properties of fuzzy sets of type 2. *Information Control*, 31: 312–340.
108. Molinas, M., Suul, J. A., and Undeland, T. (2008). Low Voltage Ride Through of Wind Farms with Cage Generators: STATCOM versus SVC. *IEEE Transactions on Power Electronics*, 23(3):1104–1117.
109. Mondol, N., Sheikh, M. R. I., and Hasan, M. R. (2015). Stabilization of wind firm integrated Hybrid Power System by using STATCOM. *International Conference on Electrical & Electronic Engineering (ICEEE)*, Rajshahi, pages 105–108.
110. Mossa, M. A. (2014). *Modeling, Analysis and Enhancement of the performance of a Wind Driven DFIG During steady state and transient conditions*. Hamburg, Anchor Academic Publishing.

111. Murthy, S. S., Singh, B., Goel, P. K., and Tiwari, S. K. (2007). A Comparative Study of Fixed Speed and Variable Speed Wind Energy Conversion Systems Feeding the Grid. *7th International Conference on Power Electronics and Drive Systems*, Bangkok, pp. pages 736–743.
112. Muyeen, S. M., Ali, M. H., and Takahashi, R. (2006). Transient Stability Analysis of Grid Connected Wind Turbine Generator System Considering Multi-Mass Shaft Modeling. *Electric Power Components and Systems*, 34 (10): 1121–1138.
113. Muyeen, S. M., Takahashi, R., Murata, T., and Tamura, J. (2005). Transient stability enhancement of wind generator by online logical controller with the consideration of initial condition settings. *International Power Electronics Conference*, Japan, pages 1–6.
114. Muyeen, S. M., Tamura, J., and Murata, T. (2009). *Stability augmentation of a grid connected wind farm*. Springer-Verlag London Ltd.
115. Muyeen, S. M., Shishido, S., Ali, M. H., Takahashi, R., Murata, T., Tamura, J. (2008). Application of energy capacitor system to wind power generation. *Wind Energy*, 11(4): 335–350.
116. Muyeen, S. M., Ali, M. H., Takahashi, R., Murata, T., and Tamura, J. (2007). Stabilization of Wind Farms Connected with Multi Machine Power System by Using STATCOM. *IEEE Lausanne Power Technology*, Lausanne, pages 299–304.
117. Muyeen, S. M., and Al-Durra, A. (2013). Modeling and Control Strategies of Fuzzy Logic Controlled Inverter System for Grid Interconnected Variable Speed Wind Generator. *IEEE Systems Journal*, 7(4): 817–824.
118. Mohan, N., Undeland, T. M., and Robbins, W. P. (1995). *Power Electronics: Converters, Applications and Design*, 2nd edition, New York: Wiley.
119. Mohsen, R., and Mostafa, P. (2010). Grid-fault ride-through analysis and control of wind turbines with doubly fed induction generators. *Electrical Power System Research*, 80(2):184–195.
120. Nayar, C. V., Islam, S. M., Dehbonei, H., Tan, K., and Sharma, H. (2011). Power electronics for renewable energy sources. In *Power Electronics Handbook*, 723–766.
121. Nie, M., and Tan, W. W. (2008). Towards an efficient type-reduction method for interval type-2 fuzzy logic systems. *IEEE International Conference on Fuzzy Systems (IEEE World Congress on Computational Intelligence)*, Hong Kong, pages 1425–1432.

122. Noureldeen, O., Rihan, M., and Hasanin, B. (2011). Stability improvement of fixed speed induction generator wind farm using STATCOM during different fault locations and durations. *Ain Shams Engineering Journal*, 2(1):1–10.
123. Ou, R., Xiao, X. Y., Zou, Z. C., Li, C. S., and Wu, D. Y. (2015). Application of SFCL to improve the transient voltage stability of grid-connected wind farm with DFIG during grid faults. *IEEE International Conference on Applied Superconductivity and Electromagnetic Devices (ASEMD)*, Shanghai, pages 240–241.
124. Ou, T. C., Lu, K. H., and Huang, C. J. (2017). Improvement of transient stability in a hybrid power multi-system using a designed NIDC (Novel Intelligent Damping Controller). *Energies*, *10*(4): 1–16.
125. Pawel, H., Girijesh, P., and McGinnity, T. (2008). Design and on-line evaluation of type-2 fuzzy logic system-based framework for handling uncertainties in BCI classification. *In Proceeding IEEE International Conference Engineering in Medicine and Biology Society*, Vancouver, pages 4242–4245.
126. Pedrycz, W., and Gomide, F. (2007). *The design of fuzzy sets*, *Fuzzy Systems Engineering: Toward human centric computing*. Whiley-IEEE Press e Book chapter, 67–100.
127. Pradhan, and C., Bhende, C. N. (2015). Adaptive Deloading of Stand-Alone Wind Farm for Primary Frequency Control. *Energy Systems*, 6(2): 109–127.
128. Pradhan, and C., Bhende, C. N. (2016). Enhancement in Primary Frequency Regulation of Wind Generator using Fuzzy-based Control. *Electric Power Components and System*s, 15(44): 1669–1682.
129. Premrudeepreechacharn, S., and Poapornsawan, T. (2000). Fuzzy logic control of predictive current control for grid-connected single phase inverter. *28th IEEE Photovoltaic Specialists Conference*, Anchorage, pages 1715–1718.
130. Poitiers, F., Bouaouiche, T., and Machmoum, M. (2009). Advanced control of a doubly fed induction generator for wind energy conversion. *Electric power system research*, 79(7):1085–1096.
131. Poultangari, I., Shahnazi, R., and Sheikhan, M. (2012). RBF neural network based PI pitch controller for a class of 5-MW wind turbines using particle swarm optimization algorithm. *ISA Transactions*, 55 (5): 641–648.
132. Qiao, W., and Harley, R. G. (2007). Power Quality and Dynamic Performance Improvement of Wind Farms Using a STATCOM. *IEEE Power Electronics Specialists Conference*, Orlando, pages 1832–1838.

133. Qilian, L., Mendel, J. M. (2000). Interval type-2 fuzzy logic systems: Theory design, IEEE Transaction Fuzzy System, 8(5): 535–550.
134. Ramirez, D., Martinez, S., Blazquez, F., and Carrero, C. (2012). Use of STATCOM in wind farms with fixed-speed generators for grid code compliance. *In Renewable Energy*, 37(1): 202–212.
135. RT-LAB Version 10.7.0.361 User Guide, Opal-RT, IIT Roorkee, Uttarakhand, India.
136. Rodriguez, A.G.G. (2006). Improvement of a Fixed-Speed Wind Turbine Soft-Starter Based on a Sliding-Mode Controller. *Doctoral Thesis*, University of Seville, Seville.
137. Saad-Saoud, Z., Lisboa, M. L., Ekanayake, J. B., Jenkins, N., and Strbac, G. (1998). Application of STATCOMs to wind farms. *IEE Proceedings-Generation, Transmission and Distribution*, 145 (5): 511–516.
138. Saffar, M., and Musilek, P. (2016). Fuzzy logic controller for large, grid-integrated wind farm under variable wind speeds. 17th *Int. Scientific Conference on Electric Power Engineering (EPE)*, Prague, pages 1–6.
139. Sakamoto R., Senjyu T., Kinjo T., Urasaki N., and Funabashi T. (2004). Output power leveling of wind turbine generator by pitch angle control using adaptive control method. *International Conference on Power System Technology*, Singapore, pages 834–839.
140. Sakamoto, R., Senjyo, T., Kaneko, T., Urasaki, N., Takagi, T., and Sugimoto, S. (2006). Output power leveling of wind turbine generator by pitch angle control using H-∞ control. *IEEE Power System Conference*, Atlanta, pages 1–6.
141. Sandhu, N. S., Vadhera, S., and Sandhu, K. S. (2014,). Identification of major control parameters of wind turbine. In *Engineering and Systems (SCES), IEEE Students Conf.* pages. 1–5.
142. Sandhu, K. S., and Vadhera, S. (2008). Reactive power requirements of grid connected induction generator in a weak grid. *WSEAS transactions on Circuits and Systems*, *7*(3): 150–159.
143. Sandhu, N.S. Vadhera, S., and Sandhu, K. S. (2014). Controlled operation of wind turbine during wind disturbances. *International journal of circuits, systems and signal processing*. 8: 417–423.
144. Santos-Martin, D., Rodriguez-Amenedo, J. L., and Arnalte, S. (2008). Direct power control applied to doubly fed induction generator under unbalanced grid voltage conditions. *IEEE Transactions Power Electronics*, 23(5): 2328–2336.

145. Sefa, I., Altin, N., Ozdemir, S., and Kaplan, O. (2015). Fuzzy PI controlled inverter for grid interactive renewable energy systems. *IET Renewable Power Generation*, 9(7): 729–738.
146. Senjyu, T., Sakamoto, R., Urasaki, N., Funabashi, T., Fujita, H., and Sekine, H. (2006). Output power leveling of wind turbine generator for all operating regions by pitch angle control. *IEEE Transactions on Energy Conversion*, 21(2): 467–475.
147. Senjyu, T., Sakamoto, R., Kaneko, T., Yona, A., and Funabashi, T. (2008). Output power leveling of wind farm using pitch angle controller with fuzzy neural networks. *Electrical Power Components and System*, 36(10): 1048–1066.
148. Sharma, P., and Bhatti, T. S. (2013). Performance investigation of isolated wind–diesel hybrid power systems with WECS having PMIG. *IEEE Transactions on Industrial Electronics*, *60*(4): 1630–1637.
149. Sheikh, M. R. I., Muyeen, S. M., Takahashi, R., and Tamura, J. (2011). Smoothing control of wind generator output fluctuations by PWM voltage source converter and chopper controlled SMES, *European Transaction on Electrical Power*, 21(1): 680–697.
150. Sheikh, M. R. I., Mondol, N., and Eva, F. (2012). Stabilization of wind generator by PWM-VSC controlled SMES. *2nd International Conference on the Developments in Renewable Energy Technology (ICDRET 2012)*, Dhaka, pages 1–5.
151. Shima, Y., Takahashi, R., and Murata, T. (2008). Transient Stability Simulation of Wind Generator Expressed by Two-Mass Model. *Electrical Engineering in Japan*, 162 (3): 855–864.
152. Shu, H., Liang, Q., and Gao, J. (2008). Wireless sensor network lifetime analysis using interval type-2 fuzzy logic systems, *IEEE Transaction Fuzzy System*, 16(2): 416–427.
153. Singh, B., Murthy, S. S., and Gupta, S. (2006). STATCOM-Based Voltage Regulator for Self-Excited Induction Generator Feeding Nonlinear Loads. *IEEE Transactions on Industrial Electronics*, 53(5): 1437–1452.
154. Sinthipsomboon, K., Hunsacharoonroj, I., Khedari, J., Po-ngaen W., and Pratumsuwan, P. (2012). *A Hybrid of Fuzzy and Fuzzy Self-Tuning PID Controller for Servo Electro-Hydraulic System*. Chapter from the book Fuzzy Controllers - Recent Advances in Theory and Applications, pages 299–314.
155. Stiebler, M. (2008).*Wind energy systems for Electric power generation*, Springer series in green energy and technology, Verlag Berlin Heidelbeng.

156. Strzelecki, R., and Benysek, G. (2008). *Power Electronics in Smart Electrical Energy Networks*. Springer, London, UK.
157. Sravanthi, P., Rani, K. R., Amarnath, J., and Kamakshaiah, S. (2014). Critical clearing time and transient stability analysis of SCIG based wind farm with STATCOM. *International Conference on Smart Electric Grid (ISEG)*, Guntur, pages 1–8.
158. Suul, J. A., Molinas, M., and Undeland, T. (2010). STATCOM-based indirect torque control of induction machines during voltage recovery after grid faults. *IEEE Transaction on Power Electroics*, 25(5): 1240–1250.
159. Suvire, G. O. (2011). *Wind farm-Impact in power system and alternatives to improve the integration*. Published by InTech Janeza Trdine 9, 51000 Rijeka, Croatia.
160. Swami Naidu, N. K., and Singh, B. (2015). Doubly Fed Induction Generator for Wind Energy Conversion Systems with Integrated Active Filter Capabilities. *IEEE Transactions on Industrial Informatics*, 11(4): 923–933.
161. Tamura, J. (2001). Transient stability simulation of power system including wind generator by PSCAD/EMTDC. *IEEE Porto Power Tech Proceedings*, Portugal, pages 1–6.
162. Tan, O., Paap, G. C., and Kolluru, M. S. (1993). Thyristor-Controlled voltage regulators for critical induction motor loads during voltage disturbances. *IEEE Transactions on Energy Conversion*, 8(1): 100–106.
163. The Wind power. http://www.thewindpower.net/windfarm_en_86_challicum-hills.php 2017 (accessed 21.03.2017).
164. Thet, A. K., and Saitoh, H. (2009). Pitch control for improving the low-voltage ride-through of wind farm. *Transmission & Distribution Conference & Exposition: Asia and Pacific*, Seoul, pages 1–4.
165. Tian, G., Wang, S., and Liu, G. (2010). Power quality and transient stability improvement of wind farm with fixed-speed induction generators using a STATCOM. *International Conference on Power System Technology*, Hangzhou, pages 1–6.
166. Tremblay, E., Atayde, S., and Chandra, A. (2011). Comparative study of control strategies for the doubly fed induction generator in wind energy conversion systems DSP-based implementations approach. *IEEE Transactions Sustainable Energy*, 2(3): 288–299.
167. Tripathy, M., and Mishra, S. (2011). Interval type-2-based thyristor controlled series capacitor to improve power system stability. *Generation Transmission and Distribution*, 5(2): 209–222.

168. Trudnowski, D. J., Gentile, A., Khan, J. M. and Petritz, E. M. (2004). Fixed-speed wind-generator and wind-park modeling for transient stability studies. *IEEE Transaction on power system*, 19(4): 1911–1917.
169. Truong, D. N. (2016). STATCOM based fuzzy logic damping controller for improving dynamic stability of a grid connected wind power system. *IEEE International Conference System Science and Engineering (ICSSE)*, pages 1–4.
170. Uddin, M. N., and Rebeiro, R. S. (2011). Improved dynamic and steady state performance of a hybrid speed controller based IPMSM drive. *IEEE Industry Applications Society Annual Meeting*, Orlando, pages 1–8.
171. Vega, D. C., Marin, J. A., and Sanchez, R. T. (2015). Pitch angle controllers design for a horizontal axis wind turbine. *IEEE International Autumn Meeting on Power, Electronics and Computing (ROPEC)*, Ixtapa, pages 1–6.
172. Venne, P., Paquin, J. N., and Belanger, J. (2010). The what, where and why of real-time simulation. *In Proceedings IEEE PES General Meeting*, pages 37–49.
173. Vera, M. A. M., Palacios, F. M., and Garcia, J. M. F. (2012). Fuzzy Control Type II in DC-DC Converters. *IEEE Ninth Electronics, Robotics and Automotive Mechanics Conference*, Cuernavaca, pages 272–276.
174. Vimalraj, M., Alex, B., and Tamilarasi, M. (2014). StatCom control for voltage stability improvement at a fixed speed wind farm under unbalanced faults. *International Conference on Information Communication and Embedded Systems (ICICES2014)*, Chennai, pages 1–6.
175. Wang, L., and Hsiung, C. T. (2011). Dynamic Stability Improvement of an Integrated Grid-Connected Offshore Wind Farm and Marine-Current Farm Using a STATCOM. *IEEE Transactions on Power Systems*, 26(2): 690–698.
176. Wasynczuk, O., Man, D. T., and Sullivan, J. P. (1981). Dynamic behavior of a class of wind turbine generator during random wind fluctuations. *IEEE Transactions on Power Apparatus and System*s, 1(6): 2873–2845.
177. Wu, B., Lang, Y., Zargari, N., Kouro, S. (2011). *Power conversion and control of wind energy systems*, John Wiley & Sons. Ltd.
178. Wu, D. and Mandel, J. M. (2009). A comparative study of ranking methods. *Similarity measures and uncertainty measures for interval type-2 fuzzy sets*, 179(8):1169–1192.
179. Wu, H. T., and Liu, Y. H. (*2011*). Novel STATCOM Control Strategy for Wind Farm Reactive Power Compensation. *Asia-Pacific Power and Energy Engineering Conference*, Wuhan, pages 1–5.

180. Xu, Z. (2015). Improvement of power quality and dynamic voltage of wind farms using an inductive filtering method. *IEEE International Conference on Environment and Electrical Engineering (EEEIC)*, Rome, pages 1611–1615.
181. Yazdani , A. and Iravani, R. (2006). An accurate model for the DC-side voltage control of the neutral point diode clamped converter. *IEEE Transactions on Power Delivery*, 21(1): 185–193.
182. Zadeh, L. A. (1965). Fuzzy sets. *Information and control*, 8, 338–353.
183. Zadeh, L. A. (1973). Outline of a new approach to the analysis of complex systems and decision processes. *IEEE Transactions on systems, Man and Cybernetics*, 3(1): 28–44.
184. Zadeh, L. A. (1975). The concept of a linguistic variable and its applications to approximated reasoning. *Information Science*, 8(3): 199–249.
185. Zadeh, L. A. (1988). Fuzzy logic, *Computer*, 21(4): 83–93.
186. Zadeh, L. A. (1998). Toward a restricting of the foundations of fuzzy logic. *IEEE International Conference on World Congress on Computational; Intelligence Fuzzy Systems*, 2: 1676–1677.
187. Zaheer, S., and Kim, J. (2011). Type-2 fuzzy airplane altitude control: A comparative study. *In Proceeding IEEE International Conference Fuzzy Systems*, Taipei, 2170–2176.
188. Zhang, J., Yin, Z., Xiao, X., and Di, Y. (*2009*). Enhancement voltage stability of wind farm access to power grid by novel SVC. *4thIEEE Conference on Industrial Electronics and Applications*, Xian, pages 2262–2266.
189. Zhang, K., Mao, C., Lu, J., Wang, D., Chen, X., and Zhang, J. (2014). Optimal control of state-of-charge of superconducting magnetic energy storage for wind power system, *IET Renewable Power Generation*, 8(1): 58–66.
190. Zhao, Y., Shi, L., Ni, Y., and Yao, L. (2012). Modeling and Real-time simulation of wind farm. *Power & Energy Engineering Conference*, Shanghai, pages 1–4.
191. Zhou, D., and Blaabjerg, F. (2017). Bandwidth oriented proportional-integral controller design for back-to-back power converters in DFIG wind turbine system. *IET Renewable Power Generation*, 11(7): 941–951.
192. Zhu, W., and Cao, R. F. (2009). Improved low voltage ride-through of wind farm using STATCOM and pitch control. *IEEE 6thInternational Power Electronics and Motion Control Conference*, Wuhan, pages 2217–222.

193. Zwang, L., and Truong, D. N. (2013). Stability enhancement of DFIG-based offshore wind farm fed to a multi-machine system using a STATCOM. *IEEE transactions on power systems*, 28(3): 2882–2889.
194. Zwu,D., and Tan,W.W.(2010).Interval type-2 fuzzy pi controllers: Why they are more robhust. *IEEE International conference on Granular Computing, 2010*, pages 802-807.

APPENDIX

FIXED SPEED WIND ENERGY SYSTEM PARAMETERS FOR SIMULATION

Table i: Wind turbine parameters

Parameters	Values
Rated power	1.5 MW
Rotor diameter	64m
Number of blades	3
Cut-in wind speed (V_{wCI})	4 m/s
Cut-out wind speed (V_R)	25 m/s
Rated wind speed (V_{wR})	14 m/s
Generator	SCIG

Table ii: SCIG generator parameters

Parameters	Values
P_{rated} , V_{rated}	1.5 MW, 0.69 kV
R_s, R_r	0.004843 p.u., 0.004377 p.u.
L_s, L_r	0.1248 p.u., 0.1791p.u.
L_m, H	6.77 p.u., 5.04s
C	200 kVAR

Table iii: Transformer parameters

Parameters	Values
MVA	47MVA
$V_{\text{rated step-up}}$	25kV/120kV
Winding resistance	0.08/30 p.u.
Winding reactance	0.08 p.u.
Magnetizing resistance	500 p.u.
Magnetizing reactance	500 p.u.

VARIABLE-SPEED WIND ENERGY SYSTEM PARAMETERS

Table iv: DFIG studied system parameters

Parameters	Values
DFIG	1.5MW
Voltage rating	575V
Frequency	60Hz
Stator resistance	0.00706 p.u.
Stator inductance	0.171 p.u.
Rotor resistance	0.005 p.u.
Rotor inductance	0.156 p.u.
Mutual inductance	2.9 p.u.
Inertia constant	2.04 s
Transformer rating	47MVA, 25kV/120kV
Winding resistance	0.08/30 p.u.
Winding reactance	0.08 p.u.
Magnetizing resistance	500 p.u.
Magnetizing reactance	500 p.u.

MODELLING OF SYNCHRONOUS GENERATOR

Practically, the Park's "two reaction theory" of synchronous machine model is used in power system studies. Thus, the fundamental assumptions considered for modelling of a synchronous generator (SG) are well known and are not repeated here. The resulting set of machine differential algebraic equations (DAEs) changes with the dynamic order and the detail of the transfer functions. A modular approach is provided in this section to model the synchronous machine. The system model has been developed by reducing the SG equations in an appropriate form and then combining them with the network equations. This model is applicable to the three time frames: sub transient, transient and steady state. The differential equations of the SG are described as follows :

$$\begin{aligned} \dot{\delta} &= \Omega_b(\omega - \omega_s) \\ \dot{\omega} &= \frac{1}{2H}(\tau_m - \tau_e - D(\omega - \omega_s)) \end{aligned} \tag{i}$$

Where the electromagnetic torque is:

$$\tau_e = \psi_d i_q - \psi_q i_d \tag{ii}$$

where, Ω_b is the base synchronous frequency in rad/s (377 rad/s at 60Hz) and ω_s is the reference frequency approximated to the per unit value of ω_s is equal to 1.0 pu.

$$\begin{aligned} \dot{e}_q^{'} &= (-e_q^{'} - (x_d - x_d^{'} - \gamma_d)i_d + (1 - \frac{T_{AA}}{T_{do}^{'}})v_f) / T_{d0}^{'} \\ \dot{e}_d^{'} &= (-e_d^{'} + (x_q - x_q^{'} - \gamma_q)i_q) / T_{q0}^{'} \\ \dot{e}_q^{''} &= (-e_q^{''} + e_q^{'} - (x_d^{'} - x_d^{''} + \gamma_d)i_d + \frac{T_{AA}}{T_{do}^{'}} v_f) / T_{d0}^{''} \\ \dot{e}_d^{''} &= (-e_d^{''} + e_d^{'} + (x_q^{'} - x_q^{''} + \gamma_q)i_q) / T_{q0}^{''} \end{aligned} \tag{iii}$$

where, coefficients γ_q and γ_d are expressed as:

$$\begin{aligned} \gamma_q &= \frac{T_{q0}^{''}}{T_{q0}^{'}} \frac{x_q^{''}}{x_q^{'}} (x_q - x_q^{'}) \\ \gamma_d &= \frac{T_{d0}^{''}}{T_{d0}^{'}} \frac{x_d^{''}}{x_d^{'}} (x_d - x_d^{'}) \end{aligned} \tag{iv}$$

Finally the model complete with the following algebraic equations:

$$\begin{aligned} 0 &= \psi_d + x_d^{''} i_d - e_q^{''} \\ 0 &= \psi_q + x_q^{''} i_q + e_d^{''} \end{aligned} \tag{v}$$

By assuming *d*-axis additional leakage time constant $T_{AA} = 0$

Table v: synchronous generator parameters

Parameters	Values
S_{rated} , V_{rated}	100 MVA, 11kV
Inertia H	3.5s
r_a , x_l	0.003p.u , 0.15p.u
x_d , $x_d^{'}$	1.81p.u , 0.30p.u
$x_d^{''}$, x_q	0.23p.u , 1.76p.u
$x_q^{'}$, $x_q^{''}$	0.65p.u , 0.25p.u
$T_{d0}^{'}$, $T_{d0}^{''}$	8.00s , 0.03s
$T_{q0}^{'}$, $T_{q0}^{''}$	1.00s , 0.07s

REAL TIME SIMULATIONS

I. REAL TIME DIGITAL SIMULATOR

OPAL-RT lab, fully integrated with MATLAB/Simulink, is the open Real-Time Simulation software environment that has revolutionized the way model-based design is performed. RT-LAB's flexibility and scalability allow it to be used in virtually any simulation or control system application, and to add computing power to simulations, where and when it is needed. This simulator was developed with the aim of meeting the transient simulation needs of electric systems while solving the limitations of traditional real-time simulators. It is based on a central principle: the use of widely available, user-friendly, highly commercial products (PC platform, Simulink ^{TM}).

The real-time simulator consists of two main tools: a real-time distributed simulation package (RT-LAB) for the execution of Simulink block diagrams on a PC-cluster, and algorithmic toolboxes designed for the fixed time- step simulation of stiff electric circuits and their controllers. Real-time simulation and Hardware-in-the-Loop (HIL) applications are increasingly recognized as essential tools for engineering design and especially in electric power systems and power electronics.

II. EVOLUTION OF REAL-TIME SIMULATORS

Simulator technology has evolved from physical/analogue simulators (HVDC simulators &TNAs) for EMT and protection and control studies, to hybrid TNA/Analogue/Digital simulators capable of studying EMT behavior, to fully digital real-time simulators, as illustrated in Figure i. With the development of microprocessor and floating-point DSP technologies, physical simulators have been gradually replaced with fully digital real-time simulators. DSP-based real-time simulators were developed using proprietary technology, and used for HIL studies. These are the first new breed of digital simulator to become commercially available. However, the limitations of using proprietary hardware were recognized quickly, leading to the development of commercial supercomputer- based simulators, such as HYPERSIM from Hydro-Quebec, which is no longer commercially available.

Attempts have been made by the researchers to develop fully digital real-time simulators using low-cost standard PC technology, in an effort to eliminate the high costs associated with the use of high-end supercomputers. Such development was very difficult due to the lack of fast, low cost inter-computer communication links. However, the advent of low-cost, readily available multi-core processors (from INTEL and AMD) and related COTS computer

components has directly addressed this issue, clearing the way for the development of much lower cost and easily scalable real-time simulators. In fact, today's low-cost computer boards equipped with eight processor cores provide greater performance than 24-CPU supercomputers that were available only 10 years ago. The availability of this low-cost, high performance processor technology has also reduced the need to cluster multiple PCs to conduct complex parallel simulation, thereby reducing dependence on sometimes-costly inter-computer communication technology.

COTS-based high-end real-time simulators equipped with multi-core processors have been used in aerospace, robotics, automotive and power electronic system design and testing for a number of years. Recent advancements in multi-core processor technology means that such simulators are now available for the simulation of EMT expected in large-scale power grids, micro grids, wind farms and power systems installed in all-electric ships and aircraft. These simulators, operating under Windows, LINUX and standard real-time operating systems, have the potential to be compatible with a large number of commercially available power system analysis software tools, such as PSS/E, EMTP-RV and PSCAD, as well as multi domain software tools such as SIMULINK and DYMOLA. The integration of multi-domain simulation tools with electrical simulators enables the analysis of interactions between electrical, power electronic, mechanical and fluid dynamic systems.

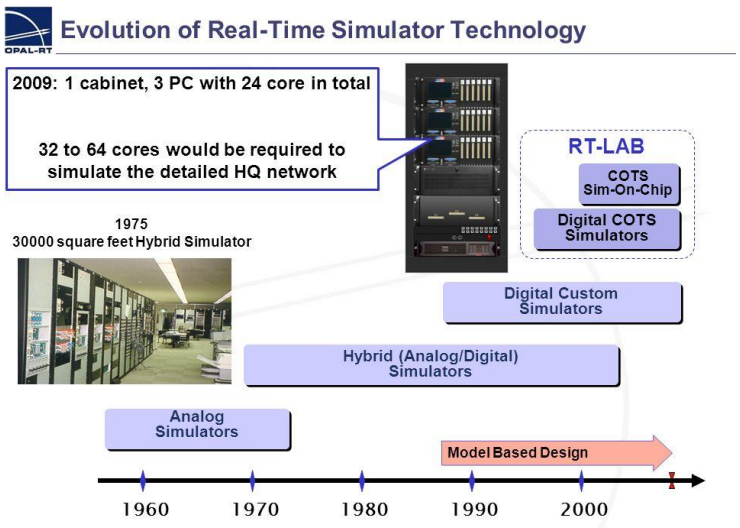

Figure i: Evolution of Real-Time Simulation Technologies

The latest trend in real-time simulation consists of exporting simulation models to real time digital simulator (RTDS). This approach has many advantages. First, computation time within each time step is almost independent of system size because of the parallel nature of

RTDS. Second, overruns cannot occur once the model is running and timing constrains are met.

III. SIMULATOR CONFIGURATION

Real-time simulators are typically used in three different application categories, as illustrated in Figure ii.

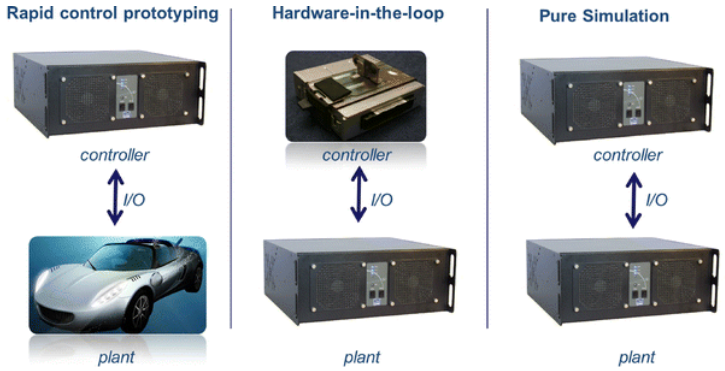

Figure ii: Different Real-Time Simulation configurations

i. Rapid Control Prototyping (RCP):

In RCP applications, a plant controller is implemented using a real-time simulator and is connected to a physical plant. RCP offers many advantages over implementing an actual controller prototype. A controller prototype developed using a real-time simulator is more flexible, faster to implement and easier to debug. The controller prototype can be tuned on the fly or completely modified with just a few mouse clicks. In addition, since every internal controller state is available, an RCP can be debugged faster without having to take its cover off.

ii. *Hardware-in-the-Loop (HIL):*

For HIL applications, a physical controller is connected to a virtual plant executed on a real-time simulator, instead of to a physical plant. Figure ii illustrates a small variation to HIL; an implementation of a controller using RCP is connected to a virtual plant via HIL. In addition to the advantages of RCP, HIL allows for early testing of controllers when physical test benches are not available. Virtual plants also usually cost less and are more constant. This allows for more repeatable results and provides for testing conditions that are unavailable on real hardware, such as extreme events testing.

iii. *Pure simulation/Software in the loop (SIL):*

SIL represents the third logical step beyond the combination of RCP and HIL. With a powerful enough simulator, both controller and plant can be simulated in real time in the

same simulator. SIL has the advantage over RCP and HIL that no inputs and outputs are used, thereby preserving signal integrity. In addition, since both the controller and plant models run on the same simulator, timing with the outside world is no longer critical; it can be slower or faster than real-time with no impact on the validity of results, making SIL ideal for a class of simulation called accelerated simulation. In accelerated mode, a simulation runs faster than real-time, allowing for a large number of tests to be performed in a short period. For this reason, SIL is well suited for statistical testing such as Monte-Carlo simulations.

IV. THE WORKING PROCESS OF RT-LAB

RT-LAB allows the user to readily convert simulink models, via Real-time workshop (RTW), and then to conduct Real-time simulation of those models executed on multiple target computers equipped with multi-core PC processors. This is used particularly for Hardware-in-loop (HIL) and rapid control prototyping (RCP) and SIL applications. RTLAB transparently handles synchronization, user interaction, and real world interfacing using I/O boards and data exchanges for seamless distributed execution.

V. SIMULATOR SOLVERS

The RT-LAB electrical simulator uses advanced fixed time step solvers and computational techniques designed for the strict constraints of real-time simulation of stiff systems. They are implemented as a Simulink toolbox called ARTEMIS, which is used with the sim Power Systems/ Power System Block-set (PSB). PSB is a Simulink toolbox that enables the simulation of electric power circuits within the Simulink environment. While PSB supports a fixed-time-step solver based on the Tustin method, dynamic computation of circuit matrices, un-damped switching oscillations, and the need for a very small step size which greatly slows down the simulation. The ARTEMIS solver uses a high-order fixed time- step integration algorithm that is not prone to numerical oscillations, and advanced computational techniques necessary for the real-time simulation.

VI. RT-LAB SIMULATION DEVELOPMENT PROCEDURE

Electric and power electronic systems are created on the host personal computer by interconnecting:

- Electrical components from component model libraries available in the Power System Block-set
- Controller components and other components from Simulink and its toolboxes that are supported by Real- Time-Workshop

- I/O blocks from the simulator I/O tool boxes. The easy to- use drag-and-drop Simulink interface issued at all stages of the process.
- These systems are then simulated and tuned off-line in the MATLAB/Simulink environment. ARTEMIS fixed step solvers are used for the electric part and Simulink native solvers for the controller and other block-diagram parts. Finally, the model is automatically compiled and loaded to the PC-Cluster with RTLAB simulation interface.

VII. OP5600 SIMULATOR

The OP5600 is a complete simulation system capable of operating with either Spartan 3 or Vertex 6 FPGA platforms. It is designed to be used either as a desktop (or shelf top) or as a more traditional rack mount. It contains a powerful Target Computer and a flexible, high-speed Front End Processor and a signal conditioning stage. The new design makes it easier to use with standard connectors (DB37, RJ45 and mini-BNC) without the need for input/output adaptors and allows quick connections for monitoring. The typical diagram of OP5600 HIL box is as shown in Figure iii.

The front of the chassis provides the monitoring interfaces and monitoring connectors, while the back of the chassis provides access to the FPGA monitoring connections, all I/O connectors, power cable and main power switch.

Inside, the main housing is divided into two sections, each with a specific purpose and connected only by a DC power cable and a PCIe cable:

Figure iii: OP5600 HIL box

i. Front view configuration:

The front view of the OP5600 chassis is shown in Figure iv.

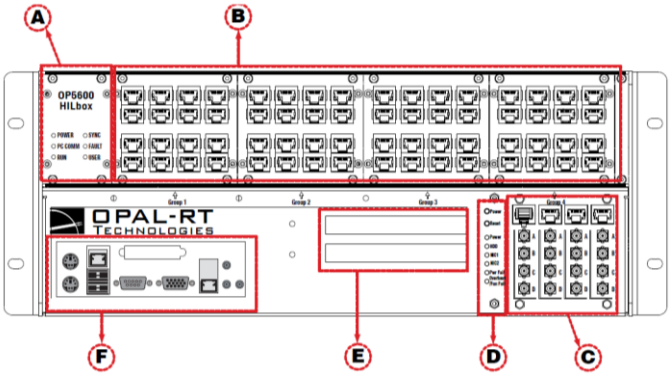

Figure iv: OP5600 front connector panels

A. Inactive section. These functions are currently in development and unavailable.

B. 4 panels of RJ45 connectors provide connections to monitor output from mezzanine I/O boards. Each connector is linked to front and back mezzanines on the carrier board. Analog mezzanines (channels 0-15) will use only the first column of connectors. Digital mezzanines will use both columns (channels 0-15 in the first column and channels 16-31 on the second column of connectors). See "DB37F Connections" and "RJ45 connections" for more detailed information.

C. Monitoring RJ45 connectors with mini-BNC terminals: RJ45 cables connect from a channel on an RJ45 panel (B) to one of four RJ45 monitoring connectors (C). Mini-BNC connectors allow for quick cable connections to monitoring devices (such as an oscilloscope). See "connecting monitoring devices" for details.

D. Target computer monitoring interface. Two push buttons include POWER in top position to start the target computer and RESET in the bottom position to reset the target computer. There are 6 LED indicators:

LED	**NAME**	**Description**
Green	Power	On indicates that the unit is powered up.
Green	HDD	On indicates that the hard disk drive is operating.
Green	NIC1	On indicates that network port 1 is in use.
Green	NIC2	On indicates that network port 2 is in use.
Red	Power Fail	On indicates a power fault.
Red	Overheat/Fan Fail	On indicates either that unit has overheated or a fan fault.

E. Optional PCI or PCIe connector slots (by default, these spaces will be covered by blank plates if there are no optional PCI cards. If there are PCI cards installed, the spaces will contain the PCI connectors).

F. F. Standard computer connectors (left to right): mouse and keyboard, USB ports, monitor, network ports. Although use of these connectors is optional but not required to use the OP5600, one network port is required for network connection.

ii. Back view configuration:

Figure v represents the back view configuration of the OP5600 chassis.

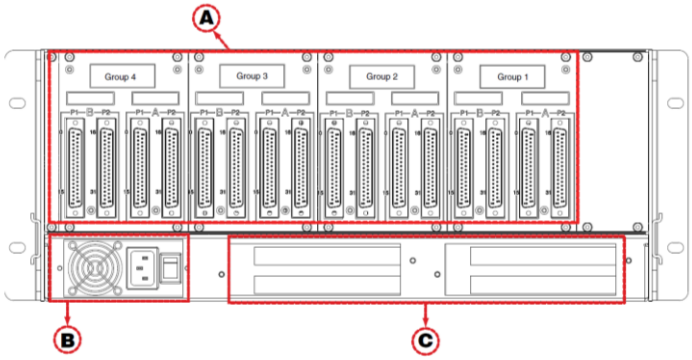

Figure v: OP5600 back connector panels

A. DB37F I/O connectors (see "Table vi and vi: Pin Assignments" for more details). The image (opposite) illustrates the links between the mezzanines and the DB37 I/O connectors

B. Power connector and power On/Off switch.

C. Optional PCI or PCIe connector slots.

Table vi: OP5600 DB37 pin assignments

Connector A Ch. 0-15				**Connector A Ch. 16-31**			
DB37	**Module pin assign ment**	**DB37**	**Module pin assign ment**	**DB37**	**Module pin assign ment**	**DB37**	**Module pin assign ment**
1	+CH00	20	-CH00	1	+CH16	20	-CH16
2	+CH01	21	-CH01	2	+CH17	21	-CH17
3	+CH02	22	-CH02	3	+CH08	22	-CH18
4	+CH03	23	-CH03	4	+CH19	23	-CH19
5	+CH04	24	-CH04	5	+CH20	24	-CH20
6	+CH05	25	-CH05	6	+CH21	25	-CH21
7	+CH06	26	-CH06	7	+CH22	26	-CH22
7	+CH07	27	-CH07	7	+CH23	27	-CH23
9	+CH08	28	-CH08	9	+CH24	28	-CH24
10	+CH09	29	-CH09	10	+CH25	29	-CH25
11	+CH10	30	-CH10	11	+CH26	30	-CH26
12	+CH11	31	-CH11	12	+CH27	31	-CH27
13	+CH12	32	-CH12	13	+CH28	32	-CH28
14	+CH13	33	-CH13	14	+CH29	33	-CH29
15	+CH14	34	-CH14	15	+CH30	34	-CH30
16	+CH15	35	-CH15	16	+CH31	35	-CH31
17		36		17		36	
18	Vuser 1 A*	37	Vrtn 1 A*	18	Vuser 2 A*	37	Vrtn 2 A*
19				19			

Table vii: OP5600 DB37 pin assignments

Connector B Ch. 0-15				Connector B Ch. 16-31			
DB37	**Module pin assignment**	**DB37**	**Module pin assignment**	**DB37**	**Module pin assignment**	**DB37**	**Module pin assignment**
1	+CH00	20	-CH00	1	+CH16	20	-CH16
2	+CH01	21	-CH01	2	+CH17	21	-CH17
3	+CH02	22	-CH02	3	+CH08	22	-CH18
4	+CH03	23	-CH03	4	+CH19	23	-CH19
5	+CH04	24	-CH04	5	+CH20	24	-CH20
6	+CH05	25	-CH05	6	+CH21	25	-CH21
7	+CH06	26	-CH06	7	+CH22	26	-CH22
7	+CH07	27	-CH07	7	+CH23	27	-CH23
9	+CH08	28	-CH08	9	+CH24	28	-CH24
10	+CH09	29	-CH09	10	+CH25	29	-CH25
11	+CH10	30	-CH10	11	+CH26	30	-CH26
12	+CH11	31	-CH11	12	+CH27	31	-CH27
13	+CH12	32	-CH12	13	+CH28	32	-CH28
14	+CH13	33	-CH13	14	+CH29	33	-CH29
15	+CH14	34	-CH14	15	+CH30	34	-CH30
16	+CH15	35	-CH15	16	+CH31	35	-CH31
17		36		17		36	
18	Vuser 1 B*	37	Vrtn 1 B*	18	Vuser 2 B*	37	Vrtn 2 B*
19				19			

iii. RJ45 Channel assignments

Each mezzanine is assigned two columns of RJ45 connectors. Each column represents a series of channels, divided into 4 channels per jack, as shown in Figure vi.

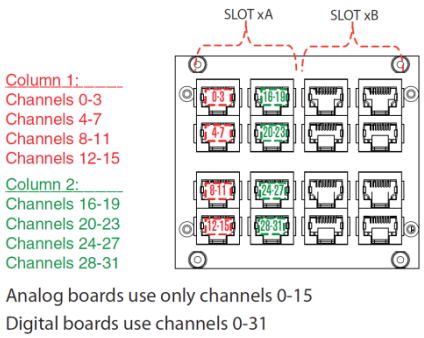

Figure vi: RJ45 channel assignments

iv. Connecting monitoring devices

The OP5600 simulator offers quick, single-ended connections, through RJ45 and mini BNC connectors, to any monitoring device (i.e. oscilloscope, etc.). These mini-BNC jacks let you monitor 4 channels individually. Simply follow these instructions (as illustrated in Figure vii):

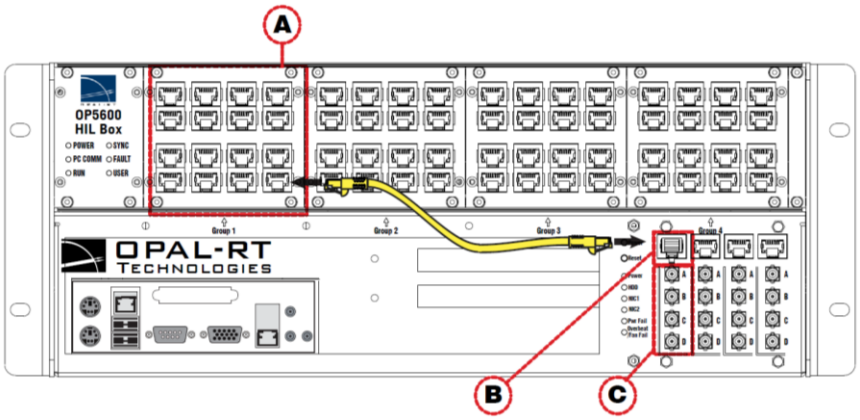

Figure vii: How to connect cables for monitoring

1. Connect one end of the RJ45 cable to the desired channels (A). See Figure vi for RJ45 connector pinouts
2. Connect the other end of the RJ45 cable to the monitoring connector (B)
3. Connect a mini-BNC cable to each BNC jack (C) and connect the other end of the cable to the desired monitoring device. The mini-BNC jacks each connect to one of the 4 channels of the RJ45 Connector (A). In the example shown in Figure vi, the RJ45 cable is connected to channels 28-31. The mini-BNC cable jacks, identified as A, B, C, D, represent each channel in the following order;
   A = channel 28,
   B = channel 29,
   C = channel 30
   D = channel 31.

v. OP5330 Digital to analog converter

The OP5330 digital to analog converter (DAC) provides 16 single-ended digital output channels. Each channel uses a 16-bit resolution digital-to-analog converter. It is a part of the OP5000 series of optional modules for OPAL-RT's state of the art HIL (hardware-in-the-loop) systems, intended for use with OPAL-RT carrier boards.

Each OP5330 can sample up to 1 MS/s, giving a total throughput of 8 MS/s, all channels are simultaneously sampled. The onboard EEPROM provides offset and gain data adjustment written during the calibration process, as well as over-voltage protection.

By default, the maximum output signal is set to ±16 volts.

vi. OP5340 Analog to digital converter

The OP5340 Analog to Digital converter (ADC) is a part of the OP5000 series of optional modules for OPAL-RT's state of the art HIL (hardware-in-the-loop) systems, intended for use with OPAL-RT carrier boards. Designed for OPAL-RT's simulation systems, the OP5340 converts analog signals to digital.

The OP5340 module provides 16 differential analog input channels. Each channel uses a 16- bit resolution analog-to-digital converter. The OP5340 module also has input signal conditioning capabilities that allow the user to apply a signal range from ±20v up to ±120v on the inputs. By default, the maximum input signal is set to ±20 volts.

VIII. PROCEDURE FOR IMPLEMENTATION OF A MODEL FROM MATLAB TO REAL-TIME

The execution process allows user to run the Simulink model with Opal-RT's software and hardware. It is based on eight (8) main steps:

i. Open a model

ii. Edit a model in MATLAB

iii. Compilation

iv. Assign nodes

v. Synchronization Mode

vi. Loading

vii. Execution / Pause

viii. Reset

i. Open a Model

In the Main Control window, the Open Model button allows user to open the model. Right-click button is used to open a recently used model. Simulink, System Build & EMTP models can be opened. When a model is open, its path will appear in the top display. Opening of a Simulink model using RT-LAB is shown in Figure viii.

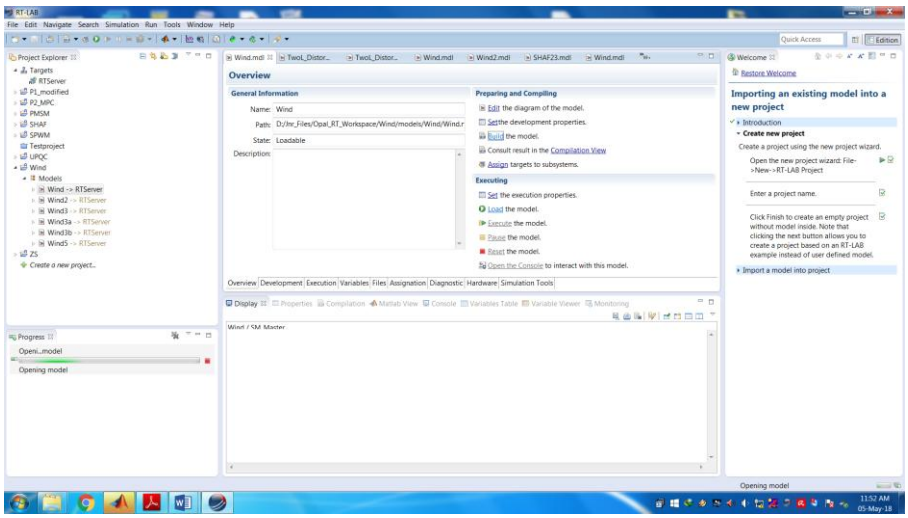

Figure viii: Opening of MATLAB model using RT-LAB

ii. Edit a Model

In the Main Control window, the Edit button allows user to edit Simulink model using MATLAB. Simulink model consists of Master and Console subsystems which are shown in Figure ix.

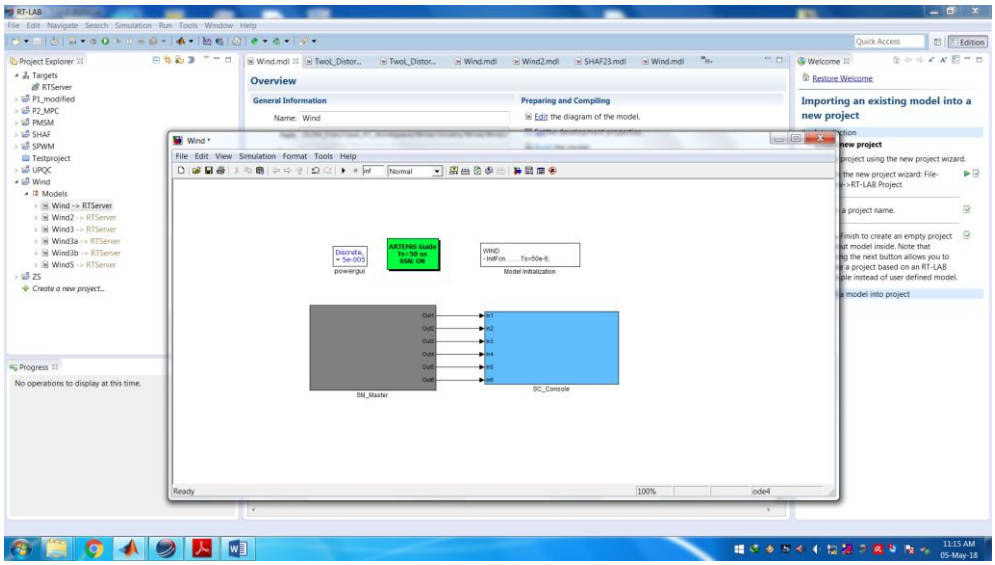

Figure ix: Model consist of Master and Consloe sub systems

SM Master Subsystem

- Prefix Identifier: SM_
- Number of SM subsystems allowed in a model: 1 (always)
- Content: All the computational elements of the model, the mathematical operations, the I/O blocks, the signal generators, etc.

- Note: This is the main subsystem and every model must have one SM_subsystem. If double click on the SM_Master block the computing system inside the SM_Master subsystem is display and as shown in Figure x.

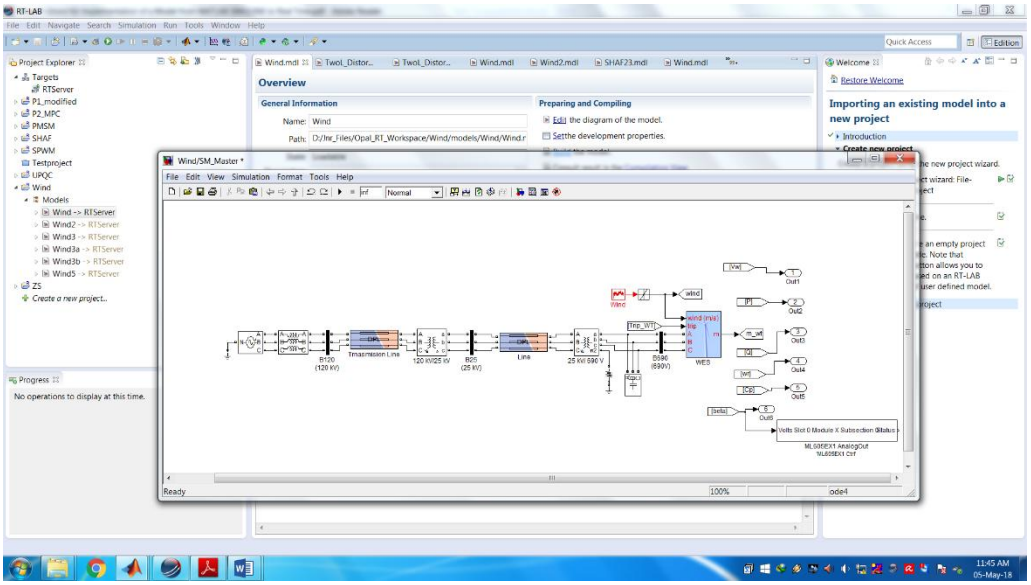

Figure x: SM_Master computing sub system

SC Console Subsystem

- Prefix Identifier: SC_
- Number of SC subsystems allowed in a model: 0 or 1
- Content: All user interface blocks (scopes, displays, switches, etc)
- Note: This is the only subsystem that will be available to us during execution. It enables us to interact with the system while it is running. The console runs asynchronously from the other subsystems. It is also the only subsystem that is not linked to a computation node (core). Therefore, there should be no signal generation or important mathematical operations included in this subsystem.

Add the OpComm Block

RT-LAB uses OpComm blocks to enable and save communication setup information. This includes both communication between the console and the computation nodes and communication between the multiple computation nodes in a distributed simulation scenario. All subsystems inputs must first go through an OpComm block before any operations can be done on the signals they are associated with. The OpComm block must be inserted after the subsystems creation and renaming. In general, only one OpComm block must be used even if there are multiple inputs in one subsystem. Double-click on the block to select the number of inputs required. The typical OpComm block for studied system is shown in Figure xi.

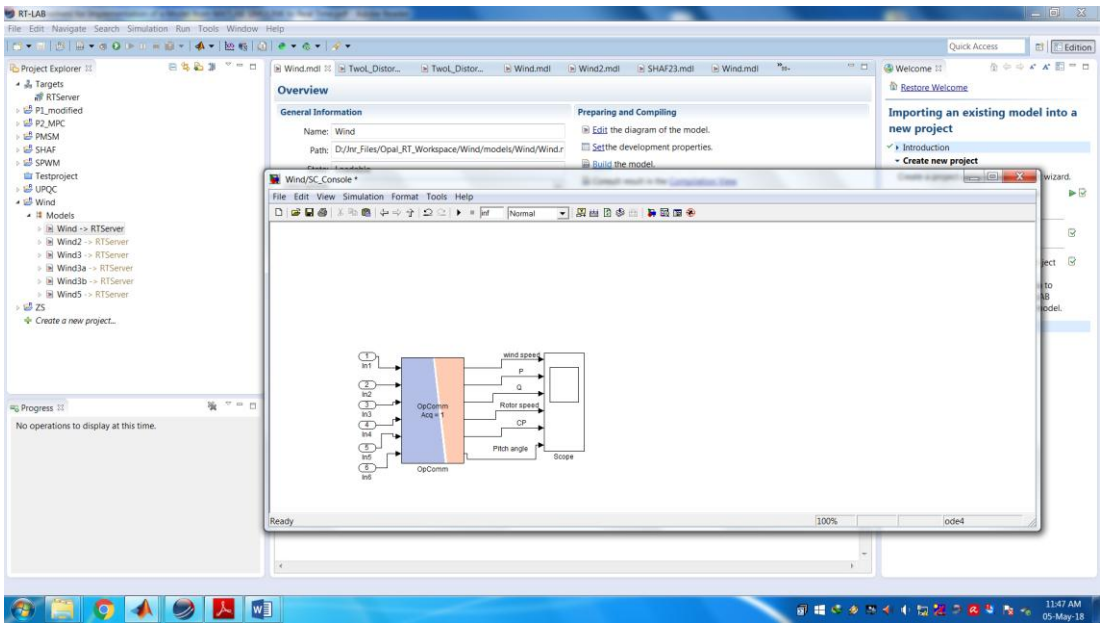

Figure xi: SC_Console sub system

Set the Real-Time Parameters

A real-time model can only run in Fixed-Step mode as real time is fixed-step. The Fixed-Step size (fundamental sample time) must be chosen carefully regarding the needs of the simulation, the dynamics of the model and must take in account the software/hardware capability. A typical mechanical application may run around 1millisec while a typical electrical system may run around 50microsec.

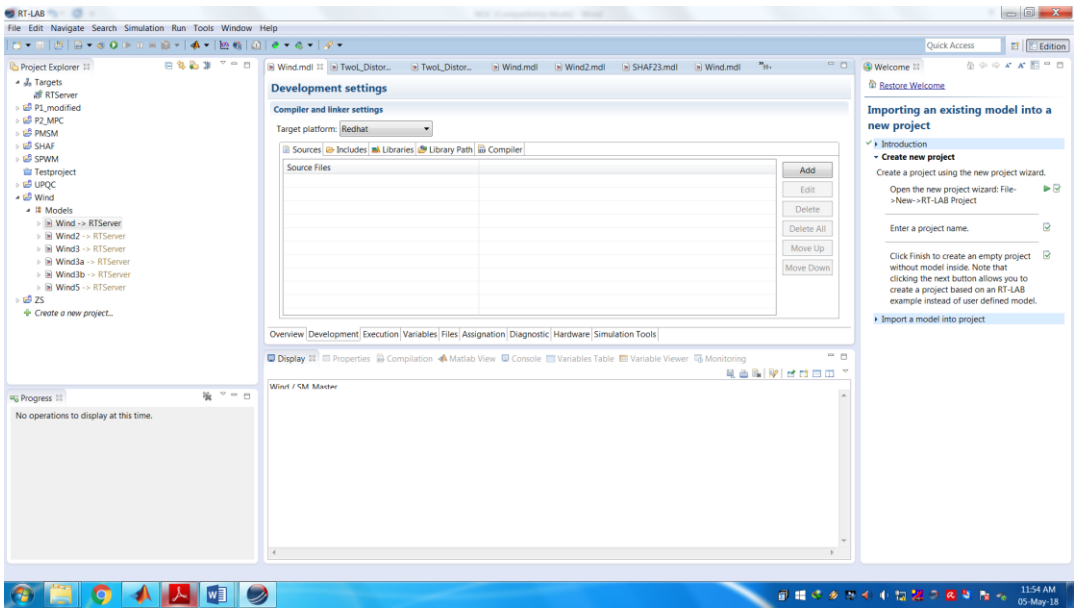

Figure xii: Setting of redhat mode for MATLAB model using RT-LAB

In most cases, we want the console (SC) to run indefinitely. In order to do so, the simulation's stop time must be set to ''INF''. With this parameter set, the console will be

stopped only when us decides to reset his model. This parameter does not apply to the simulation duration; only to the console. To develop a model in RT-LAB, target platform should be set in Red hat mode this is shown in Figure xii.

iii. Compilation

In the Main Control window, the Compile button allows us to compile the Simulink model. Right-click button is used to select only specific steps of the compilation. If for any reason us wants to stop the compilation while it is launched, the Compile button is changed to ‘‘Abort’’ and is available to stop the process. Compilation of a Simulink model using RT-LAB is shown in Figure xiii.

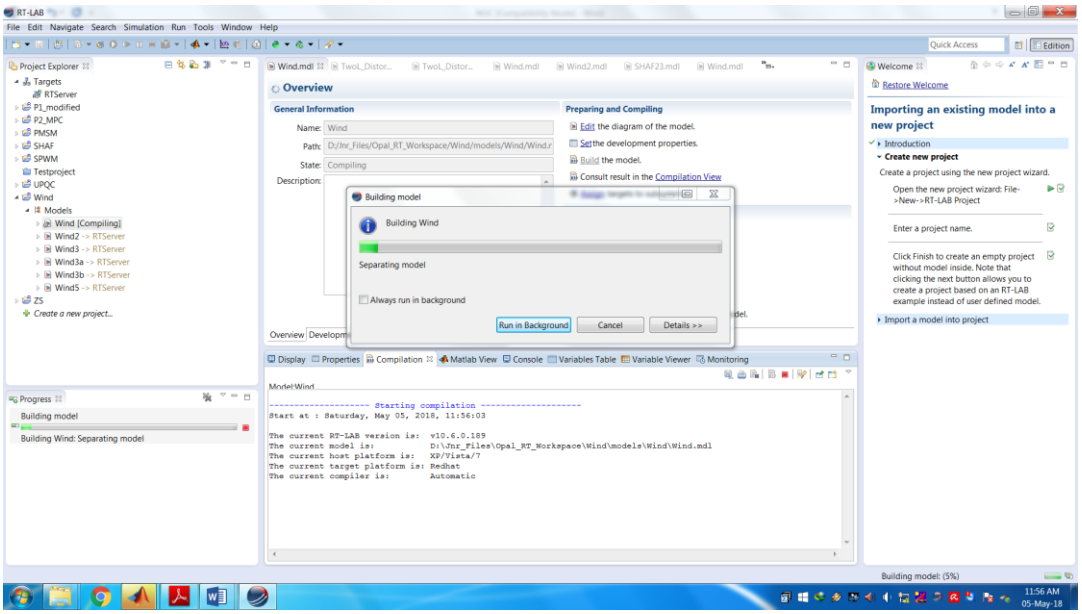

Figure xiii: Compilation of Simulink model using RT-LAB

iv. Assign nodes

In the Main Control window, the Assign Nodes button allows us to link the model’s subsystems to the targets. The list of available nodes is on the right side. ‘‘Target Info’’ will provide us very useful information about the target selected. ‘‘Target Info’’ will provide us very useful information about the target selection, which is shown in Figure xiv.

v. Synchronization Mode

There are 4 synchronization modes available in RT-LAB:

(a) Simulation

(b) Software Synchronized

(c) Hardware Synchronized

(d) Simulation with low priority

The synchronization mode can be set at any time before loading a model. After the loading step, the simulation mode list will be disabled and the model must be reset if a simulation mode change is required. Hardware Synchronization of Simulink model using RT-LAB is shown in Figure xv.

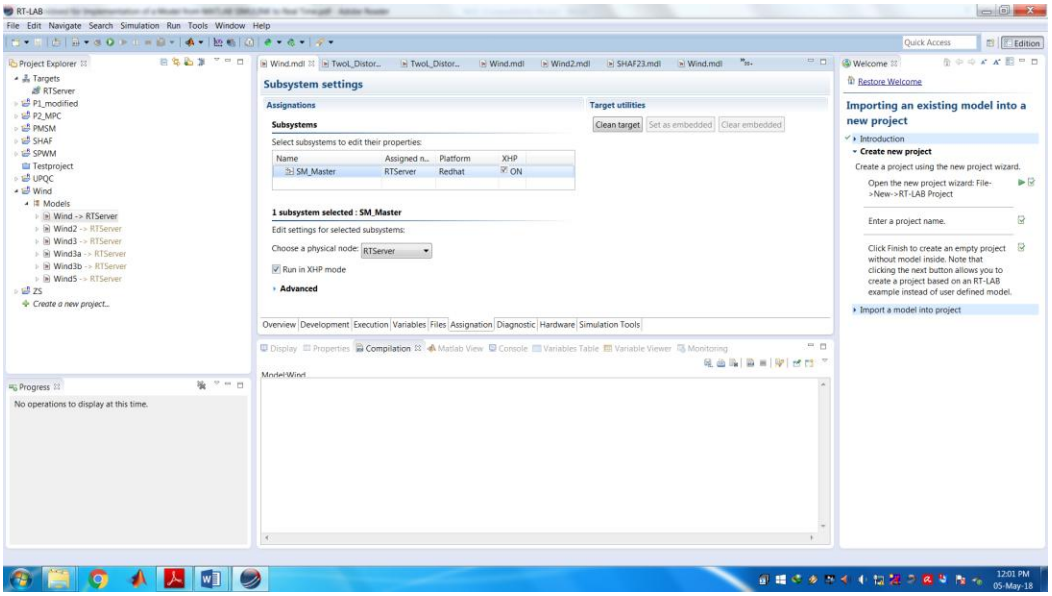

Figure xiv: Assigning nodes using RT-LAB

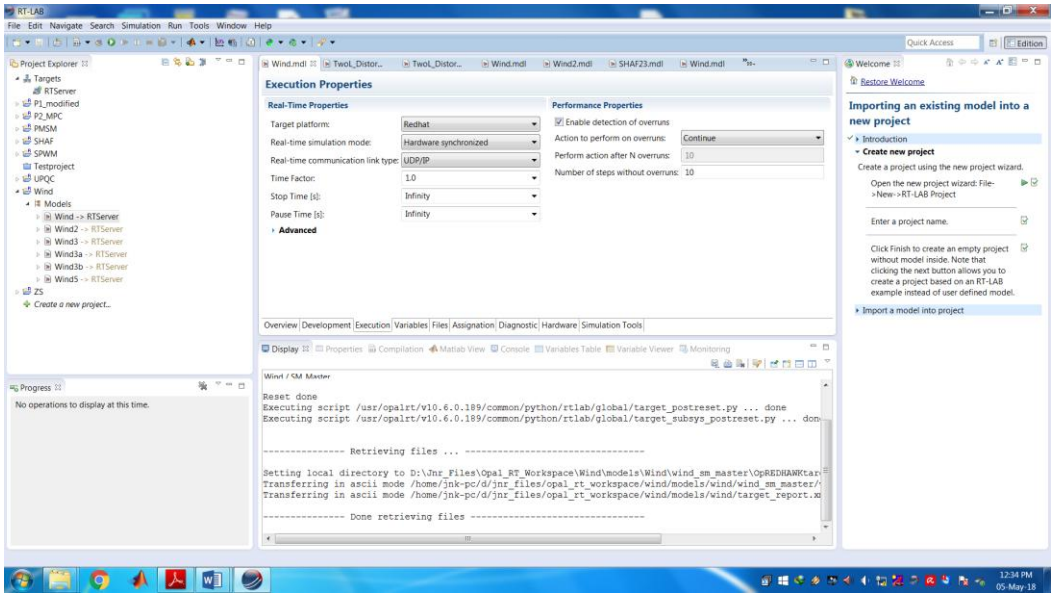

Figure xv: Hardware synchronization using RT-LAB

vi. Load

In the Main Control window, the Load button allows us to load the Simulink model on the target(s). This is the last step before executing the model. The console will open and be ready for execution. There is one log window for each real time subsystem (SM or SS). Loading Simulink model and opening of console block using RT-LAB is shown in Figure xvi.

vii. Execution

In the Main Control window, the Execute button allows us to execute the Simulink model. During execution, we can change the controls found in the console and witness changes displayed in scopes, displays, etc. We can pause or reset the model at any time. Execution of Simulink model using RT-LAB is shown in Figure xvii.

viii. Reset

When we want to stop definitely our model from running, we must use the reset button found in the Main Control window. This will stop the acquisition (software & hardware) and the console will close.

IX. RT-LAB APPLICATION FIELD

- Electrical (Power Electronics & Power Systems)
- Aerospace & Defence
- Automotive
- Academic & Research

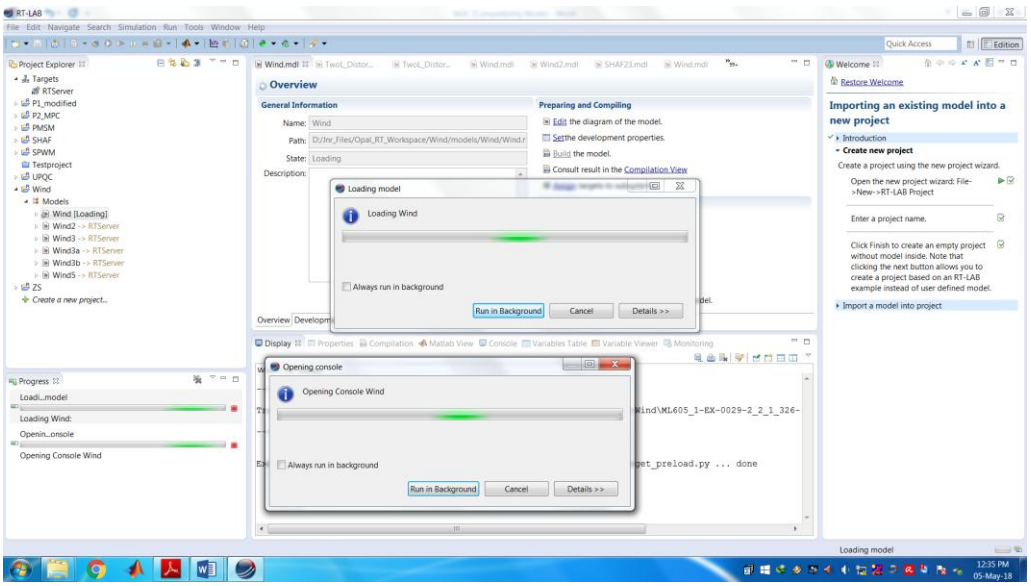

Figure xvi: Loading model using RT-LAB

- 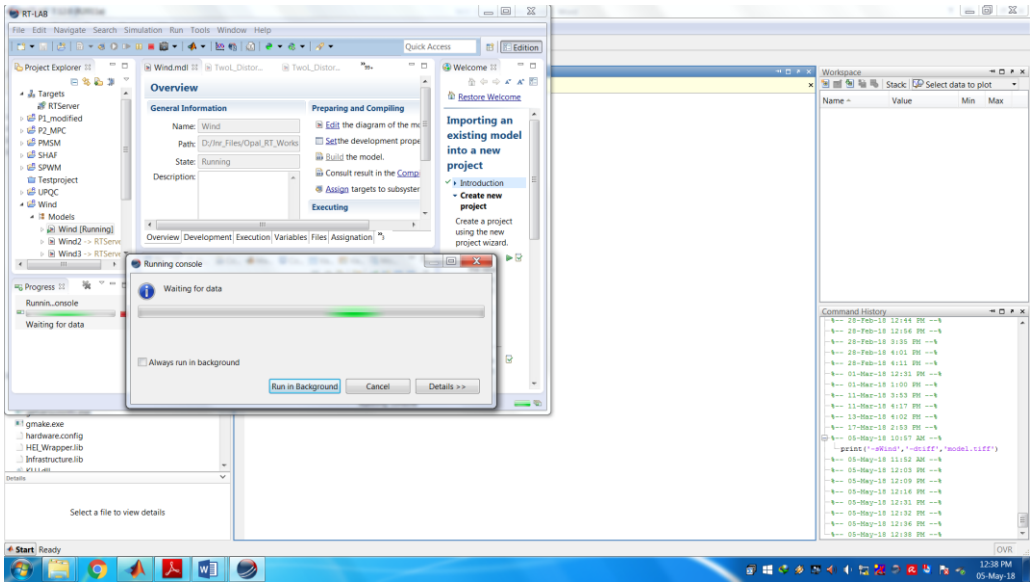

- Figure xvii: Execution of simulink model using RT-LAB

LIST OF PUBLICATIONS

List of Journal Papers:

1. Kanasottu Anil Naik and Chandra Prakash Gupta "Output power smoothing and voltage regulation of a fixed speed wind generator in partial load region using STATCOM and pitch angle controller," *Energies,* Vol. 11, No. 1, 2018, pp.1-18.
2. K. A. Naik, C. P. Gupta and E. Fernandez. "Performance improvement of a wind energy system using fuzzy logic based pitch angle control strategy." in *AST System Journal*, vol.3, no.3, 2018, pp-30-37.
3. K. A. Naik and C. P. Gupta "Power Smoothing of Wind Energy System using Type-2 Fuzzy-Logic Pitch-Angle Controller," **Minor Revision Submitted** in *Electric Power Components and Systems Journal.*
4. K. A. Naik and C. P. Gupta "Output power smoothing of wind energy system using Type-2 Fuzzy logic based pitch angle controller in all operating regions," **Under review** in *Journal of electrical engineering and technology*.
5. K. A. Naik, C. P. Gupta and E. Fernandez "Improved low voltage-ride-through capability of a fixed speed wind energy system using STATCOM and pitch angle control," **Under review** in *International Journal of Emerging Electric Power Systems.*
6. K. A. Naik, C. P. Gupta and E. Fernandez "Advanced Type-2 Fuzzy Logic Based Pitch Angle Control strategy for stability enhancement of wind energy system," **Under review** in *Wind engineering*.
7. K. A. Naik, C. P. Gupta and E. Fernandez "Design and implementation of adaptive type-2 FLC-PI controller DFIG based wind energy system", **Communicated** in *IET Renewable power generation.*

List of Conference Papers:

1. K. A. Naik and C. P. Gupta, "Improved oscillatory behavior of a grid connected wind farm using PI based pitch angle controller," *IEEE Int. Conf. on Power Systems (ICPS)*, New Delhi, 2016, pp. 1-6.
2. K. A. Naik and C. P. Gupta, "Improved fluctuation behavior of SCIG based wind energy system using hybrid pitch angle controller," *IEEE Int. Conf. on Electrical, Computer and Electronics Engineering (UPCON)*, Varanasi, 2016, pp. 508-514.

3. K. A. Naik and C. P. Gupta, "Transient stability enhancement of wind energy system using fuzzy logic based pitch angle controller," *2017 4th IEEE Uttar Pradesh Section International Conference on Electrical, Computer and Electronics (UPCON)*, Mathura, India, 2017, pp. 78-83.
4. K. A. Naik and C. P. Gupta, "Fuzzy logic based pitch angle controller for SCIG based wind energy system," *IEEE Int.Conf. on Recent Developments in Control, Automation & Power Engineering (RDCAPE)*, Noida, 2017, pp. 60-65.
5. K. A. Naik and C. P. Gupta, "Performance comparison of Type-1 and Type-2 fuzzy logic systems," *IEEE 4th International Conference on Signal Processing, Computing and Control (ISPCC)*, Solan, 2017, pp. 72-76.
6. K. A. Naik and C. P. Gupta "A Fuzzy based Novel Pitch Angle Control Strategy for Wind Energy System," *IEEE int.Conf. INDICON*, IIT Roorkee, 15st-17th December, 2017.
7. K. A. Naik, C. P. Gupta and E. Fernandez "Implementation of grid connected wind driven induction generator from MATLAB/Simulink to Real-Time," *Communicated to IEEE, ICPEICES*, DTU Delhi, October 22-24, 2018.
8. K. A. Naik, C. P. Gupta and E. Fernandez "Investigations on fixed speed farm stabilization using STATCOM," *Communicated to IEEE CIPECH*, November 1-2, 2018.